The University of Nottingham

UNITED KINGDOM • CHINA • MALAYSIA

Division of Drug Delivery and Tissue Engineering

School of Pharmacy

DEVELOPMENT OF FUNCTIONAL MICELLES FROM BIODEGRADABLE AMPHIPHILIC BLOCK COPOLYMERS FOR DRUG DELIVERY AND TUMOUR THERAPY

Muhammad Gulfam

Thesis submitted to the University of Nottingham for the degree of Doctor of Philosophy

October 2017

ABSTRACT

Drug delivery systems in the size range of ~ 10-250 nm are enabling tools for site-specific targeting and controlled release applications. To take advantage of these capabilities, various nanocarriers e.g., micelles, dendrimers, liposomes, nanoparticles, nanocapsules, nanotubes, and nanogels, have been designed for drug delivery. Specifically, micelle-based drug carrier systems have emerged as promising tools for site-specific delivery and controlled release applications. Despite several advantages over conventional drugs, some limitations of micelle-based drug delivery have also been reported. These drawbacks include low stability *in vivo*, poor penetration, modest accumulation in tumour tissues, and inadequate control over drug release.

To overcome these limitations, stimuli-responsive or smart polymeric nanocarriers have been developed for drug delivery and tumour therapy, previously. The most well-known internal stimuli in cancerous regions include higher acidity associated with dysregulated metabolism in tumour tissues, elevated levels of glutathione in the cytosol and nucleus of cancer cells, and altered degradative enzymes in the lysosomes, and reactive oxygen species in the mitochondria. These intrinsic microenvironments can be exploited as internal stimuli to attain active drug release in the tumour tissues or cancer cells.

In particular, the reducing potential inside the cancer cells is considerably higher than found in the extracellular environment and bloodstream. Such varying redox potential can be exploited for tumour-specific drug delivery and controlled release applications. Various types of redox-responsive micelles have been developed, previously. Generally, redox-responsive micelles have disulfide linkages that undergo rapid cleavage in the presence of reducing agents in the intracellular components, however, are stable at oxidising extracellular environment. The redox-responsive disulfide bridges can be incorporated into nanocarriers by placing multiple disulfide bonds in the hydrophobic backbone or by conjugating therapeutic agents to the side chain of the polymer via a disulfide linker. Another strategy to construct redox-responsive linkages is to crosslink the polymeric nanocarriers with a disulfide crosslinker. Studies have shown that polymeric micelles can dissociate, especially upon administration when they are diluted below their critical micelle concentration. The stability of polymeric micelles can be enhanced by chemical crosslinking. Various types of crosslinked micelles can be prepared subjected to the localisation of the crosslinking, e.g. shell crosslinked micelles, and core crosslinked micelles. Introducing redox-responsive bridges through disulfide crosslinkers may not only provide stability to nano-carriers against dilutions during circulation, but also render them responsive to reducing conditions.

Specifically, redox-responsive core-crosslinked micelles have demonstrated good stability and better 'stealth' properties, nevertheless, the hydrophobic core of most of the existing core-crosslinked micelles have been based on

non-degradable polymers such as polyacrylamide or polyacrylate. The non-degradable constituent of the block copolymer may cause complications in clinical applications. Therefore, reduction-responsive core-crosslinked micelles comprising entirely of biologically inert or biocompatible and biodegradable polymers would be better candidates for drug delivery and controlled release application.

To overcome these limitations, micelles based on polyesters (a class of aliphatic biodegradable polymers) can used for drug delivery application. In the last few decades, various FDA approved aliphatic polyesters e.g. poly(lactic-co-glycolic acid) (PLGA), poly(ε-caprolactone), and poly(lactic acid), have been intensively studied to exploit their potential in drug, gene and protein delivery and controlled release applications. Nevertheless, most of these polyesters lack functional groups, making it difficult to incorporate redox-responsive linkages to core-crosslink their micelles.

To address these issues, we have synthesised functional biodegradable and biocompatible block copolymers based on methoxypoly(ethyleneglycol)-*b*-poly(ε-caprolactone-*co*-α-azido-ε-caprolactone) (mPEG-*b*-poly(εCL-*co*-$\alpha N_3 \varepsilon$CL)). The pendent chloro groups of the block copolymer were converted into azides using nucleophilic substitution reaction to obtain mPEG-*b*-poly(εCL-*co*-αN_3CL) block copolymer as a precursor of reactive polymeric micelles. The synthesised polymers were characterised by NMR, FT-IR and size exclusion chromatography (SEC). Micelles were prepared using the dialysis method and methotrexate (an anticancer drug) was

loaded into the hydrophobic core of the reactive micelles. Micelles were subsequently crosslinked by a redox-responsive bis-alkyne ethyl disulfide crosslinker. The size distributions and morphology of core-crosslinked micelles were assessed using dynamic light scattering (DLS) and transmission electron microscopy. The drug release studies were performed under simulated non-reducing and reducing conditions. Cellular uptake studies in human breast cancer cells (MCF7 cells) were performed using Oregon-green loaded core-crosslinked micelles. The MTX-loaded core-crosslinked micelles were assessed for their cytotoxicity in human breast cancer cells by MTT assays. The apoptosis inducing potential of MTX-loaded core-crosslinked micelles was analysed using Hoechst/PI assays and was further probed by annexin-V/PI assays. The data from these studies indicate that drug release from these crosslinked micelles can be controlled and that redox-responsive micelles are more effective carriers for MTX than non-cross-linked analogues in the cell lines tested.

In another strategy, a multifunctional amphiphilic block copolymer based on α-amine-PEG-*b*-poly(εCL-*co*-$\alpha N_3\varepsilon$CL) was synthesised and subsequently was used to conjugate methotrexate on the hydrophilic block for receptor mediated targeting of breast cancer cells. Cellular uptake studies revealed 2.3-fold higher uptake of MTX-conjugated micelles as compared with un-conjugated micelles. The blank micelles showed low cytotoxicities in breast cancer cells, however, MTX-conjugated micelles exhibited greater antitumor activity in contrast to the free-MTX. We hypothesise that these

functional micelles could be potentially powerful nanocarriers for stimuli-responsive controlled release, active tumour targeting, and cancer therapy.

TABLE OF CONTENTS

List of Figures

List of Tables

List of Schemes

Acknowledgement

I am heartily thankful and truly indebted to my principal supervisor Prof. Cameron Alexander for all his guidance, motivation and support during my studies. I am especially indebted to my co-supervisors, Prof. Christine Jerome (University of Liege, Belgium) and Prof. Steve Howdle for all the support, encouragement and help. I would also like to thank Dr. Keith Spriggs and Dr. Hilary Collins and Dr. Teresa Matini for helping me in cell culture experiments.

Many thanks also go to Dr. Raphael Riva (University of Liege, Belgium) for helping me in polymer synthesis. I would also like to extend my gratitude to Mss. Patrícia-Monteiro for her help in polymer synthesis and transmission electron microscopy. I must also give special thanks to all former and present students and postdoctoral researchers in B-15 lab and my other friends for their help and for providing a warm, friendly atmosphere throughout my stay in the lab.

I also express my profound gratitude to the European Commission, Education, Audiovisual and Cultural Executive Agency, (EACEA) for an Erasmus Mundus fellowship under the NanoFar Joint Doctoral Program, which allowed me to follow my dreams of higher education in Belgium and the United Kingdom.

Finally, I would like to show my appreciation to my family members and friends for their continuous moral support, without which this work would not have been possible.

Abbreviation List

ATRP	Atom transfer radical polymerisation
CMC	Critical micelle concentrations
CuAAC	Copper-catalysed azide–alkyne cycloaddition
DC	Drug content
DCM	Dichloromethane
DLS	Dynamic light scattering
DMAP	4-(Dimethylamino) pyridine
DMSO	Dimethyl sulfoxide
DP	Degree of polymerisation
DSC	Differential scanning calorimetry
DTT	Dithiothreitol
EDAC	*N*-(3-Dimethylaminopropyl)-*N'*-ethylcarbodiimide hydrochloride
EDTA	Ethylenediaminetetraacetic acid
EE	Encapsulation Efficiency
FBS	Fetal bovine serum
FDA	Food and drug administration
FTIR	Fourier Transform Infrared Spectroscopy
GPC	Gel permeation chromatography
GSH	Glutathione
HATU	1-[Bis(dimethylamino)methylene]-1*H*-1,2,3-triazolo[4,5-*b*]pyridinium 3-oxid hexafluorophosphate
IR	Infrared spectroscopy
KDa	Kilo Dalton
M_n	Number average molecular weight
mPEG	methoxy poly(ethylene glycol)
MTT	3-[4,5-dimethylthiazol-2-yl]-2,5-diphenyltetrazolium bromide; thiazolyl blue
MTX	Methotrexate

M_w	Weight average molecular weight
MWCO	Molecular weight cut off
NMR	Nuclear Magnetic Resonance
OG	Oregon-Green
PBS	Phosphate buffer saline
PCL	Polycaprolactone
PD	Polydispersity
PDI	Polydispersity index
PEG	Polyethylene glycol
PI	Propidium iodide
PLA	Polylactide
PLGA	Poly (lactide-co-glycolide)
RAFT	Reversible addition-fragmentation chain transfer
ROP	Ring opening polymerisation
RT	Room temperature
SEC	Size exclusion chromatography
TEM	Transmission electron microscope
THF	Tetrahydrofuran
T_m	Melting temperature
UV-Vis	Ultraviolet-visible
αClεCL	α-Chloro-ε-caprolactone
εCL	ε-caprolactone

Chapter 1: GENERAL INTRODUCTION

1.1. Nano-carriers in drug delivery

Cancer and various other dysfunctions such as autoimmune, neurodegenerative, and metabolic diseases are highly complex and are difficult to treat with systemically-delivered therapeutic agents.[1] Generally, these disorders are treated by small molecular weight therapeutic compounds such as anti-metabolites, alkylating agents, topoisomerase inhibitors, anti-microtubule agents, and cytotoxic inhibitors. Although, these small molecular weight therapeutic compounds proved effective against various malignancies, several side effects have also been reported, including damage to bone marrow and gastrointestinal tract, hyper-immune system, and inflammation.[2] These side effects are due to various limitations of many current drugs such as their poor solubility, rapid clearance, limited stability, nonspecific toxicity to normal tissues, and need for frequent and high dose administration to achieve a therapeutic effect.[3, 4] To overcome limitations of conventional chemotherapy, various novel drug delivery and controlled release systems have been developed.[4, 5] Particularly, nano-carrier based drug delivery systems (10-250 nm in size) are enabling tools for the site-specific targeting and controlled release of anti-cancer agents, vaccines, nucleic acids, and recombinant proteins.[6] Owing to their small size, nano-scaled materials can show various properties that differ from the bulk materials.[6] These so-called 'nano-carriers' have the ability to encapsulate or bind drug molecules and can deliver them to the target site.[7, 8] To take advantage of these capabilities,

various nano-carriers e.g., micelles, dendrimers, liposomes, nanoparticles, nano-capsules, nanotubes, and nano-gels have been designed for drug delivery and controlled release applications (figure 1-1).

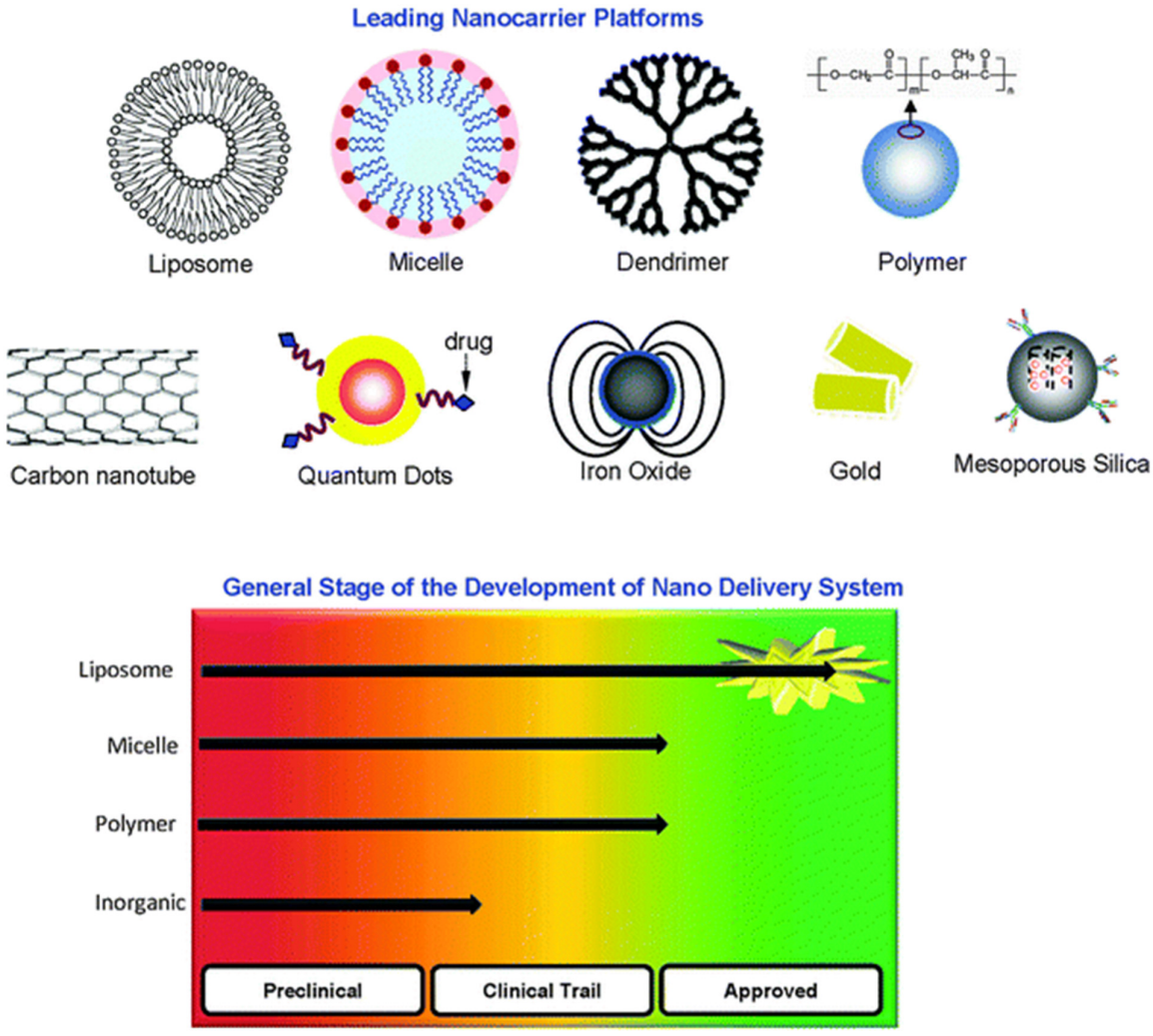

Figure 1-1. Various nano-scaled drug delivery systems and stages of development.[9]

Some of the drug delivery systems in the nano-scale size range, for instance, Doxil® (doxorubicin loaded liposome),[10] Genexol® (paclitaxel

loaded PEG-PLA micelles) and Opaxio® (paclitaxel conjugated to polyglutamate nanoparticles)[11] are already in regular clinical use, while several others are at advanced stages of their development.[9]

Drug delivery systems in general can be designed from a variety of materials e.g., polymers,[12] mesoporous silica,[13] calcium carbonate,[14] calcium-deficient hydroxyapatite,[15] chitosan,[16] iron oxide, gold and other metals.[17] The majority of these existing 'nano-carriers' are comprised of a non-targeted drug delivery system and a therapeutic molecule, therefore can be referred as first generation nano-therapeutics.[18] In contrast to more conventional drug delivery, the first generation nano-carrier systems offer several advantages such as improved bioavailability and half-life of the hydrophobic drugs, less immunogenic response, sustained release and low side effects.[19]

1.2. Polymers in drug delivery

Polymers are a versatile class of materials and have gained great importance in our daily life. Polymers exhibit great diversity in topology, chemistry, and dimensions, enabling them to form a group of materials which can be specifically adapted for drug delivery and controlled release applications.[20] Polymer therapeutics consist of rationally developed macromolecular drugs, polymeric micelles, nano-capsules, core-shell particles, nano-gels, polymer-drug conjugates, and polyplexes as

illustrated in figure 1-2.[12] The key advantage of polymer therapeutics is their flexibility to chemical modification, leading to discrete chemical composition and tailored surface properties.[21]

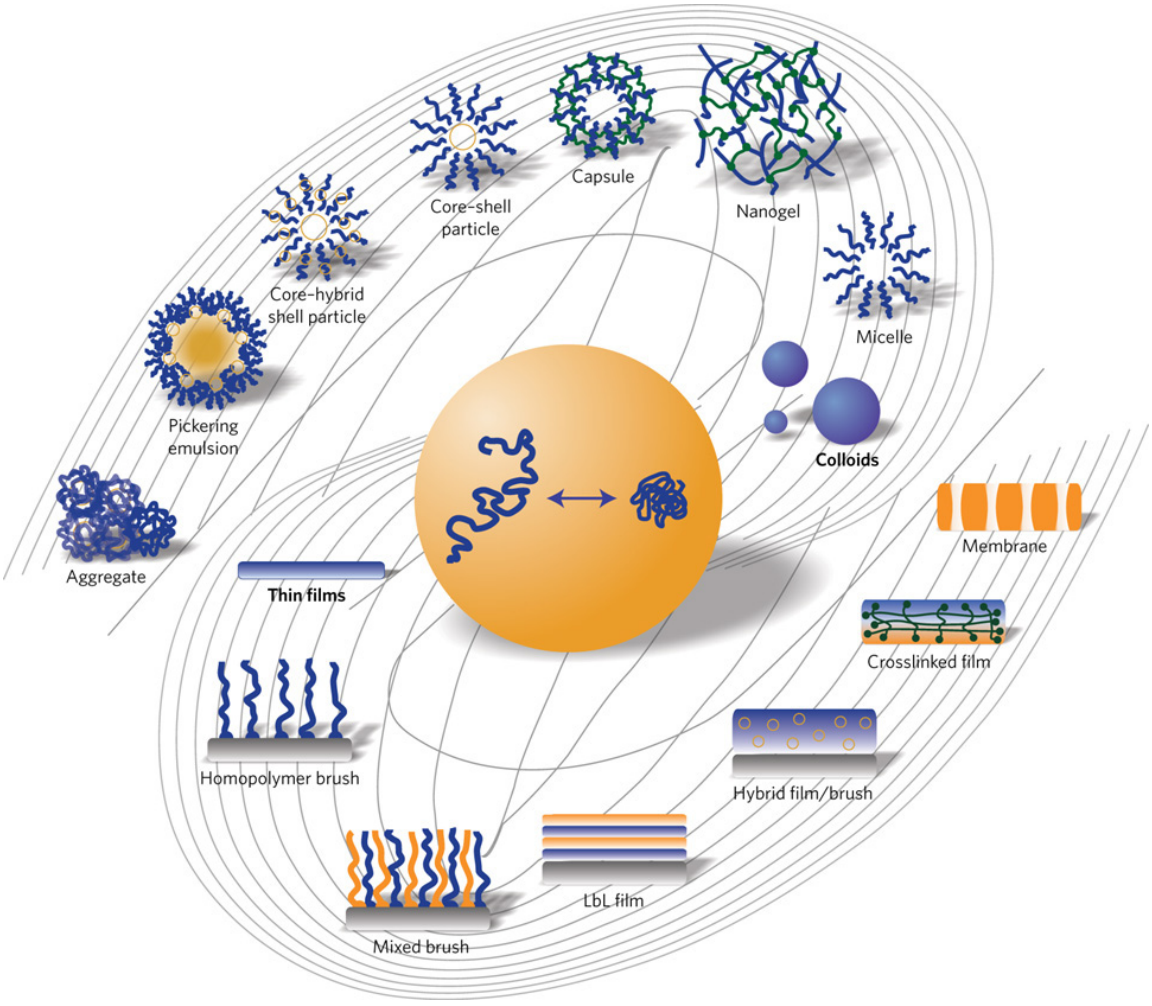

Figure 1-2. Various types of nanostructured polymer materials.[22]

Polymers used in biomedical applications can be derived either from natural materials (e.g. dextran, dextrin, chitosan, and hyaluronic acid) or synthetic components (such as poly(ethylene glycol), poly(ethyleneimine), N-(2-

hydroxypropyl) methacrylamide, poly(vinylpyrrolidone), and linear polyamidoamines).[23,24]

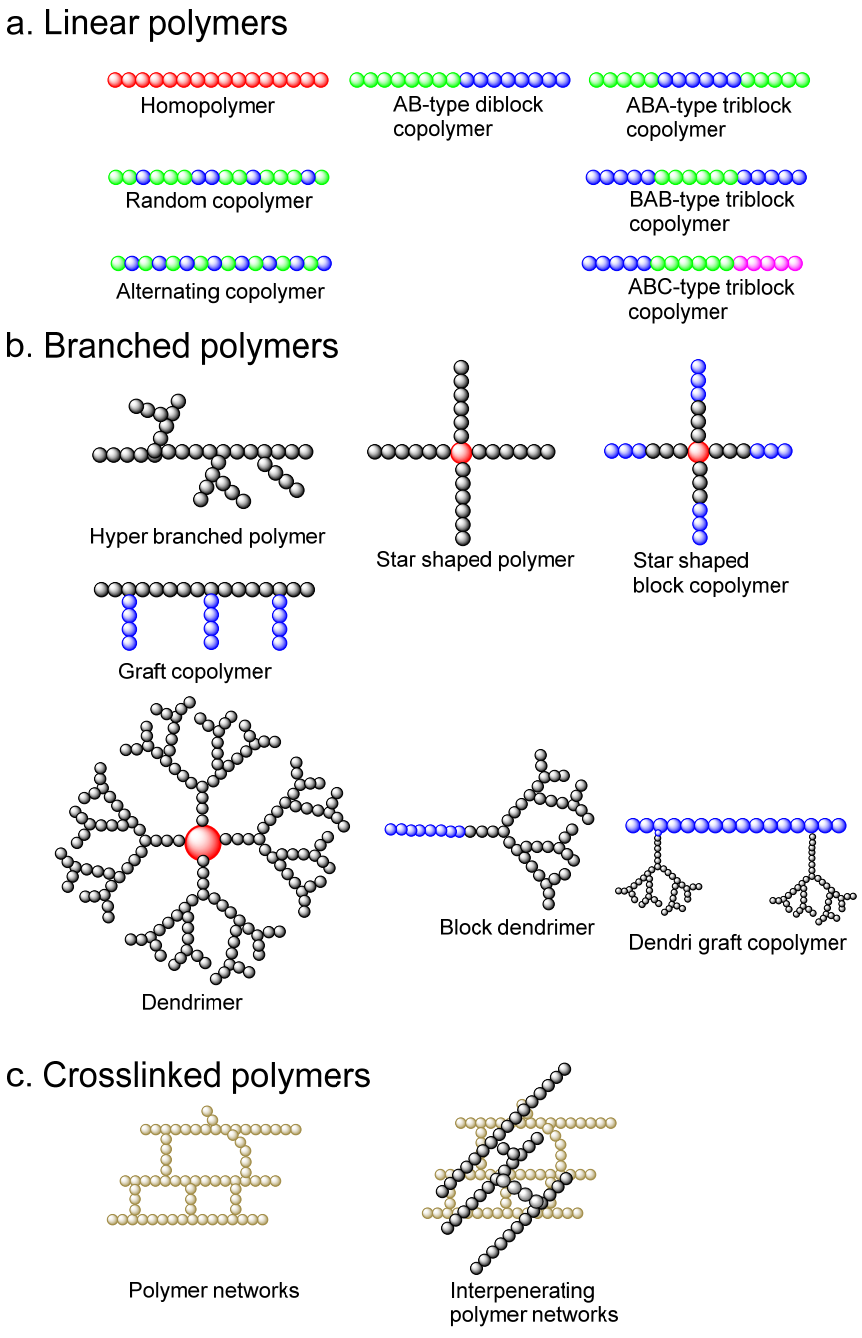

Figure 1-3. Various architectures of polymers (a) Linear, (B) Branched, and (c) Crosslinked.

Polymers also exhibit various architectures such as linear, branched, block, graft, dendritic, cross-linked and star-shaped (figure 1-3). The polymer architectures play a vital role in stability, water solubility, drug loading, release, and biodistribution.[20]

1.3. Biodegradable polymers

For drug delivery applications, polymer in generals should be biocompatible and biodegradable, unless they are considered for certain oral administrations where they may be excreted unchanged.[25] Biocompatibility refers to the extent to which biomaterials can interact with living systems without causing any undesirable harm or toxicities.[26] In the case of biodegradable polymers, the drug-carrying materials must not induce any allergic, inflammatory, carcinogenic or cytotoxic effect to normal tissues, and upon degradation, must not produce toxic by-products.[27] The degradation of polymers in drug delivery applications can occur via a range of mechanisms, including chain cleavage by hydrolysis, oxidation, thermal activation or by enzymes.[28] Both natural and synthetic polymers have been studied as biodegradable materials for drug delivery application. The polymers from natural origin are often chosen because of their susceptibility to degrade by enzymatic activity, whereas, synthetic polymers are generally designed to degrade via hydrolysis.[29]

The natural biodegradable polymers, for instance, hyaluronic acid, chitosan, and gelatin etc., have been used for drug delivery applications.[30, 31] However, undesirable immunogenic response, chance of disease transmission, batch-to-batch variations in composition and difficulties in purification limit their further application as drug delivery vehicles.[26] In contrast, synthetic polymers are usually biologically inert with highly predictable properties and less batch-to-batch variations. The synthetic biodegradable polymers used most frequently in drug delivery include polyesters, polyanhydrides, polyacetals, polyorthoesters, polycarbonates, polyurethanes, polyphosphazenes, and polyphosphoesters.[32]

1.4. Polyesters in drug delivery

Polyesters are a class of biodegradable polymers containing hydrolytically cleavable ester linkages in their backbone.[33] Polyesters can be synthesised from a variety of monomers. Various polyesters have been developed for biomedical applications, for instance, polyglycolide,[34] polylactides,[35] poly(lactide-co-glycolide),[36] polycaprolactone,[37] polydioxanone,[38] and poly(trimethylene carbonate).[39]

1.4.1. Synthesis of polyesters

Polyesters can be synthesised either by step growth polymerisation (polycondensation) or by chain growth polymerisation (e.g. ring opening polymerisation).

a. Step growth polymerisation (polycondensation)

The step growth polymerisation involves the condensation of a carboxylic acid and an alcohol (scheme 1-1). The substrate acids or alcohols can be part of separate molecules or on the same molecule.

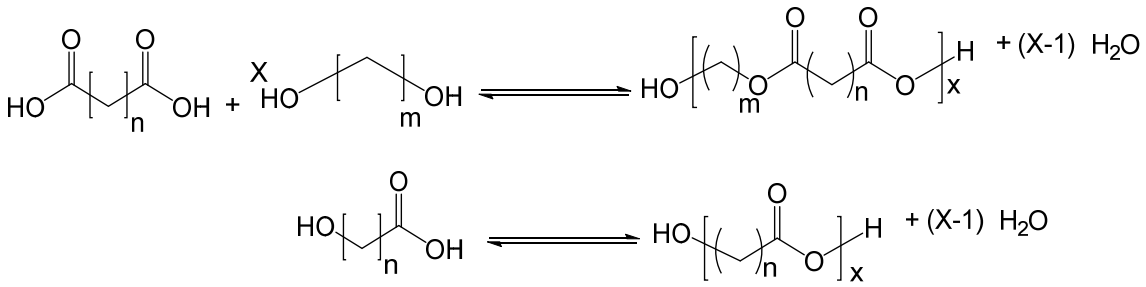

Scheme 1-1. Step-growth polymerisation for the synthesis of polyesters.

The major disadvantages of this route are high temperature and long reaction times which may result in side reactions.[40] Furthermore, water produced during condensation reaction must be removed continuously to shift the established equilibrium. Moreover, higher molecular weight polyesters may not be obtained by this method because even slight deviations of the stoichiometry of di-acids and diols adversely affects the chain growth.[41]

b. Ring opening polymerisation

Ring opening polymerisation (ROP) is a well-known route to obtain aliphatic polyesters from cyclic esters. In contrast to polycondensation, high molecular weight polyesters with tailor-made properties can be synthesised

in a straightforward manner via ROP.[42] In addition, ROP can be accomplished under comparatively mild conditions and short reaction times. Depending upon the catalyst, ROP may proceed via 3 main mechanisms, namely, anionic, cationic, and coordination–insertion mechanism.

The anionic ring opening polymerisation (scheme 1-2) proceeds with the formation of a negatively charged species which subsequently attacks the carbonyl carbon or the carbon atom next to the acyl oxygen of the monomer to yield linear polyesters. Alkali metals and alkali metal oxides are commonly used initiators in anionic ring opening polymerisation.[43] The major downside of this route is inter and intra-molecular transesterification owing to the highly reactive nature of the anionic initiators. This leads to wider polydispersity and low molecular weight of resultant polyesters.

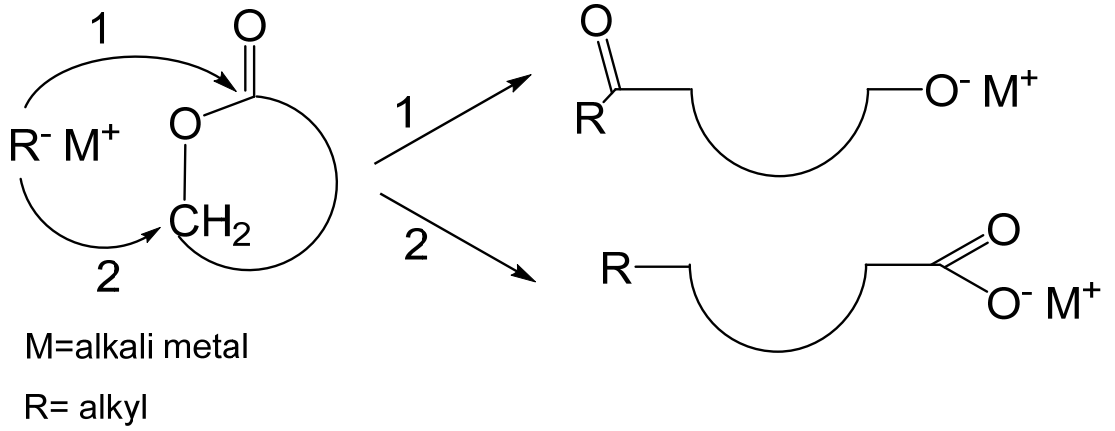

Scheme 1-2. Ring opening polymerisation of cyclic ester via anionic mechanism by the cleavage of (1) acyl-oxygen bond and (2) alkyl-oxygen bond.

On the other hand, the cationic ring opening polymerisation (scheme 1-3) proceeds via the formation of a positively charged initiator species which is then attacked by the carbonyl-oxygen of the cyclic ester monomer through a bimolecular nucleophilic substitution reaction.[44, 45]

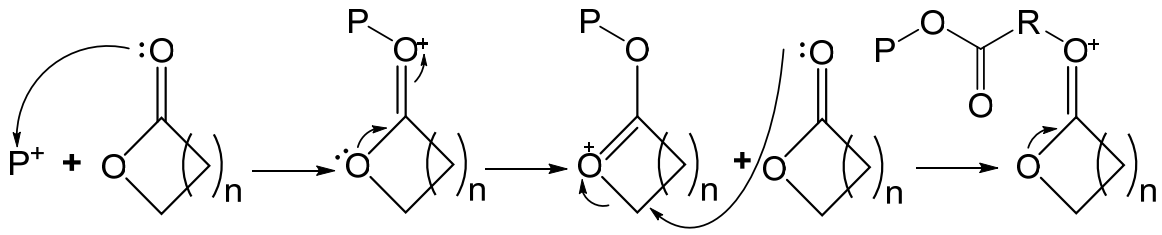

P^+= positively charged species (a cation)

Scheme 1-3. Ring opening polymerisation of cyclic esters via cationic mechanism.

The coordination-insertion mechanism (scheme 1-4) is the most common route for ring opening polymerisation of cyclic esters.[46] In this route, metal alkoxides are common initiators, which first coordinate with the exocyclic carbonyl oxygen atom of the ester monomer. In the later stage, acyl-oxygen bond of the lactone is broken, opening the chain of lactone ring to insert into the tin-oxygen bond. The propagation is proceeded by identical mechanism and continues as additional lactone units are inserted into the tin-oxygen bond.[47, 48]

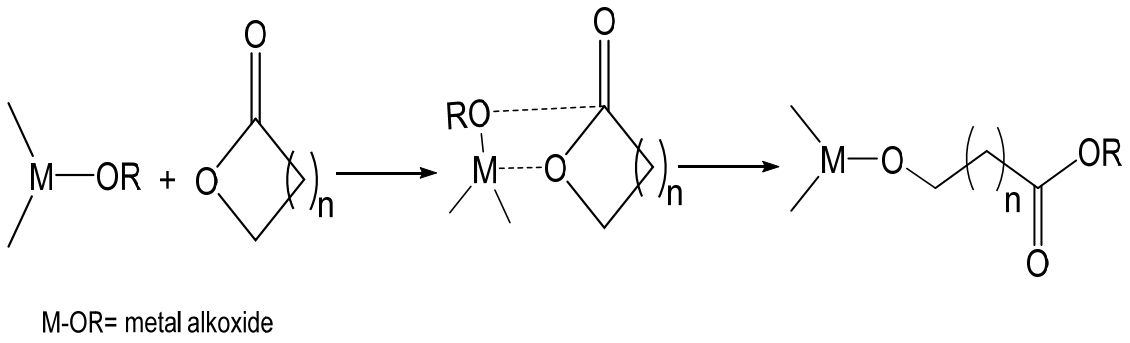

Scheme 1-4. Ring opening polymerisation of cyclic ester via coordination-insertion mechanism.

1.5. Stimuli responsive micelles

Stimuli-responsive micelles are developed from polymers that undergo structural changes in response to internal or external stimuli.[49] Owing to their rapid and reversible response to changes in the surrounding milieu, these micelles are often called "smart" or "intelligent" drug delivery vehicles.[50] The stimuli-triggered feedback in the polymers may lead to fragmentation, destabilisation, or agglomeration of micelles resulting in drug release at the response site. The origin of the stimuli can be external or internal depending on the state and chemical compositions of micelles as illustrated in figure 1-4.

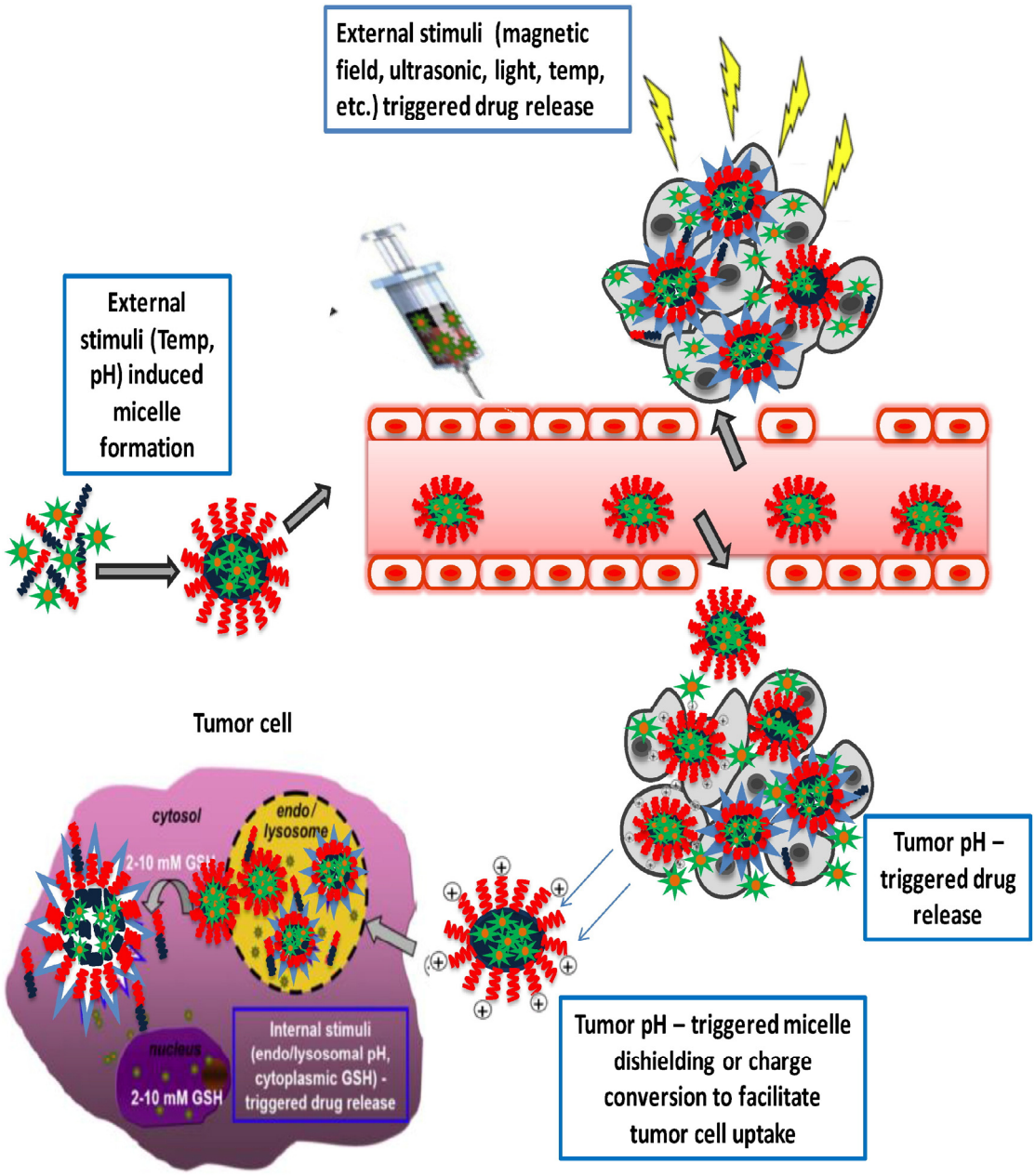

Figure 1-4. Schematic illustration of various external and internal stimuli and mechanism of responsive drug release from polymeric micelles.[51] The applied external stimulus (e.g. temperature and pH) can trigger the formation of micelles. Whereas, drug release can be programmed in response to external stimulus (temperature, light, magnetic field, ultrasound etc.). In contrast, internal stimulus (e.g. change in pH or redox potential) can be exploited to release the drug at the target site.

The stimuli for drug delivery systems can further be categorised into physical, chemical or biological origins. The physical stimuli may alter the chain dynamics (energy level of polymer-solvent system) of polymers and include light, magnetic field, temperature, and ultrasound etc.[52] Chemical stimuli such as pH, redox-potential, and ionic strength generally modify molecular interactions between polymer chains.[53] On the other hand, stimuli of biological origins (e.g. enzymes, receptors etc.) can trigger specific functioning of molecules i.e. enzymatic reactions, or receptor recognition.[54] Specifically, stimuli in the tumour microenvironment include low pH, elevated temperature, redox potential, and existence of certain overexpressed enzymes.[55]

In particular, the dysregulated metabolism in the tumour tissues leads into enhanced acidity, which can be used as an internal stimulus for responsive release of drugs from micelles. To exploit this stimulus, various pH responsive micelles have been developed. Generally, pH responsive amphiphilic block copolymers comprise either ionic blocks (e.g. (poly(acrylic acid), poly(methacrylic acid), poly(glutamic acid), poly(vinyl pyridine), and poly(histidine) etc.)[51] that help their destabilisation or acid labile bonds (e.g. hydrazone, acetal, ortho-esters, and benzoic imine)[56-60] that trigger their degradation at low pH in a tumour site. For instance, pH sensitive micelles comprising of naphthalene-terminated poly(ethylene glycol) (PEG-Np) and methyl viologen functioned doxorubicin (MV-DOX) were prepared using cucurbit[8]uril (CB (8)) as a linker (figure 1-5).[61] The ternary complex micelles retained the drug at pH 7.4, whereas rapid release

of doxorubicin was observed under acidic conditions (pH 5) and inhibited the growth of human liver carcinoma cells (HepG2 cells).

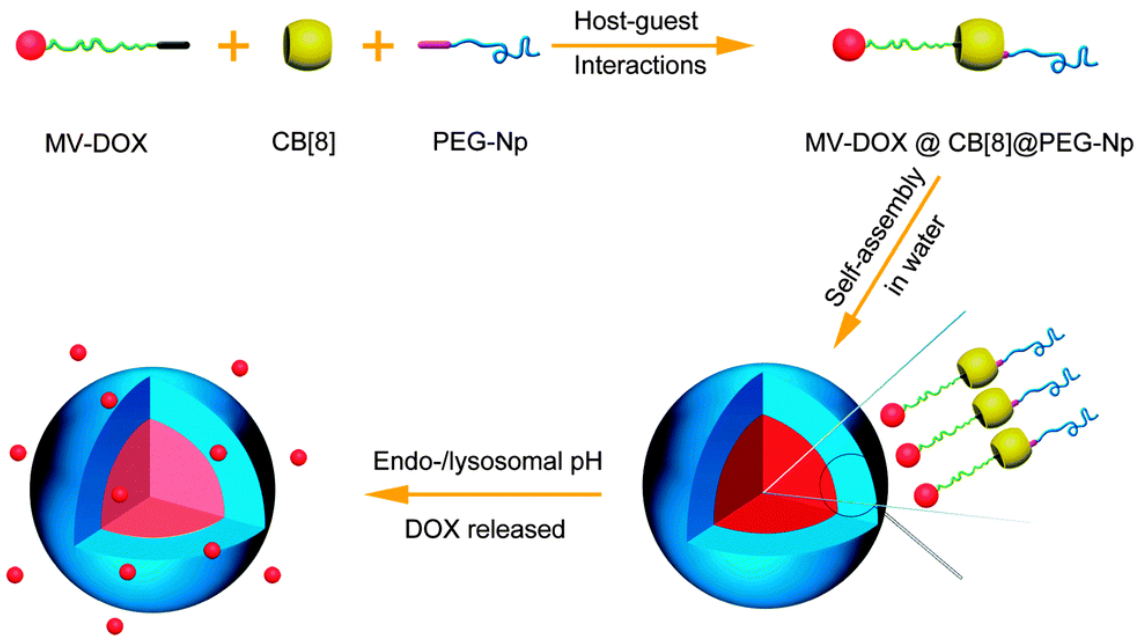

Figure 1-5. Preparation of pH responsive micelles of MV-DOX-CB(8)-PEG-Np micelles and controlled release of doxorubicin.[61]

Thermo-responsive polymeric micelles are another type of stimuli responsive nanocarriers to exploit tumour microenvironments. The temperature sensitive micelles are generally prepared from 'pro-amphiphilic' materials such as poly(*N*-isopropyl acrylamide) (PNIPAAM), Pluronics®, or poly(hydroxy propyl methacrylamide-lactate), which are soluble in water below their lower critical solution temperature (LCST), however, precipitate above LCST as depicted in figure 1-6.[62]

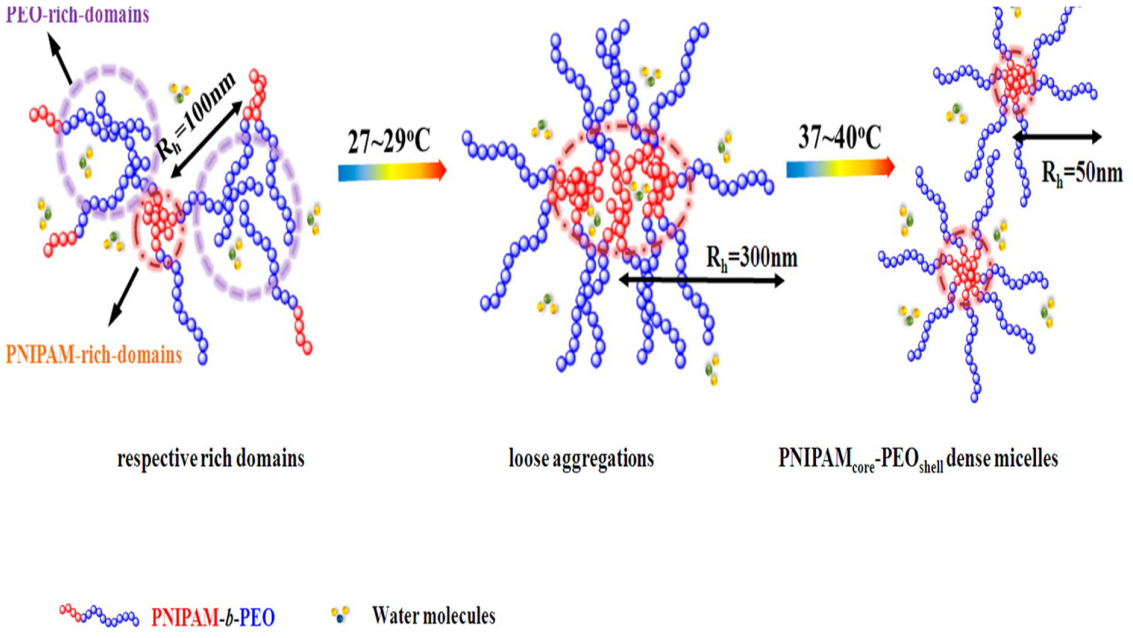

Figure 1-6. Phase transition of PEO-*b*-PNIPAM during the heating process.[63]

The higher levels of redox-potential in tumour tissues and inside certain cancerous regions is another important stimulus to develop redox responsive micelles. Generally, redox responsive polymers have disulfide linkages that undergo rapid cleavage in the presence of reducing agents in the intracellular components, however, they are stable at extracellular environment.[64, 65] Redox responsive disulfide bridges can be incorporated in the backbone or in side chain, or as crosslinker in the architecture of micelles (figure 1-7).[64, 66]

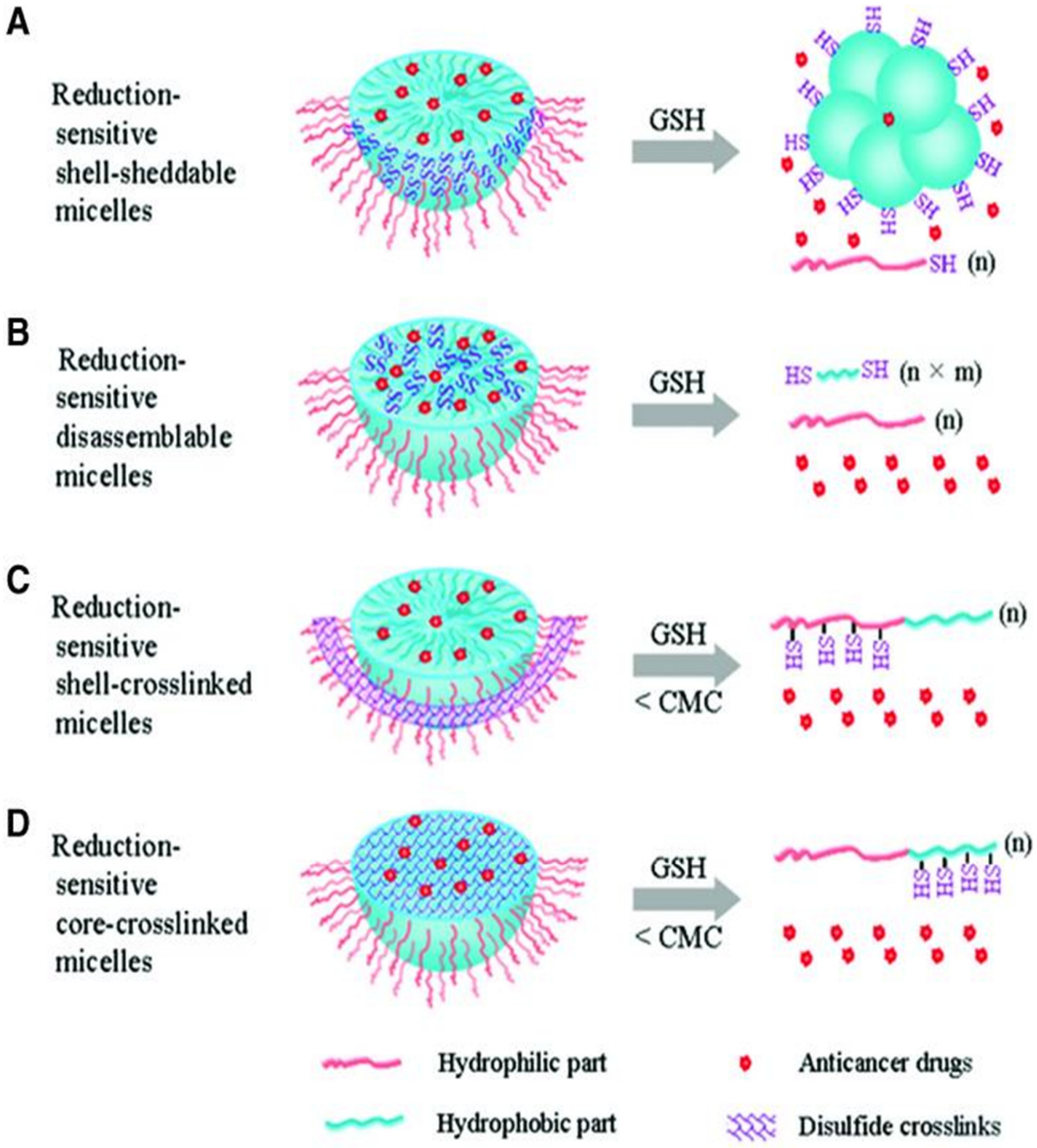

Figure 1-7. Design of various reduction-sensitive micelles for the delivery of anticancer drugs.[67] (A) Shell-sheddable redox-responsive micelles, (B) dis-assemblable redox-responsive micelles (C) redox-responsive shell crosslinked micelles, and (D) redox-responsive core-crosslinked micelles. CMC = critical micelle concentration.

1.6. Micelles in drug delivery

Polymeric micelles are supramolecular core-shell nano structures (figure 1-8) of amphiphilic block copolymers. These polymers comprise at least two blocks of a discrete chemical nature that exhibit phase separation as a result of chain association in aqueous solution that selectively dissolves one of the constituents.[68, 69]

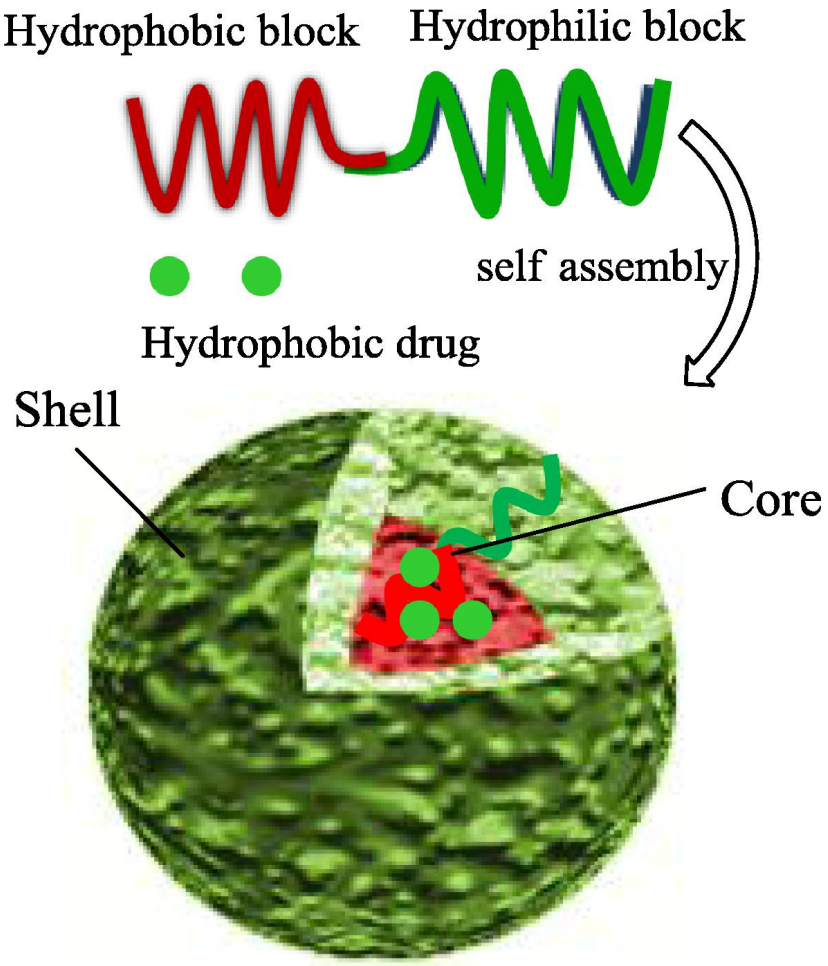

Figure 1-8. Illustration of the self-assembly of amphiphilic block copolymers into micelles.[70]

The formation or self-assembly of micelles takes place when the concentration of block copolymer rises above a certain threshold, called the critical micelle concentration (CMC). At the CMC, the hydrophobic constituents of di-block copolymers begin to associate to decrease the interaction with the aqueous environment, resulting into a vesicular or core-shell structure.

The polymeric micelles have emerged as attractive carriers for the delivery of poorly water soluble drugs due to their capability to encapsulate such drugs in their inner core.[71] Owing to their core-shell structure, micelles are often comparable to natural existing structures (e.g. viruses or lipoproteins), which protect their payload while it is delivered to the target cell.[72]

The micelle shell usually comprises biocompatible hydrophilic polymers such as poly(ethylene glycol) (PEG) which impart stability to micelles and are also responsible for suppressing the interactions with plasma proteins and cell membranes.[73] Some other polymers e.g. poly(*N*-isopropylacrylamide) (PNIPAM)[74-76] , and poly(alkylacrylic acid)[76] could be employed to build temperature or pH-responsive polymeric micelles.[77] The hydrophobic core usually comprises a biodegradable macromolecule e.g. poly(DL-lactic acid) (PDLLA),[78] poly(β-benzyl-L-aspartate) (PBLA),[79] or poly(ϵ-caprolactone) (PCL),[80, 81] and works as a container for a hydrophobic drug, shielding it from interaction with the aqueous environment.

The drug-loaded amphiphilic block copolymer micelles can be obtained by various methods e.g., nano-precipitation, dialysis, oil-in-water, and solid dispersion methods.[82] Drug loading can be performed either by chemical conjugation,[83] or by physical encapsulation within the inner core of the micelles.[84] The drug release from micelles mainly relies on the type of encapsulation. The bulk degradation of polymer matrix or surface erosion is responsible for the release of chemically conjugated drug, whereas, physically entrapped drugs are mainly released by diffusion.

1.7. Active tumour targeting

Generally, nano-carrier based drug delivery systems rely on passive targeting exploiting the typical features of tumour tissues due to the enhanced permeability and retention (EPR) effect.[85] However this route has several limitations.[82] For instance, not all tumours exhibit an enhanced permeability and retention (EPR) effect and the permeability of vessels is not consistent throughout a single solid tumour.[86] In addition, nano-carrier based passive targeting is not inherently selective to tumour tissues as administered nano-carriers have been reported to accumulate in organs including the liver, lungs and spleen, resulting in non-specific toxicities.[87] To overcome these drawbacks, active drug targeting has been used in which nano-carriers are modified to bind selectively to components on or in the specific cells.[88-90] The active targeting may be attained by grafting targeting agents (e.g. antibodies, ligands, nucleic acids and peptides) to

the surface of nanocarriers.[91] These targeting agents selectively bind to various receptors overexpressed on the surface of cancer cells[92] (figure 1-9)[51], such as the folate receptor,[92] transferrin receptor,[93] and epidermal growth factor receptor etc.[94, 95]

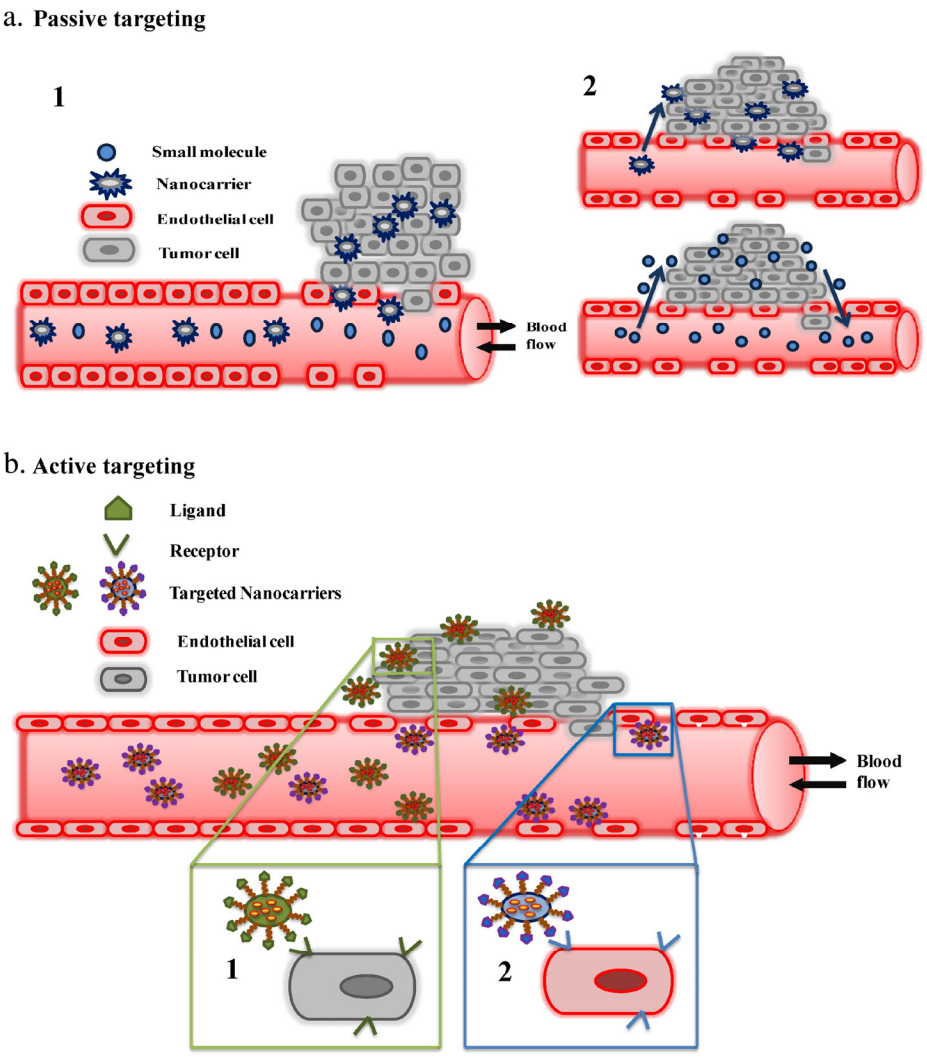

Figure 1-9. Tumour targeting by active and passive routes.[51] (a) Passive targeting using nano-carriers. (1) Leaky vascular around the tumour allows nano-carriers to permeate through the tumour cells. (2) Size dependent retention of nano-carriers. (b) Schematic illustration of active targeting. (1) Cancer cells or (2) Angiogenic endothelial cells.

1.8. Endocytosis of micelles

Drug-loaded nanocarriers must pass through various transport barriers to reach their targets. Specifically, translocation of nanocarriers across the plasma membrane barrier is a prerequisite.[96] Plasma membranes are complicated components of the body and play an important role in control of cellular communication and cell division regulated by endocytosis. Cells use endocytosis for internalisation of important nutrients, extracellular fluids, proteins, and lipids, and in downregulation of growth factor receptors and in controlling the cell signalling.[97]

There are various forms of endocytosis (phagocytosis and pinocytosis) through which nanocarriers are internalised into the cells (figure 1-10), however, all internalisation pathways involve formation of new intracellular membrane-enclosed vesicles following invagination of the plasma membrane.[98-101] In particular, particles larger than 500 nm are taken up by cells through phagocytosis, a form of endocytosis characterised by the generation of a large size vesicle known as phagosome.[102] Small particles (10-100 nm) and fluids are taken up through pinocytosis. The pinocytosis pathway is further subcategorised into micropinocytosis, caveolin-mediated endocytosis, clathrin-mediated endocytosis, and caveolin and clathrin-independent endocytosis.[103, 104]

Macro-pinocytosis is an actin-driven form of endocytosis which involves the protrusion at the outer plasma membrane which later on again fuses with the plasma membrane to engulf large entities or debris.[100] Clatherin-

mediated endocytosis (a type of receptor-mediated pinocytosis) is characterised by the construction of "coated pits" comprising transmembrane receptors and cytosolic proteins (e.g. clathrin). The low-density lipoproteins and transferrin are mostly taken up by clathrin-mediated endocytosis.[105, 106]

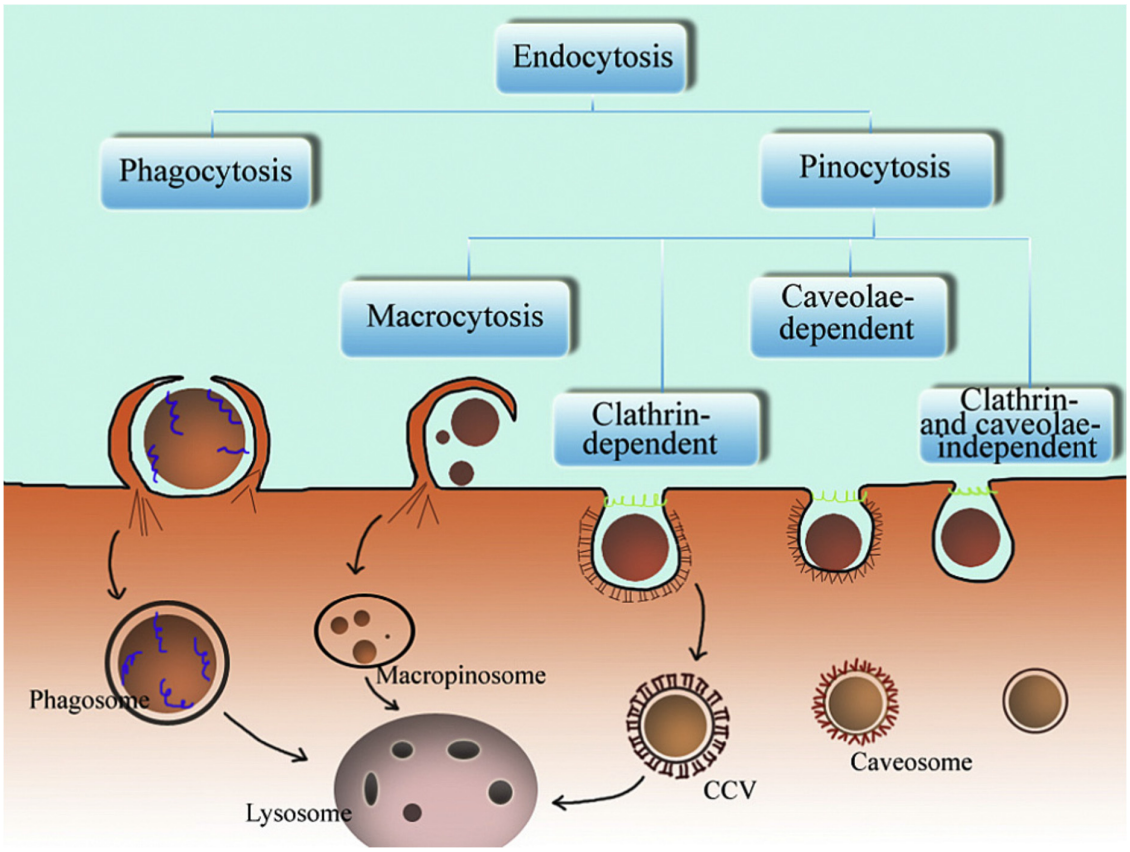

Figure 1-10. Various forms of endocytosis for uptake of nano-carriers by mammalian cells. (CCV = clathrin coated vesicle).[107]

In contrast, caveolin-mediated endocytosis is a receptor independent type of endocytosis which is initiated by the creation of flask-shaped infolded caveolae, and is mainly accountable for the homeostasis of cholesterol.[108]

In addition to the above mentioned uptake pathways, passive diffusion of nanocarriers across cell membranes as well as clathrin- and caveolin-independent endocytosis have also been reported.[109] After being internalised, some nano-carriers have been shown to be entrapped into the endocytic vesicles (endosome) formed during endocytosis, and subsequently transferred into lysosomes. The endosomes and lysosomes are acidic vesicles packed with various enzymes that can help to degrade their contents, for example biodegradable polymer micelles, this resulting in drug release.[110, 111]

1.9. Challenges in the design of micelle based drug delivery systems

The nano-carrier based drug delivery systems are promising candidates for tumour targeting and therapy. However, it has been reported in the literature that only a small proportion of administered nano-carriers appear to be delivered to a solid tumour.[112] This has resulted into a negative impact on the translation of nano-carrier based drug delivery systems into clinical applications. A possible reason for the failure of nano-carrier based drug delivery systems may be a gap in the understanding of the framework guiding nano-carrier design.[113] The therapeutic agents must complete an exhaustive journey before their actual therapeutic action inside a tumour cell.[114] The journey commences with the injection of drug-loaded or

conjugated nano-carriers into the bloodstream and continues to the phases of circulation, accumulation, distribution, cellular uptake, endosomal escape, intercellular accumulation, and therapeutic action.

Specifically, nano-carriers must pass through various transport barriers to reach their targets (figure 1-11). After systemic administration, mononuclear phagocytic system, reticuloendothelial system, and renal clearance compete with malignant cells for nano-carriers.

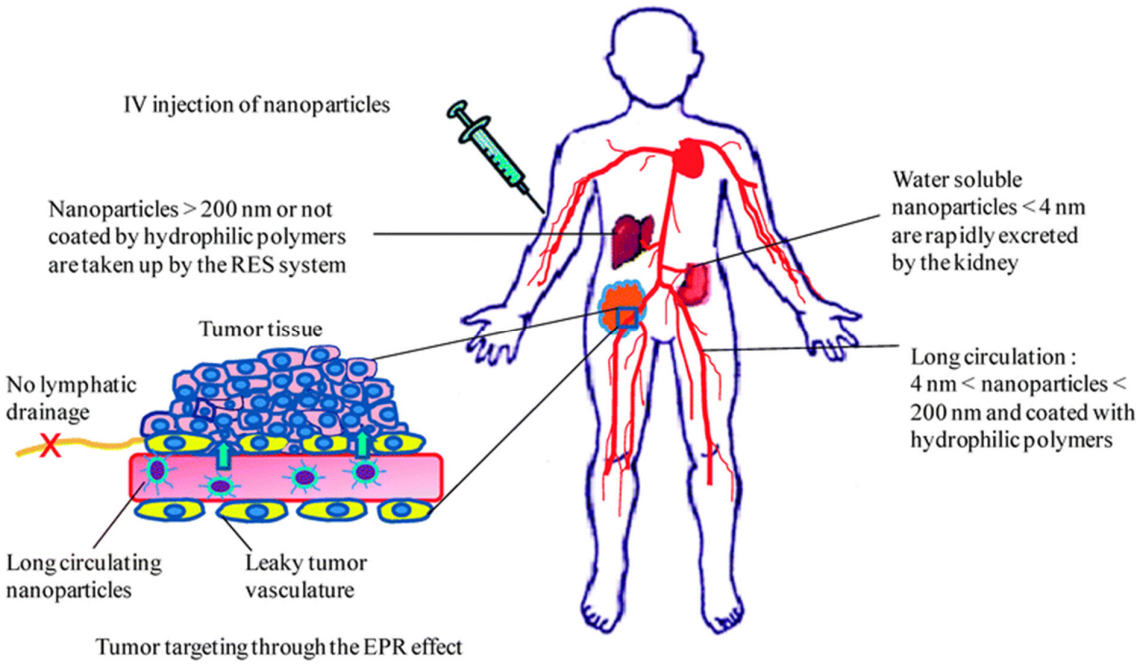

Figure 1-11. Scheme for the bio-distribution of intravenously injected nanoparticles.[115]

Nano-carriers that succeed to escape these barriers have a chance to interact with cancerous tissues. Any drug molecules localised away from the malignant cells could be potentially toxic to normal cells. To prevent

uptake by the mononuclear phagocytic and reticuloendothelial system, the surface of nano-carriers can be coated with a hydrophilic polymer e.g. poly(ethylene glycol) (PEG) or by developing the nano-carriers from amphiphilic block copolymers based on PEG and biodegradable polyesters. By incorporating PEG, opsonisation can be decreased resulting into prolonged circulation of these nano-carriers in the bloodstream.[91, 116] This phenomenon is called as the "stealth effect" and is reported to enhance the circulation time of nano-carriers in the blood stream. The stealth properties of PEG can essentially be attributed to the creation of a dense hydrophilic layer of long PEG chains on the surface of nano-carriers which prevents the hydrophobic interaction with mononuclear phagocytic system[117].

Another strategy to improve the stealth properties of nano-carriers is to introduce functional moieties, which can be achieved by post-polymerisation functionalisation. However, the possibility of side reactions decreases the applicability of this route. Furthermore, synthesis of amphiphilic di-block copolymers by this process is not straightforward. Hence, post-polymerisation functionalisation is not an ideal technique to obtain functional polyesters. To synthesise functional polyesters, a commonly used technique is to polymerise a functional monomer via polycondensation, ring opening, and enzymatic polymerisation.[118-120] The functional lactone monomers can be easily purified by fractional distillation or by re-crystallisation, enabling them to be good candidates towards functional polyesters.[40, 120-122] Another challenge for the micelle based drug delivery systems is the disassembly of micelles especially upon

administration when they are diluted below their critical micelle concentration.[123] Therefore, micelles also need to be stabilise using various techniques (e.g. crosslinking) for better stability and antitumor activity.

1.10. AIMS AND OBJECTIVES

The main aims of this thesis involve the synthesis of novel amphiphilic macromolecules in order to build redox-responsive and multifunctional well-defined nanocarriers. Specifically, the synthesised amphiphilic copolymers will be formulated into functional nano-carriers for bio-responsive drug delivery, controlled release and active tumour targeting. By encapsulating hydrophobic anti-cancer therapeutic molecules in the cores of micelles, it is hypothesised that drug release can be programmed with minimal side effects to the normal tissues. The proposed macromolecules can be synthesised from PEG, ε-caprolactone, and a functional monomer i.e. α-chloro-ε-caprolactone using the ring opening polymerisation technique, followed by the displacement of chloro atoms with the azide group. The redox-responsive characteristics can be incorporated by either crosslinking the reactive micelles with a redox-responsive crosslinker or by introducing a redox-responsive spacer in the polymer-drug conjugate. Whereas, active tumour targeting can be achieved by functionalising the surface of micelles with a targeting ligand.

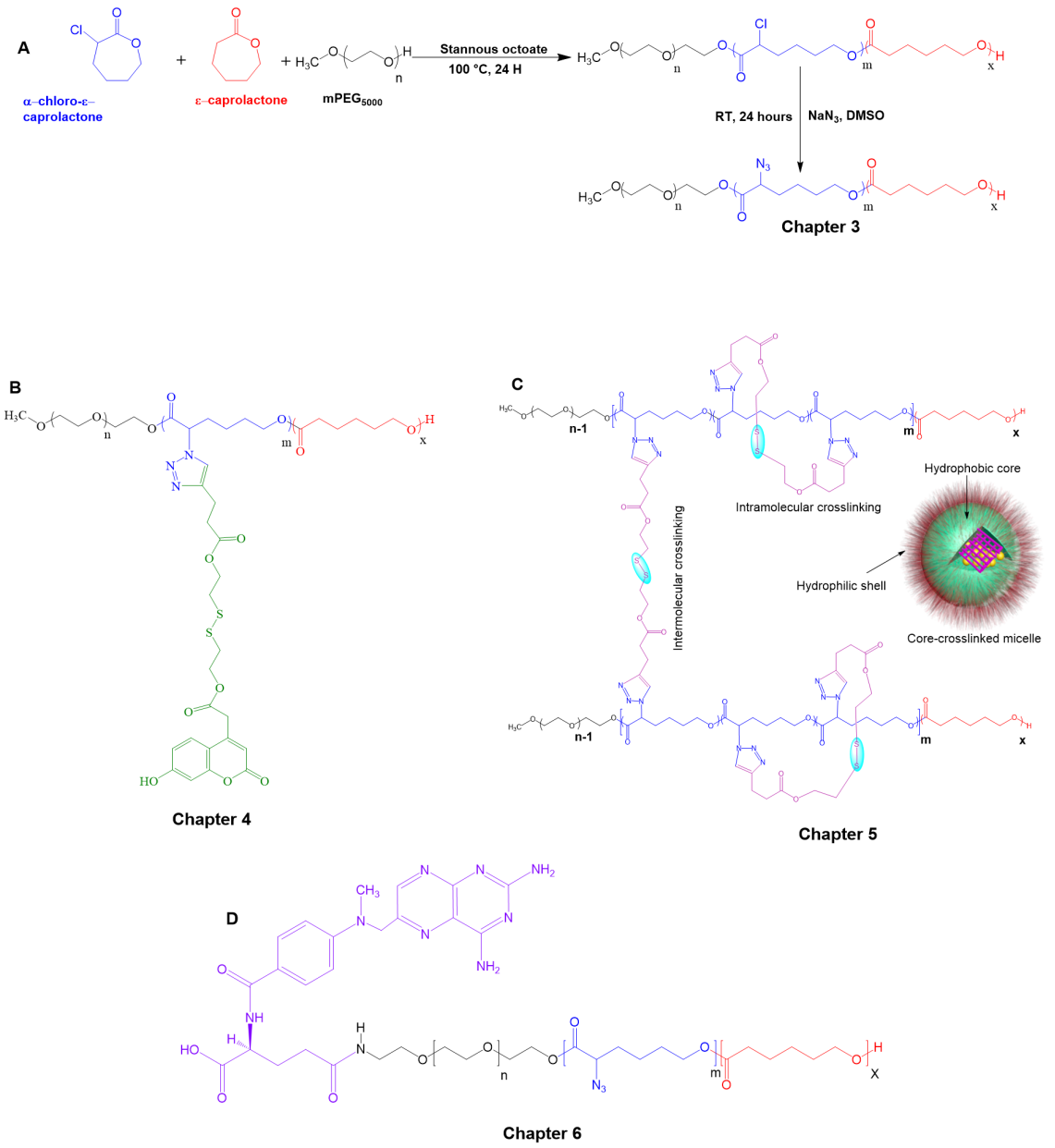

Scheme 1-5. Schematic illustration of some important amphiphilic block copolymers proposed to synthesise in this thesis (scheme 1-5A). These polymers will be subsequently functionalised to obtain either redox-responsive polymer-drug conjugate (scheme 1-5B) or redox-responsive core-crosslinked micelles (scheme 1-5C). Moreover, these polymers will be functionalised to obtain micelles possessing active tumour-targeting properties (scheme 1-5D).

The main objectives of the work include:

- Synthesis of a functional monomer (α-chloro-ε-caprolactone) as a precursor for functional polyesters
- Synthesis of novel amphiphilic block copolymers based on mPEG-*b*-poly($\alpha N_3\varepsilon CL$), and mPEG-*b*-poly(εCL-co-$\alpha N_3\varepsilon CL$)
- Design of redox-responsive polymer-drug conjugate and core-crosslinked micelles as bio-responsive drug delivery systems
- Design of multi-functional polymeric micelles for active tumour targeting
- *In-vitro* drug release, cellular uptake and cytotoxicity studies of the engineered polymeric micelles

1.11. REFERENCES

1. W. B. Liechty, D. R. Kryscio, B. V. Slaughter and N. A. Peppas, *Annual Review of Chemical and Biomolecular Engineering*, 2010, **1**, 149-173.
2. C. M. Dawidczyk, L. M. Russell and P. C. Searson, *Frontiers in Chemistry*, 2014, **2**, 69.
3. C. E. Ashley, E. C. Carnes, G. K. Phillips, D. Padilla, P. N. Durfee, P. A. Brown, T. N. Hanna, J. Liu, B. Phillips, M. B. Carter, N. J. Carroll, X. Jiang, D. R. Dunphy, C. L. Willman, D. N. Petsev, D. G. Evans, A. N. Parikh, B. Chackerian, W. Wharton, D. S. Peabody and C. J. Brinker, *Nature Materials*, 2011, **10**, 389-397.

4. S. Nie, Y. Xing, G. J. Kim and J. W. Simons, *Annual Review of Biomedical Engineering*, 2007, **9**, 257-288.

5. R. K. Jain and T. Stylianopoulos, *Nature Reviews Clinical Oncology*, 2010, **7**, 653-664.

6. O. Kayser, A. Lemke and N. Hernandez-Trejo, *Current Pharmaceutical Biotechnology*, 2005, **6**, 3-5.

7. S. M. Moghimi, A. C. Hunter and J. C. Murray, *Faseb Journal*, 2005, **19**, 311-330.

8. D. Peer, J. M. Karp, S. Hong, O. C. Farokhzad, R. Margalit and R. Langer, *Nature Nanotechnology*, 2007, **2**, 751-760.

9. W. X. Mai and H. Meng, *Integrative Biology*, 2013, **5**, 19-28.

10. D. W. Northfelt, F. J. Martin, P. Working, P. A. Volberding, J. Russell, M. Newman, M. A. Amantea and L. D. Kaplan, *Journal of Clinical Pharmacology*, 1996, **36**, 55-63.

11. J. W. Singer, S. Shaffer, B. Baker, A. Bernareggi, S. Stromatt, D. Nienstedt and M. Besman, *Anti-cancer Drugs*, 2005, **16**, 243-254.

12. R. Duncan, *Nature Reviews Drug Discovery*, 2003, **2**, 347-360.

13. J.-F. Chen, H.-M. Ding, J.-X. Wang and L. Shao, *Biomaterials*, 2004, **25**, 723-727.

14. Y. Ueno, H. Futagawa, Y. Takagi, A. Ueno and Y. Mizushima, *Journal of Controlled Release*, 2005, **103**, 93-98.

15. T.-Y. Liu, S.-Y. Chen, D.-M. Liu and S.-C. Liou, *Journal of Controlled Release*, 2005, **107**, 112-121.

16. M. Bodnar, J. F. Hartmann and J. Borbely, *Biomacromolecules*, 2005, **6**, 2521-2527.

17. M. Z. Ahmad, S. Akhter, G. K. Jain, M. Rahman, S. A. Pathan, F. J. Ahmad and R. K. Khar, *Expert Opinion on Drug Delivery*, 2010, **7**, 927-942.

18. K. Riehemann, S. W. Schneider, T. A. Luger, B. Godin, M. Ferrari and H. Fuchs, *Angewandte Chemie (International ed. in English)*, 2009, **48**, 872-897.

19. J. Shi, A. R. Votruba, O. C. Farokhzad and R. Langer, *Nano Letters*, 2010, **10**, 3223-3230.

20. L. Qiu and Y. Bae, *Pharmaceutical Research*, 2006, **23**, 1-30.

21. M. Goldberg, R. Langer and X. Jia, *Journal of Biomaterials Science. Polymer Edition*, 2007, **18**, 241-268.

22. M. A. C. Stuart, W. T. S. Huck, J. Genzer, M. Muller, C. Ober, M. Stamm, G. B. Sukhorukov, I. Szleifer, V. V. Tsukruk, M. Urban, F. Winnik, S. Zauscher, I. Luzinov and S. Minko, *Nature Materials*, 2010, **9**, 101-113.

23. A. O. Elzoghby, W. S. Abo El-Fotoh and N. A. Elgindy, *Journal of Controlled Release*, 2011, **153**, 206-216.

24. Y. Lu and S. C. Chen, *Advanced Drug Delivery Reviews*, 2004, **56**, 1621-1633.

25. B. D. Ulery, L. S. Nair and C. T. Laurencin, *Journal of Polymer Science. Part B, Polymer Physics*, 2011, **49**, 832-864.

26. M. Navarro, A. Michiardi, O. Castaño and J. A. Planell, *Journal of the Royal Society Interface*, 2008, **5**, 1137-1158.

27. A. W. Lloyd, *Medical Device Technology*, 2002, **13**, 18-21.

28. L. S. Nair and C. T. Laurencin, *Progress in Polymer Science*, 2007, **32**, 762-798.

29. D. S. Katti, S. Lakshmi, R. Langer and C. T. Laurencin, *Advanced Drug Delivery Reviews*, 2002, **54**, 933-961.

30. N. Bhattarai, J. Gunn and M. Zhang, *Advanced Drug Delivery Reviews*, 2010, **62**, 83-99.

31. J. M. Dang and K. W. Leong, *Advanced Drug Delivery Reviews*, 2006, **58**, 487-499.

32. K. S. Soppimath, T. M. Aminabhavi, A. R. Kulkarni and W. E. Rudzinski, *Journal of Controlled Release*, 2001, **70**, 1-20.

33. P. P. DeLuca, R. C. Mehta, A. G. Hausberger and B. C. Thanoo, in *Polymeric Delivery Systems*, American Chemical Society, 1993, vol. 520, ch. 4, pp. 53-79.

34. K. J. Dickers, H. Huatan and R. E. Cameron, *Journal of Applied Polymer Science*, 2003, **89**, 2937-2939.

35. F. Rancan, D. Papakostas, S. Hadam, S. Hackbarth, T. Delair, C. Primard, B. Verrier, W. Sterry, U. Blume-Peytavi and A. Vogt, *Pharmaceutical Research*, 2009, **26**, 2027-2036.

36. I. Bala, S. Hariharan and M. N. Kumar, *Critical Reviews in Therapeutic Drug Carrier Systems*, 2004, **21**, 387-422.

37. B. Rai, S. H. Teoh, D. W. Hutmacher, T. Cao and K. H. Ho, *Biomaterials*, 2005, **26**, 3739-3748.

38. N. Goonoo, R. Jeetah, A. Bhaw-Luximon and D. Jhurry, *European Journal of Pharmaceutics and Biopharmaceutics : official journal of Arbeitsgemeinschaft fur Pharmazeutische Verfahrenstechnik e.V*, 2015, **97**, 371-391.

39. D. Neut, O. S. Kluin, B. J. Crielaard, H. C. van der Mei, H. J. Busscher and D. W. Grijpma, *Acta Orthopaedica*, 2009, **80**, 514-519.

40. C. Jérôme and P. Lecomte, *Advanced Drug Delivery Reviews*, 2008, **60**, 1056-1076.

41. S.-H. Hyon, K. Jamshidi and Y. Ikada, *Biomaterials*, 1997, **18**, 1503-1508.

42. S. Penczek, M. Cypryk, A. Duda, P. Kubisa and S. Słomkowski, *Progress in Polymer Science*, 2007, **32**, 247-282.

43. K. M. Stridsberg, M. Ryner and A.-C. Albertsson, in *Degradable Aliphatic Polyesters*, Springer Berlin Heidelberg, Berlin, Heidelberg, 2002, pp. 41-65.

44. H. Wu, Y. Ji, Z. Li, X. Wang, Q. Zhang, S. Cui, W. Wu, J. Liu and K. Guo, *Journal of Polymer Science Part A: Polymer Chemistry*, 2015, **53**, 729-736.

45. M. Labet and W. Thielemans, *Chemical Society Reviews*, 2009, **38**, 3484-3504.

46. J. Liu, J. Ling, X. Li and Z. Shen, *Journal of Molecular Catalysis A: Chemical*, 2009, **300**, 59-64.

47. A.-C. Albertsson and I. K. Varma, *Biomacromolecules*, 2003, **4**, 1466-1486.

48. K. Shinno, M. Miyamoto, Y. Kimura, Y. Hirai and H. Yoshitome, *Macromolecules*, 1997, **30**, 6438-6444.

49. Q. Zhang, N. Re Ko and J. Kwon Oh, *Chemical Communications*, 2012, **48**, 7542-7552.

50. J.-O. You, D. Almeda, G. J. Ye and D. T. Auguste, *Journal of Biological Engineering*, 2010, **4**, 1-13.

51. S. Biswas, P. Kumari, P. M. Lakhani and B. Ghosh, *European Journal of Pharmaceutical Sciences*, 2016, **83**, 184-202.

52. N. Rapoport, *Progress in Polymer Science*, 2007, **32**, 962-990.

53. W. B. Liechty, D. R. Kryscio, B. V. Slaughter and N. A. Peppas, *Annual Review Of Chemical And Biomolecular Engineering*, 2010, **1**, 149-173.

54. M. Delcea, H. Mohwald and A. G. Skirtach, *Advanced Drug Delivery Reviews*, 2011, **63**, 730-747.

55. R. Cheng, F. Meng, C. Deng and Z. Zhong, *Nano Today*, 2015, **10**, 656-670.

56. Y. Bae and K. Kataoka, *Advanced Drug Delivery Reviews*, 2009, **61**, 768-784.

57. D.-W. Dong, S.-W. Tong and X.-R. Qi, *Journal of Biomedical Materials Research Part A*, 2013, **101A**, 1336-1344.

58. W. Chen, F. Meng, F. Li, S.-J. Ji and Z. Zhong, *Biomacromolecules*, 2009, **10**, 1727-1735.

59. C. Masson, M. Garinot, N. Mignet, B. Wetzer, P. Mailhe, D. Scherman and M. Bessodes, *Journal of Controlled Release*, 2004, **99**, 423-434.

60. H. Deng, Y. Zhang, X. Wang, Jianhuazhang, Y. Cao, J. Liu, J. Liu, L. Deng and A. Dong, *Acta Biomaterialia*, 2015, **11**, 126-136.

61. Y. Wang, D. Li, H. Wang, Y. Chen, H. Han, Q. Jin and J. Ji, *Chemical Communications*, 2014, **50**, 9390-9392.

62. Y.-Z. You and D. Oupický, *Biomacromolecules*, 2007, **8**, 98-105.

63. Q. Wang, H. Tang and P. Wu, *Langmuir*, 2015, **31**, 6497-6506.

64. D. Roy, J. N. Cambre and B. S. Sumerlin, *Progress in Polymer Science*, 2010, **35**, 278-301.

65. E. Fleige, M. A. Quadir and R. Haag, *Advanced Drug Delivery Reviews*, 2012, **64**, 866-884.

66. J. Li, M. Huo, J. Wang, J. Zhou, J. M. Mohammad, Y. Zhang, Q. Zhu, A. Y. Waddad and Q. Zhang, *Biomaterials*, 2012, **33**, 2310-2320.

67. H. Sun, F. Meng, R. Cheng, C. Deng and Z. Zhong, *Antioxidants & Redox Signaling*, 2014, **21**, 755-767.

68. G. Riess, *Progress in Polymer Science (Oxford)*, 2003, **28**, 1107-1170.

69. M. C. Jones and J. C. Leroux, *European Journal of Pharmaceutics and Biopharmaceutics*, 1999, **48**, 101-111.

70. X.-B. Xiong, Z. Binkhathlan, O. Molavi and A. Lavasanifar, *Acta Biomaterialia*, 2012, **8**, 2017-2033.

71. G. S. Kwon and T. Okano, *Advanced Drug Delivery Reviews*, 1996, **21**, 107-116.

72. V. S. Trubetskoy and V. P. Torchilin, *S.T.P. Pharma Sciences*, 1996, **6**, 79-86.

73. M.-C. Jones and J.-C. Leroux, *European Journal of Pharmaceutics and Biopharmaceutics*, 1999, **48**, 101-111.

74. S. Cammas, K. Suzuki, C. Sone, Y. Sakurai, K. Kataoka and T. Okano, *Journal of Controlled Release*, 1997, **48**, 157-164.

75. J. E. Chung, M. Yokoyama, K. Suzuki, T. Aoyagi, Y. Sakurai and T. Okano, *Colloids and Surfaces B: Biointerfaces*, 1997, **9**, 37-48.

76. W. Y. Chen, P. Alexandridis, C. K. Su, C. S. Patrickios, W. R. Hertler and T. A. Hatton, *Macromolecules*, 1995, **28**, 8604-8611.

77. T. Inoue, G. Chen, K. Nakamae and A. S. Hoffman, *Journal of Controlled Release*, 1998, **51**, 221-229.

78. J. Connor, N. Norley and L. Huang, *BBA - General Subjects*, 1986, **884**, 474-481.

79. S. B. La, T. Okano and K. Kataoka, *Journal of Pharmaceutical Sciences*, 1996, **85**, 85-90.

80. I. G. Shin, S. Y. Kim, Y. M. Lee, C. S. Cho and Y. K. Sung, *Journal of Controlled Release*, 1998, **51**, 1-11.

81. S. Cajot, P. Lecomte, C. Jerome and R. Riva, *Polymer Chemistry*, 2013, **4**, 1025-1037.

82. U. Kedar, P. Phutane, S. Shidhaye and V. Kadam, *Nanomedicine: Nanotechnology, Biology and Medicine*, 2010, **6**, 714-729.

83. N. Nishiyama, S. Okazaki, H. Cabral, M. Miyamoto, Y. Kato, Y. Sugiyama, K. Nishio, Y. Matsumura and K. Kataoka, *Cancer Research*, 2003, **63**, 8977-8983.

84. J. M. Chan, L. Zhang, K. P. Yuet, G. Liao, J. W. Rhee, R. Langer and O. C. Farokhzad, *Biomaterials*, 2009, **30**, 1627-1634.

85. Y. Matsumura and H. Maeda, *Cancer Res*, 1986, **46**, 6387-6392.

86. R. K. Jain, *Scientific American*, 1994, **271**, 58-65.

87. Y. H. Bae and K. Park, *Journal of Controlled Release*, 2011, **153**, 198-205.

88. C. H. J. Choi, C. A. Alabi, P. Webster and M. E. Davis, *Proceedings of the National Academy of Sciences*, 2010, **107**, 1235-1240.

89. K. Y. Choi, H. Chung, K. H. Min, H. Y. Yoon, K. Kim, J. H. Park, I. C. Kwon and S. Y. Jeong, *Biomaterials*, 2010, **31**, 106-114.

90. A. Béduneau, P. Saulnier and J.-P. Benoit, *Biomaterials*, 2007, **28**, 4947-4967.

91. L. E. van Vlerken, T. K. Vyas and M. M. Amiji, *Pharmaceutical Research*, 2007, **24**, 1405-1414.

92. X. Pan and R. J. Lee, *Expert Opinion on Drug Delivery*, 2004, **1**, 7-17.

93. T. Kakudo, S. Chaki, S. Futaki, I. Nakase, K. Akaji, T. Kawakami, K. Maruyama, H. Kamiya and H. Harashima, *Biochemistry*, 2004, **43**, 5618-5628.

94. A. Kikuchi, S. Sugaya, H. Ueda, K. Tanaka, Y. Aramaki, T. Hara, H. Arima, S. Tsuchiya and T. Fuwa, *Biochemical and Biophysical Research Communications*, 1996, **227**, 666-671.

95. S. Acharya, F. Dilnawaz and S. K. Sahoo, *Biomaterials*, 2009, **30**, 5737-5750.

96. V. P. Chauhan and R. K. Jain, *Nature Materials*, 2013, **12**, 958-962.

97. T.-G. Iversen, T. Skotland and K. Sandvig, *Nano Today*, 2011, **6**, 176-185.

98. K. Sandvig, M. L. Torgersen, H. A. Raa and B. van Deurs, *Histochemistry and Cell Biology*, 2008, **129**, 267-276.

99. M. Wieffer, T. Maritzen and V. Haucke, *Cell*, 2009, **137**, 382.e381-383.

100. G. J. Doherty and H. T. McMahon, *Annual Review of Biochemistry*, 2009, **78**, 857-902.

101. M. T. Howes, S. Mayor and R. G. Parton, *Current Opinion in Cell Biology*, 2010, **22**, 519-527.

102. M. Rabinovitch, *Trends in Cell Biology*, 1995, **5**, 85-87.

103. H. Hillaireau and P. Couvreur, *Cellular and Molecular Life Sciences,* 2009, **66**, 2873-2896.

104. S. D. Conner and S. L. Schmid, *Nature*, 2003, **422**, 37-44.

105. S. L. Schmid, *Annual Review of Biochemistry*, 1997, **66**, 511-548.

106. F. M. Brodsky, C. Y. Chen, C. Knuehl, M. C. Towler and D. E. Wakeham, *Annual Review of Cell and Developmental Biology*, 2001, **17**, 517-568.

107. L. Kou, J. Sun, Y. Zhai and Z. He, *Asian Journal of Pharmaceutical Sciences*, 2013, **8**, 1-10.

108. K. L. Douglas, C. A. Piccirillo and M. Tabrizian, *European Journal of Pharmaceutics and Biopharmaceutics : Official Journal of Arbeitsgemeinschaft fur Pharmazeutische Verfahrenstechnik e.V*, 2008, **68**, 676-687.

109. B. Rothen-Rutishauser, C. Muhlfeld, F. Blank, C. Musso and P. Gehr, *Particle and Fibre Toxicology*, 2007, **4**, 9.

110. K. Miyata, N. Nishiyama and K. Kataoka, *Chemical Society Reviews*, 2012, **41**, 2562-2574.

111. M. Elsabahy and K. L. Wooley, *Chemical Society Reviews*, 2012, **41**, 2545-2561.

112. S. Wilhelm, A. J. Tavares, Q. Dai, S. Ohta, J. Audet, H. F. Dvorak and W. C. W. Chan, *Nature Reviews Materials*, 2016, **1**, 16014.

113. J. W. Nichols and Y. H. Bae, *Nano Today*, 2012, **7**, 606-618.

114. A. S. Mikhail and C. Allen, *Journal of Controlled Release*, 2009, **138**, 214-223.

115. G. M. Soliman, A. Sharma, D. Maysinger and A. Kakkar, *Chemical Communications*, 2011, **47**, 9572-9587.

116. L. E. van Vlerken, T. K. Vyas and M. M. Amiji, *Pharmaceutical Research*, 2007, **24**, 1405-1414.

117. S. Kommareddy, S. B. Tiwari and M. M. Amiji, *Technology in Cancer Research & Treatment*, 2005, **4**, 615-625.

118. D. E. Noga, T. A. Petrie, A. Kumar, M. Weck, A. J. García and D. M. Collard, *Biomacromolecules*, 2008, **9**, 2056-2062.

119. M. Leemhuis, C. F. Van Nostrum, J. A. W. Kruijtzer, Z. Y. Zhong, M. R. Ten Breteler, P. J. Dijkstra, J. Feijen and W. E. Hennink, *Macromolecules*, 2006, **39**, 3500-3508.

120. P. Lecomte, C. Detrembleur, X. Lou, M. Mazza, O. Halleux and R. Jérôme, *Macromolecular Symposia*, 2000, **157**, 47-60.

121. X. Lou, C. Detrembleur and R. Jérôme, *Macromolecular Rapid Communications*, 2003, **24**, 161-172.

122. C. K. Williams, *Chemical Society Reviews*, 2007, **36**, 1573-1580.

123. Y. Lu and K. Park, *International Journal of Pharmaceutics*, 2013, **453**, 198-214.

Chapter 2: MATERIALS AND METHODS

2.1. MATERIALS

2.1.1. General chemicals

All chemicals were used as obtained without additional purification unless otherwise stated and purchased from standard suppliers. 2-Chlorocyclohexanone (98%), 3-chloroperoxybenzoic acid (70%), monomethoxy poly(ethylene glycol) (mPEG, M_n-5000 g/mol), poly(ethylene glycol) (PEG, M_n-4000), ε-caprolactone (97%), tin(II) 2-ethylhexanoate (92.5-100%), sodium azide (≥99.5%), propargylamine (98%), triethylamine (≥99%), copper (II) sulfate (99.9%), copper (I) bromide (99.9%), ascorbic acid sodium salt (≥98%), pyrene (≥99%), *N*-(3-dimethylaminopropyl)-*N*′-ethylcarbodiimide hydrochloride (EDAC, 99%), 4-(dimethylamino) pyridine (≥99%), Tween 80, 2-hydroxyethyl disulfide (90%), 4-pentynoic acid (95%), 4-fluororesorcinol (97%), 1,2,4-benzenetricarboxylic anhydride (trimellitic anhydride, ≥97%), ethylenediaminetetra acetic acid disodium salt dihydrate (99%), dithiothreitol (98%), rhodamine B (95%), fluorescein isothiocyanate isomer I (≥97.5%), 7-hydroxycoumarinyl-4-acetic acid (97%), *p*-toluenesulfonyl chloride (99%), triphenylphosphine (≥99%) and all deuterated solvents were purchased form Sigma-Aldrich. 1-[Bis(dimethylamino)methylene]-1*H*-1,2,3-triazolo[4,5-*b*]pyridinium 3-oxid hexafluorophosphate (HATU, 99%), was procured from Alfa Aesar. Methotrexate hydrate (≥98%) was obtained from VWR International. All other solvents were purchased from Fischer Scientific.

2.1.2. Cell culture reagents

Cells from a human breast cancer cell line (MCF7) were obtained from American Type Cell Culture Collection (ATCC). Dulbecco's Modified Eagle Medium (DMEM), fetal bovine serum, L-glutamine, trypsin-EDTA solution (10 ×), 3-(4,5-dimethyl-2-thiazolyl)-2,5-diphenyl-2*H*-tetrazolium bromide (MTT, 97.5%) and annexin V-FITC apoptosis detection kit was purchased from Sigma-Aldrich. Propidium iodide (1mg/mL solution) and Hoechst 33342 stains were purchased from Fisher Scientific UK. CellMask Deep Red plasma membrane stain was procured from Invitrogen (Thermo Fisher Scientific).

2.2. INSTRUMENTS AND METHODS

2.2.1. Nuclear magnetic resonance (NMR) spectroscopy

NMR spectra were recorded on a Bruker 400 spectrometer operating at 399.8 MHz (^{1}H) and 100.5 MHz (^{13}C), respectively. All chemical shifts were recorded in ppm using deuterated solvents and referenced against tetramethylsilane (0 ppm). NMR spectra were analysed using MestRENova 6.0.2 software (Mestrelab Research S.L).

2.2.2. Fourier transform infrared (FTIR) spectroscopy

FTIR spectra were recorded on an Agilent Technologies Cary 630 FTIR spectrophotometer fitted with a diamond single reflection ATR unit. All spectra were acquired by directly placing a small amount of a dried sample on a clean crystal of the instrument and were referenced against background spectra obtained by scanning the clean crystal before addition of the sample. Transmittances were recorded in the range 4000-650 cm^{-1} and data were processed using the Agilent MicroLab software suite.

2.2.3. Size exclusion chromatography (SEC).

SEC was performed on a Polymer Laboratories GPC 50 equiped with a differential refractive index detector. The mobile phase was HPLC grade $CHCl_3$ at 30 °C and a flow rate of 1 mL/min. Separations were performed on a pair of PLgel Mixed-D columns (300 × 7.8 mm, 5 μm bead size, Polymer Labs UK) fitted with a matching guard column (50 × 7.8 mm). The number average molecular weight (M_n), weight average molecular weight (M_w), and polydispersity were calculated based on a standard calibration method using poly(styrene) narrow molecular weight standards in the range of 100 Da–500 kDa.

Chromatograms were analysed using Polymer Labs Cirrus 3.0 software. Some samples were also analysed using HPLC grade tetrahydrofuran as the eluent at 40 °C.

2.2.4. Ultraviolet-visible spectroscopy (UV-Vis)

All UV-Vis spectra were recorded on a Beckman Coulter DU 800 UV spectrophotometer using quartz cuvettes. A sample volume of 700 µL was used and all spectra were referenced against a background of pure DMSO.

2.2.5. Fluorescence spectroscopy

Fluorescence spectra were recorded using an Agilent Cary Eclipse fluorescence spectrophotometer. The fluorescence intensities were measured against appropriate blank solutions at room temperature using a quartz cuvette. The excitation and emission slit width of 5 nm was selected for all measurements.

2.2.6. Differential scanning colorimeter (DSC)

Thermal properties of block copolymers were investigated using a Q2000 differential scanning calorimeter (TA Instruments, Leatherhead, UK). Typically, 5-10 mg sample was placed in a pre-weighed DSC pans with pin holed lids (TA Instruments, Brussels, Belgium) to measure melting temperature (T_m) and glass transition temperature (T_g), using empty pans as references. Nitrogen gas with a flow rate of 50 cm^3/min was used to purge the DSC cell and measurements were recorded by performing two heating/cooling cycles from -40 to 120 °C at a heating rate of 10 °C/min.

The recorded data were analysed usning Thermal Analysis Software (Version 4.5.05A, TA Instruments).

2.2.7. Particle size distribution and zeta potential

The size distributions of micelles were measured by dynamic light scattering (DLS) using a Malvern Zetasizer (Nano-ZS, Malvern Instruments Ltd., UK). Samples were prepared in Milli-Q water and measurements were recorded at 25 °C and at a 173-degree angle as aqueous suspension in polystyrene disposable cuvettes. Samples were illuminated using 633 nm wavelength (4mW) laser and data were analysed using Malvern ZetaSizer software version 7.11.

For zeta potential measurements, the micellar solutions were diluted in NaCl solution (final concentration of NaCl ~ 5 mmol) and measurements were recorded in an electrophoretic cell at an electric field of 15.24 V/cm using the NanoZS instrument (Malvern, UK).

Zeta potential of nanocarriers can be estimated by applying an electric field across the colloids or nanoparticles dispersion and then by measuring the electrophoretic mobility by laser doppler velocimetry. The measured electrophoretic mobility was converted into zeta potential using the Henry equation.

2.2.8. Transmission electron microscopy (TEM)

The morphologies of micelles were characterised by a Tecnai G2 (FEI, Oregon, USA) transmission electron microscope at electron voltages of 100 kV. TEM samples were prepared by placing a drop of micellar solution onto Formvar® coated copper grids and the suspensions were allowed to settle for few minutes. The excess of solution was removed with a filter paper and the samples allowed to air dry prior to analysis.

2.2.9. Critical micelle concentration (CMC)

The critical micelle concentration (CMC) of block copolymers was measured by fluorescence spectroscopy using pyrene as a probe. Pyrene is one of the most frequently used fluorescent probe to determine CMC of surfactants and amphiphilic block copolymers.1 The fluorescence intensity peaks of pyrene at λmax=373 (I1) and 383 nm (I3) are sensitive to its surroundings. Any variation in polarity around pyrene molecule can alter its fluorescence intensity.2 Specifically, the intensity of peak I1 decreases when pyrene moves from a polar to non-polar region. In contrast, the intensity of peak I3 increases in non-polar region, providing a convenient way to estimate the CMC of block copolymers. When amphiphilic block copolymers start to assemble into micelles in solution, the environment of pyrene changes from hydrophilic to hydrophobic, therefore, intensity of I1 decreases while that of I3 increases. Therefore, the CMC of amphiphilic block copolymers can be determined from the change of intensity ratio of I1/I3.

To estimate CMC, a stock solution of pyrene was prepared in acetone and a known volume was transferred into a number of vials to obtain $6x10^{-7}$ M of pyrene in each vial. The vials were then placed in the dark for four hours at room temperature in a fume cupboard to allow evaporation of acetone. Block copolymer solutions ranging from 0.1-100 µg/mL were added into the pyrene-containing vials. The vials containing block copolymer solution and pyrene were then agitated overnight (in dark). Fluorescence spectra of solutions were recorded in the range of 350 to 450 nm after excitation at 335 nm. The slit width was set at 5 nm for both excitation and emission. The ratio of the peak intensities at 373 and 383 nm (I_1/I_3) was plotted against the logarithm of polymer concentration to find the inflection point. The corresponding concentration at this point was considered to be the polymer CMC.

2.2.10. Electrospray ionisation mass spectrometry

Electrospray ionisation mass spectrometry was performed on a Micromass LCT KC453 spectrometer. Mass spectra were recorded using electrospray (ES+) or (ES-). Samples were prepared as diluted solution in acetonitrile or HPLC grade methanol.

2.2.11. Freeze dryer

Lyophilisation of aqueous solutions was carried out in a GIROVAC LTD GVD3 freeze dryer equipped with a high vacuum pump. Liquid nitrogen was used to freeze samples before placing in the dryer.

2.2.12. Rotary evaporator

Organic solvents were removed under reduced pressure using a Buchi rotavapor R-200 fitted with a B490 heating bath.

2.2.13. Thin layer chromatography (TLC)

Thin layer chromatography (TLC) was carried out on ALUGRAM®SIL G/UV254 pre-coated TLC sheets procured from Macherey-Nagel. TLC sheets were visualised by staining with potassium permanganate.

2.2.14. Column chromatography

Column chromatography was carried out using silica 60 A (Fischer Chemicals, particle size 35-70 μm) as the stationary phase with solvents of analytical purity as the mobile phase.

2.2.15. Microplate reader

The formazan contents in the MTT assay were quantified using a BioTek microplate reader (Synergy 2 Multi-Mode Reader) at a wavelength of 570 nm. The percent cell metabolic activity was calculated using untreated cells (without micelles) as a negative control (100% metabolic activity).

2.2.16. Fluorescence microscopy

Fluorescence microscopy was performed using an inverted fluorescence microscope EVOS™ FL Cell Imaging System equipped with a Sony ICX285AQ colour CCD camera.

2.2.17. Confocal laser scanning microscopy

The cellular uptake of micelles was observed using a Zeiss 510 Meta Confocal microscope. A 488-nm wavelength laser was used to excite the Oregon-green (excitation/emission maxima = 495/521 nm) and CellMask™ deep red plasma membrane stain (excitation/emission maxima = 649/666) was excited with a laser of 633 nm wavelength. The Hoechst 33342 stain (excitation/emission maxima = 350/461) was illuminated with a 100-watt high-pressure mercury plasma arc-discharge lamp (HBO 100). The control untreated cells (without micelles) were used to subtract the background or auto fluorescence.

2.2.18. Flow cytometry

Flow cytometry analysis was performed using a Beckman Coulter FC 500 flow cytometer equipped with 488 and 633 nm co-linear lasers. Fluorescence assisted cell sorting (FACS) or flow cytometry is an important tool to quantify the cellular uptake of nano-carriers. FACS can also be employed to sort live, apoptotic or dead cells. It allows the fast and high-throughput screening of cells and provide data with high statistical significance. FACS involves the hydrodynamic focusing of a cell suspension through a chamber using a laminar flow of sheath fluid, which allows cells to pass one at a time through one or more laser. As each cell passes through the laser beam, light scattering and fluorescence intensities are measured, letting various parameters to be assessed simultaneously. The control or untreated cells are used to direct the auto fluorescence. Forward scattering (FS) can be integrated to get information about size of the cells, whereas cell morphology and granularity can be estimated using side scattering (SS). The fluorescence and scattered parameters can be combined in the form of a dot plot to estimate cellular uptake of nanocarriers or to resolve subpopulations such as live or dead cells. The histograms of control and treated samples can be overlaid to quantify the percentage of population which has taken up the nanocarriers.[3, 4] Moreover, the percentages of live or dead cells are calculated using multiple fluorescent dyes which may interact or bind with various cellular components such as RNA or DNA. Furthermore, various antibodies or

proteins conjugated to fluorescent dyes can be used to detect apoptotic cells.

2.2.19. Cell culture

Human breast cancer cells (MCF7) were cultured in Dulbecco's Modified Eagle Medium (DMEM) containing 10% fetal bovine serum (FBS) and 1% *L*-glutamine at 37 °C with 5% CO_2. Cells were split after reaching 90% confluency using fresh cell culture medium. Trypsin/EDTA was used to detach the cells that were adhered to tissue culture flask. Cell counting was performed using a haemocytometer.

2.3. REFERENCES

1. J. Aguiar, P. Carpena, J. A. Molina-Bolívar and C. Carnero Ruiz, *Journal of Colloid and Interface Science*, 2003, **258**, 116-122.
2. G. Basu Ray, I. Chakraborty and S. P. Moulik, *Journal of Colloid and Interface Science*, 2006, **294**, 248-254.
3. K. L. Robertson and J. L. Liu, *Wiley Interdisciplinary Reviews. Nanomedicine and Nanobiotechnology*, 2012, **4**, 511-524.
4. O. Gladkovskaya, V. A. Gerard, M. Nosov, Y. K. Gun'ko, G. M. O'Connor and Y. Rochev, *RSC Advances*, 2015, **5**, 42250-42258.

Chapter 3: ENGINEERING OF FUNCTIONAL AMPHIPHILIC BLOCK COPOLYMERS AS PRECURSORS OF REACTIVE MICELLES FOR DRUG DELIVERY APPLICATIONS

3.1. INTRODUCTION

Polyesters are a class of biodegradable polymers and have been broadly used in various biomedical applications such as tissue engineering, drug delivery, controlled release, and surgical repair.[1-3] In the last few decades, various FDA approved[4] aliphatic polyesters e.g. poly(lactic-*co*-glycolic acid) (PLGA), poly(ε-caprolactone) (PCL), and poly(lactic acid) (PLA), have been intensively studied to exploit their potential in drug, gene and protein delivery and controlled release applications.[5] Such polyesters are mainly derived from ε-caprolactone, lactide, and glycolide (figure 3-1).[6-8] It has been reported that polyesters are biocompatible and biodegradable and possess excellent moulding and shaping properties, rendering them suitable for biomedical applications. They degrade by bulk or surface erosion and the degradation is induced through the hydrolysis of ester bonds.[9, 10]

Specifically, aliphatic polyesters have gained great interest in drug delivery and controlled release systems. For instance, PLGA micro and nano-carriers have been used for the delivery and controlled release of low molecular weight drugs, nucleic acids and proteins.[11-13] However, due to the acidic nature of the PLGA monomer, the pH drop in the nano-carriers upon their degradation, may result in the chemical modification, instability and aggregation of the loaded therapeutic agent.[10, 11] Moreover, the resulting aggregates can cause immunogenic reactions suggesting that PLGA is not ideal for all drugs or bioactive molecules.[14-17]

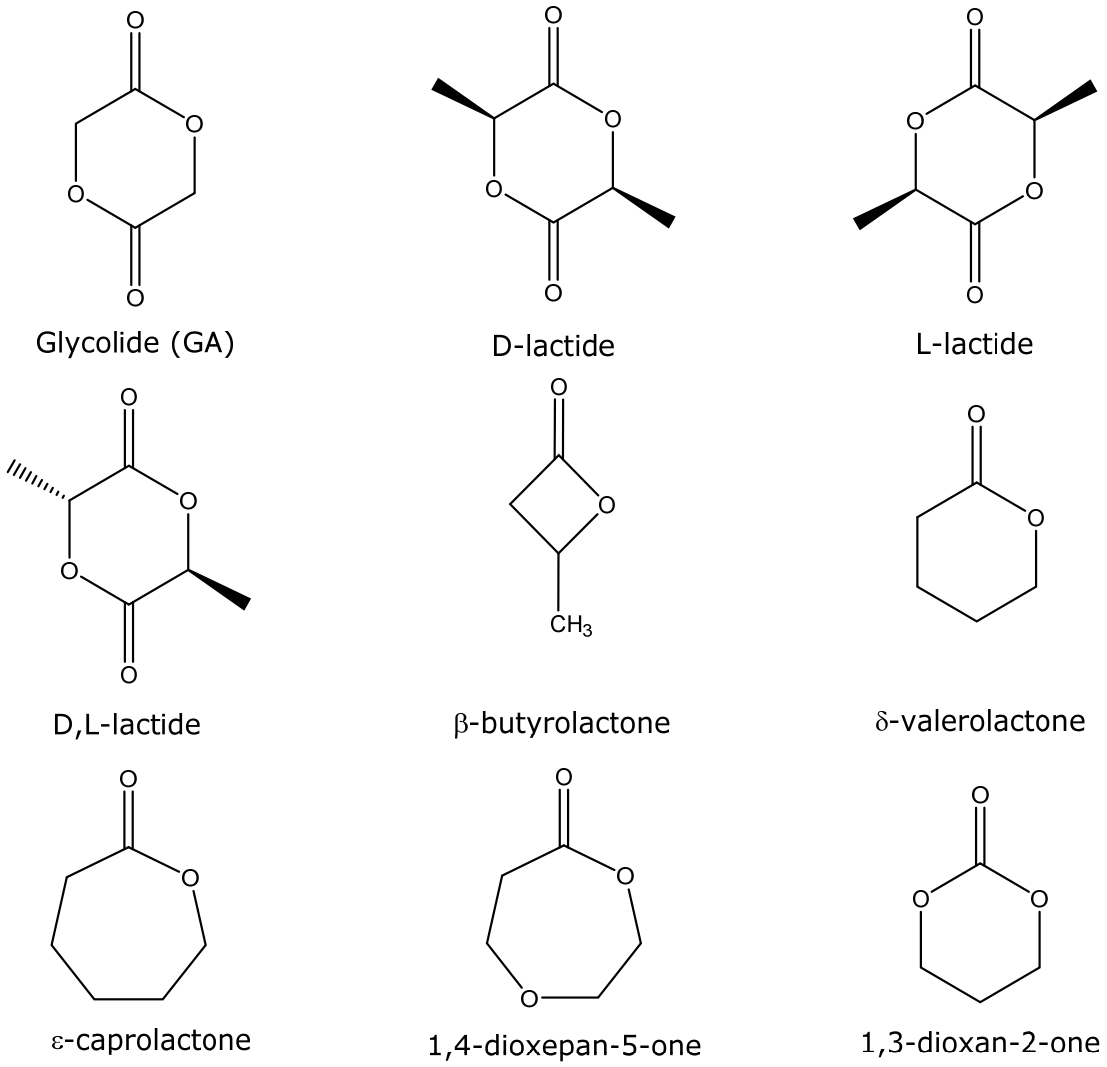

Figure 3-1. Chemical structure of some commonly used precursors for polyester synthesis.

Poly-ε-caprolactone (PCL) is another example of aliphatic biodegradable polyesters. It is a semi-crystalline, hydrophobic polymer and has been widely used in drug delivery, controlled release applications and tissue engineering scaffolds.[18-20] It has been reported that PCL is non-toxic and is well-tolerated in numerous body tissues. Moreover, good compatibility of PCL with a wide range of drugs has been shown, as well as desirable

mechanical properties, enabling PCL to be considered as a good candidate for drug delivery applications.[21, 22]

However, a high degree of crystallinity and intrinsic hydrophobicity results in slow degradation of PCL limiting its further clinical applications.[23] Moreover, inflammation, local tissue necrosis, and thrombosis have also been reported due to the inappropriate interaction between PCL and cells.[24] The hydrophilicity, biodegradability and mechanical properties of PCL can be improved by copolymerising it with poly(ethylene glycol) (PEG).[25-27] PEG is a hydrophilic polymer with good biocompatibility, non-toxicity, and non-immunogenicity. [28] Additionally, PEG has also established its importance to prevent protein adsorption and non-specific interactions of biomaterials with biological systems, hence, PEG has been intensively used as a hydrophilic block to improve the properties of polyesters.[29] Another limitation of PCL is the lack of any functional pendent group along the hydrophobic chain. The functional moieties along the hydrophobic backbone not only provide the opportunity to covalently graft therapeutic molecules or fluorescent probes of biological importance, but also can tailor the macroscopic properties of the polymer such as biodegradation rate, bioadhesion, crystallinity, hydrophilicity, and mechanical properties.[30]

Functional groups can be introduced into the hydrophobic backbone by various methods e.g. post-polymerisation functionalisation,[1] and by polymerisation of previously functionalised ε–caprolactone monomer.[31] The post-polymerisation functionalisation is generally performed by removal of

protons from the polyester by reacting it with a base, followed by introducing an electrophilic compound (e.g., a halogen or a carbonyl containing reagent).[32] For instance, PCL possessing various functional groups was obtained by anionic activation of PCL chain using lithium di-isopropyl amide as shown in scheme 3-1.[33]

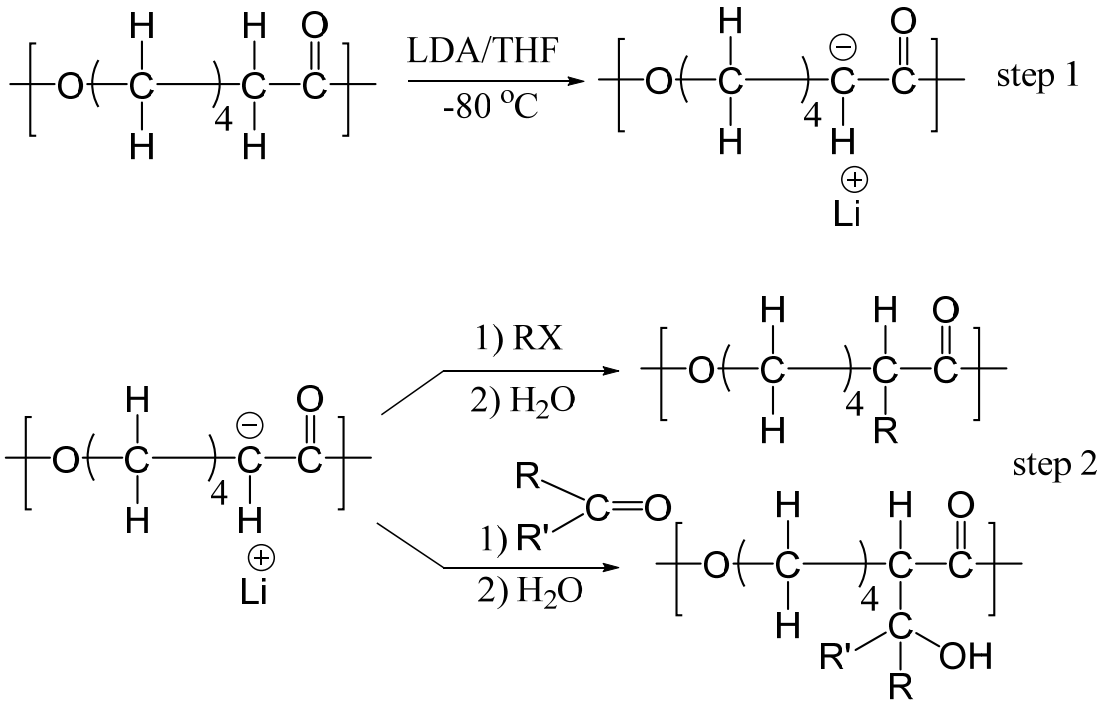

Scheme 3-1. Chemical modification of polycaprolactone via anionic route.[33]

This activation resulted into a poly-carbanion onto which several electrophiles such as benzyl chloroformate, benzaldehyde, iodomethane and naphthoyl chloride were attached. However, low efficiency of functionalisation, inevitable chain degradation and the possibility of side reactions decreases the applicability of this route. Furthermore, synthesis

of amphiphilic di-block copolymers by this process is not straightforward. Hence, post-polymerisation functionalisation is not the favoured technique to obtain functional polyesters.

To synthesise functional polyesters, a commonly used technique is to polymerise a functional (co)monomer via polycondensation, ring-opening, or enzymatic polymerisation, the ring-opening pathway being one of the best methods, thanks to the livingness of such polymerisation process.[34-36] For this process, the required functional lactone monomers can be easily purified by fractional distillation or by recrystallization, enabling them to be good candidates towards functional polyesters.[36-39] For example, 2-oxepane-1,5-dione (OPD) was synthesised by Baeyer-Villiger oxidation of 1,4-cyclohexanedione by *m*-chloroperbenzoic acid.[31] The synthesised functional monomer was used to obtain poly(OPD) via ring opening polymerisation using stannous octoate as catalyst and 1-phenyl-2-propanol as an initiator. The resulting polyester was semicrystalline with high melting temperature (147 °C).

In another approach, γ-bromo-εCL (γBrεCL) has been synthesised previously, as a precursor of functional PCL.[40] Briefly, bicyclic cyclohexane-1,4-oxide was reacted with hydrobromic acid to generate trans-4-bromocyclohexanol, which was subsequently oxidized to 4-bromocyclohexanone using pyridinium chlorochromate. In a later step, 4-bromocyclohexanone was further oxidized into γ-bromo-εCL using Bayer-Villiger oxidation as shown in scheme 3-2.

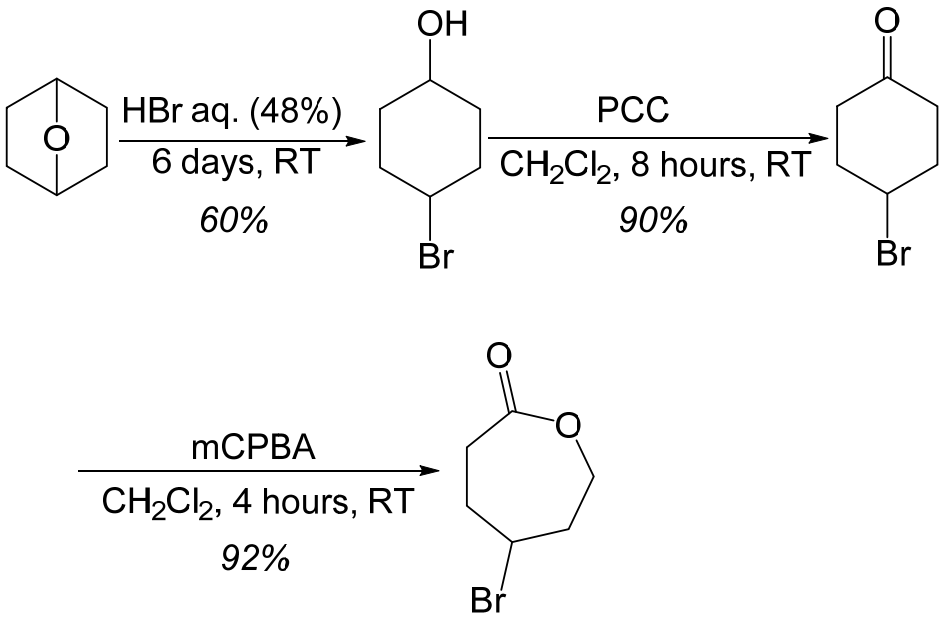

Scheme 3-2. Multi-step reaction route for the synthesis of γ-bromo-εCL (γBrCL).[40]

The synthesised γ-bromo-εCL was successfully used to produce homo and copolymers (i.e. poly(γBrεCL-*co*-εCL)) with predictable molecular weights and narrow molecular weight distribution using aluminium isopropoxide as an initiator. However, synthesis of this functional lactone was not straightforward and required multiple steps to obtain γBrεCL.

In this work, a functional caprolactone (α-chloro-ε-caprolactone) was synthesised in one step from the oxidation of 2-chlorocyclohexanone using 3-chloroperoxybenzoic acid (*m*CPBA) as oxidising agent.[41] The functional lactone monomer was purified by silica gel column chromatography with high yield and high purity as reported elsewhere. The ring opening polymerisation of this functional lactone monomer was carried out to generate amphiphilic block copolymers based on mPEG-*b*-poly(αClεCL) and

mPEG-*b*-poly(εCL-*co*-αClεCL) comprising various molar masses. Tin octoate was used as catalyst and PEG bearing one OH functional group at the ω-chain end, was used as a macro-initiator. In a second step, pendent chloro groups of amphiphilic block copolymers were substituted by the azide group via nucleophilic substitution reaction using sodium azide following a reported process.[42]

The synthesised functional amphiphilic block copolymers were characterised by ^{1}H NMR, ^{13}C NMR, FT-IR and size exclusion chromatography (SEC). The characterisation data revealed good quantitative conversion of monomers generating amphiphilic block copolymers of predictable molecular weights and narrow polydispersity without apparent transesterification. Therefore, functional amphiphilic block copolymers based on mPEG-*b*-poly(αN_3εCL) and mPEG-*b*-poly(εCL-*co*-αN_3CL) comprising various molar masses can be used as precursors of reactive polymeric nanocarriers.

3.2. RESULTS

3.2.1. Synthesis of α-chloro-ε-caprolactone

The functional caprolactone i.e. α-chloro-ε-caprolactone was obtained from the oxidation of 2-chlorocyclohexanone by Baeyer-Villiger oxidation reaction,[43] using 3-chloroperoxybenzoic acid (*m*CPBA) as an oxidising

agent as shown in scheme 3-3.

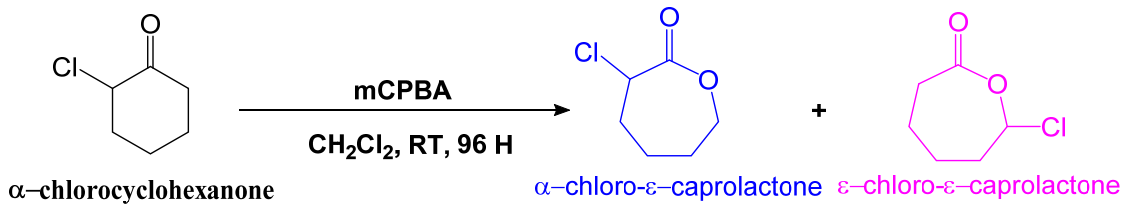

Scheme 3-3. Synthesis of α-chloro-ε-caprolactone by Baeyer-Villiger oxidation reaction.

The crystals of unreacted *m*CPBA and its reduced form (*m*-chloro benzoic acid) were removed by filtration, whereas, the remaining residues of both acids in the product mixture were quenched and removed by extraction with saturated solutions of sodium thiosulfate and sodium bicarbonate. The Baeyer-Villiger oxidation of 2-chlorocyclohexanone resulted in two isomers i.e. αClεCL, and εClεCL (scheme 3-3), in a 95:5 molar ratio. The isomers could be separated either by fractional distillation under reduced pressure,[44] or by silica gel column chromatography.[45] In this work, the αClεCL was purified by silica gel column chromatography with high yield (70%) and with high purity, as also revealed by ^{1}H and ^{13}C NMR spectroscopy (figure 3-2). The appearance of chemical shifts at 4.69 and 4.29 ppm in ^{1}H NMR spectrum, and 69.52 ppm in ^{13}C spectrum confirmed the formation of the functional lactone.

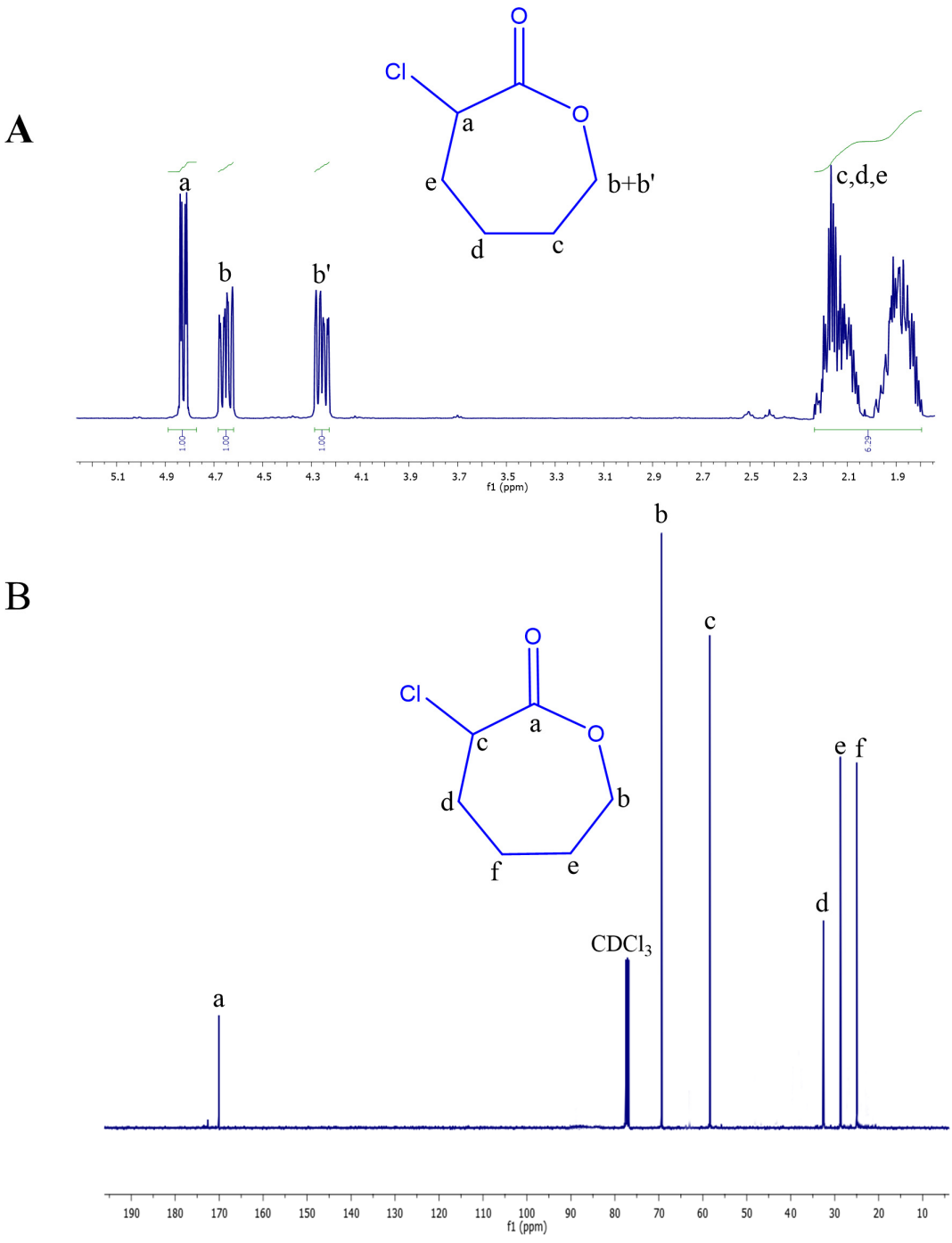

Figure 3-2. NMR characterisation of α-chloro-ε-caprolactone in $CDCl_3$. (A) ^{1}H NMR spectrum and (B) ^{13}C NMR spectrum.

3.2.2. Synthesis and characterisation of amphiphilic block copolymers

A mixture of functional mPEG-*b*-poly(αClεCL) and mPEG-*b*-poly(εCL-*co*-αClεCL) block copolymers comprising various molar masses, were synthesised by ring-opening polymerisation of αClεCL and or εCL. The PEG bearing one OH functional group at the ω-chain end was used as an initiator, whereas, tin octoate was used as a catalyst (scheme 3-4).

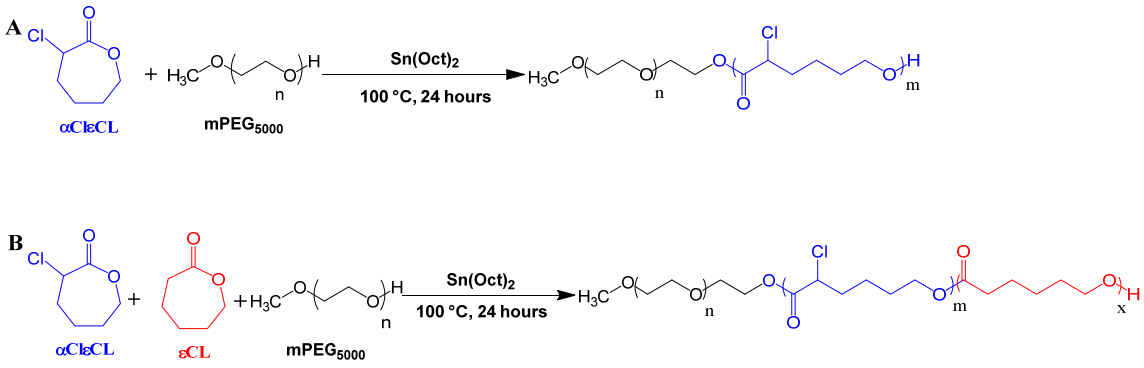

Scheme 3-4. Ring-opening polymerisation to synthesise (A) mPEG-*b*-poly(αClεCL), and (B) mPEG-*b*-poly(εCL-*co*-αClεCL).

To obtain mPEG-*b*-poly(αClεCL) and mPEG-*b*-poly(εCL-*co*-αClεCL) block copolymers with various molar masses, the molar feed ratio of mPEG was kept constant in the reaction mixture, whereas, the molar feed ratio of αClεCL and or εCL monomers were changed. The polymerisation was performed in bulk (without solvent) at 100 °C. The block copolymers were purified by precipitation in diethyl ether to remove un-converted monomer and catalyst residues. The characterisation data of mPEG-*b*-poly(αClεCL)

and mPEG-*b*-poly(εCL-*co*-αClεCL) block copolymers with various molar masses are shown in figure 3-3 to 3-12. The disappearance of monomer signals in ^{1}H NMR spectra revealed quantitative conversion of both monomers after 24 hours. The comparison of the relative intensities of protons of the methoxy end group of mPEG (3.40 ppm, peak "a" in figure 3-3A) and the C$\underline{H}_2$-CHCl protons (2.05 ppm, peak "g", in figure 3-3A) of poly(αClεCL) was used to estimate the molar mass of mPEG-*b*-poly(αClεCL). The integrations of NMR spectra revealed that the molar masses of synthesised mPEG-*b*-poly(αClεCL) block copolymers were 6.8, 9.4, 14.3, and 19.4 kDa, with 12, 30, 62, and 97 degrees of polymerisation of poly(αClεCL), respectively. The increase in molar masses of poly(αClεCL) can be observed by the increase in signal intensities as indicated by the upward arrows in figure 3-3B. The synthesised block copolymers of mPEG-*b*-poly(αClεCL) were further characterised by ^{13}C NMR (figure 3-4) and FT-IR spectroscopy (figure 3-5).

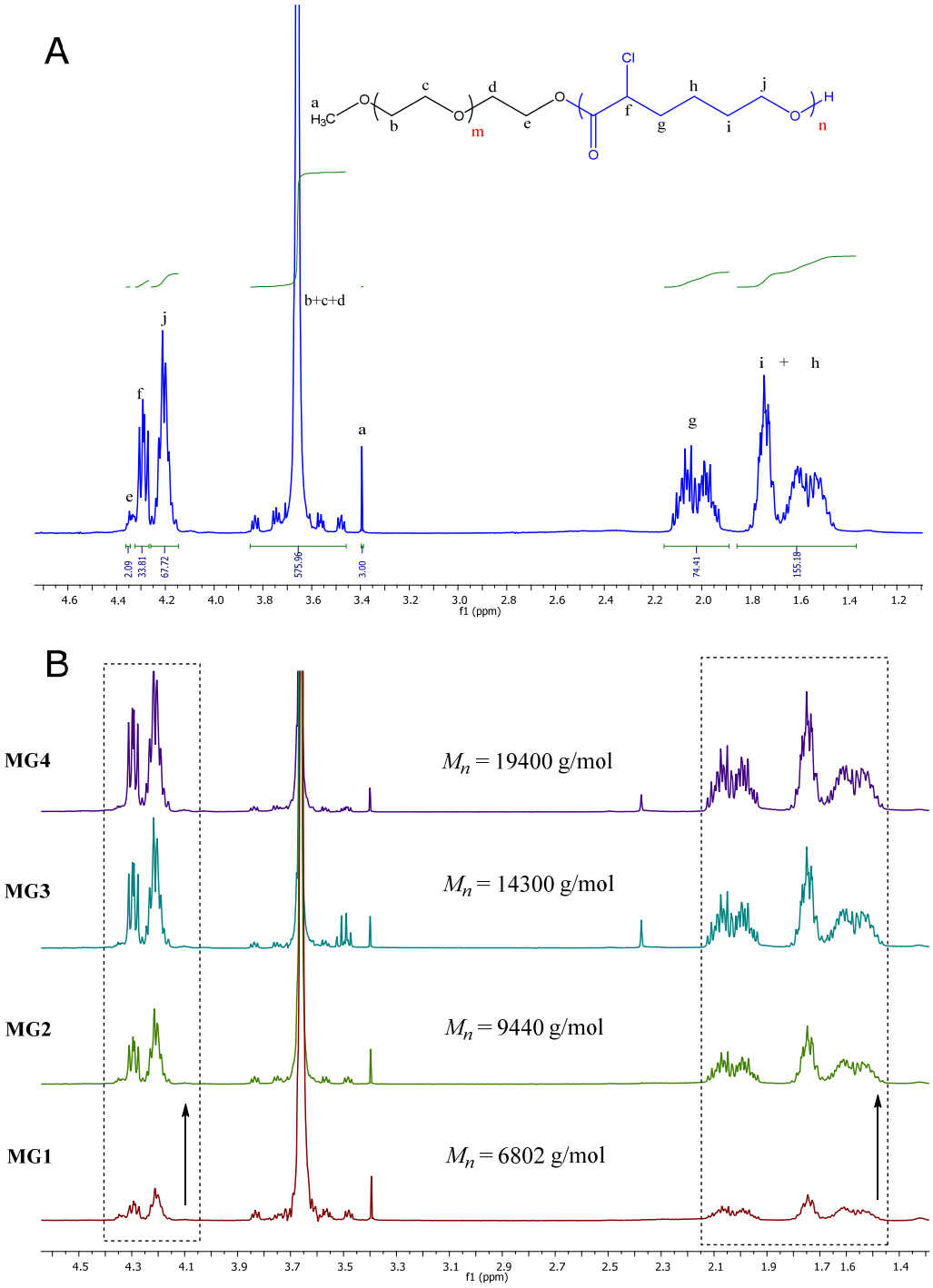

Figure 3-3. (A) ^{1}H NMR spectrum of mPEG-*b*-poly(αClεCL) block copolymer (MG2) and (B) Overlaid ^{1}H NMR spectra of mPEG-*b*-poly(αClεCL) block copolymers with various molar masses. Arrows showing the increase in signal intensity.

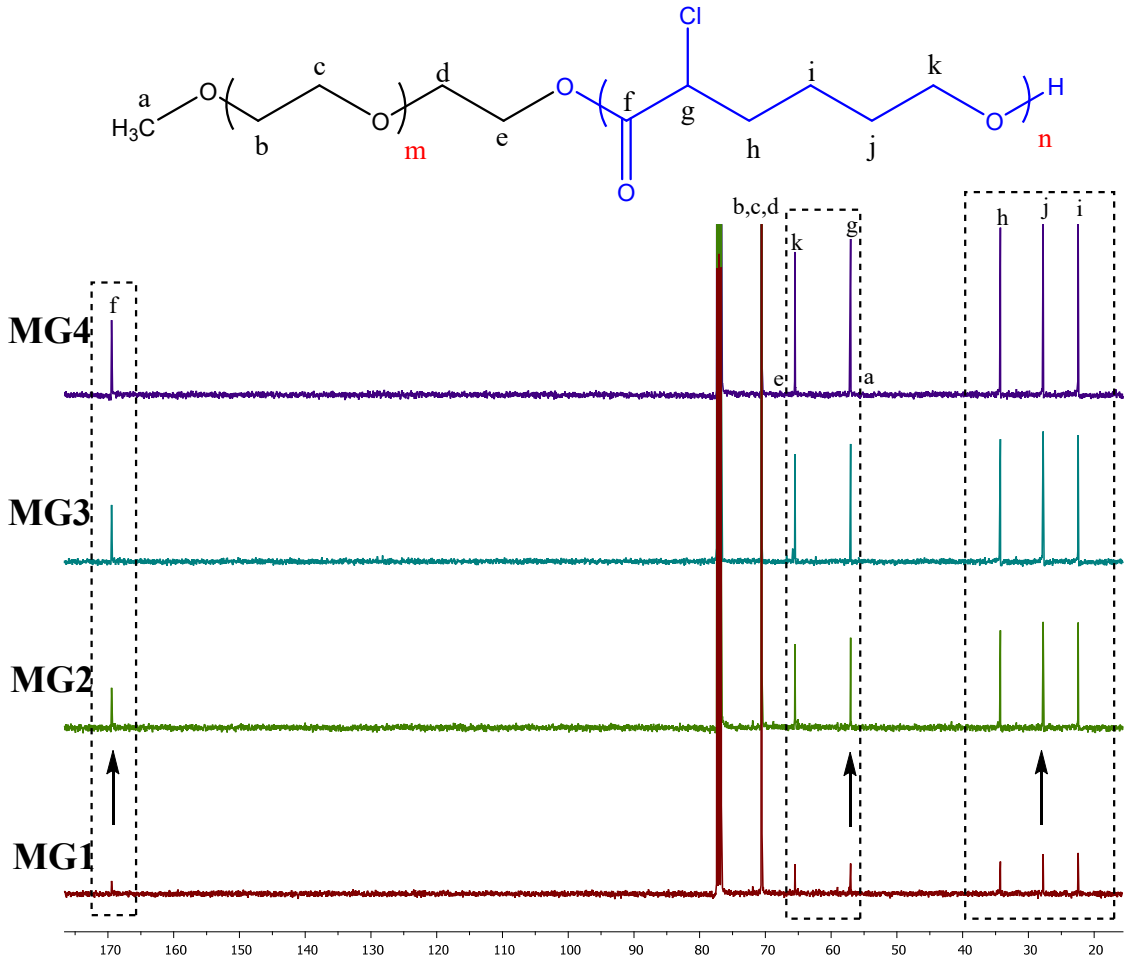

Figure 3-4. (A) ^{13}C NMR spectra of mPEG-*b*-poly(αClεCL) block copolymer with various molar masses. Arrows indicating the increase in signal intensity.

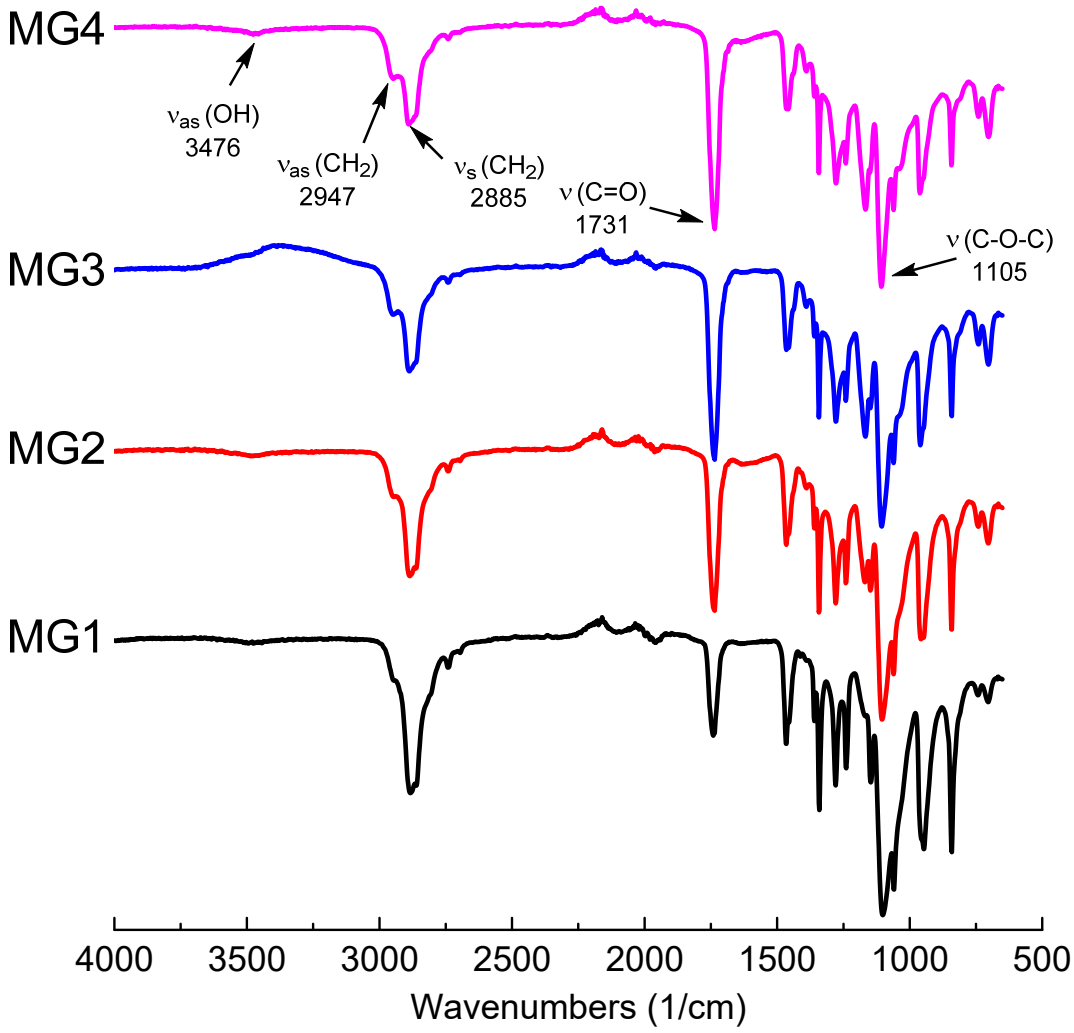

Figure 3-5. FT-IR spectra of mPEG-*b*-poly(αClεCL) block copolymers with different molar masses.

The differential scanning calorimetry (DSC) analysis showed a slight decrease in the melting temperatures of mPEG-*b*-poly(αClεCL) block copolymers with the increase in molecular weights as shown in figure 3-6. Specifically, mPEG-*b*-poly(αClεCL) block copolymers having 6.8, 9.4, 14.3, and 19.4 kDa number average molecular weights showed melting temperatures of 58.35, 55.16, 54.62, and 52.86 °C, respectively.

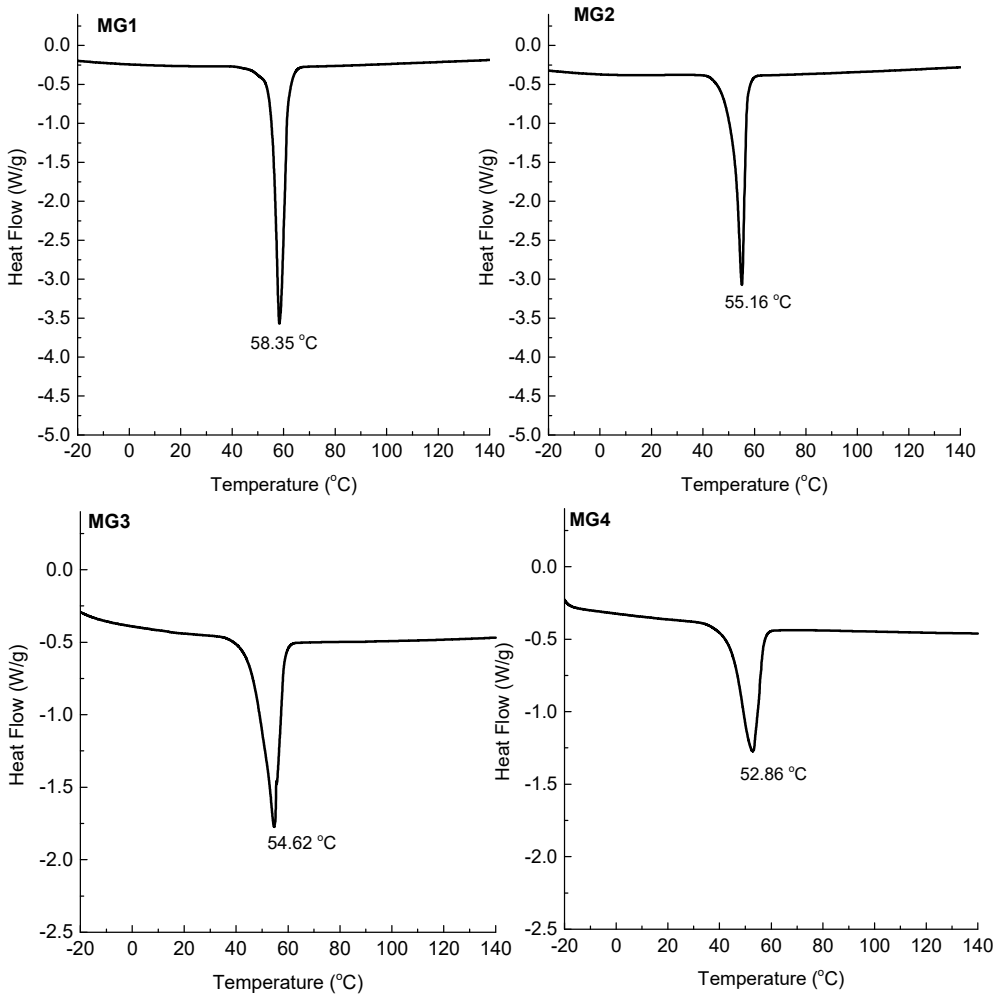

Figure 3-6. DSC thermograph of mPEG-*b*-poly(αClεCL) block copolymers with different molar masses.

The molecular weights of mPEG-*b*-poly(εCL-*co*-αClεCL) copolymers were calculated by the comparison of the relative intensity of the proton of PCL at 2.33 ppm (C$\underline{H_2}$-C(O), peak "k", in figure 3-7A) and relative intensity of the proton of poly(αClεCL) at 4.21 ppm (CO–CH(Cl)–CH_2–CH_2–CH_2–C$\underline{H_2}$–O–, peak "j", in figure 3-7A) with the methoxy end group of the mPEG. The block copolymers of mPEG-*b*-poly(εCL-*co*-αClεCL) resulted into molar masses of 6.6, 10.0, 14.9, and 19.8 kDa (determined by ^{1}H NMR

integration), with 8, 35, 79, and 122 degrees of polymerisation of εCL, and 5, 7, 6, and 6 degrees of polymerisation of αClεCL, respectively.

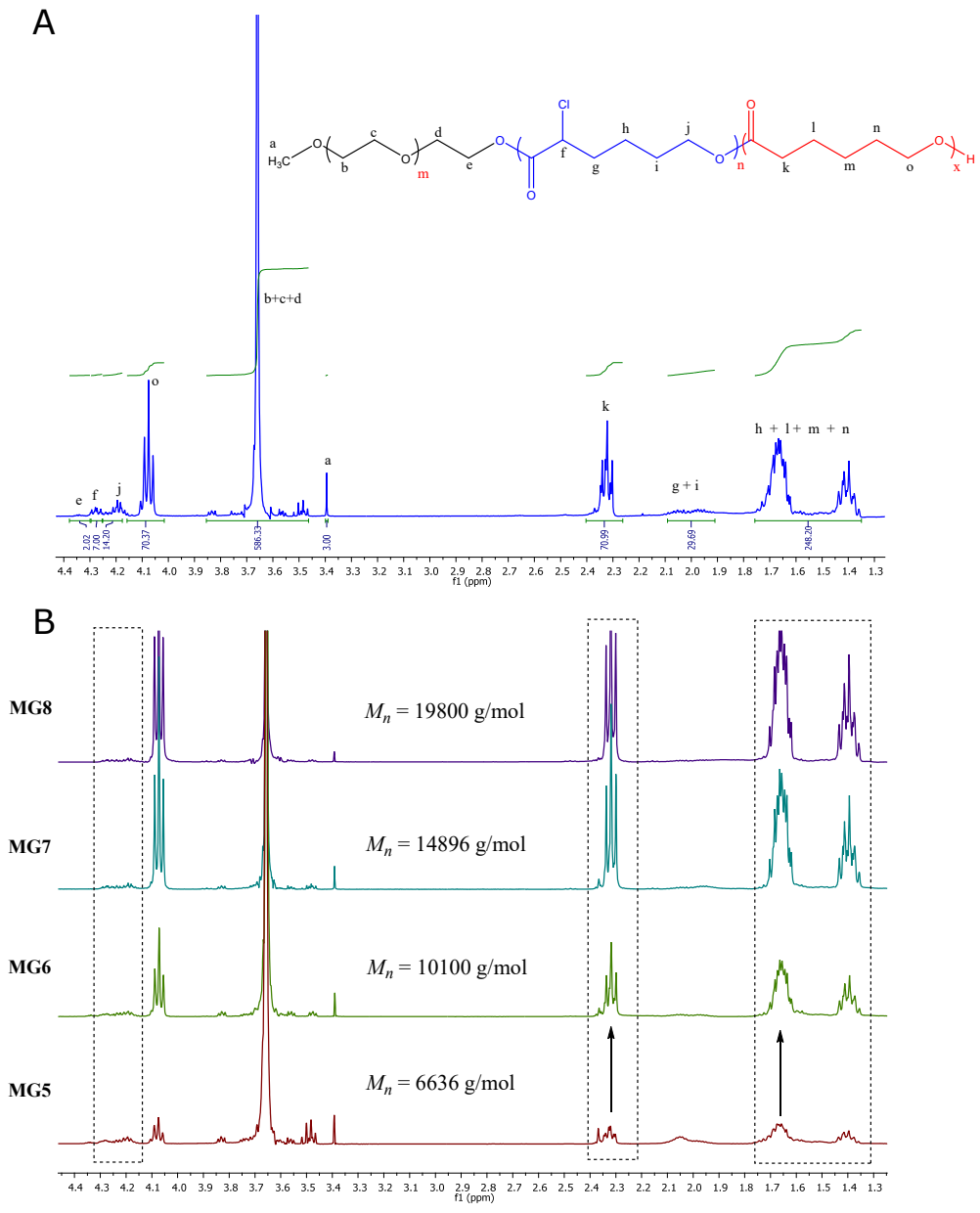

Figure 3-7. (A) ^{1}H NMR spectrum of mPEG-*b*-poly(εCL-*co*-αClεCL) (MG6) and (B) Overlaid ^{1}H NMR spectra of mPEG-*b*-poly(εCL-*co*-αClεCL) block copolymers with different molar masses. Upwards arrows showing the increase in signal intensity.

The ^{1}H NMR-derived experimental molecular weights were in good agreement with the theoretically calculated molar masses values for all the block copolymers. The ^{13}C NMR (figure 3-8) and FT-IR (figure 3-9) characterisation of mPEG-*b*-poly(εCL-*co*-αClεCL) showed good conformation to the chemical structures.

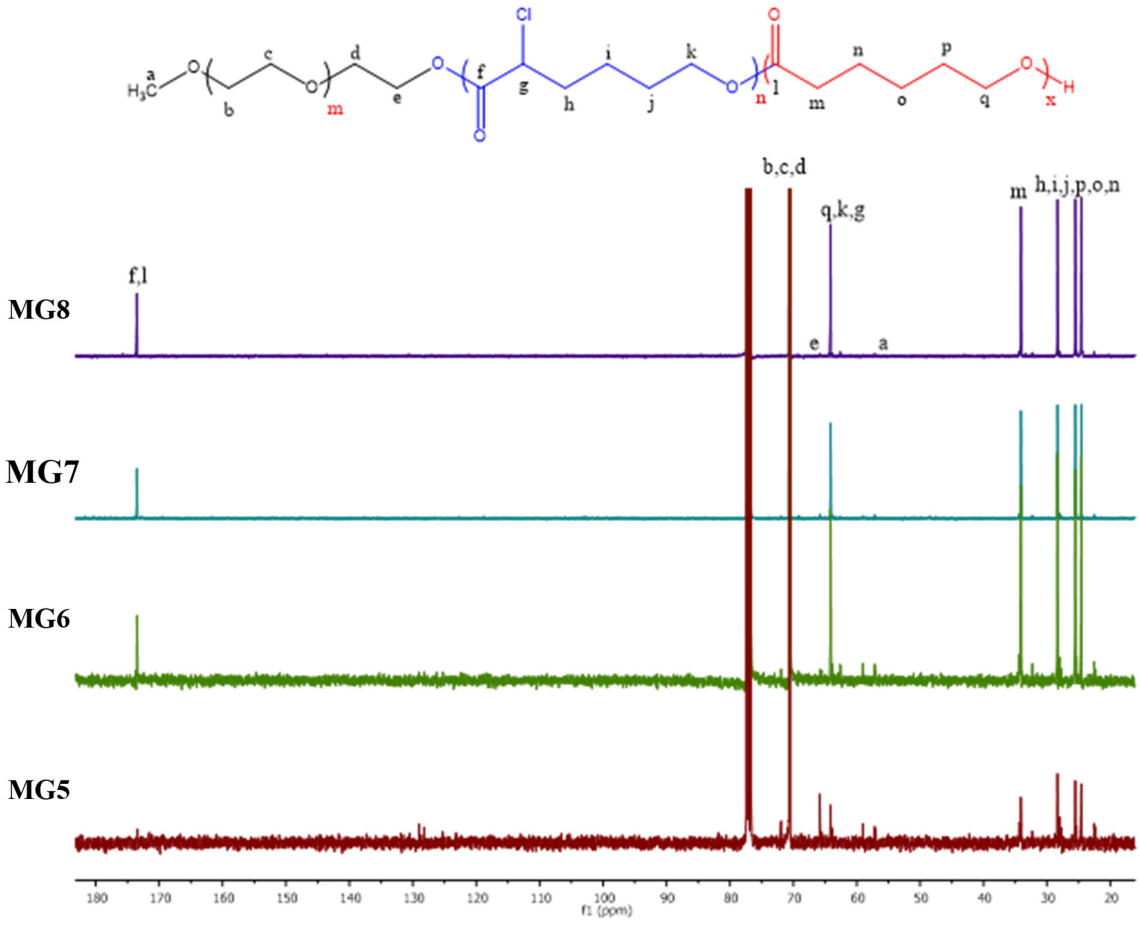

Figure 3-8. ^{13}C NMR spectra of mPEG-*b*-poly(εCL-*co*-αClεCL) block copolymer with various molar masses. Arrows showing the increase in signal intensity.

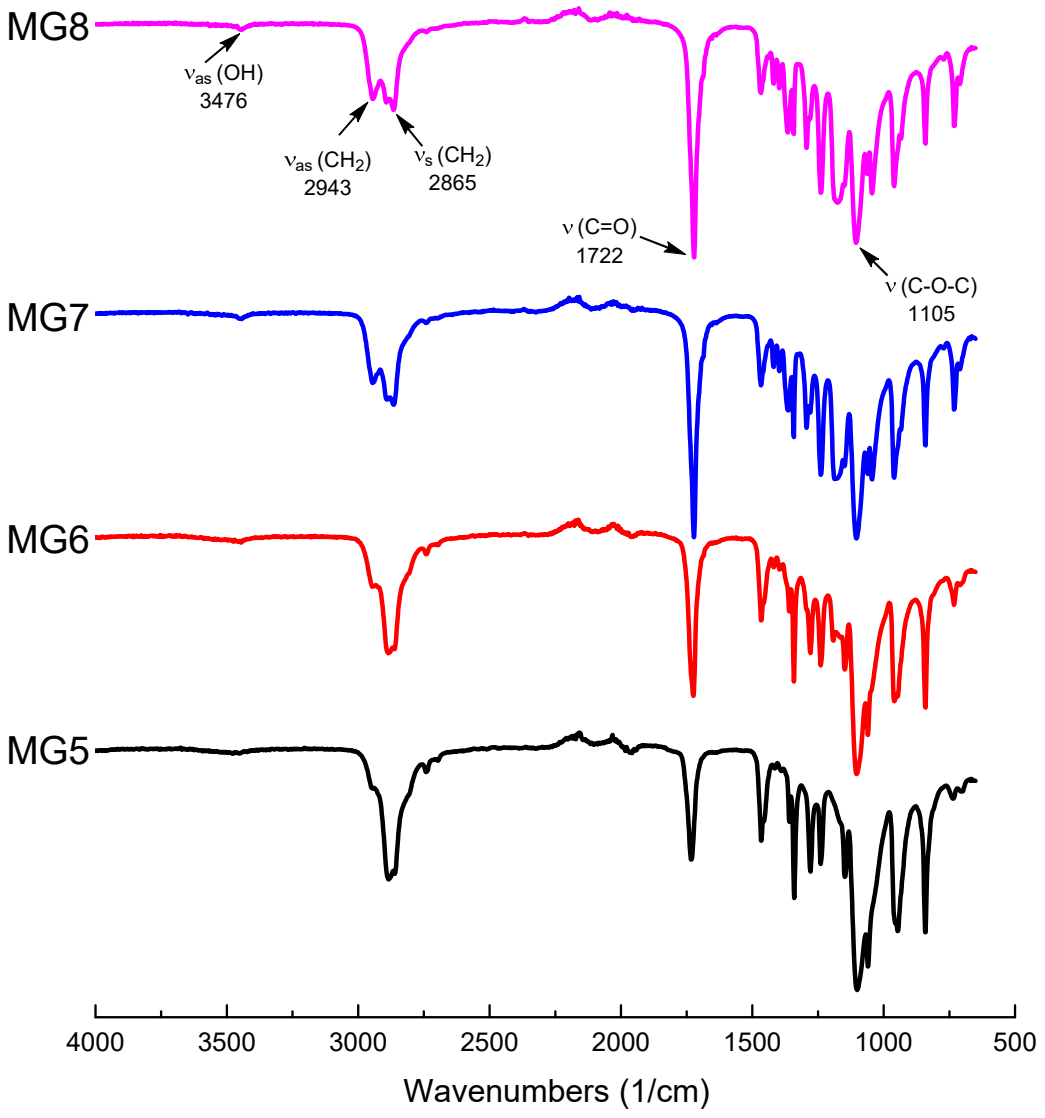

Figure 3-9. FT-IR spectra of mPEG-*b*-poly(εCL-*co*-αClεCL) block copolymers with different molar masses.

The differential scanning calorimetry (DSC) analysis of mPEG-*b*-poly(εCL-*co*-αClεCL) block copolymers with molar masses of 6.6, 10.0, 14.9, and 19.8 kDa demonstrated the melting temperatures of 58.58, 55.54, 55.48, and 50.04 °C, respectively (figure 3-10).

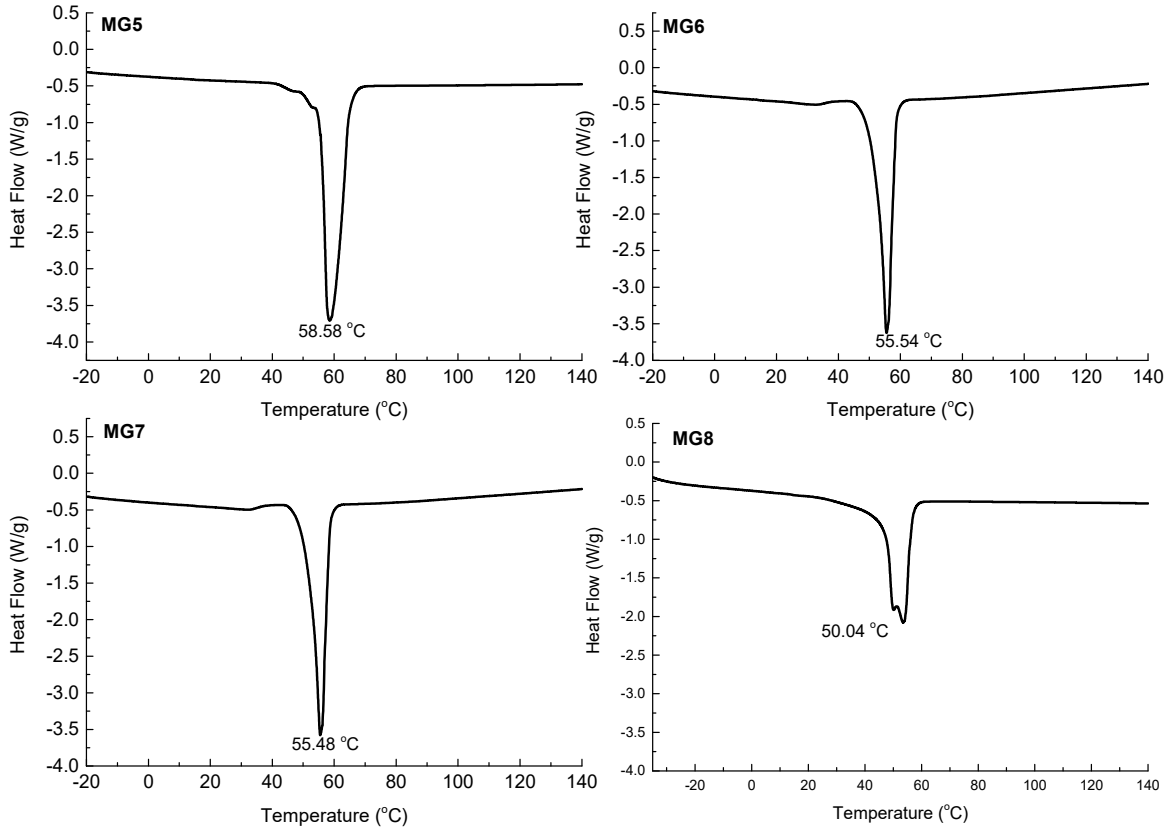

Figure 3-10. DSC of mPEG-*b*-poly(εCL-*co*-αClεCL) block copolymers with different molar masses.

The number average molecular weight (M_n) and PD (polydispersity) were also analysed by size exclusion chromatography (SEC). The shift towards lower elution time of mPEG-*b*-poly(αClεCL) (figure 3-11), and mPEG-*b*-poly(εCL-*co*-αClεCL) (figure 3-12) showed growing molar masses with the increase in feeding ratio of αClεCL and or εCL. The SEC analysis of mPEG-*b*-poly(αClεCL) showed block copolymers with apparent number average molecular weights (M_n) of 11.5, 12.8, 13.7, and 15.5 kDA, and poly dispersities of 1.07, 1.10, 1.24, and 1.16, respectively. Whereas, mPEG-*b*-poly(εCL-*co*-αClεCL) block copolymers showed apparent number average

molecular weights of 12.3, 13.5, 14.5, and 17.7 kDA with polydispersities of 1.11, 1.09, 1.72, and 1.73, respectively.

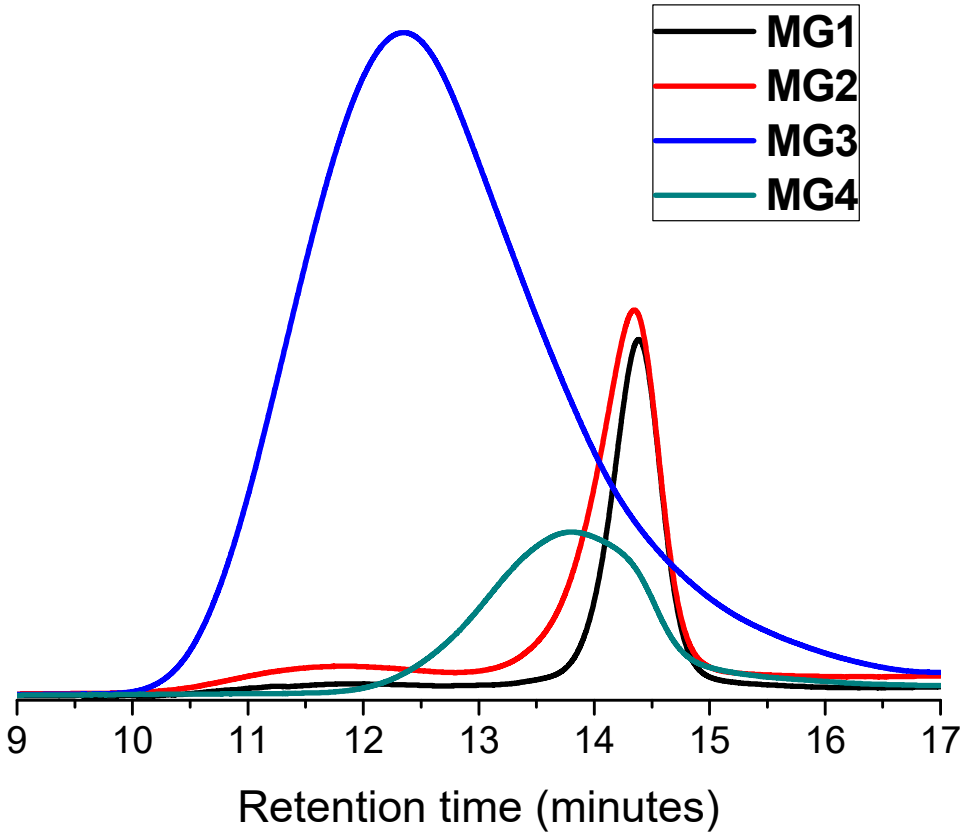

Figure 3-11. Size exclusion chromatography in $CHCl_3$ of mPEG-*b*-poly(αClεCL) block copolymers with different molar masses (PS calibration).

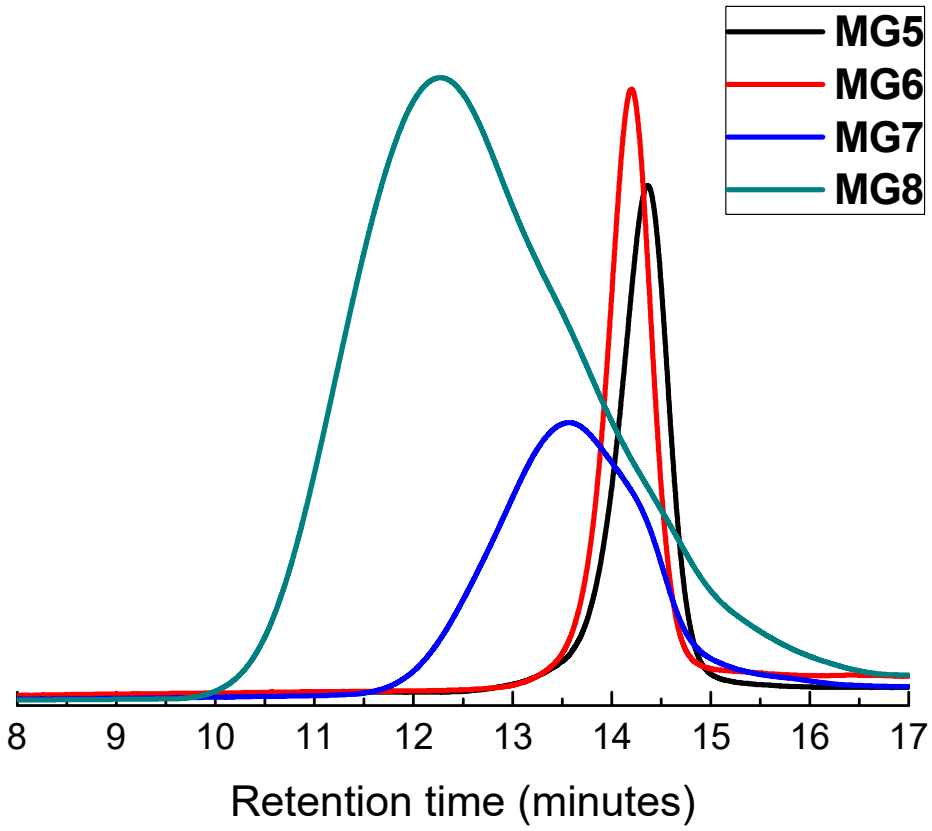

Figure 3-12. Size exclusion chromatography in $CHCl_3$ of mPEG-*b*-poly(εCL-*co*-αClεCL) block copolymers with different molar masses (PS calibration).

3.2.3. Substitution of chloro atoms into azide groups

The pendent chloro atoms of mPEG-*b*-poly(αClεCL) and mPEG-*b*-poly(εCL-co-αClεCL) were converted into azides by a nucleophilic substitution reaction in order to synthesise clickable polyesters. To avoid side reactions and degradation of copolymers, the substitution reaction was performed under mild conditions at room temperature in DMSO, in the presence of sodium azide (scheme 3-5), as reported earlier.[44]

Table 3-1. Characterisation of mPEG-*b*-poly(αClεCL) block-copolymer with various molar masses obtained by ring-opening polymerisation of αClεCL initiated from mPEG.

Entry	M_n (Theoretical) (kDA)	M_n (NMR) (kDA)	M_n (SEC) (kDA)	PD (SEC) (M_w/M_n)	Conversion (NMR) (%)	D_p (αClεCL)	T_m (ºC)	ΔH (J/g)
MG1	7.0	6.8	11.5	1.07	90.1	12	58.35	99.9
MG2	10.0	9.4	12.8	1.10	88.8	30	55.16	78.1
MG3	15.0	14.3	13.7	1.24	93.0	62	54.62	61.5
MG4	20.0	19.4	15.5	1.16	96.0	97	52.86	45.9

The ^{1}H and ^{13}C NMR of mPEG-*b*-poly(αN_3εCL) (figure 3-13 and figure 3-14, respectively) and mPEG-*b*-poly(εCL-co-αN_3εCL) (figure 3-15 and figure 3-16, respectively) revealed the complete conversion of chloro atoms into azides. Specifically, the chemical shifts at 4.27 ppm for the C<u>H</u>-Cl protons in ^{1}H NMR spectra noticeably disappeared in corresponding to a new peak at 3.89 ppm, typical of C<u>H</u>-N_3.

Table 3-2. Characterisation of mPEG-*b*-poly(εCL-*co*-αClεCL) block-copolymers with various molar masses obtained by ring-opening polymerisation of εCL and αClεCL initiated from mPEG.

Entry	M_n (Theoretical) (kDA)	M_n (NMR) (kDA)	M_n (SEC) (kDA)	PD (SEC) (M_w/M_n)	Conversion (NMR) (%)	D_p (εCL)	D_p (αClεCL)	T_m (°C)	ΔH (J/g)
MG5	7.0	6.6	12.3	1.11	80.0	8	5	58.58	146.8
MG6	10.0	10.0	13.5	1.09	100.0	35	7	55.54	100.2
MG7	15.0	14.9	14.5	1.72	99.0	79	6	55.48	65.2
MG8	20.0	19.8	17.7	1.73	98.6	122	6	50.04	92.1

The substitution of chloro atoms of mPEG-*b*-poly(αClεCL) and mPEG-*b*-poly(εCL-co-αClεCL) with azides was also confirmed by FT-IR (figure 3-17, and 3-18, respectively). The IR spectra of amphiphilic block copolymers before and after azide substitution reaction, clearly showed characteristics absorption peaks of PEG, poly(αN_3εCL), and or PCL. In IR spectra, the absorption peak at 1729 cm^{-1} is characteristic of C=O stretching vibrations of the ester carbonyl group, whereas, the absorption band at 1177 cm^{-1} is attributed to the C–O–C stretching vibrations of the repetitive $–OCH_2CH_2$ components of mPEG. All the C–H stretching bonds are confined at 2946

and 2867 cm^{-1}.

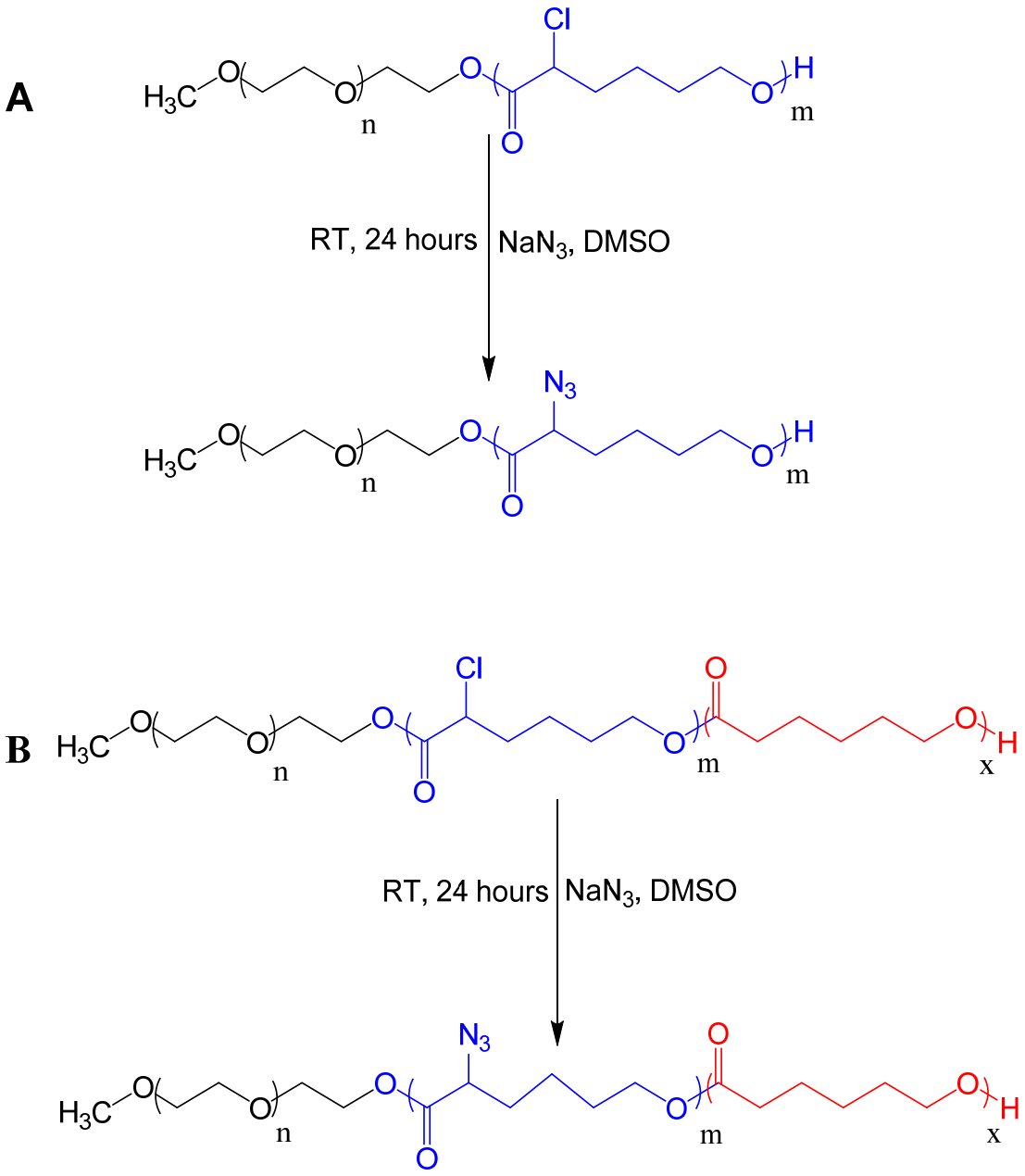

Scheme 3-5. Substitution of chloro atoms into azide groups to obtain (A) mPEG-*b*-poly(αN₃εCL) and (B) mPEG-*b*-poly(εCL-co-αN₃εCL).

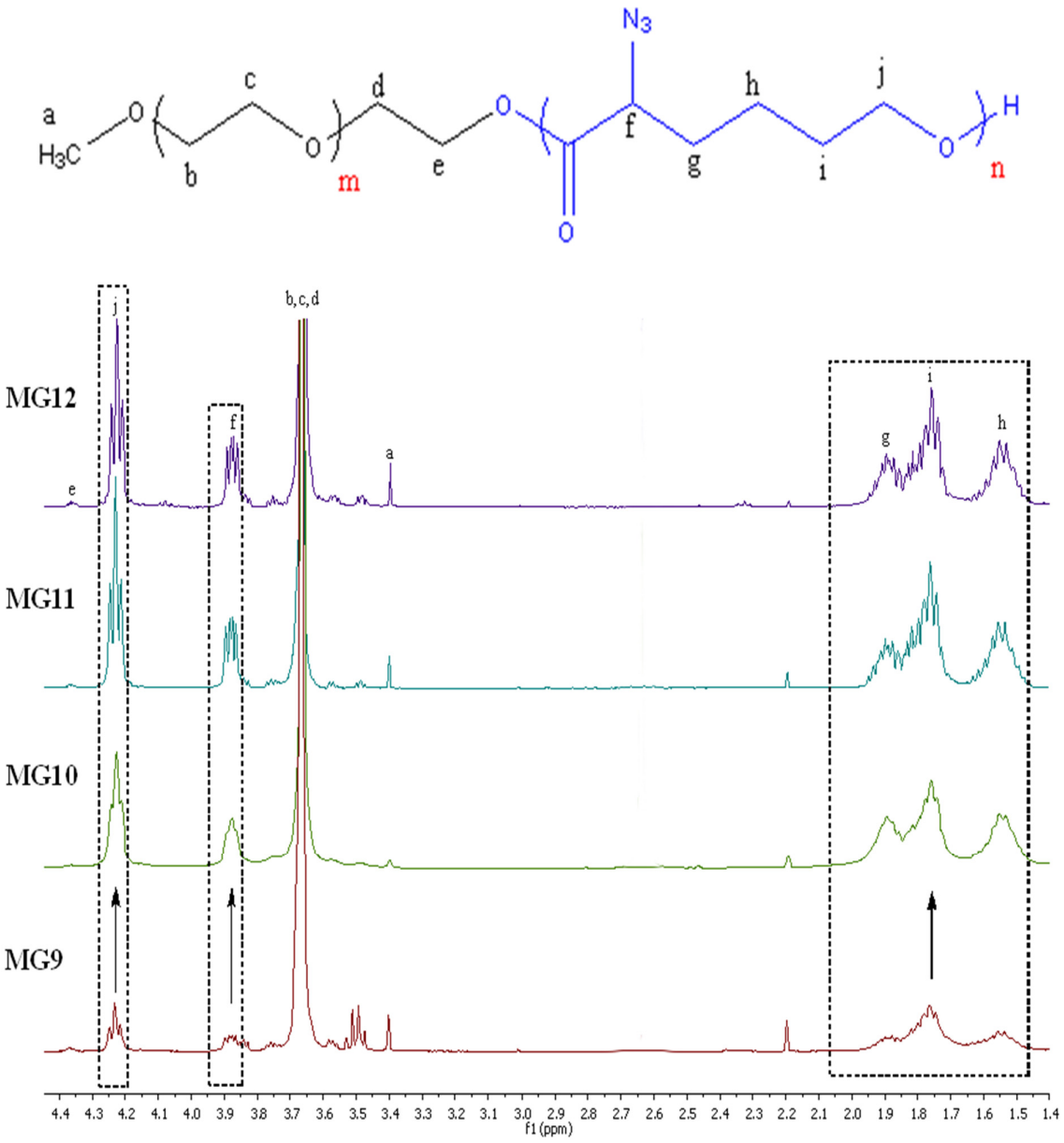

Figure 3-13: ^{1}H NMR spectra of mPEG-*b*-poly(αN$_3$εCL) block copolymers with different molar masses. Arrows showing the increase in signal intensity.

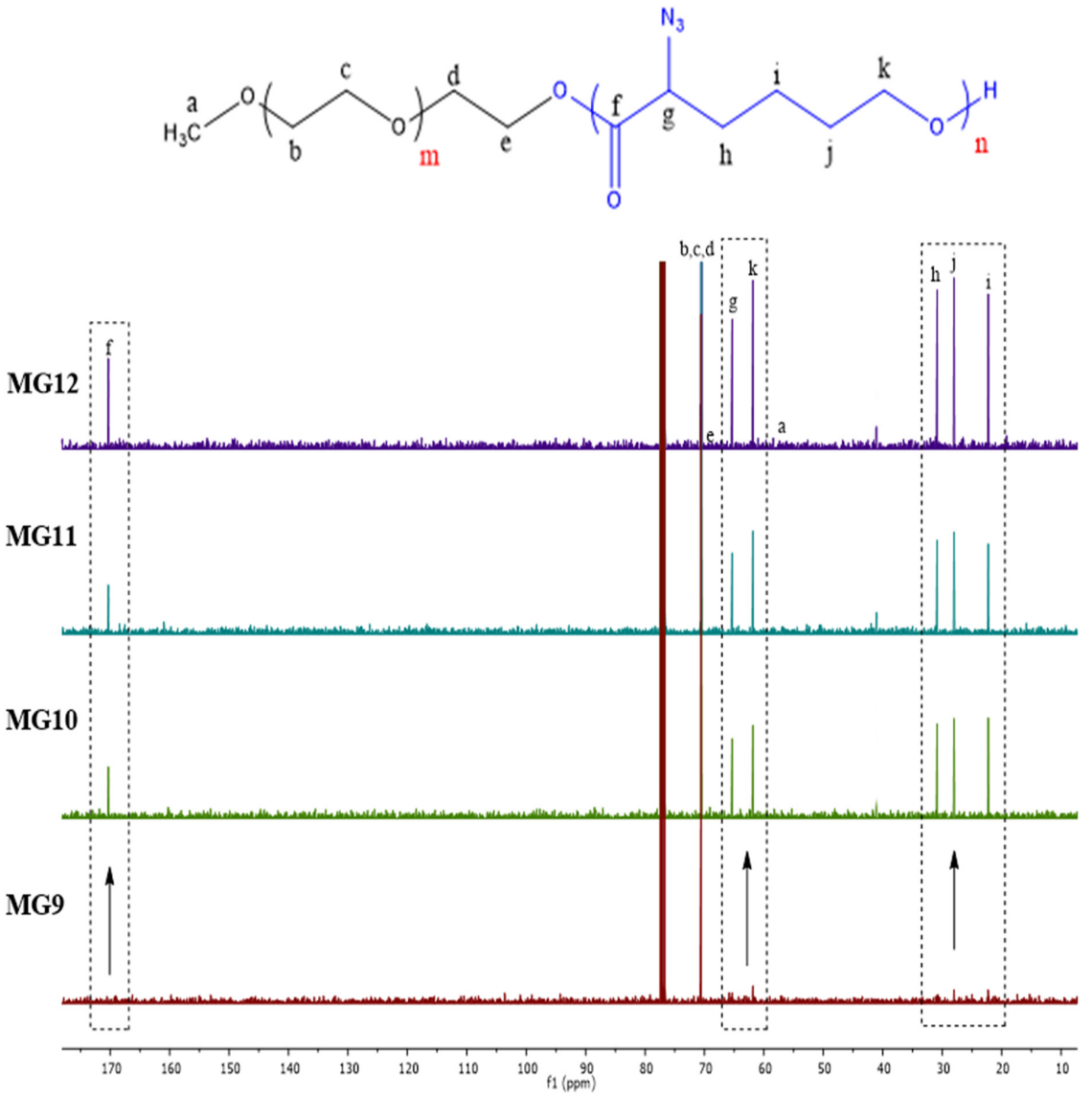

Figure 3-14. ^{13}C NMR spectra of mPEG-*b*-poly(αN_3CL) with various molar masses. ^{13}C NMR spectra were recorded in $CDCl_3$ and arrows indicating the increase in signal intensity.

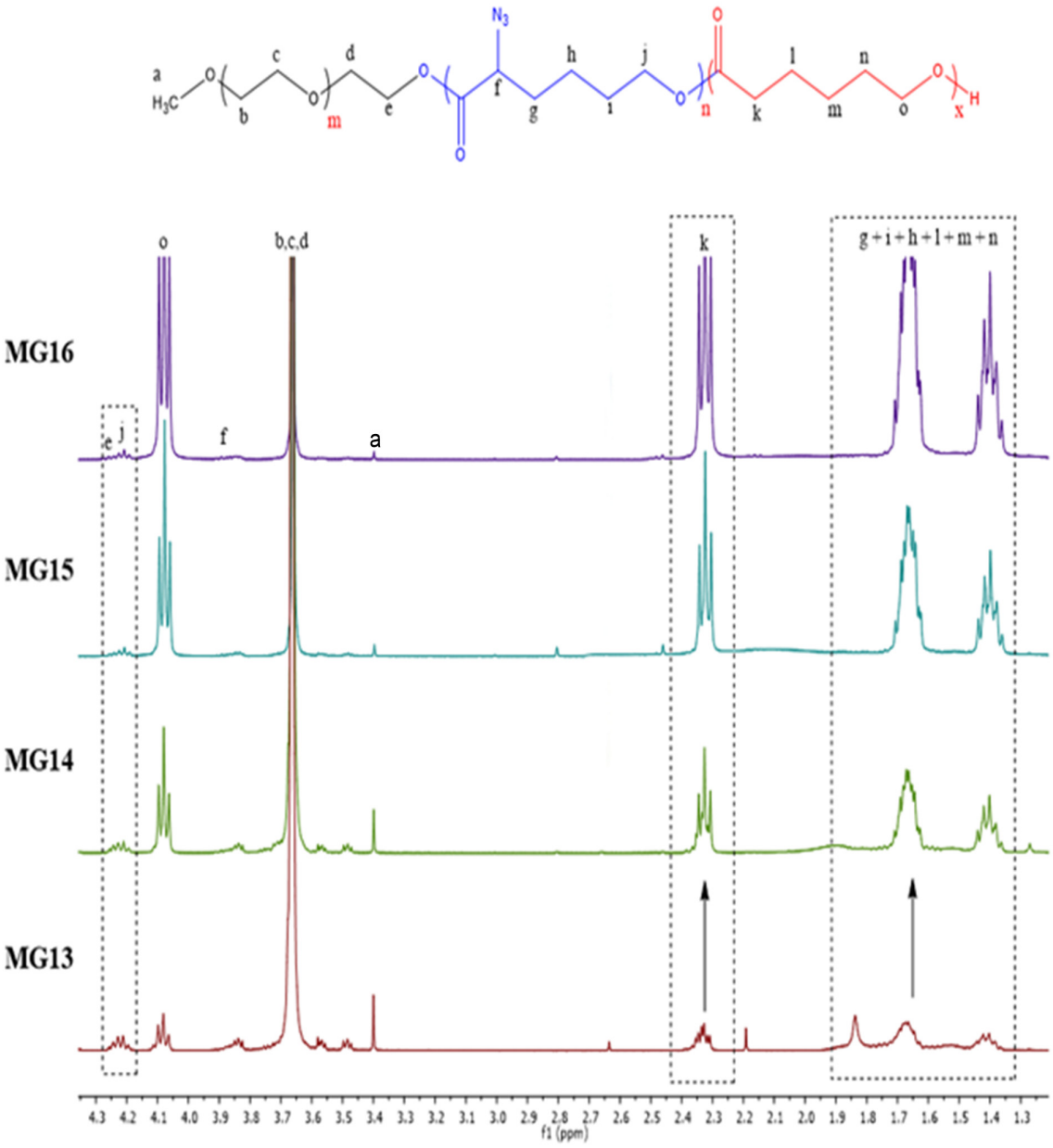

Figure 3-15. ^{1}H NMR spectra of mPEG-*b*-poly(εCL-co-αN$_3$εCL) block copolymers with different molar masses. ^{13}C NMR spectra were recorded in $CDCl_3$ and arrows indicating the increase in signal intensity.

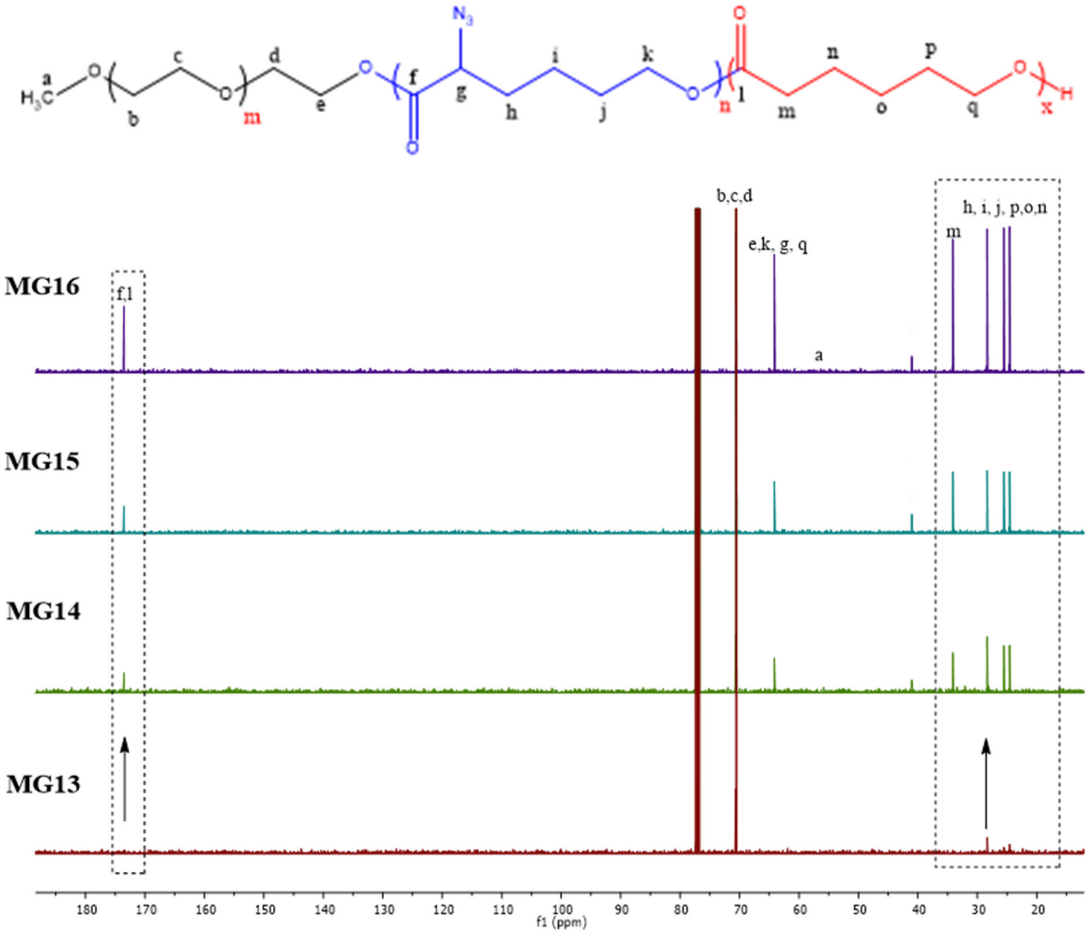

Figure 3-16. ^{13}C NMR spectra of mPEG-*b*-poly(εCL-co-αN$_3$εCL) block copolymer with various molar masses. Arrows showing the increase in signal intensity.

Specifically, the IR spectra of (mPEG-*b*-poly(αN$_3$CL) and mPEG-*b*-poly(εCL-*co*-αN$_3$εCL) expectedly showed a new peak at 2106 cm^{-1}, typical of the azide group. These signals indicated that substitution reaction has been completed without the degradation of the block copolymers.

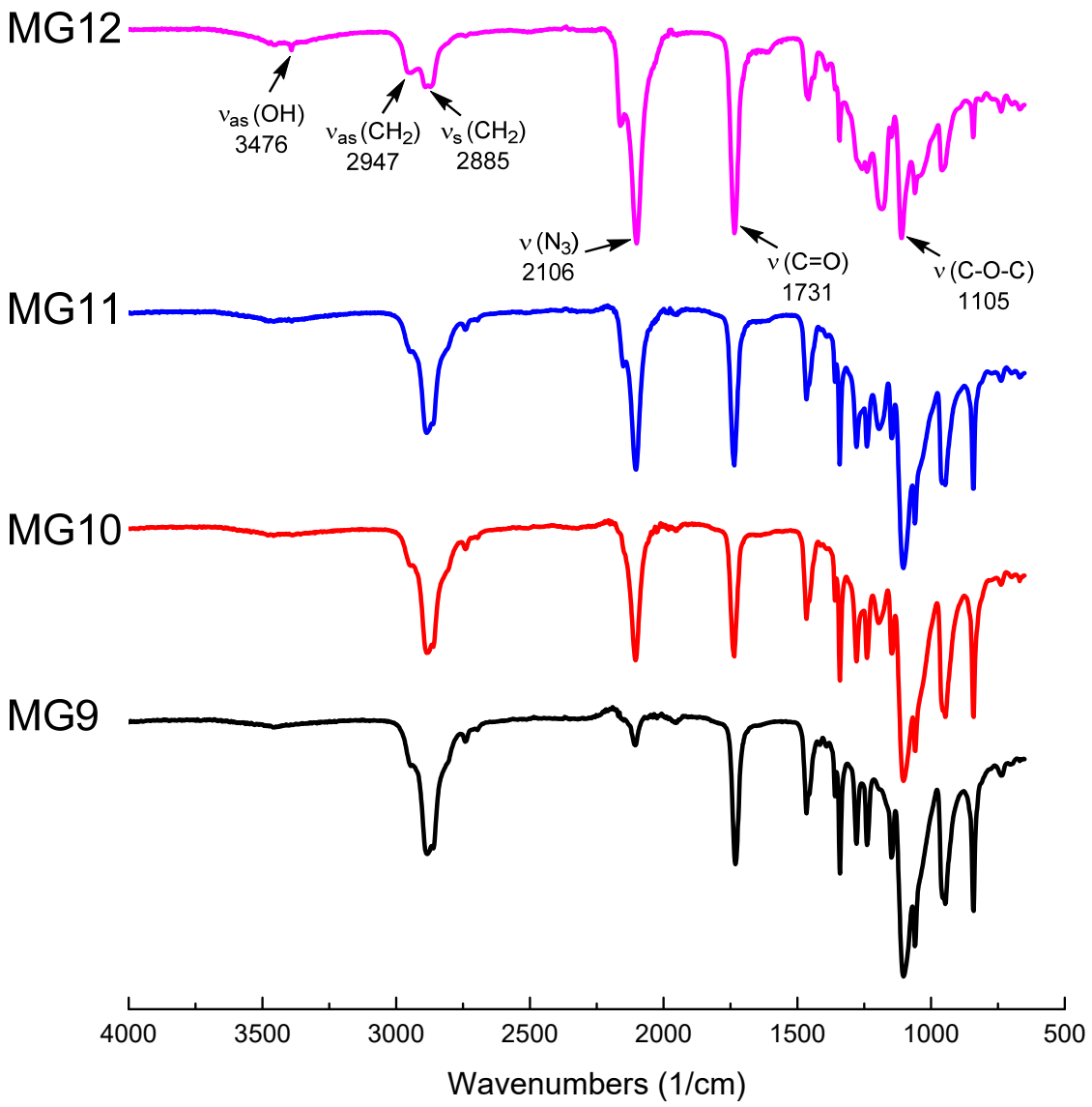

Figure 3-17. FT-IR spectra of mPEG-*b*-poly(αN$_3$CL) block copolymers with different molar masses.

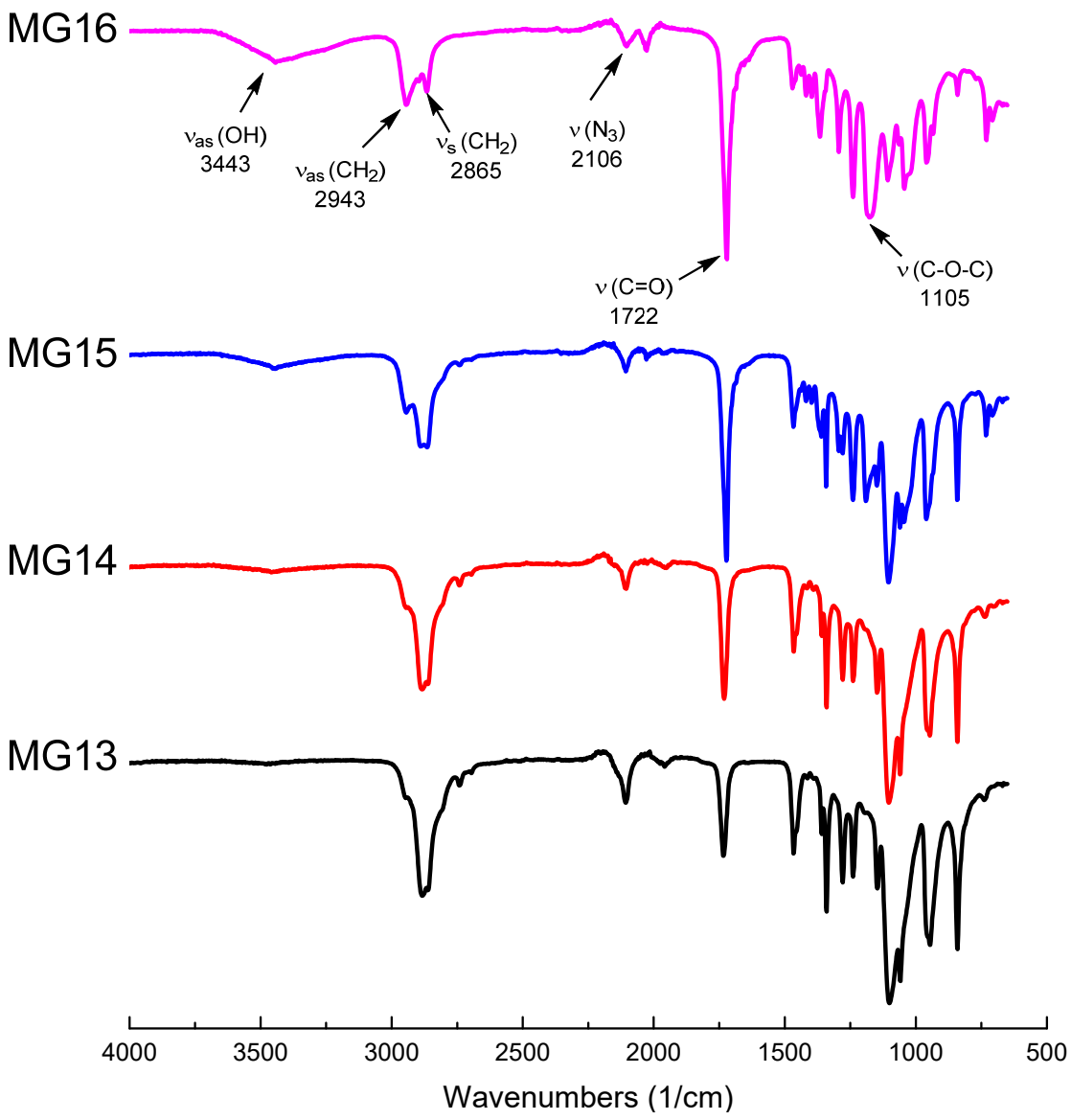

Figure 3-18. FT-IR spectra of mPEG-*b*-poly(εCL-co-αN$_3$εCL) block copolymer with various molar masses. IR absorption peaks at 2106 cm^{-1} represents the azides.

The DSC characterisation of mPEG-*b*-poly(εCL-co-αN$_3$εCL) block copolymer with various molar masses of 6.7, 10.1, 14.9, and 19.8 kDa revealed melting temperatures of 57.65, 57.62, 50.20, and 50.44 °C, respectively (figure 3-19). Whereas, DSC analysis of azide bearing block copolymer

based on mPEG-*b*-poly(αN$_3$CL) with various molar masses of 6.8, 9.6, 14.6, and 20.0 kDA demonstrated melting temperatures of 59.35, 58.89, 56.78, and 49.17 °C, respectively, as shown in figure 3-20.

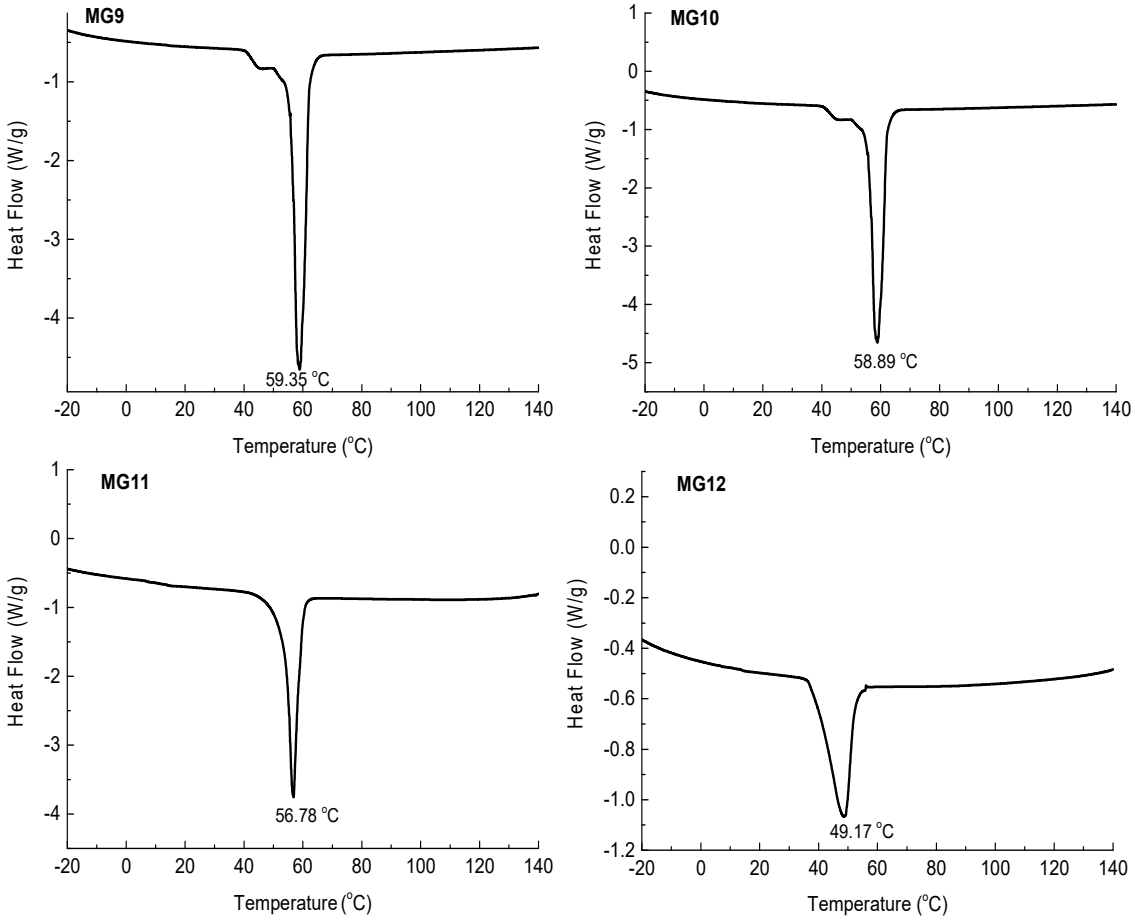

Figure 3-19. DSC analysis of mPEG-*b*-poly(αN$_3$CL) block copolymers with different molar masses.

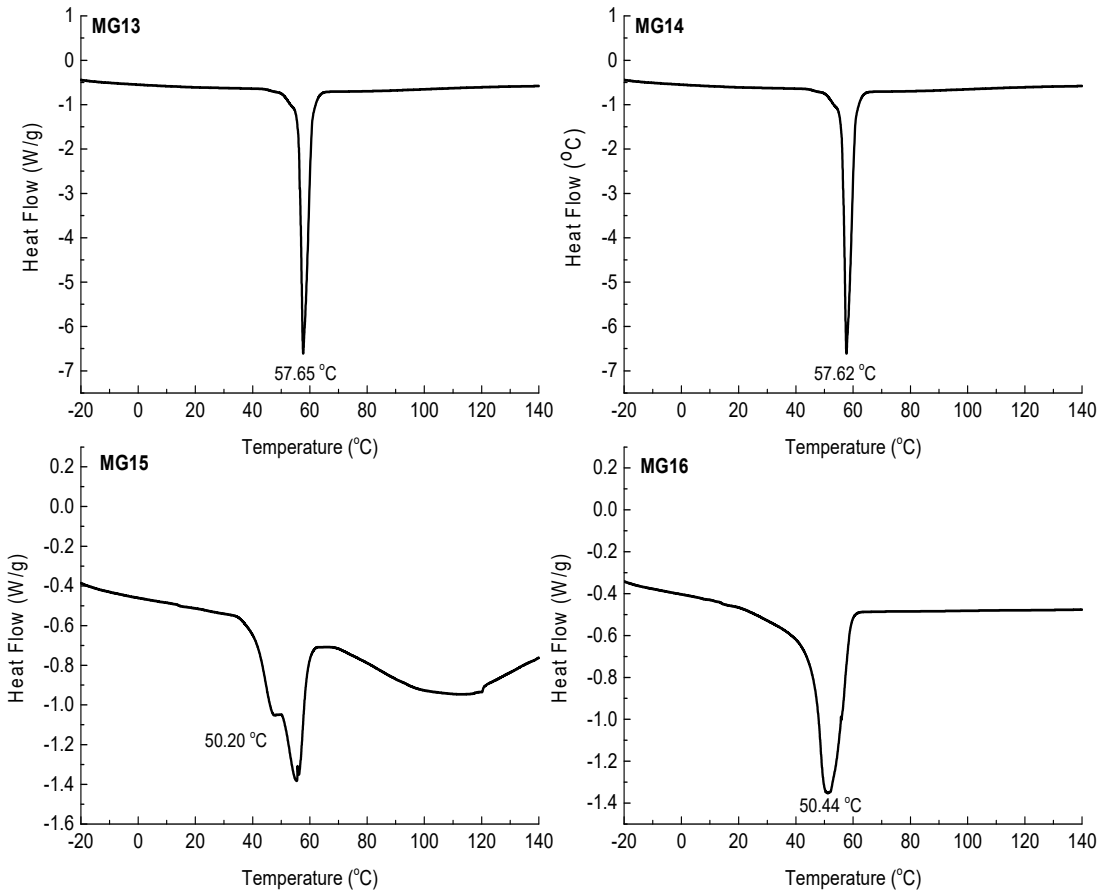

Figure 3-20. DSC of mPEG-*b*-poly(εCL-co-αN$_3$εCL) block copolymer with various molar masses.

Table 3-3. DSC Characterisation of mPEG-*b*-poly(αN$_3$εCL) and mPEG-*b*-poly(εCL-co-αN$_3$εCL) block-copolymers with various molar masses.

Polymer type	Code	T_m (^oC)	ΔH(J/g)
mPEG-*b*-poly(αN$_3$εCL)	MG9	59.35	128.0
	MG10	58.89	88.8
	MG11	56.78	59.7
	MG12	49.17	22.2
mPEG-*b*-poly(εCL-co-αN$_3$εCL)	MG13	57.65	143.1
	MG14	57.62	112.9
	MG15	50.20	66.5
	MG16	50.44	35.5

3.3. DISCUSSION

In this study, a functional lactone (α-chloro-ε-caprolactone) was synthesised from the oxidation of 2-chlorocyclohexanone using 3-chloroperoxybenzoic acid (*m*CPBA) as an oxidising agent via the Baeyer-Villiger reaction. The mechanism of peroxy acid catalysed Baeyer-Villiger oxidation reaction is illustrated in scheme 3-4. The reaction proceeds from the protonation of carbonyl oxygen of 2-chlorocyclohexanone followed by the addition of per-acid to yield a tetrahedral intermediate, which undergoes rearrangement where the R group migrate to the electron deficient oxygen. This is followed by deprotonation. More specifically, the

initial stage is nucleophilic addition of 3-chloroperoxybenzoic acid to the carbonyl group of the 2-chlorocyclohexanone, whereas, in later stages alkyl group migrates to oxygen. The relatively weak oxygen-oxygen bond breaks down in this step generating a 7-membred ring structure i.e. α-chloro-ε-caprolactone. This compound is thus readily synthesised from a commercially available precursor on a large scale and can be kept at -20 °C for few weeks without degradation or substantial loss of ability to polymerise.[46]

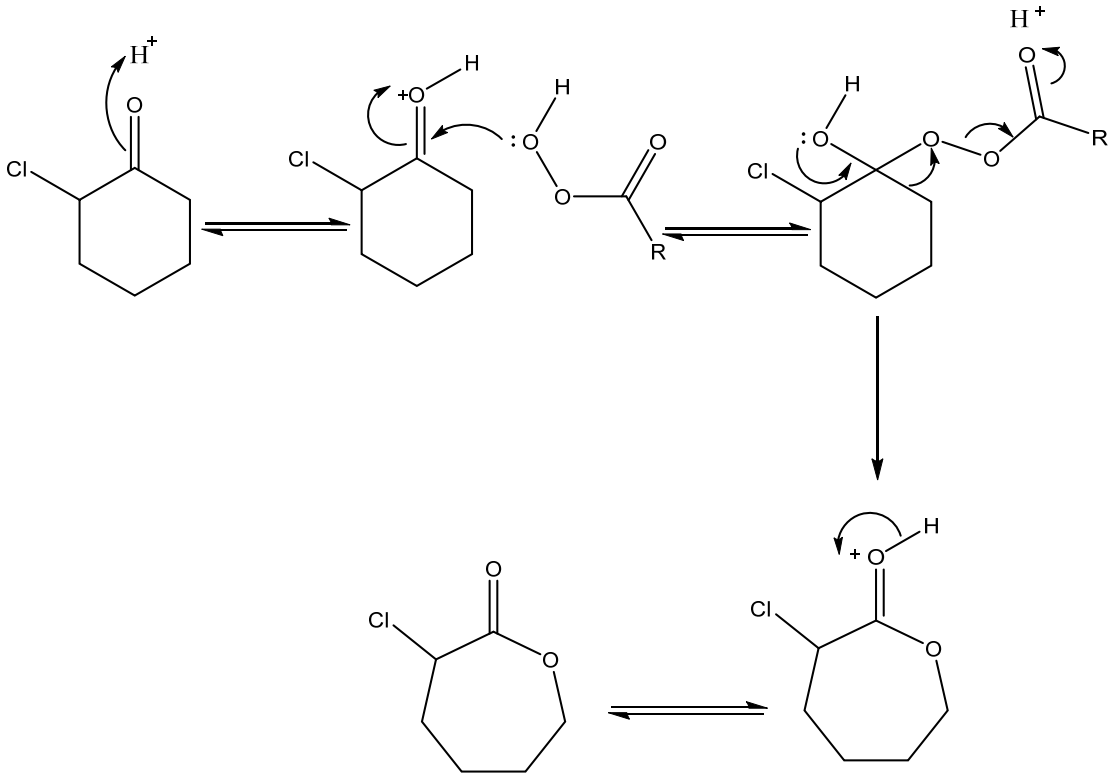

Scheme 3-6. General reaction mechanism for peroxy acid catalysed Baeyer-Villiger oxidation reaction.

It is worth mentioning that functional lactone can also be obtained by direct functionalisation of the commercially available ε-CL monomer. For instance, α-iodo-εCL has been synthesised by anionic activation at alpha-position of ε-CL monomer. The reaction was performed at -78 °C using a non-nucleophilic strong base (lithium diisopropylamide). In a second step, the resulting lithium carbanion was quenched with iodine mono chloride via electrophilic substitution to generate α-iodo-εCL.[47] In a similar approach, α-benzyl carboxy-εCL was also synthesised but the lithium carbanion was quenched with benzyl chloroformate to obtain the functional lactone.[48] However, these reactions resulted into low yield of functionalised caprolactone probably due to the formation of side products by transesterification or by anionic polymerisation of caprolactone.

The functional moieties can also be introduced into the polyesters by post-polymerisation functionalisation.[1,32,33] However, the possibility of side reactions decreases the applicability of this route. To synthesise the functional polyesters, a commonly used technique is to polymerise a functional monomer via polycondensation, ring opening, or enzymatic polymerisation.[34-36] Functional lactone monomer (α-chloro-ε-caprolactone) can easily be purified by fractional distillation, column chromatography or by recrystallisation, it is a good monomer for the ring-opening polymerisation in functional polyesters.[36-39]

The synthesised α-chloro-ε-caprolactone monomer was used as a co-monomer to generate functional amphiphilic block copolymers of mPEG-*b*-

poly(αClεCL) and mPEG-*b*-poly(εCL-co-αClεCL) via ring opening polymerisation using stannous octoate as a catalyst. Ring-opening polymerisation has extensively been used for the synthesis of polyesters from lactones or lactides.[49] The ring-opening polymerisation could be initiated by various mechanisms i.e. anionic, cationic, and coordination insertion polymerisation, depending on the type of initiator.[50] The stannous octoate [$Sn(Oct)_2$] or Tin(II) 2-ethylhexanoate is most extensively investigated catalyst for ring opening polymerisation of lactones and lactides. It has been approved by the Food and Drug Administration (FDA) to be use as a food additive.

For the synthesis of block copolymers with mPEG as a first block, the ring opening polymerisation of lactones using stannous octoate as a catalysts can be performed by using mPEG-OH as initiator.[51] It is admitted that this polymerisation follows a coordination-insertion mechanism. In this mechanism, the alcohol initiator (e.g. PEG) is thought to first react with the stannous octoate to form a tin alkoxide initiating complex by ligand exchange (scheme 3-7). In the next step, the exocyclic carbonyl oxygen atom of the lactone monomer coordinates with the tin atom of the tin alkoxide. In the later stage, acyl-oxygen bond of the lactone is broken, opening the chain of lactone ring to insert into the tin-oxygen bond. The propagation is proceeded by an identical mechanism and continues as additional lactone units are inserted into the tin-oxygen bond.[49, 52]

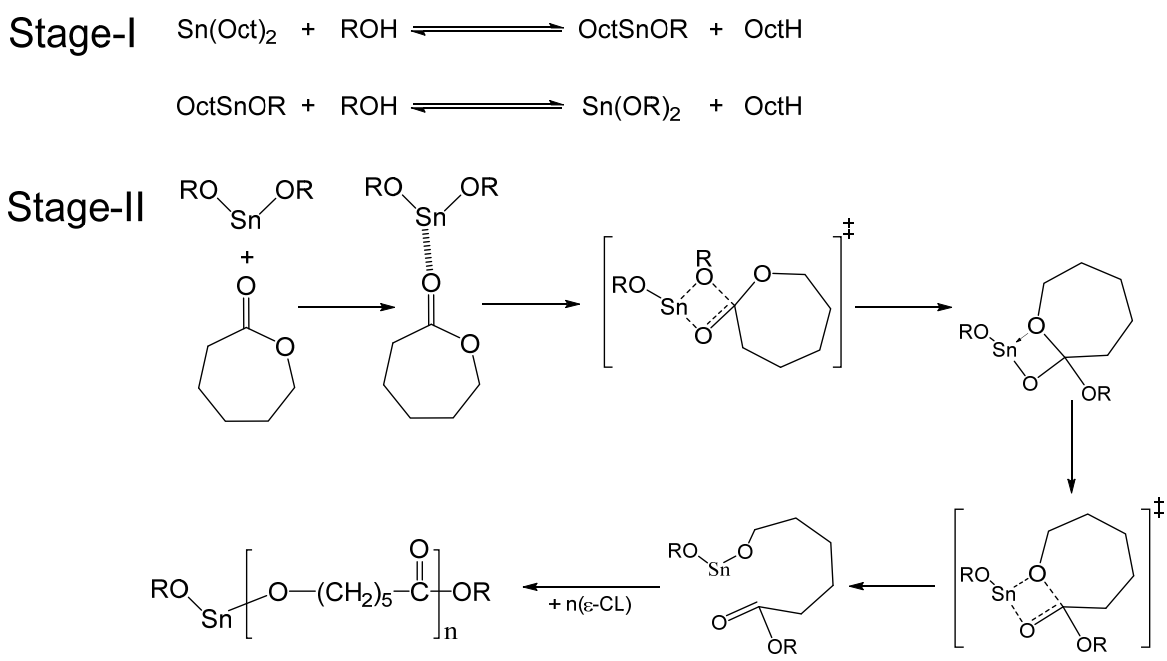

Scheme 3-7. Coordination-insertion mechanism of ring opening polymerisation of εCL initiated by tin (II) alkoxide.

It has already been reported that mPEG macro-initiator (5000 kDA molar mass), when copolymerised with εCL, resulted into 'stealth' micelles with spherical morphology.[53] Therefore, in this study, mPEG having molar mass of 5000 g mol^{-1} was chosen as an initiator. To generate amphiphilic block copolymers with various architecture and different molecular weights, the molar feed ratio of mPEG was kept constant and the feeding quantity of caprolactone based monomers was adjusted to attain various degrees of polymerisation of αClεCL and or εCL to generate functional block copolymers.

The NMR and FTIR spectroscopic analysis showed all the characteristic peaks that confirmed the formation of block copolymers with good

quantitative conversion. For all the amphiphilic block copolymers, unimodal molecular weight distributions were observed in the SEC chromatograms. The narrow polydispersities and the absence of residual mPEG indicated the quantitative initiation as also have been reported previously.[41] However, block copolymers of mPEG-*b*-poly(αClεCL) (MG3 and MG4) and mPEG-*b*-poly(εCL-*co*-αClεCL) (MG7, and MG8) with higher molecular weights, showed a clear broadening of the SEC chromatograms which is an indication that some transesterification reactions are occurring in these cases. Nevertheless, no trace of un-reacted mPEG macro-initiator was observed by SEC showing the complete initiation of the lactone polymerisation by the macro-initiator.

After synthesis of mPEG-*b*-poly(αClεCL) and mPEG-*b*-poly(εCL-co-αClεCL) amphiphilic block copolymers with various molar masses, their chloro atoms were substituted with azides via nucleophilic substitution reaction to obtain clickable block copolymers. The reaction was carried out under mild conditions using NaN_3 as an azide source. The nucleophilic substitution reactions in polymer-halide proceed by the attack of a nucleophile (e.g. azide ion) on the electrophilic α-carbon from the side opposite to halogen. This initiates a covalent bond formation between the nucleophilic azide and the α-carbon, and as a result, carbon-halogen bond weakens and stretches. The halogen atom eventually leaves as an anion and reacts with the cation to form its related salt as a by-product.[54] This nucleophilic substitution is thought to be S_N2 type reaction, where formation and breaking of bonds

take place simultaneously in one step.[55] Various aliphatic polyesters have been functionalised using this nucleophilic substitution reaction, previously.[56] [44]

It is also worth pointing that chloro atoms of functional monomer (αClεCL) could easily be converted into azide groups,[45] however, degradation of monomer and the safety concerns of azide bearing organic compounds (high reaction temperature in tin octoate catalysed ring-opening polymerisation) limits the use of the azide bearing monomer. Therefore, the substitution reaction was performed after the synthesis of block copolymers. The synthesised azide bearing block copolymers based on mPEG-*b*-poly(αN_3εCL) and mPEG-*b*-poly(εCL-co-αN_3εCL) showed strong signals relating to the presence of the azide moiety in both NMR and IR spectra, revealing the complete conversion of Cl into N_3 without any apparent degradation of polyester backbone, as also reported previously.[57]

These functional amphiphilic block copolymers with various architectures and different degree of polymerisation can have various biomedical applications. For instance, multiple azide units of block copolymers offer an opportunity to crosslink the micelles core using click reaction.[58] Moreover, alkyne functionalised or alkyne bearing molecules of therapeutic importance or fluorescence tags can be grafted on the hydrophobic backbone. Furthermore, azide units of block copolymers can be reduced into amines to directly graft the anticancer drugs or other therapeutic molecules.

3.4. CONCLUSIONS

In this work, a functional caprolactone (α-chloro-ε-caprolactone) was synthesised as a precursor of functional amphiphilic block copolymers. The ring opening polymerisation of the functional lactone monomer was carried out by using PEG-OH as initiator to generate amphiphilic block copolymers based on mPEG-*b*-poly(αClεCL) and mPEG-*b*-poly(εCL-*co*-αClεCL) comprising various molar masses. The characterisation data revealed good quantitative conversion of monomers generating amphiphilic block copolymers of predictable molecular weights and narrow polydispersity with limited transesterification. In a second step, pendent chloro groups of amphiphilic block copolymers were substituted by azides via nucleophilic substitution reaction. The functional amphiphilic block copolymers based on mPEG-*b*-poly(αN_3εCL) and mPEG-*b*-poly(εCL-*co*-αN_3CL) comprising various molar masses can be used as precursors of reactive polymeric nano-carriers.

3.5. EXPERIMENTAL

3.5.1. Synthesis of α-chloro-ε-caprolactone

The αClεCL monomer was synthesised from the oxidation of 2-chlorocyclohexanone with *m*-chloroperoxybenzoic acid (mCPBA). Briefly, 2-chlorocyclohexanone (5 g, 37.5 mmol) was dissolved in 50 mL dichloromethane in a round bottom glass flask and the solution was cooled to 0 °C using an ice bath. Afterwards, 10 g (40.5 mmol) of mCPBA was carefully introduced into the reaction mixture within 10 minutes. The reaction mixture was stirred at room temperature for 96h, and was subsequently cooled to -20 °C. After filtration, the filtrate was washed with saturated solutions of $Na_2S_2O_3$ (3 X 100 mL), $NaHCO_3$ (3 X 100 mL) and brine (100 mL). Finally, the organic phase was washed with deionised water (3 X 100 mL). After drying over magnesium sulphate, the organic phase was filtered again, and the organic solvent was removed by rotary evaporator to obtain a pale viscous liquid. Finally, the product was purified by silica gel column chromatography with solvents of analytical purity as mobile phase (hexane: ethyl acetate 9:2, R_f 0.36) to obtain α-chloro-ε-caprolactone (3.50 g, 70% yield, pale viscous liquid).

^{1}H NMR (400 MHz, $CDCl_3$) δ (ppm) 4.85-4.81 (COC<u>H</u>Cl, m, 1H), 4.69-4.63 ($CH_2C\underline{H}_2O$, m, 1H), 4.29-4.23 ($CH_2C\underline{H}_2O$, m, 1H), 2.23-1.77 ($ClCHC\underline{H}_2C\underline{H}_2C\underline{H}_2$, m, 6H). ^{13}C NMR (101 MHz, $CDCl_3$) δ 170.06 (<u>C</u>=O),

69.52 ($CH_2\underline{C}H_2O$), 58.54 ($CO\underline{C}HCl$), 32.55 ($ClCH\underline{C}H_2CH_2CH_2$), 28.70($ClCHCH_2CH_2\underline{C}H_2$), 24.98 ($ClCHCH_2\underline{C}H_2CH_2$).

3.5.2. Synthesis of mPEG-*b*-poly(αClεCL)

Amphiphilic block copolymers based on mPEG-*b*-poly(αClεCL) were synthesised by the ring opening polymerisation of αClεCL initiated by mPEG using stannous octoate as a catalyst. A series of mPEG-*b*-poly(αClεCL) block copolymers was synthesised, where the molar mass of mPEG was kept constant (5000 DA) and molar mass of poly(αClεCL) was targeted to 2000, 5000, 10000, and 15000 DA (at 100% conversion, theoretically). For this, the ratios of mPEG: αClεCL in the reaction mixture were 1:13, 1:34, 1:67, and 1:101, respectively (table 3-4). Briefly, mPEG and αClεCL were dissolved in anhydrous toluene and dried by azeotropic distillations (3 times) in a glass reactor. Afterwards, the reaction mixture was purged with nitrogen before adding $SnOct_2$ (1.5 wt % in CH_2Cl_2) via a glass syringe. The CH_2Cl_2 was removed by purging with nitrogen gas and the reaction was stirred at 100 °C for 24 hours. Finally, the polymers were recovered by precipitation in diethyl ether and characterised by GPC, NMR, FTIR and DSC. Data were compared with the previously reported results.[51, 57]

Table 3-4. Ingredients for ring-opening polymerisation to synthesise mPEG-*b*-poly(αClεCL) with various molecular weights. I ~ initiator (mPEG, 5000 g/mol), M ~ monomer (αClεCL, 148.46 g/mol).

Polymer	Code	Reagents (mmol)			Molar ratio (I:M)
		mPEG (I)	αClεCL (M)	Stannous octoate	
mPEG-*b*-poly(αClεCL)	MG1	0.100	1.347	0.013	1:13
	MG2	0.100	3.367	0.034	1:34
	MG3	0.100	6.730	0.067	1:67
	MG4	0.100	10.100	0.100	1:101

MG1:

M_n = 6.8 kDa (^{1}H NMR). ^{1}H NMR (400 MHz, $CDCl_3$) δ (ppm) 4.35 (C$\underline{H}_2$–O–CO, t, 2H), 4.27 (CO–C$\underline{H}$(Cl)–CH_2–CH_2–CH_2–CH_2–O–, m, 12H), 4.21 (CO–CH(Cl)–CH_2–CH_2–CH_2–C$\underline{H}_2$–O–, m, 24H), 3.66 (O–C$\underline{H}_2$–C$\underline{H}_2$–O–, m, 586H), 3.40 (C$\underline{H}_3$–O–, s, 3H), 2.0 (CO-CH(Cl)–C$\underline{H}_2$–CH_2–CH_2–CH_2–O–, m, 24H), 2.12-1.28, (CO–CH(Cl)–C$\underline{H}_2$–C$\underline{H}_2$–C$\underline{H}_2$–CH_2–O–, m, 48H). ^{13}C NMR (101 MHz, $CDCl_3$) δ (ppm) 169.45 (C=O), 70.57 (-O–C$\underline{H}_2$–C$\underline{H}_2$–O–), 65.50 (CO–CH(Cl)–CH_2–CH_2–CH_2–C$\underline{H}_2$–O–), 57.04 (CO–C$\underline{H}$(Cl)–CH_2–CH_2–CH_2–CH_2–O–), 34.27 (CO-CH(Cl)–C$\underline{H}_2$–CH_2–CH_2–CH_2–O–), 27.75 (CO-CH(Cl)–CH_2–

CH_2–$\underline{C}H_2$–CH_2–O–), 22.42 (CO-CH(Cl)–CH_2–$\underline{C}H_2$–CH_2–CH_2–O–). IR: ν max/cm^{-1}: 1105 (C-O-C stretching), 1731 (C=O stretching), 2885 (symmetric CH_2 stretching), 2947 (asymmetric CH_2 stretching) 3476 (OH stretching). T_m (DSC) = 58.35 °C.

MG2:

M_n = 9.4 kDa (^{1}H NMR). ^{1}H NMR (400 MHz, $CDCl_3$) δ (ppm) 4.35 (C$\underline{H}_2$–O–CO, t, 2H), 4.27 (CO–C$\underline{H}$(Cl)–CH_2–CH_2–CH_2–CH_2–O–, m, 30H), 4.21 (CO–CH(Cl)–CH_2–CH_2–CH_2–C$\underline{H}_2$–O–, m, 60H), 3.66 (O–C$\underline{H}_2$–C$\underline{H}_2$–O–, m, 575H), 3.40 (C$\underline{H}_3$–O–, s, 3H), 2.0 (CO-CH(Cl)–C$\underline{H}_2$–CH_2–CH_2–CH_2–O–, m, 60H), 2.12-1.28 and, CO–CH(Cl)–C$\underline{H}_2$–C$\underline{H}_2$–C$\underline{H}_2$–CH_2–O–, m, 120H). ^{13}C NMR (101 MHz, $CDCl_3$) δ (ppm) 169.45 (C=O), 70.57 (-O–$\underline{C}H_2$–$\underline{C}H_2$–O–), 65.50 (CO–CH(Cl)–CH_2–CH_2–CH_2–$\underline{C}H_2$–O–), 57.04 (CO–$\underline{C}$H(Cl)–CH_2–CH_2–CH_2–CH_2–O–), 34.27 (CO-CH(Cl)–$\underline{C}H_2$–CH_2–CH_2–CH_2–O–), 27.75 (CO-CH(Cl)–CH_2–CH_2–$\underline{C}H_2$–CH_2–O–), 22.42 (CO-CH(Cl)–CH_2–$\underline{C}H_2$–CH_2–CH_2–O–). IR: ν max/cm^{-1}: 1105 (C-O-C stretching), 1731 (C=O stretching), 2885 (symmetric CH_2 stretching), 2947 (asymmetric CH_2 stretching) 3476 (OH stretching). T_m (DSC) = 55.16 °C.

MG3:

M_n = 14.3 kDa (^{1}H NMR). ^{1}H NMR (400 MHz, $CDCl_3$) δ (ppm) 4.35 (C$\underline{H}_2$–O–CO, t, 2H), 4.27 (CO–C$\underline{H}$(Cl)–CH_2–CH_2–CH_2–CH_2–O–, m, 62H), 4.21 (CO–CH(Cl)–CH_2–CH_2–CH_2–C$\underline{H}_2$–O–, m, 124H), 3.66 (O–C$\underline{H}_2$–C$\underline{H}_2$–O–, m, 544H), 3.40 (C$\underline{H}_3$–O–, s, 3H), 2.0 (CO-CH(Cl)–C$\underline{H}_2$–CH_2–CH_2–CH_2–O–, m, 124H), 2.12-1.28 and, CO–CH(Cl)–C$\underline{H}_2$–C$\underline{H}_2$–C$\underline{H}_2$–CH_2–O–, m, 248H). ^{13}C

NMR (101 MHz, $CDCl_3$) δ (ppm) 169.45 (C=O), 70.57 (-O–$\underline{C}H_2$–$\underline{C}H_2$–O–), 65.50 (CO–CH(Cl)–CH_2–CH_2–CH_2–$\underline{C}H_2$–O–), 57.04 (CO–$\underline{C}$H(Cl)–CH_2–CH_2–CH_2–CH_2–O–), 34.27 (CO-CH(Cl)–$\underline{C}H_2$–CH_2–CH_2–CH_2–O–), 27.75 (CO-CH(Cl)–CH_2–CH_2–$\underline{C}H_2$–CH_2–O–), 22.42 (CO-CH(Cl)–CH_2–$\underline{C}H_2$–CH_2–CH_2–O–). IR: ν max/cm^{-1}: 1105 (C-O-C stretching), 1731 (C=O stretching), 2885 (symmetric CH_2 stretching), 2947 (asymmetric CH_2 stretching) 3476 (OH stretching). T_m (DSC) = 54.62 °C.

MG4:

M_n = 19.4 kDa (^{1}H NMR). ^{1}H NMR (400 MHz, $CDCl_3$) δ (ppm) 4.35 (C$\underline{H}_2$–O–CO, t, 2H), 4.27 (CO–C$\underline{H}$(Cl)–CH_2–CH_2–CH_2–CH_2–O–, m, 97H), 4.21 (CO–CH(Cl)–CH_2–CH_2–CH_2–C$\underline{H}_2$–O–, m, 194H), 3.66 (O–C$\underline{H}_2$–C$\underline{H}_2$–O–, m, 577H), 3.40 (C$\underline{H}_3$–O–, s, 3H), 2.0 (CO-CH(Cl)–C$\underline{H}_2$–CH_2–CH_2–CH_2–O–, m, 194H), 2.12-1.28 and, CO–CH(Cl)–C$\underline{H}_2$–C$\underline{H}_2$–C$\underline{H}_2$–CH_2–O–, m, 388H). ^{13}C NMR (101 MHz, $CDCl_3$) δ (ppm) 169.45 (C=O), 70.57 (-O–$\underline{C}H_2$–$\underline{C}H_2$–O–), 65.50 (CO–CH(Cl)–CH_2–CH_2–CH_2–$\underline{C}H_2$–O–), 57.04 (CO–$\underline{C}$H(Cl)–CH_2–CH_2–CH_2–CH_2–O–), 34.27 (CO-CH(Cl)–$\underline{C}H_2$–CH_2–CH_2–CH_2–O–), 27.75 (CO-CH(Cl)–CH_2–CH_2–$\underline{C}H_2$–CH_2–O–), 22.42 (CO-CH(Cl)–CH_2–$\underline{C}H_2$–CH_2–CH_2–O–). IR: ν max/cm^{-1}: 1105 (C-O-C stretching), 1731 (C=O stretching), 2885 (symmetric CH_2 stretching), 2947 (asymmetric CH_2 stretching) 3476 (OH stretching). T_m (DSC) = 52.86 °C.

3.5.3. Synthesis of mPEG-*b*-poly(εCL-*co*-αClεCL)

A series of block copolymers based on mPEG-*b*-poly(εCL-*co*-αClεCL) was synthesised, where molar masses of mPEG and poly(αClεCL) were kept constant (5000 and 1040 DA, respectively) and molar mass of poly(εCL) was targeted to 960, 3960, 8960., and 13960 DA (at 100% conversion, theoretically). For this, the molar feed ratios of mPEG: εCL: αClεCL in the reaction mixture was 1:8:7, 1:35:7, 1:78:7, and 1:122:7, respectively (table 3-5).

Briefly, mPEG and αClεCL were dissolved in anhydrous toluene and dried by azeotropic distillations (3 times) in a glass reactor. Afterwards, εCL was introduced via a rubber septum using a glass syringe and the mixture was heated to 50 °C and stirred for 15 minutes, until a homogeneous mixture was obtained. $SnOct_2$ 0.06 M (1.5 wt % in CH_2Cl_2) was finally introduced (under nitrogen) and the reaction was stirred at 100 °C for 24 hours. Finally, the copolymers were precipitated in anhydrous diethyl ether. The synthesised copolymers were characterised by ^{1}H NMR, SEC, and FT-IR spectroscopy.

MG5:

M_n = 6.6 kDa (^{1}H NMR). ^{1}H NMR (400 MHz, $CDCl_3$) δ (ppm) 4.35 (C$\underline{H}_2$–O–CO, t, 2H), 4.27 (CO–C$\underline{H}$(Cl)–CH_2–CH_2–CH_2–CH_2–O–, m, 5H), 4.21 (CO–CH(Cl)–CH_2–CH_2–CH_2–C$\underline{H}_2$–O–, m, 10H), 4.08 (CO–CH_2–CH_2–CH_2–CH_2–C$\underline{H}_2$–O–H, m, 16H), 3.66 (O–C$\underline{H}_2$–C$\underline{H}_2$–O–, m, 594H), 3.40 (C$\underline{H}_3$–O–, s, 3H), 2.33 (CO–C$\underline{H}_2$–CH_2–CH_2–CH_2–CH_2–O–H, m, 16H), 2.0 (CO-CH(Cl)–C$\underline{H}_2$–CH_2–C$\underline{H}_2$–CH_2–O–, m, 20H), 1.76-1.32 (CO–CH_2–C$\underline{H}_2$– C$\underline{H}_2$–C$\underline{H}_2$–CH_2–

O– and, CO–CH(Cl)–CH_2–CH_2–CH_2–CH_2–O–, m, 42H). ^{13}C NMR (101 MHz, $CDCl_3$) δ (ppm) 173.61 (C=O), 71.93 (-O–CH_2–CH_2–O–), 64.14 (CO–CH(Cl)–CH_2–CH_2–CH_2–CH_2–O–, CO–CH_2–CH_2–CH_2–CH_2–CH_2–O–H), 34.45 (CO–CH_2–CH_2–CH_2–CH_2–CH_2–O–H), 28.88-20.77 (CO–CH(Cl)–CH_2–CH_2–CH_2–CH_2–O–, CO–CH_2–CH_2–CH_2–CH_2–CH_2–O–H). IR: ν max/cm^{-1}: 1105 (C-O-C stretching), 1731 (C=O stretching), 2885 (symmetric CH_2 stretching), 2947 (asymmetric CH_2 stretching) 3476 (OH stretching). T_m (DSC) = 58.58 ^{o}C.

MG6:

M_n = 10.0 kDa (^{1}H NMR). ^{1}H NMR (400 MHz, $CDCl_3$) δ (ppm) 4.35 (CH_2–O–CO, t, 2H), 4.27 (CO–CH(Cl)–CH_2–CH_2–CH_2–CH_2–O–, m, 7H), 4.21 (CO–CH(Cl)–CH_2–CH_2–CH_2–CH_2–O–, m, 14H), 4.08 (CO–CH_2–CH_2–CH_2–CH_2–CH_2–O–H, m, 70H), 3.66 (O–CH_2–CH_2–O–, m, 586H), 3.40 (CH_3–O–, s, 3H), 2.33 (CO–CH_2–CH_2–CH_2–CH_2–CH_2–O–H, m, 70H), 2.0 (CO-CH(Cl)–CH_2–CH_2–CH_2–CH_2–O–, m, 28H), 1.76-1.32 (CO–CH_2–CH_2– CH_2–CH_2–CH_2–O– and, CO–CH(Cl)–CH_2–CH_2–CH_2–CH_2–O–, m, 248H). ^{13}C NMR (101 MHz, $CDCl_3$) δ (ppm) 173.61 (C=O), 71.93 (-O–CH_2–CH_2–O–), 64.14 (CO–CH(Cl)–CH_2–CH_2–CH_2–CH_2–O–, CO–CH_2–CH_2–CH_2–CH_2–CH_2–O–H), 34.45 (CO–CH_2–CH_2–CH_2–CH_2–CH_2–O–H), 28.88-20.77 (CO–CH(Cl)–CH_2–CH_2–CH_2–CH_2–O–, CO–CH_2–CH_2–CH_2–CH_2–CH_2–O–H). IR: ν max/cm^{-1}: 1105 (C-O-C stretching), 1731 (C=O stretching), 2885 (symmetric CH_2 stretching), 2947 (asymmetric CH_2 stretching) 3476 (OH stretching). T_m (DSC) = 55.54 ^{o}C.

MG7:

M_n = 14.9 kDa (^{1}H NMR). ^{1}H NMR (400 MHz, $CDCl_3$) δ (ppm) 4.35 (C$\underline{H}_2$–O–CO, t, 2H), 4.27 (CO–C$\underline{H}$(Cl)–CH_2–CH_2–CH_2–CH_2–O–, m, 6H), 4.21 (CO–CH(Cl)–CH_2–CH_2–CH_2–C$\underline{H}_2$–O–, m, 12H), 4.08 (CO–CH_2–CH_2–CH_2–CH_2–C$\underline{H}_2$–O–H, m, 158H), 3.66 (O–C$\underline{H}_2$–C$\underline{H}_2$–O–, m, 554H), 3.40 (C$\underline{H}_3$–O–, s, 3H), 2.33 (CO–C$\underline{H}_2$–CH_2–CH_2–CH_2–CH_2–O–H, m, 158H), 2.0 (CO-CH(Cl)–C$\underline{H}_2$–CH_2–C$\underline{H}_2$–CH_2–O–, m, 24H), 1.76-1.32 (CO–CH_2–C$\underline{H}_2$– C$\underline{H}_2$–C$\underline{H}_2$–CH_2–O– and, CO–CH(Cl)–CH_2–C$\underline{H}_2$–CH_2–CH_2–O–, m, 474H). ^{13}C NMR (101 MHz, $CDCl_3$) δ (ppm) 173.61 (C=O), 71.93 (-O–C$\underline{H}_2$–C$\underline{H}_2$–O–), 64.14 (CO–C$\underline{H}$(Cl)–CH_2–CH_2–CH_2–C$\underline{H}_2$–O–, CO–CH_2–CH_2–CH_2–CH_2–C$\underline{H}_2$–O–H), 34.45 (CO–C$\underline{H}_2$–CH_2–CH_2–CH_2–CH_2–O–H), 28.88-20.77 (CO–CH(Cl)–C$\underline{H}_2$–C$\underline{H}_2$–C$\underline{H}_2$–CH_2–O–, CO–CH_2–C$\underline{H}_2$–C$\underline{H}_2$–C$\underline{H}_2$–CH_2–O–H). IR: ν max/cm^{-1}: 1105 (C-O-C stretching), 1731 (C=O stretching), 2885 (symmetric CH_2 stretching), 2947 (asymmetric CH_2 stretching) 3476 (OH stretching). T_m (DSC) = 55.48 ^{o}C.

MG8:

M_n = 19.8 kDa (^{1}H NMR).

^{1}H NMR (400 MHz, $CDCl_3$) δ (ppm) 4.35 (C$\underline{H}_2$–O–CO, t, 2H), 4.27 (CO–C$\underline{H}$(Cl)–CH_2–CH_2–CH_2–CH_2–O–, m, 6H), 4.21 (CO–CH(Cl)–CH_2–CH_2–CH_2–C$\underline{H}_2$–O–, m, 12H), 4.08 (CO–CH_2–CH_2–CH_2–CH_2–C$\underline{H}_2$–O–H, m, 244H), 3.66 (O–C$\underline{H}_2$–C$\underline{H}_2$–O–, m, 538H), 3.40 (C$\underline{H}_3$–O–, s, 3H), 2.33 (CO–C$\underline{H}_2$–CH_2–CH_2–CH_2–CH_2–O–H, m, 244H), 2.0 (CO-CH(Cl)–C$\underline{H}_2$–CH_2–C$\underline{H}_2$–CH_2–O–, m, 24H), 1.76-1.32 (CO–CH_2–C$\underline{H}_2$– C$\underline{H}_2$–C$\underline{H}_2$–CH_2–O– and, CO–CH(Cl)–CH_2–C$\underline{H}_2$–CH_2–CH_2–O–, m, 744H). ^{13}C NMR (101 MHz, $CDCl_3$) δ (ppm) 173.61 (C=O), 71.93 (-O–C$\underline{H}_2$–C$\underline{H}_2$–O–), 64.14 (CO–C$\underline{H}$(Cl)–CH_2–CH_2–CH_2–C$\underline{H}_2$–

O–, CO–CH_2–CH_2–CH_2–CH_2–$C\underline{H}_2$–O–H), 34.45 (CO–$\underline{C}H_2$–CH_2–CH_2–CH_2–CH_2–O–H), 28.88-20.77 (CO–CH(Cl)–$\underline{C}H_2$–$\underline{C}H_2$–$\underline{C}H_2$–CH_2–O–, CO–CH_2–$\underline{C}H_2$–$\underline{C}H_2$–$\underline{C}H_2$–CH_2–O–H). IR: ν max/cm^{-1}: 1105 (C-O-C stretching), 1731 (C=O stretching), 2885 (symmetric CH_2 stretching), 2947 (asymmetric CH_2 stretching) 3476 (OH stretching). T_m (DSC) = 50.04 °C.

Table 3-5. Ingredients for ring opening polymerisation to synthesise mPEG-*b*-poly(εCL-*co*-αClεCL) with various molecular weights. I ~ initiator (mPEG, 5000 g/mol), M_1 ~ εCL (148.46 g/mol), M_2 ~ αClεCL (148.46 g/mol).

Polymer	Code	Reagents (mmol)				Molar ratio (I:M_1:M_2)
		mPEG (I)	εCL M_1	αClεCL M_2	Stannous octoate	
mPEG-*b*-poly(εCL-*co*-αClεCL)	MG5	0.100	0.842	0.700	0.014	1:8:7
	MG6	0.100	3.470	0.700	0.034	1:35:7
	MG7	0.100	7.800	0.700	0.067	1:78:7
	MG8	0.100	12.246	0.700	0.101	1:122:7

3.5.4. Synthesis of mPEG-*b*-poly(αN_3εCL)/mPEG-b-poly(εCL-co-αN_3εCL)

The azide bearing amphiphilic block copolymers based on mPEG-*b*-poly(αN_3εCL)/mPEG-*b*-poly(εCL-*co*-αN_3εCL) were obtained via the

substitution of chloro atoms of mPEG-*b*-poly(αClεCL) or mPEG-*b*-poly(εCL-co-αClεCL) by an azide group. Briefly, 500 mg of mPEG-*b*-poly(αClεCL) or mPEG-*b*-poly(εCL-co-αClεCL) with various molar masses were dissolved in 5 mL of DMSO. Afterwards, sodium azide (150 mol % vs. chloro atoms) was introduced and the reaction mixture was stirred at room temperature for 24 hours. The reaction mixture was diluted with a small amount of CH_2Cl_2 and polymers were recovered by precipitation in anhydrous diethyl ether. The resulting products were dissolved in toluene, and was subsequently centrifuged (4000 rpm, 10 min, RT) to remove insoluble salts. Finally, the azide bearing polymers were precipitated in anhydrous diethyl ether, filtered and were dried in vacuum and characterised by NMR and FT-

MG9:

M_n = 6.8 kDa (^{1}H NMR). ^{1}H NMR (400 MHz, $CDCl_3$) δ (ppm) 4.35 (C$\underline{H}_2$–O–CO, t, 2H), 4.23 (CO–CH(N_3)–CH_2–CH_2–CH_2–C$\underline{H}_2$–O–, t, 12H), 3.89 (CO–C$\underline{H}$(N_3)–CH_2–CH_2–CH_2–CH_2–O–, m, 6H), 3.66 (O–C$\underline{H}_2$–C$\underline{H}_2$–O–, m, 586H), 3.40 (C$\underline{H}_3$–O–, s, 3H), 1.94-1.40 CO–CH(N_3)–C$\underline{H}_2$–C$\underline{H}_2$–C$\underline{H}_2$–CH_2–O–, m, 36H). ^{13}C NMR (101 MHz, $CDCl_3$) δ (ppm) 170.31 (C=O), 70.57 (-O–$\underline{C}H_2$–$\underline{C}H_2$–O–), 65.34 (CO–$\underline{C}$H(N_3)–CH_2–CH_2–CH_2–CH_2–O–), 61.85 (CO–CH(N_3)–CH_2–CH_2–CH_2–$\underline{C}H_2$–O–), 30.86 (CO-CH(N_3)–$\underline{C}H_2$–CH_2–CH_2–CH_2–O–), 28.05 (CO-CH(N_3)–CH_2–CH_2–$\underline{C}H_2$–CH_2–O–), 22.25 (CO-CH(N_3)–CH_2–$\underline{C}H_2$–CH_2–CH_2–O–). IR: ν max/cm^{-1}: 1105 (C-O-C stretching), 1731 (C=O stretching), 2106 (N_3 stretching), 2885 (symmetric CH_2 stretching), 2947 (asymmetric CH_2 stretching) 3476 (OH stretching). T_m (DSC) = 59.35 ^{O}C.

MG10:

M_n = 9.6 kDa (^{1}H NMR). ^{1}H NMR (400 MHz, $CDCl_3$) δ (ppm) 4.35 (C$\underline{H}_2$–O–CO, t, 2H), 4.23 (CO–CH(N_3)–CH_2–CH_2–CH_2–C$\underline{H}_2$–O–, t, 60H), 3.89 (CO–C$\underline{H}$(N_3)–CH_2–CH_2–CH_2–CH_2–O–, t, 30H), 3.66 (O–C$\underline{H}_2$–C$\underline{H}_2$–O–, m, 514H), 3.40 (C$\underline{H}_3$–O–, s, 3H), 1.94-1.40 CO–CH(N_3)–C$\underline{H}_2$–C$\underline{H}_2$–C$\underline{H}_2$–CH_2–O–, m, 180H). ^{13}C NMR (101 MHz, $CDCl_3$) δ (ppm) 170.31 (C=O), 70.57 (-O–$\underline{C}H_2$–$\underline{C}H_2$–O–), 65.34 (CO–$\underline{C}$H(N_3)–CH_2–CH_2–CH_2–CH_2–O–), 61.85 (CO–CH(N_3)–CH_2–CH_2–CH_2–$\underline{C}H_2$–O–), 30.86 (CO-CH(N_3)–$\underline{C}H_2$–CH_2–CH_2–CH_2–O–), 28.05 (CO-CH(N_3)–CH_2–CH_2–$\underline{C}H_2$–CH_2–O–), 22.25 (CO-CH(N_3)–CH_2–$\underline{C}H_2$–CH_2–CH_2–O–). IR: ν max/cm^{-1}: 1105 (C-O-C stretching), 1731 (C=O stretching), 2106 (N_3 stretching), 2885 (symmetric CH_2 stretching), 2947 (asymmetric CH_2 stretching) 3476 (OH stretching). T_m (DSC) = 58.89 ^{O}C.

MG11:

M_n = 14.6 kDa (^{1}H NMR). ^{1}H NMR (400 MHz, $CDCl_3$) δ (ppm) 4.35 (C$\underline{H}_2$–O–CO, t, 2H), 4.23 (CO–CH(N_3)–CH_2–CH_2–CH_2–C$\underline{H}_2$–O–, t, 124H), 3.89 (CO–C$\underline{H}$(N_3)–CH_2–CH_2–CH_2–CH_2–O–, t, 62H), 3.66 (O–C$\underline{H}_2$–C$\underline{H}_2$–O–, m, 544H), 3.40 (C$\underline{H}_3$–O–, s, 3H), 1.94-1.40 CO–CH(N_3)–C$\underline{H}_2$–C$\underline{H}_2$–C$\underline{H}_2$–CH_2–O–, m, 372H). ^{13}C NMR (101 MHz, $CDCl_3$) δ (ppm) 170.31 (C=O), 70.57 (-O–$\underline{C}H_2$–$\underline{C}H_2$–O–), 65.34 (CO–$\underline{C}$H(N_3)–CH_2–CH_2–CH_2–CH_2–O–), 61.85 (CO–CH(N_3)–CH_2–CH_2–CH_2–$\underline{C}H_2$–O–), 30.86 (CO-CH(N_3)–$\underline{C}H_2$–CH_2–CH_2–CH_2–O–), 28.05 (CO-CH(N_3)–CH_2–CH_2–$\underline{C}H_2$–CH_2–O–), 22.25 (CO-CH(N_3)–CH_2–$\underline{C}H_2$–CH_2–CH_2–O–). IR: ν max/cm^{-1}: 1105 (C-O-C stretching), 1731 (C=O

stretching), 2106 (N_3 stretching), 2885 (symmetric CH_2 stretching), 2947 (asymmetric CH_2 stretching) 3476 (OH stretching). T_m (DSC) = 56.78 ^{O}C.

MG12:

M_n = 20.0 kDa (^{1}H NMR). ^{1}H NMR (400 MHz, $CDCl_3$) δ (ppm) 4.35 (C$\underline{H}_2$–O–CO, t, 2H), 4.23 (CO–CH(N_3)–CH_2–CH_2–CH_2–C$\underline{H}_2$–O–, t, 194H), 3.89 (CO–C$\underline{H}$(N_3)–CH_2–CH_2–CH_2–CH_2–O–, t, 97H), 3.66 (O–C$\underline{H}_2$–C$\underline{H}_2$–O–, m, 577H), 3.40 (C$\underline{H}_3$–O–, s, 3H), 1.94-1.40 CO–CH(N_3)–C$\underline{H}_2$–C$\underline{H}_2$–C$\underline{H}_2$–CH_2–O–, m, 582H). ^{13}C NMR (101 MHz, $CDCl_3$) δ (ppm) 170.31 (C=O), 70.57 (-O–$\underline{C}H_2$–$\underline{C}H_2$–O–), 65.34 (CO–$\underline{C}$H(N_3)–CH_2–CH_2–CH_2–CH_2–O–), 61.85 (CO–CH(N_3)–CH_2–CH_2–CH_2–$\underline{C}H_2$–O–), 30.86 (CO-CH(N_3)–$\underline{C}H_2$–CH_2–CH_2–CH_2–O–), 28.05 (CO-CH(N_3)–CH_2–CH_2–$\underline{C}H_2$–CH_2–O–), 22.25 (CO-CH(N_3)–CH_2–$\underline{C}H_2$–CH_2–CH_2–O–). IR: ν max/cm^{-1}: 1105 (C-O-C stretching), 1731 (C=O stretching), 2106 (N_3 stretching), 2885 (symmetric CH_2 stretching), 2947 (asymmetric CH_2 stretching) 3476 (OH stretching). T_m (DSC) = 49.17 ^{O}C.

MG13:

M_n = 6.7 kDa (^{1}H NMR). ^{1}H NMR (400 MHz, $CDCl_3$) δ (ppm) 4.35 (C$\underline{H}_2$–O–CO, t, 2H), 4.23 (CO–CH(N_3)–CH_2–CH_2–CH_2–C$\underline{H}_2$–O–, t, 10H), 4.08 (CO–CH_2–CH_2–CH_2–CH_2–C$\underline{H}_2$–O–H, t, 16H), 3.89 (CO–C$\underline{H}$(N_3)–CH_2–CH_2–CH_2–CH_2–O–, t, 5H), 3.66 (O–C$\underline{H}_2$–C$\underline{H}_2$–O–, m, 594H), 3.40 (C$\underline{H}_3$–O–, s, 3H), 2.33 (CO–C$\underline{H}_2$–CH_2–CH_2–CH_2–CH_2–O–H, t, 16H), 1.93-1.34 (CO-CH(N_3)–C$\underline{H}_2$–C$\underline{H}_2$–C$\underline{H}_2$–CH_2–O–, and, CO–CH_2–C$\underline{H}_2$– C$\underline{H}_2$–C$\underline{H}_2$–CH_2–O–H, m, 78H). ^{13}C NMR (101 MHz, $CDCl_3$) δ (ppm) 173.52 (C=O), 70.57 (-O–$\underline{C}H_2$–$\underline{C}H_2$–O–), 64.14 (CO–$\underline{C}$H(N_3)–CH_2–CH_2–CH_2–$\underline{C}H_2$–O–, CO–CH_2–CH_2–CH_2–CH_2–

$\underline{C}H_2$–O–H), 34.12 (CO–$\underline{C}H_2$–CH_2–CH_2–CH_2–CH_2–O–H), 28.35-20.77 (CO–CH(N_3)–$\underline{C}H_2$–$\underline{C}H_2$–$\underline{C}H_2$–CH_2–O–, CO–CH_2–$\underline{C}H_2$–$\underline{C}H_2$–$\underline{C}H_2$–CH_2–O–H). IR: ν max/cm^{-1}: 1105 (C-O-C stretching), 1731 (C=O stretching), 2106 (N_3 stretching), 2885 (symmetric CH_2 stretching), 2947 (asymmetric CH_2 stretching) 3476 (OH stretching). T_m (DSC) = 57.65 ^{O}C.

MG14:

M_n = 10.1 kDa (^{1}H NMR). ^{1}H NMR (400 MHz, $CDCl_3$) δ (ppm) 4.35 ($C\underline{H}_2$–O–CO, t, 2H), 4.23 (CO–CH(N_3)–CH_2–CH_2–CH_2–$C\underline{H}_2$–O–, t, 14H), 4.08 (CO–CH_2–CH_2–CH_2–CH_2–$C\underline{H}_2$–O–H, t, 70H), 3.89 (CO–$C\underline{H}$(N_3)–CH_2–CH_2–CH_2–CH_2–O–, t, 7H), 3.66 (O–$C\underline{H}_2$–$C\underline{H}_2$–O–, m, 586H), 3.40 ($C\underline{H}_3$–O–, s, 3H), 2.33 (CO–$C\underline{H}_2$–CH_2–CH_2–CH_2–CH_2–O–H, t, 70H), 1.93-1.34 (CO-CH(N_3)–$C\underline{H}_2$–$C\underline{H}_2$–$C\underline{H}_2$–CH_2–O–, and, CO–CH_2–$C\underline{H}_2$– $C\underline{H}_2$–$C\underline{H}_2$–CH_2–O–H, m, 266H). ^{13}C NMR (101 MHz, $CDCl_3$) δ (ppm) 173.52 (C=O), 70.57 (-O–$\underline{C}H_2$–$\underline{C}H_2$–O–), 64.14 (CO–$\underline{C}H$(N_3)–CH_2–CH_2–CH_2–$\underline{C}H_2$–O–, CO–CH_2–CH_2–CH_2–CH_2–$\underline{C}H_2$–O–H), 34.12 (CO–$\underline{C}H_2$–CH_2–CH_2–CH_2–CH_2–O–H), 28.35-20.77 (CO–CH(N_3)–$\underline{C}H_2$–$\underline{C}H_2$–$\underline{C}H_2$–CH_2–O–, CO–CH_2–$\underline{C}H_2$–$\underline{C}H_2$–$\underline{C}H_2$–CH_2–O–H). IR: ν max/cm^{-1}: 1105 (C-O-C stretching), 1731 (C=O stretching), 2106 (N_3 stretching), 2885 (symmetric CH_2 stretching), 2947 (asymmetric CH_2 stretching) 3476 (OH stretching). T_m (DSC) = 57.62 ^{O}C.

MG15:

M_n = 14.9 kDa (^{1}H NMR). ^{1}H NMR (400 MHz, $CDCl_3$) δ (ppm) 4.35 ($C\underline{H}_2$–O–CO, t, 2H), 4.23 (CO–CH(N_3)–CH_2–CH_2–CH_2–$C\underline{H}_2$–O–, t, 12H), 4.08 (CO–CH_2–CH_2–CH_2–CH_2–$C\underline{H}_2$–O–H, t, 158H), 3.89 (CO–$C\underline{H}$(N_3)–CH_2–CH_2–CH_2–CH_2–O–, t, 6H), 3.66 (O–$C\underline{H}_2$–$C\underline{H}_2$–O–, m, 554H), 3.40 ($C\underline{H}_3$–O–, s, 3H),

2.33 (CO–C$\underline{H}_2$–CH_2–CH_2–CH_2–CH_2–O–H, t, 158H), 1.93-1.34 (CO-CH(N_3)–C$\underline{H}_2$–C$\underline{H}_2$–C$\underline{H}_2$–CH_2–O–, and, CO–CH_2–C$\underline{H}_2$– C$\underline{H}_2$–C$\underline{H}_2$–CH_2–O–H, m, 510H). ^{13}C NMR (101 MHz, $CDCl_3$) δ (ppm) 173.52 (C=O), 70.57 (-O–C$\underline{H}_2$–C$\underline{H}_2$–O–), 64.14 (CO–C$\underline{H}$(N_3)–CH_2–CH_2–CH_2–C$\underline{H}_2$–O–, CO–CH_2–CH_2–CH_2–CH_2–C$\underline{H}_2$–O–H), 34.12 (CO–C$\underline{H}_2$–CH_2–CH_2–CH_2–CH_2–O–H), 28.35-20.77 (CO–CH(N_3)–C$\underline{H}_2$–C$\underline{H}_2$–C$\underline{H}_2$–CH_2–O–, CO–CH_2–C$\underline{H}_2$–C$\underline{H}_2$–C$\underline{H}_2$–CH_2–O–H). IR: ν max/cm^{-1}: 1105 (C-O-C stretching), 1731 (C=O stretching), 2106 (N_3 stretching), 2885 (symmetric CH_2 stretching), 2947 (asymmetric CH_2 stretching) 3476 (OH stretching). T_m (DSC) = 50.20 ℃.

MG16:

M_n = 19.8 kDa (^{1}H NMR). ^{1}H NMR (400 MHz, $CDCl_3$) δ (ppm) 4.35 (C$\underline{H}_2$–O–CO, t, 2H), 4.23 (CO–CH(N_3)–CH_2–CH_2–CH_2–C$\underline{H}_2$–O–, t, 12H), 4.08 (CO–CH_2–CH_2–CH_2–CH_2–C$\underline{H}_2$–O–H, t, 244H), 3.89 (CO–C$\underline{H}$(N_3)–CH_2–CH_2–CH_2–CH_2–O–, t, 6H), 3.66 (O–C$\underline{H}_2$–C$\underline{H}_2$–O–, m, 538H), 3.40 (C$\underline{H}_3$–O–, s, 3H), 2.33 (CO–C$\underline{H}_2$–CH_2–CH_2–CH_2–CH_2–O–H, t, 244H), 1.93-1.34 (CO-CH(N_3)–C$\underline{H}_2$–C$\underline{H}_2$–C$\underline{H}_2$–CH_2–O–, and, CO–CH_2–C$\underline{H}_2$– C$\underline{H}_2$–C$\underline{H}_2$–CH_2–O–H, m, 768H). ^{13}C NMR (101 MHz, $CDCl_3$) δ (ppm) 173.52 (C=O), 70.57 (-O–C$\underline{H}_2$–C$\underline{H}_2$–O–), 64.14 (CO–C$\underline{H}$(N_3)–CH_2–CH_2–CH_2–C$\underline{H}_2$–O–, CO–CH_2–CH_2–CH_2–CH_2–C$\underline{H}_2$–O–H), 34.12 (CO–C$\underline{H}_2$–CH_2–CH_2–CH_2–CH_2–O–H), 28.35-20.77 (CO–CH(N_3)–C$\underline{H}_2$–C$\underline{H}_2$–C$\underline{H}_2$–CH_2–O–, CO–CH_2–C$\underline{H}_2$–C$\underline{H}_2$–C$\underline{H}_2$–CH_2–O–H). IR: ν max/cm^{-1}: 1105 (C-O-C stretching), 1731 (C=O stretching), 2106 (N_3 stretching), 2885 (symmetric CH_2 stretching), 2947 (asymmetric CH_2 stretching) 3476 (OH stretching). T_m (DSC) = 50.44 ℃.

3.6. REFERENCES

1. H. Seyednejad, A. H. Ghassemi, C. F. van Nostrum, T. Vermonden and W. E. Hennink, *Journal of Controlled Release*, 2011, **152**, 168-176.
2. B. Xu, J. Yuan, T. Ding and Q. Gao, *Polymer Bulletin*, 2010, **64**, 537-551.
3. J. Zeng, X. Xu, X. Chen, Q. Liang, X. Bian, L. Yang and X. Jing, *Journal of Controlled Release*, 2003, **92**, 227-231.
4. S. K. Sahoo and V. Labhasetwar, *Drug Discovery Today*, 2003, **8**, 1112-1120.
5. N. Saito, N. Murakami, J. Takahashi, H. Horiuchi, H. Ota, H. Kato, T. Okada, K. Nozaki and K. Takaoka, *Advanced Drug Delivery Reviews*, 2005, **57**, 1037-1048.
6. L. Buttafoco, N. P. Boks, P. Engbers-Buijtenhuijs, D. W. Grijpma, A. A. Poot, P. J. Dijkstra, I. Vermes and J. Feijen, *Journal of Biomedical Materials Research Part B: Applied Biomaterials*, 2006, **79B**, 425-434.
7. S.-H. Hyon, K. Jamshidi and Y. Ikada, *Biomaterials*, 1997, **18**, 1503-1508.
8. R. J. Pounder and A. P. Dove, *Polymer Chemistry*, 2010, **1**, 260-271.
9. J. Kasperczyk, S. Li, J. Jaworska, P. Dobrzyński and M. Vert, *Polymer Degradation and Stability*, 2008, **93**, 990-999.

10. M. Vert, G. Schwach, R. Engel and J. Coudane, *Journal of Controlled Release*, 1998, **53**, 85-92.
11. K. Fu, D. W. Pack, A. M. Klibanov and R. Langer, *Pharmaceutical Research*, 2000, **17**, 100-106.
12. M. Ye, S. Kim and K. Park, *Journal of Controlled Release*, 2010, **146**, 241-260.
13. F. Ungaro, I. d' Angelo, A. Miro, M. I. La Rotonda and F. Quaglia, *Journal of Pharmacy and Pharmacology*, 2012, **64**, 1217-1235.
14. A. Kumari, S. K. Yadav and S. C. Yadav, *Colloids and Surfaces B: Biointerfaces*, 2010, **75**, 1-18.
15. S. Hermeling, D. J. A. Crommelin, H. Schellekens and W. Jiskoot, *Pharmaceutical Research*, 2004, **21**, 897-903.
16. W. Jiskoot, R. M. F. Van Schie, M. G. Carstens and H. Schellekens, *Pharmaceutical Research*, 2009, **26**, 1303-1314.
17. P. Gao, X. Nie, M. Zou, Y. Shi and G. Cheng, *The Journal of Antibiotics*, 2011, **64**, 625-634.
18. M. J. Mondrinos, R. Dembzynski, L. Lu, V. K. C. Byrapogu, D. M. Wootton, P. I. Lelkes and J. Zhou, *Biomaterials*, 2006, **27**, 4399-4408.
19. V. V. Seregin and J. L. Coffer, *Biomaterials*, 2006, **27**, 4745-4754.
20. B. Shi, C. Fang, M. You, Y. Zhang, S. Fu and Y. Pei, *Colloid and Polymer Science*, 2005, **283**, 954-967.
21. M. A. Woodruff and D. W. Hutmacher, *Progress in Polymer Science*, 2010, **35**, 1217-1256.

22. F. Sheikh, N. M. Barakat, M. Kanjwal, S. Aryal, M. Khil and H.-Y. Kim, *Journal of Materials Science: Materials in Medicine*, 2009, **20**, 821-831.

23. E. D. Yildirim, H. Ayan, V. N. Vasilets, A. Fridman, S. Guceri and W. Sun, *Plasma Processes and Polymers*, 2008, **5**, 58-66.

24. U. Hersel, C. Dahmen and H. Kessler, *Biomaterials*, 2003, **24**, 4385-4415.

25. M. F. Koenig and S. J. Huang, *Polymer*, 1995, **36**, 1877-1882.

26. H. T. Moon, Y.-K. Lee, J. K. Han and Y. Byun, *Journal of Biomaterials Science, Polymer Edition*, 2002, **13**, 817-828.

27. M.-H. Huang, S. Li, D. W. Hutmacher, J.-T. Schantz, C. A. Vacanti, C. Braud and M. Vert, *Journal of Biomedical Materials Research Part A*, 2004, **69A**, 417-427.

28. N. Rapoport, *Progress in Polymer Science*, 2007, **32**, 962-990.

29. M. Kato, H. Toyoda, T. Namikawa, M. Hoshino, H. Terai, S. Miyamoto and K. Takaoka, *Biomaterials*, 2006, **27**, 2035-2041.

30. C. Jerome and P. Lecomte, *Advanced Drug Delivery Reviews*, 2008, **60**, 1056-1076.

31. J.-P. Latere, P. Lecomte, P. Dubois and R. Jérôme, *Macromolecules*, 2002, **35**, 7857-7859.

32. B. Saulnier, S. Ponsart, J. Coudane, H. Garreau and M. Vert, *Macromolecular Bioscience*, 2004, **4**, 232-237.

33. S. Ponsart, J. Coudane and M. Vert, *Biomacromolecules*, 2000, **1**, 275-281.

34. D. E. Noga, T. A. Petrie, A. Kumar, M. Weck, A. J. García and D. M. Collard, *Biomacromolecules*, 2008, **9**, 2056-2062.

35. M. Leemhuis, C. F. Van Nostrum, J. A. W. Kruijtzer, Z. Y. Zhong, M. R. Ten Breteler, P. J. Dijkstra, J. Feijen and W. E. Hennink, *Macromolecules*, 2006, **39**, 3500-3508.

36. P. Lecomte, C. Detrembleur, X. Lou, M. Mazza, O. Halleux and R. Jérôme, *Macromolecular Symposia*, 2000, **157**, 47-60.

37. X. Lou, C. Detrembleur and R. Jérôme, *Macromolecular Rapid Communications*, 2003, **24**, 161-172.

38. C. Jérôme and P. Lecomte, *Advanced Drug Delivery Reviews*, 2008, **60**, 1056-1076.

39. C. K. Williams, *Chemical Society Reviews*, 2007, **36**, 1573-1580.

40. C. Detrembleur, M. Mazza, O. Halleux, P. Lecomte, D. Mecerreyes, J. L. Hedrick and R. Jérôme, *Macromolecules*, 2000, **33**, 14-18.

41. S. Lenoir, R. Riva, X. Lou, C. Detrembleur, R. Jérôme and P. Lecomte, *Macromolecules*, 2004, **37**, 4055-4061.

42. R. Riva, S. Schmeits, C. Jérôme, R. Jérôme and P. Lecomte, *Macromolecules*, 2007, **40**, 796-803.

43. A. Baeyer, *Berichte der Deutschen Chemischen Gesellschaft*, 1899, **32**, 2429-2447.

44. R. Riva, S. Schmeits, F. Stoffelbach, C. Jerome, R. Jerome and P. Lecomte, *Chemical Communications*, 2005,**0**, 5334-5336

45. K. Fuhrmann, J. D. Schulz, M. A. Gauthier and J.-C. Leroux, *ACS Nano*, 2012, **6**, 1667-1676.

46. M. Claes, S. Voccia, C. Detrembleur, C. Jérôme, B. Gilbert, P. Leclère, V. M. Geskin, R. Gouttebaron, M. Hecq, R. Lazzaroni and R. Jérôme, *Macromolecules*, 2003, **36**, 5926-5933.

47. S. E. Habnouni, V. Darcos and J. Coudane, *Macromolecular Rapid Communications*, 2009, **30**, 165-169.

48. A. Mahmud, X.-B. Xiong and A. Lavasanifar, *Macromolecules*, 2006, **39**, 9419-9428.

49. A.-C. Albertsson and I. K. Varma, *Biomacromolecules*, 2003, **4**, 1466-1486.

50. K. Stridsberg, M. Ryner and A.-C. Albertsson, in *Degradable Aliphatic Polyesters*, Springer Berlin Heidelberg, 2002, vol. 157, ch. 2, pp. 41-65.

51. S. Cajot and C. Jérôme, *Journal of Controlled Release*, 2011, **152, Supplement 1**, e1-e2.

52. K. Shinno, M. Miyamoto, Y. Kimura, Y. Hirai and H. Yoshitome, *Macromolecules*, 1997, **30**, 6438-6444.

53. J. Rieger, C. Passirani, J. P. Benoit, K. Van Butsele, R. Jérôme and C. Jérôme, *Advanced Functional Materials*, 2006, **16**, 1506-1514.

54. E. F. V. Scriven and K. Turnbull, *Chemical Reviews*, 1988, **88**, 297-368.

55. S. Brase, C. Gil, K. Knepper and V. Zimmermann, *Angewandte Chemie (International Edition in English)*, 2005, **44**, 5188-5240.

56. P. Lecomte, R. Riva and C. Jerome, in *New Smart Materials via Metal Mediated Macromolecular Engineering*, eds. E. Khosravi, Y. Yagci and

Y. Savelyev, Springer Netherlands, Dordrecht, 2009, DOI: 10.1007/978-90-481-3278-2_5, pp. 77-91.

57. R.-S. Lee and Y.-T. Huang, *Journal of Polymer Science Part A: Polymer Chemistry*, 2008, **46**, 4320-4331.

58. S. Cajot, N. Lautram, C. Passirani and C. Jerome, *Journal of Controlled Release*, 2011, **152**, 30-36.

Chapter 4: DEVELOPMENT OF REACTIVE MICELLES FROM BIODEGRADABLE FUNCTIONAL AMPHIPHILIC BLOCK COPOLYMERS

4.1. INTRODUCTION

Polymeric micelles have emerged as attractive carriers for the delivery of poorly water soluble drugs due to their capability to encapsulate such drugs in their inner core.[1] Polymeric micelles are supramolecular core-shell nano-structures of amphiphilic block copolymers (figure 4-1).

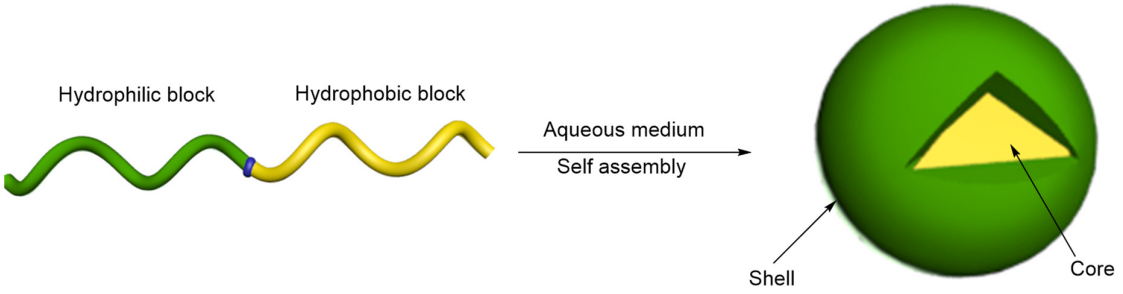

Figure 4-1. Illustration of the self-assembly of amphiphilic block copolymers into micelles.

The amphiphilic polymers comprise of at least two blocks of discrete chemical nature that exhibit phase separation as a result of chain association in aqueous solution that selectively dissolves one of the constituents.[2, 3] The formation or self-assembly of micelles takes place when concentration of block copolymer rises above a certain threshold, called the critical micelle concentration (CMC). At the CMC, the hydrophobic constituents of amphiphilic block copolymers begin to associate to decrease the interaction with the aqueous environment, resulting into a vesicular or core-shell structure. Owing to their core-shell structure, micelles are often

comparable to natural existing structures (e.g. viruses or lipoproteins), which protect their payload while it is delivered to the target cell.[4]

The micelle shell usually comprises biocompatible hydrophilic polymers such as polyethylene glycol (PEG), which impart stability to micelles and also responsible for the suppressing interactions with plasma proteins and cell membranes.[5] Some other polymers e.g. poly(*N*-isopropylacrylamide) (PNIPAM)[6-8] , and poly(alkyl-acrylic acid)[8] could be employed to build temperature or pH-responsive polymeric micelles.[9] The hydrophobic core usually comprises a biodegradable macromolecule e.g. poly(D,L-lactic acid) (PDLLA),[10] poly(β-benzyl-L-aspartate) (PBLA),[11] or poly(ϵ-caprolactone) (PCL),[12, 13] and works as a container for a hydrophobic drug, shielding it from interaction with the aqueous atmosphere.

The drug loaded amphiphilic block copolymer micelles can be obtained by various methods e.g., nanoprecipitation, dialysis, oil-in-water, and solid dispersion methods.[14] Drug loading can be performed either by chemical conjugation,[15] or by physical encapsulation within the inner core of the micelles.[16] The drug release from micelles mainly relies on the type of encapsulation. The bulk degradation of polymer matrix or surface erosion is responsible for the release of chemically conjugated drug, whereas, physically entrapped drugs are mainly released by diffusion. Parameters such as the molecular weight, chemical composition and length of hydrophilic or hydrophobic block of amphiphilic polymers can be easily tailored, allowing control over the size and morphology of micelles.[17, 18]

Beside certain advantages of micelles over other types of nanocarriers, premature drug release in the blood stream have been reported,[19-21] which may cause certain side effects to normal tissues.[22] These drawbacks can be overcome by preparing reactive micelles from functional amphiphilic block copolymers. The functional groups within the micelles core offer additional advantages. For instance, functional moieties can be used to crosslink the micelles core to provide additional stability against dilution in bloodstream, or to covalently conjugate the drug to the micelle core.[23, 24]

In this chapter, we report the preparation and characterisation of reactive micelles based on mPEG-*b*-poly($\alpha N_3\varepsilon CL$) and mPEG-*b*-poly(εCL-co-$\alpha N_3\varepsilon CL$) amphiphilic block copolymers comprising various molecular weights and different proportions of azide functional groups. The reactive micelles were prepared using the dialysis method, and were characterised for their size, morphology and zeta potential. After characterising the micelles prepared from amphiphilic block copolymers with various architecture and different molecular weights, a particular copolymer with optimum micellisation properties was selected for further investigations. A hydrophobic dye i.e. 7-hydroxy-cumarinyl-4-acetic acid (HCA) was selected as a model molecule to functionalise the selective copolymer with a redox-responsive bi-functional linker. The functionalised-HCA was covalently grafted onto the hydrophobic block of the copolymer via copper catalysed azide-alkyne cycloaddition (CuAAC) to generate HCA-linker grafted block copolymer. The dye release studies were carried out under non-reducing and reducing conditions. Such redox-responsive micelles prepared from functional

amphiphilic block copolymers could be attractive nano-carriers for bio-responsive drug delivery applications.

4.2. RESULTS

4.2.1. Preparation and characterisation of reactive micelles

The reactive micelles based on mPEG-*b*-poly(αN$_3$εCL) and mPEG-*b*-poly(εCL-*co*-αN$_3$εCL) amphiphilic block copolymers comprising various molecular weights and different ratios of functional groups, were prepared using a dialysis method. The amphiphilic block copolymers were first dissolved in DMSO and then added drop-wise into water. The organic solvent was removed by dialysis to obtain micelles with well-defined characteristics. The DLS and TEM analysis showed that with the increase in the molecular weight of hydrophobic blocks, the sizes of micelles increased correspondingly.

Specifically, amphiphilic block copolymers of mPEG-*b*-poly(αN$_3$εCL) with molecular weights of 6.8 and 9.6 kDa resulted into micelles with mean sizes of 33 ± 6, and 42 ± 8 nm, respectively, with narrow size distributions and smaller polydispersity index as observed by DLS (figure 4-2). In contrast, DLS analysis of mPEG-*b*-poly(αN$_3$εCL) with molecular weights of 14.6 kDa and 20.0 kDa showed larger sizes (59 ± 11, and 83 ± 14 nm, respectively) and wider size distributions. The morphologies of mPEG-*b*-poly(αN$_3$εCL) block copolymers micelles were investigated using TEM, showing slightly

elongated structures of micelles prepared with block copolymers having molecular weight of 6.8 kDa (figure 4-3A). Whereas, micellisation of mPEG-*b*-poly(αN$_3$εCL) with 9.6 kDa molecular weight showed well-defined and spherical morphology, without apparent aggregation or clusters as shown in the TEM micrograph in figure 4-3B. In contrast, mPEG-*b*-poly(αN$_3$εCL) with higher molecular weights of 14.6 kDa and 20.0 kDa showed formation of aggregates or clusters.

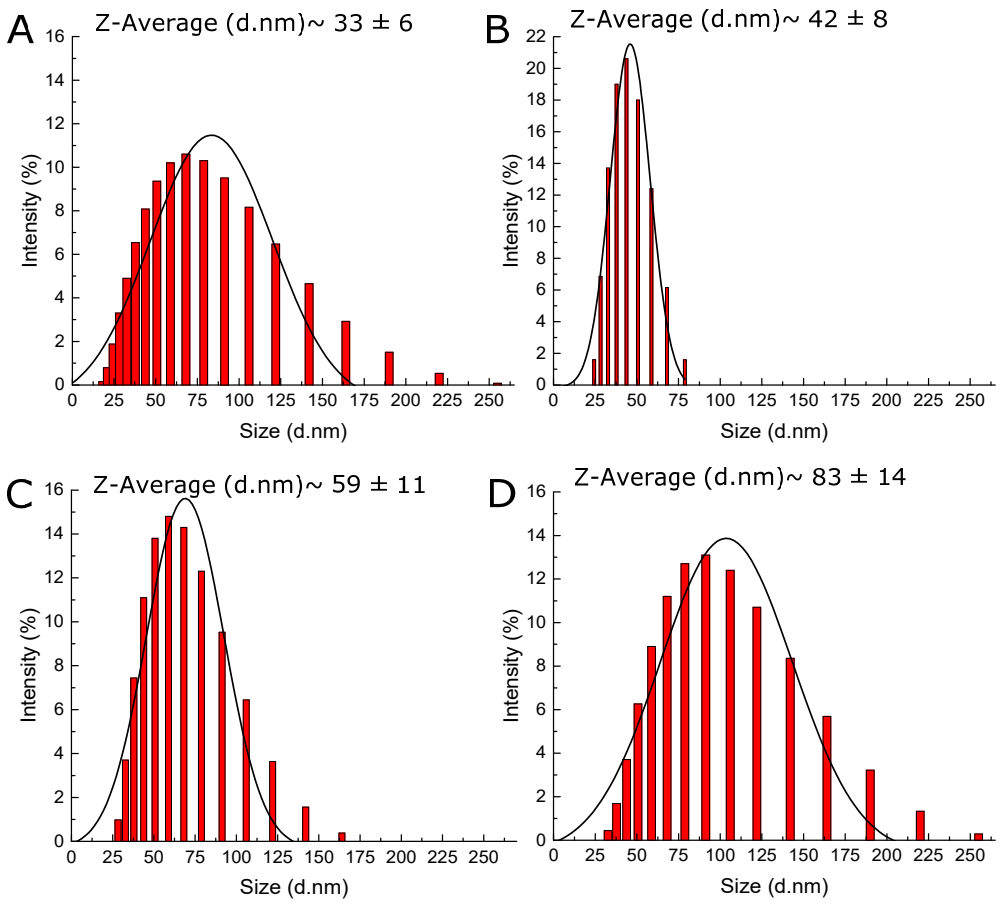

Figure 4-2. DLS characterisation of micelles prepared from mPEG-*b*-poly(αN$_3$εCL) with various molecular weights. (A) 6.8 kDa, (B) 9.6 kDa (C) 14.6 kDa, and (D) 20.0 kDa.

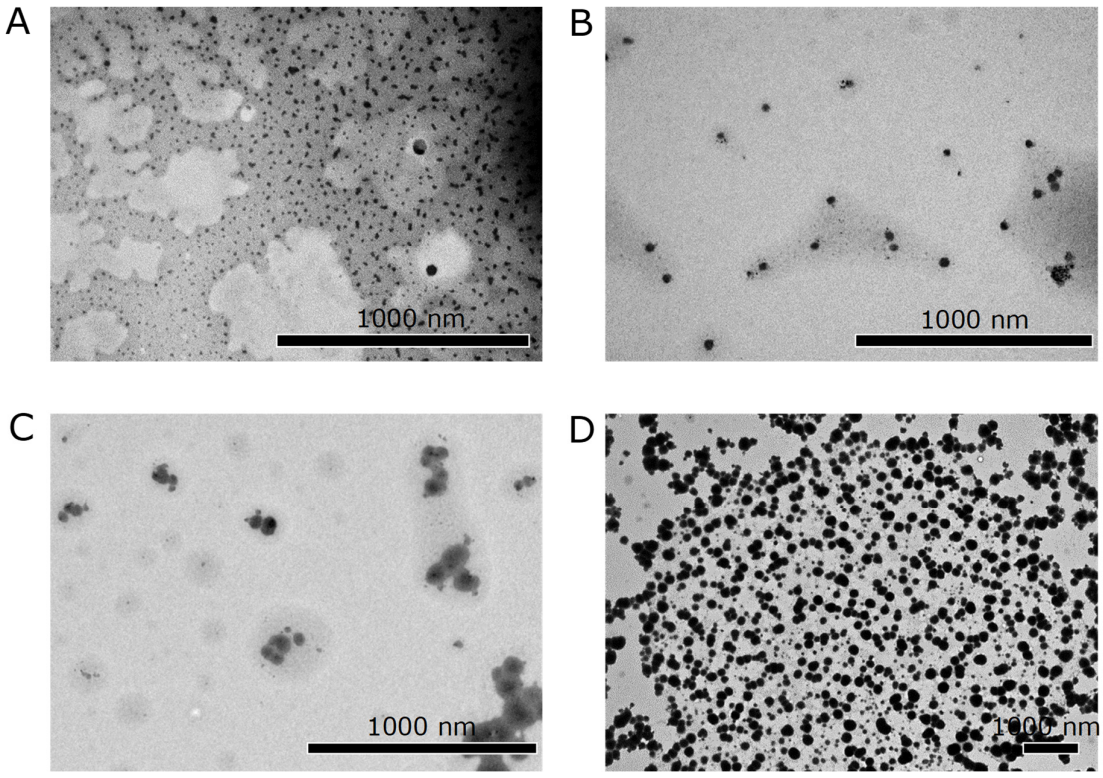

Figure 4-3. TEM micrographs of micelles prepared from mPEG-*b*-poly(αN_3εCL) with various molecular weights. (A) 6.8 kDa, (B) 9.6 kDa (C) 14.6 kDa, and (D) 20.0 kDa. Scale bars ~ 1000 nm.

The micellisation of mPEG-*b*-poly(εCL-*co*-αN_3εCL) amphiphilic block copolymers showed a similar trend in the increase of sizes with the increase in molecular weights. The DLS results showing micellisation of mPEG-*b*-poly(εCL-*co*-αN_3εCL) are presented in figure 4-4. The amphiphilic block copolymer of mPEG-*b*-poly(εCL-*co*-αN_3εCL) with lower molecular weights of 6.7 and 10.1 kDa resulted into smaller micelles with average sizes of 31 ± 4, and 36 ± 7 nm, respectively, with narrow size distributions and poly dispersity index as observed by DLS. However, mPEG-*b*-poly(εCL-*co*-

αN$_3$εCL) block copolymers with higher molecular weights of 14.9 and 19.8 kDa showed wider size distributions with average sizes of 67 ± 5 and 71 ± 10 nm, respectively.

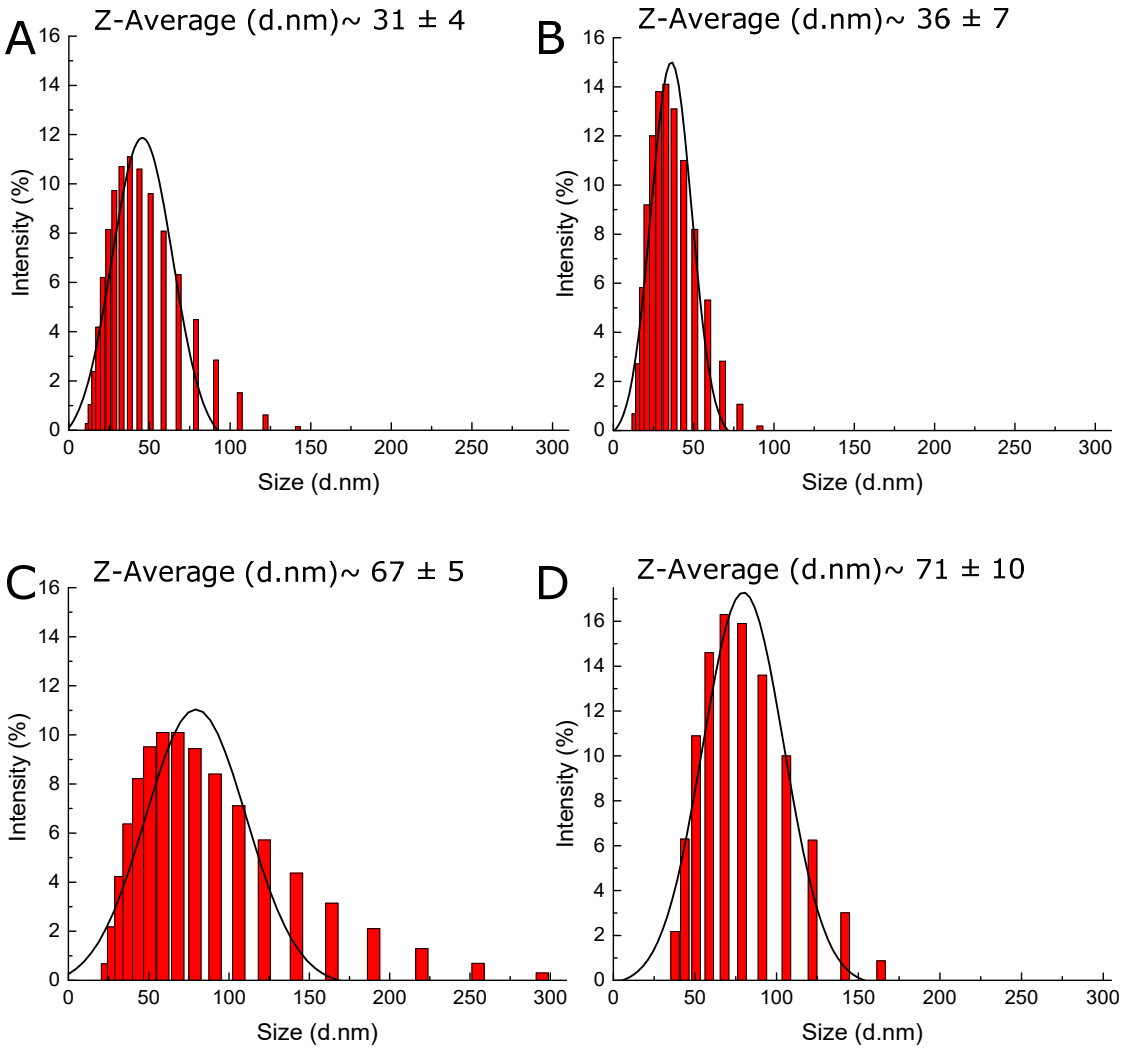

Figure 4-4. DLS characterisation of micelles prepared from mPEG-*b*-poly(εCL-*co*-αN$_3$εCL) with various molecular weights. (A) 6.7 kDa, (B) 10.1 kDa, (C) 14.9 kDa, and (D) 19.8 kDa.

The TEM analysis of micelles prepared from mPEG-*b*-poly(εCL-*co*-αN$_3$εCL) having a molecular weight of 6.7 kDa showed non-uniform morphology with spherical and some elongated micelles as shown in figure 4-5A. Whereas mPEG-*b*-poly(εCL-*co*-αN$_3$εCL) block copolymer comprising 10.1 kDa molecular weight showed uniform and spherical morphology of micelles as shown in figure 4-5B.

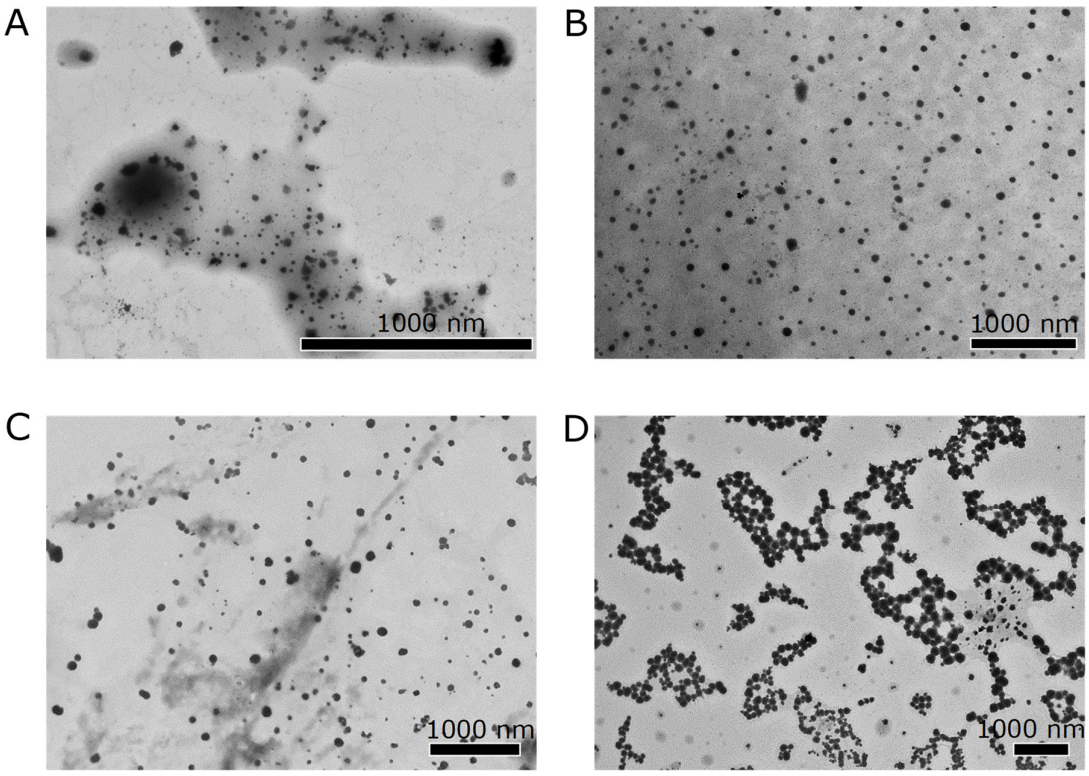

Figure 4-5. TEM micrographs of micelles prepared from mPEG-*b*-poly(εCL-*co*-αN$_3$εCL) with various molecular weights. (A) 6.7 kDa, (B) 10.1 kDa, (C) 14.9 kDa, and (D) 19.8 kDa. Scale bars ~ 1000 nm.

On the other hand, mPEG-*b*-poly(εCL-*co*-αN$_3$εCL) block copolymers with higher molecular weights of 14.9 and 19.8 kDa showed non-uniform morphologies of micelles with large numbers of clusters or aggregates.

The surface charges or zeta potentials of micelles based on mPEG-*b*-poly(αN$_3$εCL) and mPEG-*b*-poly(εCL-*co*-αN$_3$εCL) amphiphilic block copolymers were observed close to neutral or slightly negative. Specifically, mPEG-*b*-poly(αN$_3$εCL) with molecular weights of 6.8, 9.6, 14.6 and 20.0 kDa exhibited zeta potential of -8.5 ± 1.5, -4.5 ± 0.8, -4.8 ± 0.7, and -5.8 ± 0.5 mv, respectively (figure 4-6).

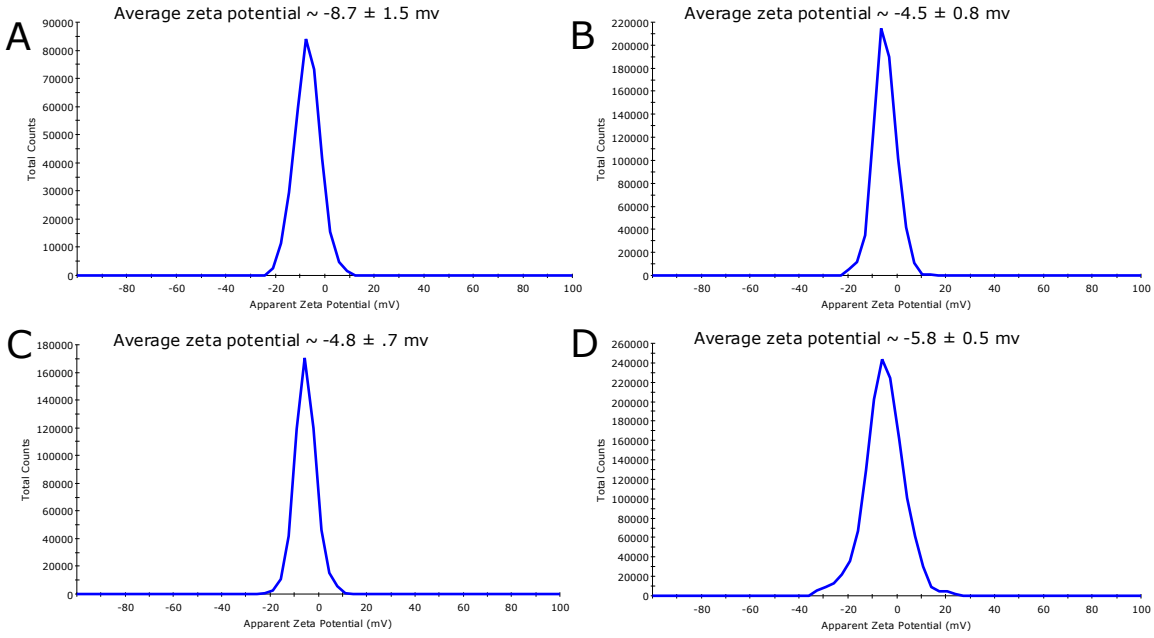

Figure 4-6. Zeta potentials of micelles prepared from mPEG-*b*-poly(αN$_3$εCL) with various molecular weights. (A) 6.8 kDa, (B) 9.6 kDa (C) 14.6 kDa, and (D) 20.0 kDa.

The mPEG-*b*-poly(εCL-*co*-αN$_3$εCL) block copolymers with molecular weights of 6.7, 10.1, 14.9, and 19.8 kDa showed zeta potentials of -4.0 ± 1.4, -2.8 ± 0.9, -3.8 ± 1.1, and -4.9 ± 1.4 mv, respectively, as shown in figure 4-7.

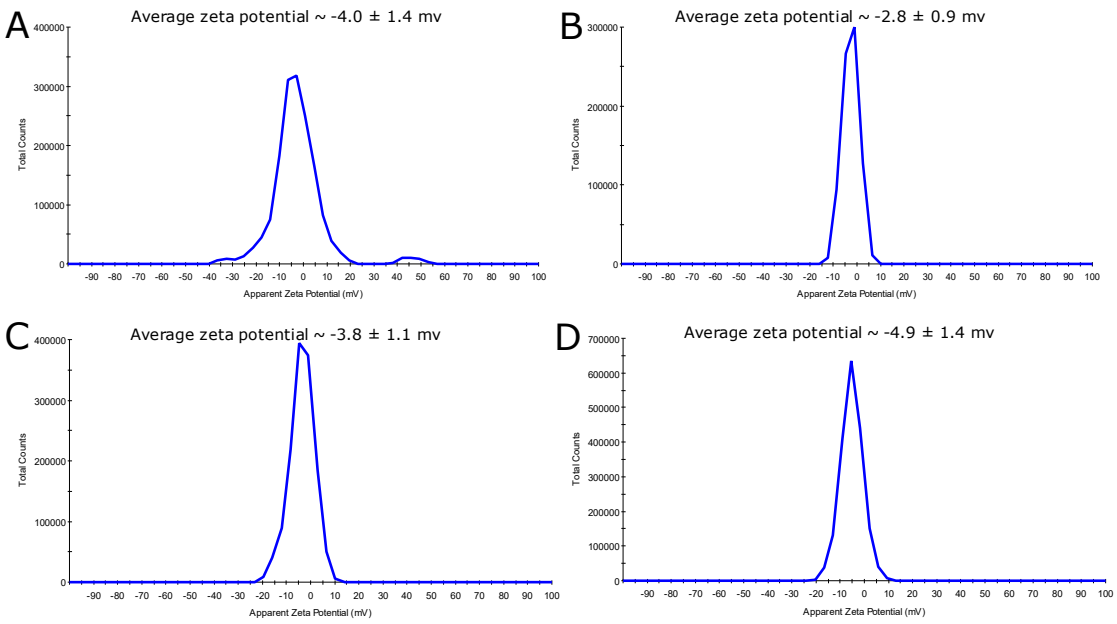

Figure 4-7. Zeta potentials of micelles prepared from mPEG-*b*-poly(εCL-*co*-αN$_3$εCL) with various molecular weights. (A) 6.7 kDa, (B) 10.1 kDa, (C) 14.9 kDa, and (D) 19.8 kDa.

4.2.2. Synthesis of polymer-dye conjugate as a model redox responsive drug delivery system

To develop redox-responsive polymer-dye conjugate as a model drug delivery system, a bi-functional alkyne linker was synthesised which was used to functionalise the 7-hydroxycoumarinyl-4-acetic acid (HCA) to generate a model alkyne bearing molecule (HCA-linker complex). The HCA-linker complex was then grafted on the copolymer backbone via a copper-

catalysed azide–alkyne cycloaddition. The bi-functional alkyne linker was synthesised by reacting equivalent molar quantities of pentynoic acid with *bis*-(2-hydroxyethyl) disulfide, using EDAC as the carboxylic acid activating agent and DMAP as a catalyst (scheme 4-1).

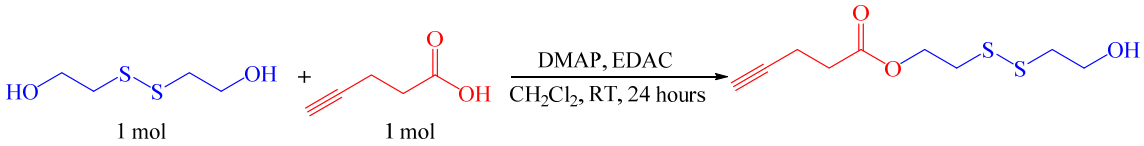

Scheme 4-1. Scheme for the synthesis of redox-responsive bi-functional linker.

The resulting reaction mixture was purified by silica gel column chromatography to obtain the redox-responsive bifunctional alkyne linker (46% yield). The synthesis of bifunctional alkyne linker was confirmed by ^{1}H NMR and ^{13}C NMR (figure 4-8A and 4-8B, respectively). The ^{1}H NMR resonances at 4.39 ppm and ^{13}C NMR resonances at 62.48 ppm confirmed the formation of the ester bond. Whereas, integration of NMR spectra revealed that bi-functional alkyne linker possessed a terminal alkyne and a terminal hydroxyl group. The synthesised redox responsive bifunctional alkyne linker was then coupled to a model molecule i.e. 7-hydroxycoumarinyl-4-acetic acid (HCA) to generate HCA-linker complex (scheme 4-2).

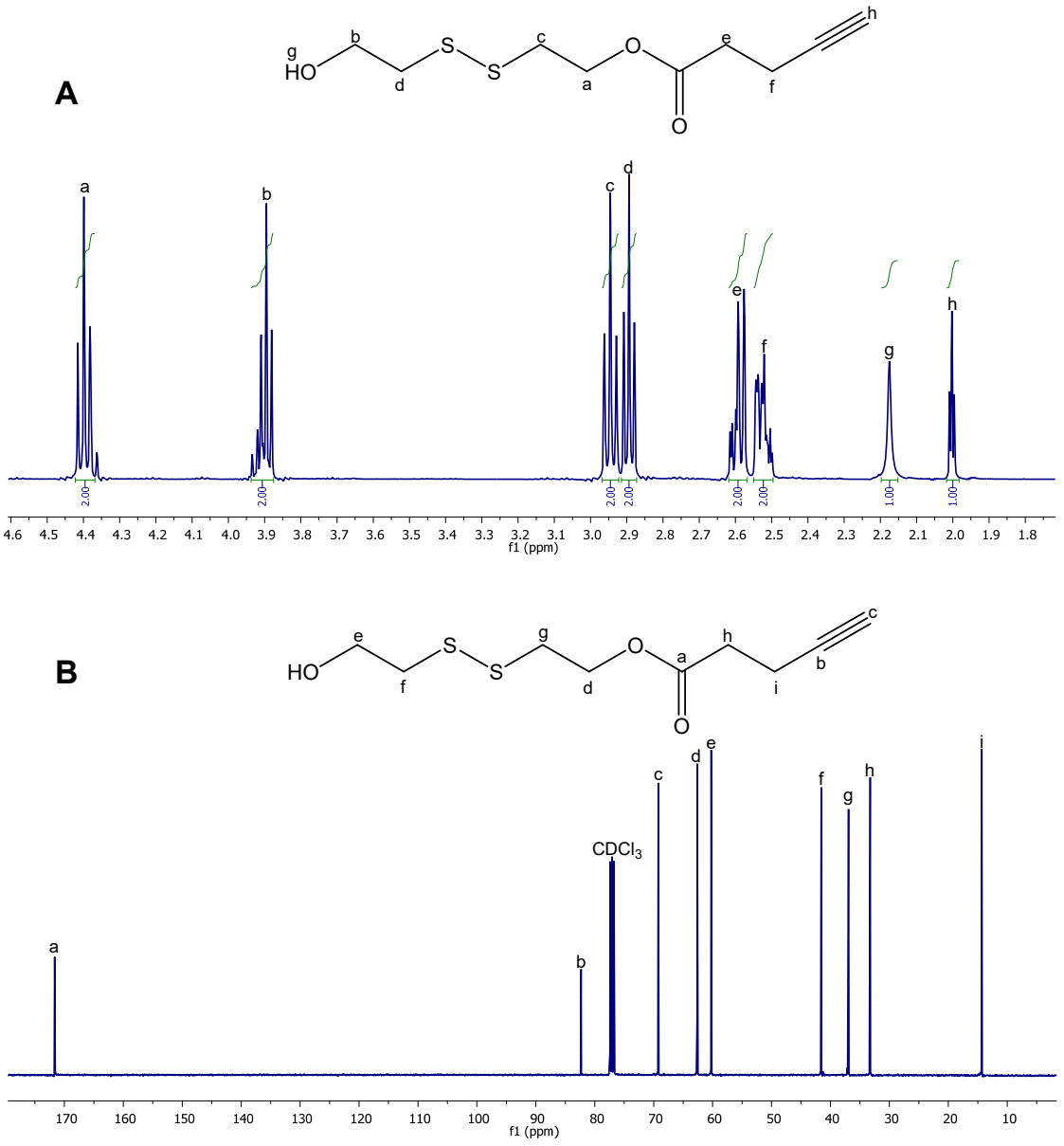

Figure 4-8. NMR spectroscopy of redox-responsive bi-functional linker in $CDCl_3$. (A) ^{1}H NMR spectrum and (B) ^{13}C NMR spectrum.

The coupling reaction proceeded with the formation of ester bond by the reaction of carboxylic acid group of the 7-hydroxycoumarinyl-4-acetic acid (HCA) with the hydroxyl group of bi-functional alkyne linker.

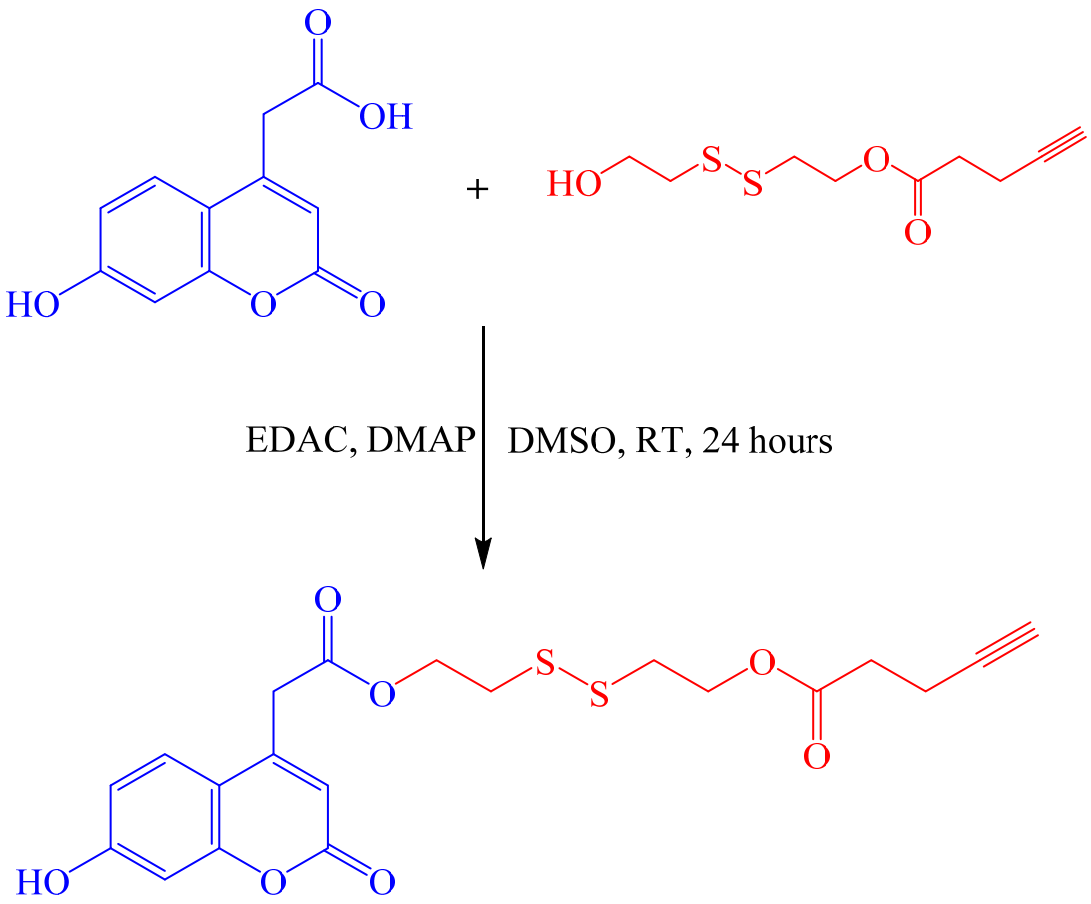

Scheme 4-2. Scheme for the synthesis of HCA-linker complex.

The structure of the HCA-linker complex was confirmed by ^{1}H NMR spectroscopy (figure 4-9). The chemical shift at 4.39 ppm in ^{1}H NMR spectrum confirmed the formation of HCA-linker complex. The HCA-linker complex was then used to study the coupling reaction with the selective azide bearing block copolymers [i.e. mPEG-*b*-poly(εCL-*co*-αN$_3$εCL), M_n ~ 10.1 kDa] via copper-catalysed azide–alkyne cycloaddition (scheme 4-3). The click reaction was continued until the infrared absorption peak corresponding to the azide group (at 2106 cm^{-1}) fully disappeared and a new peak at 1660 cm^{-1} appeared (representative of the triazole ring), as

observed by FT-IR spectroscopy (figure 4-11).The results were in complete agreement with the previously reported data.[13]

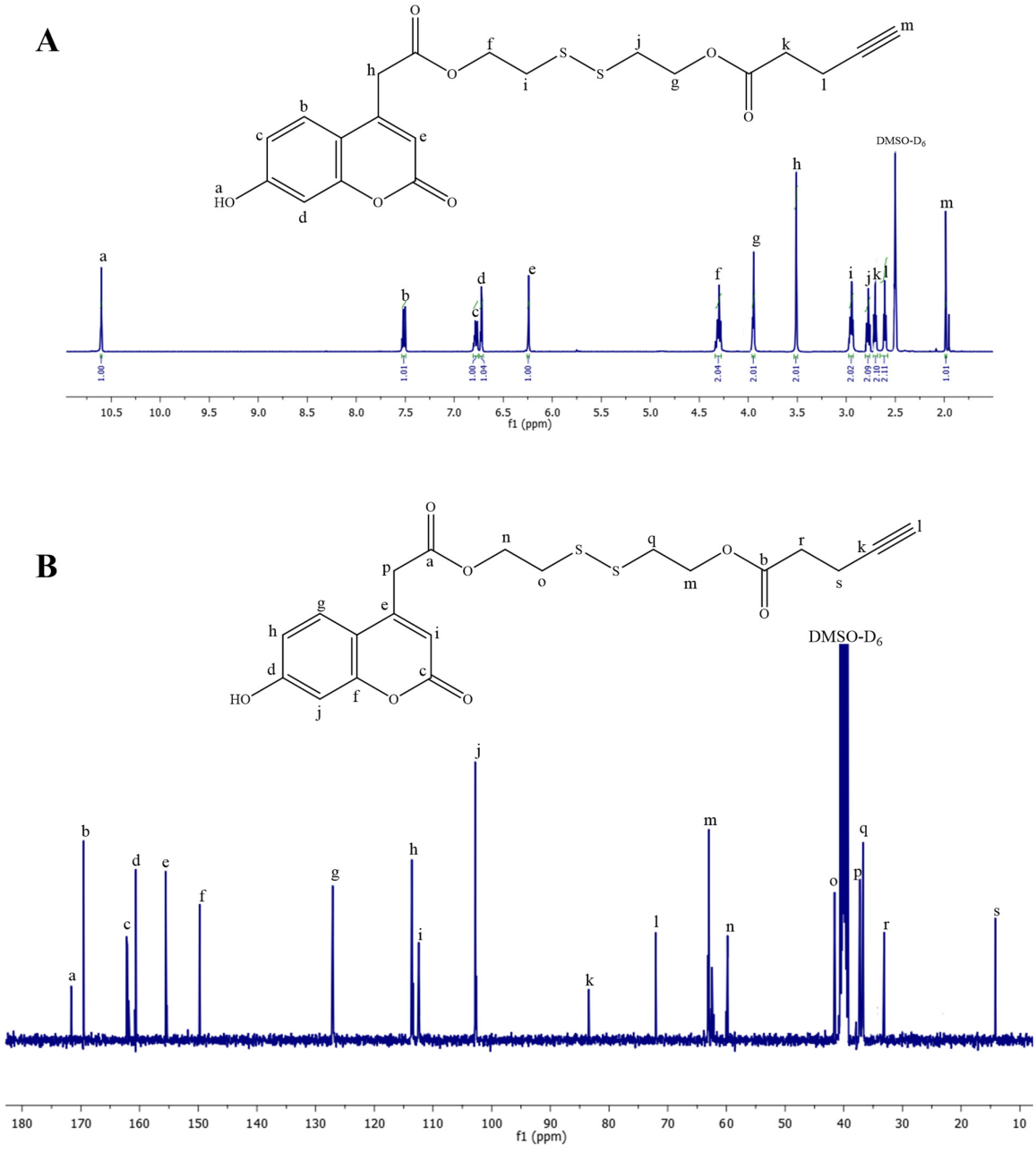

Figure 4-9. NMR spectrum of HCA-linker complex in DMSO-D_6. (A) ^{1}H NMR spectrum and (B) ^{13}C NMR spectrum.

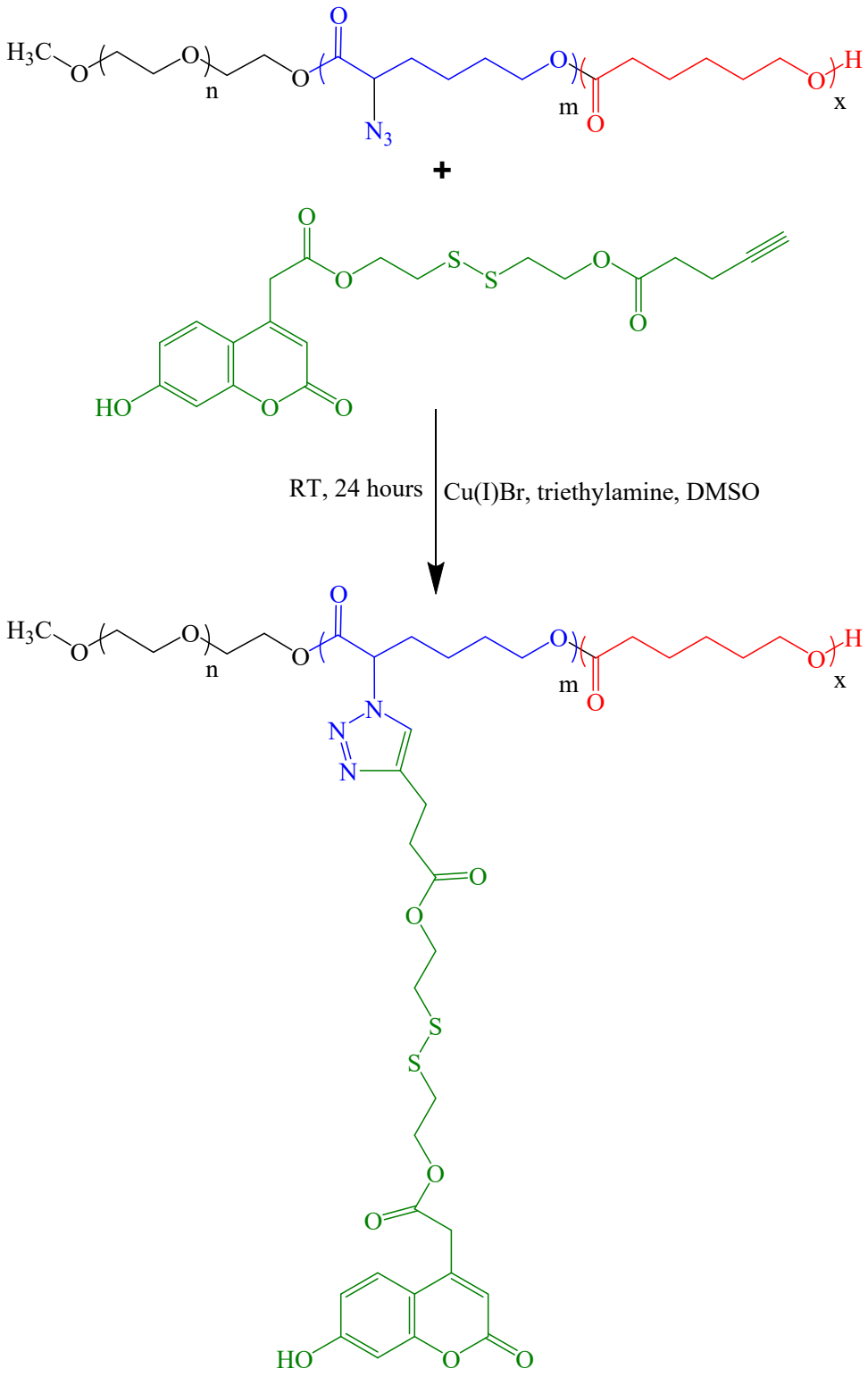

Scheme 4-3. Synthesis scheme for the grafting of HCA-linker complex onto the copolymer backbone via copper-catalysed azide–alkyne cycloaddition.

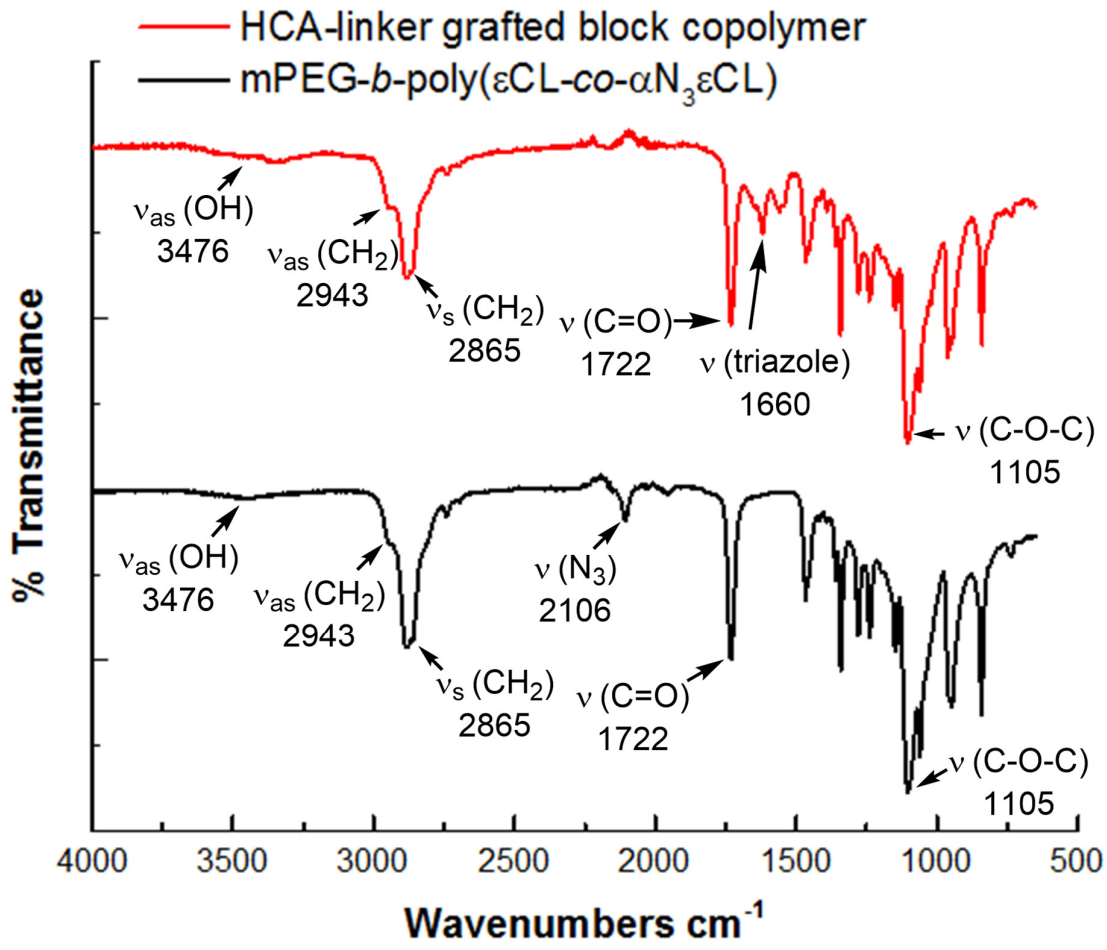

Figure 4-10. FT-IR spectrum of HCA-linker grafted block copolymer.

The micellisation of HCA-linker conjugated block copolymer was performed using same method as described for blank micelles. The size distributions and morphologies of micelles prepared from mPEG-*b*-poly(εCL-*co*-αN$_3$εCL-SS-HCA) were analysed using DLS and TEM, respectively. DLS analysis revealed that micelles of mPEG-*b*-poly(εCL-*co*-αN$_3$εCL-SS-HCA) resulted into an average size of 74 ± 8 nm (figure 4-11A), with spherical and well-defined morphologies as shown by TEM micrograph (figure 4-11B).

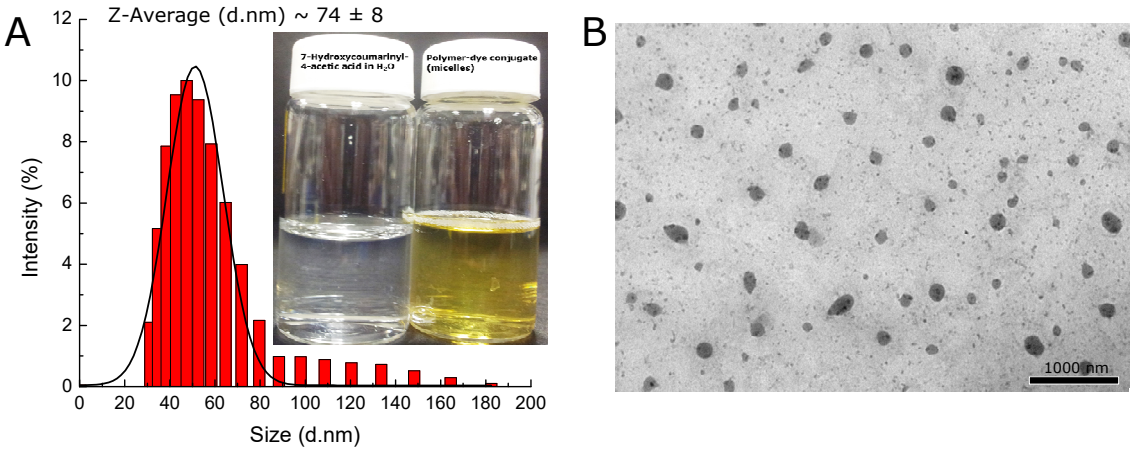

Figure 4-11. Characterisation of HCA-linker grafted block copolymer micelles. (A) Size distributions by DLS. The inset picture showing the physical appearance of the HCA in water (left vial) and HCA-linker grafted block copolymer micelles (right vial), and (B) TEM micrograph. Scale bar ~ 1000 nm.

The *in vitro* release of HCA from mPEG-*b*-poly(εCL-*co*-αN$_3$εCL-SS-HCA) micelles was investigated in non-reducing (PBS, pH 7.4) and simulated reducing conditions (10 mmol DTT in PBS) at 37 °C. The amount of dye release was measured by using UV-Vis spectrophotometry (λ_{max} = 321 nm). As shown in figure 4-12, under non-reducing conditions (pH 7.4, PBS), less than 15% HCA release was observed after 48 hours, while temporal release of the HCA was observed in reducing conditions (10 mmol DTT) showing more than 80% release of the HCA on the same length of time.

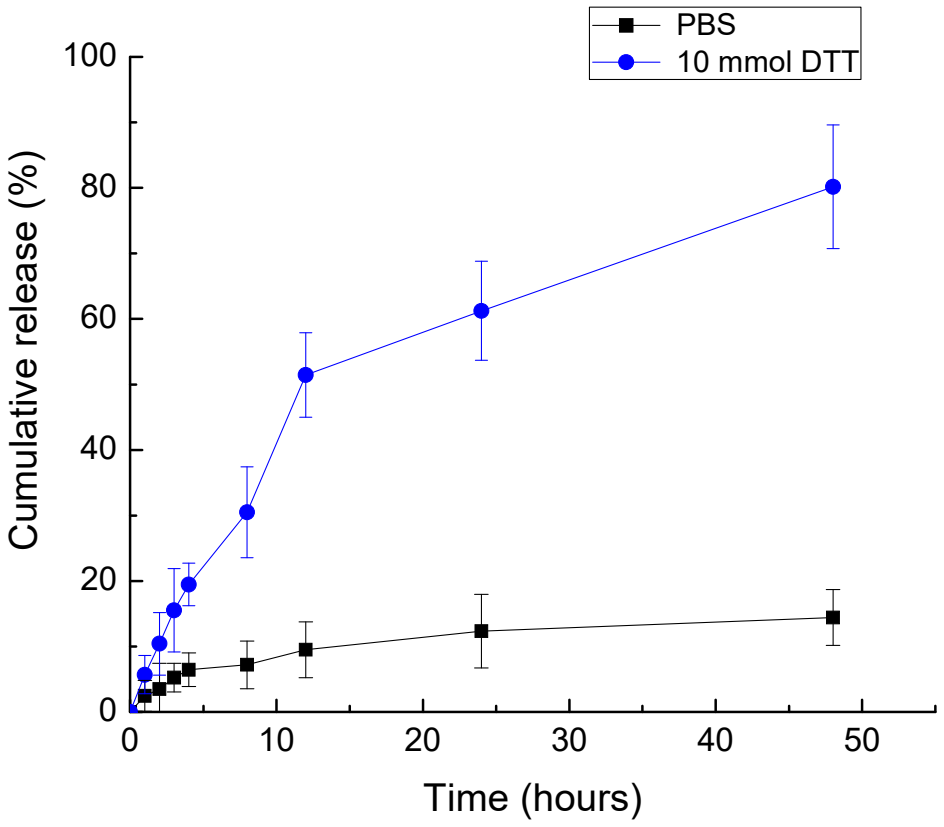

Figure 4-12. Analysis of HCA release from HCA-linker grafted block copolymer micelles in non-reducing and reducing medium at 37 °C. Error bars represent standard deviation (n=3).

4.3. DISCUSSION

The reactive micelles based on mPEG-*b*-poly(αN$_3$εCL) and mPEG-*b*-poly(εCL-*co*-αN$_3$εCL) amphiphilic block copolymers comprising various molecular weights and different ratios of functional groups, were prepared using dialysis method. The micelles of amphiphilic block copolymers can be prepared by various methods e.g., nanoprecipitation,[25] dialysis method,[26] oil-in-water emulsion method,[27] and solid dispersion method.[14] However, due to the high molecular weight of semi-crystalline polyethylene glycol

and the presence of multiple azide groups in poly(αN$_3$εCL), a good solvent (e.g. DMF or DMSO) for both the blocks is highly desirable to obtain micelles with well-defined morphology and narrow size distributions.[26] Therefore, the dialysis method was used to obtain micelles of mPEG-*b*-poly(αN$_3$εCL) and mPEG-*b*-poly(εCL-*co*-αN$_3$εCL) amphiphilic block copolymers using DMSO as a co-solvent. This method involved the dissolution of block copolymer in water-miscible DMSO followed by the drop-wise addition of this mixture into water (i.e., non-solvent for hydrophobic block). The drop-wise addition of copolymer-solvent mixture was controlled using a syringe pump by optimizing the flow rate to obtain uniform size micelles. The micellar solution was dialysed over night to gradually replace DMSO with water which caused the self-assembly of block copolymers into micelles. [28, 29]

The DLS analysis revealed that micelles sizes increased with the increase in the molecular weights of the block copolymers as summarised in table 4-1. Since the molecular weight of the mPEG block was same (i.e., 5 kDa) in all amphiphilic block copolymers, therefore, increase in the micelle size could be attributed to the increase in the molecular weights of hydrophobic poly(αN$_3$εCL) and or PCL.[30] The micelles prepared from mPEG-*b*-poly(αN$_3$εCL) block copolymers with lower molecular weights (6.8 and 9.6 kDa) showed narrow size distributions and poly dispersity index, however, micelles developed from the same block copolymer having higher molecular weights (14.6 and 20.0 kDa) showed broader size distributions. The mPEG-*b*-poly(αN$_3$εCL) block copolymers with lower molecular weights exhibited

well-defined spherical morphology of micelles without aggregations. However, same block copolymer with higher molecular weights showed presence of clusters or aggregates. The micellisation of mPEG-*b*-poly(εCL-*co*-αN$_3$εCL) followed similar trend in sizes and morphologies as the micellisation of mPEG-*b*-poly(αN$_3$εCL) block copolymers.

Table 4-1. Summary of the characterisation data of reactive micelles prepared from various functional block copolymers.

Polymer(s)	M_n (kDa)	Micelles size (d. nm) ± SD	Poly dispersity index ± SD	Zeta potential (mv) ± SD
mPEG-*b*-poly(αN$_3$εCL)	6.8	33 ± 6	0.20 ± 0.01	-8.7 ± 1.5
	9.6	42 ± 8	0.11 ± 0.09	-4.5 ± 0.8
	14.6	59 ± 11	0.12 ± 0.05	-4.8 ± 0.7
	20.0	83 ± 14	0.14 ± 0.07	-5.8 ± 0.5
mPEG-*b*-poly(εCL-*co*-αN$_3$εCL)	6.7	31 ± 4	0.13 ± 0.01	-4.0 ± 1.4
	10.1	36 ± 7	0.21 ± 0.02	-2.8 ± 0.9
	14.9	67 ± 5	0.24 ± 0.03	-3.8 ± 1.1
	19.8	71 ± 10	0.12 ± 0.05	-4.9 ± 1.4

The presence of clusters or aggregates in micelles prepared from higher molecular weight block copolymers could be attributed the strong hydrophobic-hydrophobic interactions amongst the core of micelles. The lower ratio of shell forming PEG to core forming PCL in higher molecular weight amphiphilic block copolymers could also be responsible for the aggregation of micelles due to the greater micelle-micelle interactions, as reported previously.[31] However, aggregation of micelles in lower molecular weights block copolymers was not found because of the higher proportion

of PEG in these block copolymers which might formed a dense brush like shell, therefore, limiting the micelle-micelle or hydrophobic-hydrophobic interactions.

The surface charges or zeta potentials of all the micelles appeared close to neutral or slightly negative. The neutral surface charges of micelles can be attributed to the neutral hydrophilic PEG shell that could shield the micelles in such a way that long loops and tails of PEG extend out in the solution and inhibit the aggregation of micelles through steric stabilisation. Therefore, near to zero or neutral zeta potential may not affect the stability of micelles due to the steric stabilisation by PEG.[32]

The self-assembly of these functional block copolymers into spherical micelles in the aqueous media could make them attractive candidates for novel drug delivery systems. Specifically, the existence of multiple azide groups in the core of these micelles could be useful to tag them with a fluorescent probe for cell imaging or to monitor intra-cellular trafficking and to covalently graft a drug for controlled release applications (figure 4-13). To prove this concept, a model molecule i.e. 7-hydroxycoumarinyl-4-acetic acid (HCA) was functionalised with an alkyne-bearing redox responsive bifunctional linker, and was subsequently grafted onto the hydrophobic backbone of a selected block copolymer (i.e., mPEG-*b*-poly(εCL-*co*-αN$_3$εCL), M_n ~ 10.1 kDa) via copper-catalysed azide–alkyne cycloaddition. The micellisation of polymer-dye conjugate resulted into spherical micelles with narrow size distributions. However, the average sizes of the micelles

prepared from the polymer-dye conjugate was larger when compared with the same polymer without dye conjugation. The larger sizes of the dye-conjugated micelles might be due to the existence of HCA and formation of triazole ring in the core of micelles during click reaction.[33]

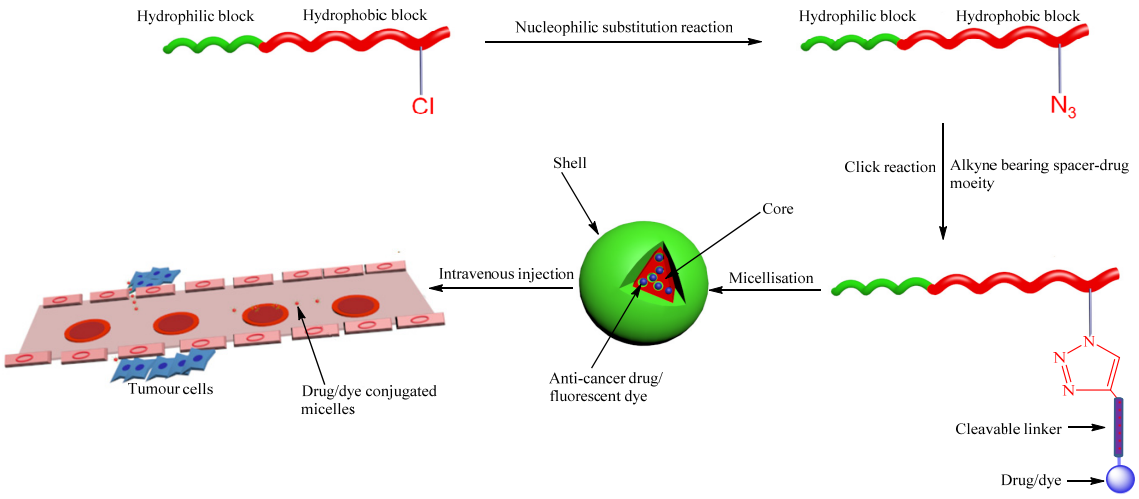

Figure 4-13. Schematic illustration for the synthesis of polymer-drug/dye conjugate and micellisation.

The release studies revealed that micelles of polymer-dye conjugate efficiently retained the HCA under non-reducing medium, however, temporal release of the HCA was observed in the reducing medium. The temporal release of the HCA under reductive environment was primarily due to the reduction of disulfide bonds resulting into the cleavage of the linker, and subsequently release of dye as reported previously.[34, 35] These redox-sensitive polymer-dye/drug conjugated micelles can be utilised to release the drug in response to naturally occurring reductive environment

within the cancer cells. Such linkages are stable in the blood circulation and in the extracellular environment, but might be susceptible to rapid cleavage under a reductive environment.[36] This rapid response chemical degradation characteristic is different from typical hydrolytically degradable polymers. In particular, the polyesters generally undergo gradual degradation kinetics inside the body ranging from days to months.[25] Therefore, incorporating a redox-responsive linker in amphiphilic block copolymeric micelles could enable them to be attractive candidates for the responsive delivery and controlled release of anti-cancer agents.

4.4. CONCLUSIONS

The reactive micelles based on mPEG-*b*-poly(αN$_3$εCL) and mPEG-*b*-poly(εCL-*co*-αN$_3$εCL) amphiphilic block copolymers comprising various molecular weights and different ratios of functional groups were prepared using dialysis method. The micelles prepared from mPEG-*b*-poly(αN$_3$εCL) with molecular weights of 6.8 and 9.6 kDa showed smaller sizes and approximately spherical morphologies as compared with the micelles developed with higher molecular weights of 14.6 and 20.0 kDa which showed larger sizes and formation of clusters or aggregates. The micelles prepared with mPEG-*b*-poly(εCL-*co*-αN$_3$εCL) exhibited similar trend in sizes and morphologies i.e., by increasing the molecular weights of hydrophobic poly(αN$_3$εCL) and or PCL, micelle size increased as did the formation of aggregates with higher molecular weight block copolymers. The surface

charges of micelles prepared from all the tested amphiphilic block copolymers were slightly negative or near neutral due to the neutral mPEG corona.

The azide-bearing hydrophobic backbone of a selected amphiphilic block copolymer ((mPEG-*b*-poly(εCL-*co*-αN$_3$εCL), M_n ~ 10.1 kDa) was used to conjugate an alkyne functionalised model molecule (HCA-linker) to develop redox-responsive polymer-dye conjugate as a model responsive drug delivery system. The resultant micelles of mPEG-*b*-poly(εCL-*co*-αN$_3$εCL-SS-HCA) efficiently retained the HCA in the non-reducing medium, while, temporal release of HCA was observed in the reducing medium.

4.5. EXPERIMENTAL

4.5.1. Micellisation of amphiphilic block copolymers

Empty micelles of mPEG-*b*-poly(αN$_3$εCL) and mPEG-*b*-poly(εCL-*co*-αN$_3$εCL) block copolymers with different molecular weights were prepared by the dialysis method using DMSO (a good co-solvent for both the blocks). The copolymers (50 mg) were dissolved in 5 mL DMSO and was introduced into Milli-Q water (20 mL) under vigorous stirring, using a syringe pump with a flow rate of 0.20 mL/min. The solution was stirred for 2 hours at room temperature and polymer micelles were purified by dialysis overnight against 1 L of Milli-Q water using a cellulose dialysis membrane

(Spectrapor, cut-off 3500) to remove the DMSO solvent. Micelles were characterised for their size distributions, morphologies and zeta potentials.

4.5.2. Synthesis of bi-functional redox-responsive linker [2-((2-hydroxyethyl)disulfaneyl)ethyl pent-4-ynoate]

2-hydroxyethyl disulfide (1.31 g, 8.50 mmol), 4-pentynoic acid (0.416 g, 4.24 mmol), and *N*-(3-dimethylaminopropyl)-*N′*-ethylcarbodiimide hydrochloride (0.814 g, 4.24 mmol) were introduced into a round bottom flask containing dry dichloromethane (50 mL, precooled to 0 °C using an ice bath). Afterwards, 4-(dimethylamino) pyridine (0.026 g, 0.21 mmol) was added drop wise and the reaction contents were stirred for 48 hours at room temperature. Afterwards, the organic phase was washed with 3x100 mL of 1M hydrochloric acid solution, 3x100 mL of 1M sodium hydroxide solution, and 1M sodium chloride solution (200 mL). The water residues of organic layer were removed with anhydrous $MgSO_4$ overnight. The organic phase was filtered and the solvent was removed by rotary evaporator. The final product was purified by silica gel column chromatography (hexane: ethyl acetate 4:3, R_f 0.40, 46% yield), and characterised by electrospray ionisation mass spectrometry (see appendix figure 8-4), ^{1}H NMR, and ^{13}C NMR. ^{1}H NMR (400 MHz, $CDCl_3$) δ (ppm): 4.45 – 4.35 ($C\underline{H}_2$-O-C=O, t, *J* = 6.4 Hz, 2H), 3.96 – 3.85 ($C\underline{H}_2$-OH, t, *J* = 5.8 Hz, 2H), 2.97 – 2.92 (S-S-$C\underline{H}_2$-CH_2-O-C=O, t, *J* = 6.4 Hz, 2H), 2.89 (S-S-$C\underline{H}_2$-CH_2-OH, t, *J* = 5.8 Hz, 2H), 2.62 – 2.56 (O=C-$C\underline{H}_2$-CH_2-C≡CH, m, 2H), 2.55 – 2.50 (O=C-CH_2-$C\underline{H}_2$-C≡CH, m, 2H), 2.18 (CH_2-O$\underline{H}$, s, 1H), 2.00 (C≡C$\underline{H}$, s, 1H). ^{13}C NMR

(101 MHz, $CDCl_3$) δ (ppm): 171.66 (C=O), 82.31 (C≡CH), 69.23 (C≡CH), 62.62 (CH_2-O-C=O), 60.25 (CH_2-OH), 41.56 (S-S-CH_2-CH_2-OH), 36.93 (S-S-CH_2-CH_2-O-C=O), 33.24 (O=C-CH_2-CH_2-C≡CH), 14.32 (O=C-CH_2-CH_2-C≡CH). Data were compared with the previously reported results by Jain *et. al*.[37]

4.5.3. Synthesis of HCA-linker complex [2-((2-(2-(7-hydroxy-2-oxo-2H-chromen-4-yl)acetoxy)ethyl)disulfaneyl)ethyl pent-4-ynoate]

7-Hydroxycoumarinyl-4-acetic acid (HCA, 200 mg, 0.91 mmol), 267 mg (1.14 mmol) of alkyne-2-hydroxyethyl disulfide (linker), and *N*-(3-dimethylaminopropyl)-*N'*-ethylcarbodiimide hydrochloride (174 mg, 0.91 mmol) were dissolved in dimethyl sulfoxide (5 mL) in a round bottom glass flask. The reaction mixture was purged with nitrogen gas before the dropwise addition of 4-(dimethylamino) pyridine (11 mg, 0.09 mmol). The reaction was carried out under stirring for 24 hours at room temperature. The product mixture was then dissolved in ethyl acetate (100 mL), and was washed with 1M HCl solution (100 mL) and finally with 100 mL brine. The organic phase was dried over anhydrous $MgSO_4$, filtered, and the solvent was removed by rotary evaporator and the final product was characterised by electrospray ionisation mass spectrometry, and ^{1}H NMR. ^{1}H NMR (400 MHz, DMSO) δ (ppm): 10.61 (s, 1H), 7.52 (d, 1H), 6.79 (d, 1H), 6.73 (s, 1H), 6.25 (s, 1H), 4.39 – 4.23 (m, 4H), 4.03 (m, 2H), 3.96 (s, 2H), 2.96

(t, 2H), 2.83 – 2.72 (m, 2H), 1.98 (s, 1H). ^{13}C NMR (101 MHz, DMSO) δ (ppm): 171.60, 169.53, 162.21, 160.62, 155.55, 149.80, 127.13, 113.61, 112.50, 102.81, 83.36, 71.92, 63.00, 60.01, 41.56, 37.30, 36.71, 33.12, 14.20.

4.5.4. Grafting of HCA-linker onto copolymer and micellisation

The block copolymer coded as MG14 (*Mn* ~ 10145 g/mol, D_p of PCL ~ 35, D_p of poly(αN3εCL) ~ 7) was selected to graft a model molecule (7-hydroxycoumarinyl-spacer) (HCA-linker) using copper catalysed alkyne-azide cycloaddition (CuAAC). Briefly, 600 mg (approximately 0.059 mmol) of mPEG-*b*-poly(εCL-*co*-αN_3εCL) was dissolved in DMSO (5 mL) and was purged with nitrogen gas for 30 minutes. Afterwards, HCA-linker complex (201 mg, 0.46 mmol, 1.1 mol equi. *vs* azide group), copper(I) bromide (12 mg, 0.08 mmol, 0.20 mol equi. *vs* azide group), and triethylamine (8 mg, 0.084 mmol, 0.20 mol equi. *vs* azide group) were introduced into the system. The reaction contents were stirred at 36 °C for 24 hours and the kinetics of reaction was monitored by FT-IR spectroscopy. The polymer-dye conjugate was precipitated in anhydrous diethyl ether, filtered, and dried under vacuum and was characterised by FT-IR spectroscopy. IR: ν max/cm^{-1}: 1096 (C-O-C stretching), 1660 (triazole ring stretching), 1727 (C=O stretching), 2885 (symmetric CH_2 stretching), 2999 (asymmetric CH_2 stretching), 3427 (OH stretching).

The micelles of polymer-dye conjugate were prepared using same method as described for the preparation of blank micelles.

4.5.5. *In vitro* release studies

The *in vitro* HCA release studies from micelles were carried out in non-reducing (PBS, pH 7.4) and reducing (10 mmol DTT in PBS, pH 7.4) media. 10 mg of freeze dried mPEG-*b*-poly(εCL-*co*-αN_3εCL-SS-HCA) micelles were re-dispersed in 2mL PBS (pH 7.4) and the solution was placed in a dialysis device (Slide-A-Lyzer™ mini dialysis device, 3.5K MWCO, Thermo Scientific). The micellar solution was dialysed against 45 mL of release media at 37 °C and samples (1 mL) were taken at appropriate time points and replaced with 1 mL fresh medium. The collected samples were freeze dried and dissolved in DMSO. The amount of HCA was calculated using UV-Vis spectrophotometer (λ_{max} = 321 nm) via a standard calibration curve of HCA in DMSO.

4.6. REFERENCES

1. G. S. Kwon and T. Okano, *Advanced Drug Delivery Reviews*, 1996, **21**, 107-116.
2. G. Riess, *Progress in Polymer Science (Oxford)*, 2003, **28**, 1107-1170.

3. M. C. Jones and J. C. Leroux, *European Journal of Pharmaceutics and Biopharmaceutics*, 1999, **48**, 101-111.
4. V. S. Trubetskoy and V. P. Torchilin, *S.T.P. Pharma Sciences*, 1996, **6**, 79-86.
5. M.-C. Jones and J.-C. Leroux, *European Journal of Pharmaceutics and Biopharmaceutics*, 1999, **48**, 101-111.
6. S. Cammas, K. Suzuki, C. Sone, Y. Sakurai, K. Kataoka and T. Okano, *Journal of Controlled Release*, 1997, **48**, 157-164.
7. J. E. Chung, M. Yokoyama, K. Suzuki, T. Aoyagi, Y. Sakurai and T. Okano, *Colloids and Surfaces B: Biointerfaces*, 1997, **9**, 37-48.
8. W. Y. Chen, P. Alexandridis, C. K. Su, C. S. Patrickios, W. R. Hertler and T. A. Hatton, *Macromolecules*, 1995, **28**, 8604-8611.
9. T. Inoue, G. Chen, K. Nakamae and A. S. Hoffman, *Journal of Controlled Release*, 1998, **51**, 221-229.
10. J. Connor, N. Norley and L. Huang, *BBA - General Subjects*, 1986, **884**, 474-481.
11. S. B. La, T. Okano and K. Kataoka, *Journal of Pharmaceutical Sciences*, 1996, **85**, 85-90.
12. I. G. Shin, S. Y. Kim, Y. M. Lee, C. S. Cho and Y. K. Sung, *Journal of Controlled Release*, 1998, **51**, 1-11.
13. S. Cajot, P. Lecomte, C. Jerome and R. Riva, *Polymer Chemistry*, 2013, **4**, 1025-1037.
14. U. Kedar, P. Phutane, S. Shidhaye and V. Kadam, *Nanomedicine: Nanotechnology, Biology and Medicine*, 2010, **6**, 714-729.

15. N. Nishiyama, S. Okazaki, H. Cabral, M. Miyamoto, Y. Kato, Y. Sugiyama, K. Nishio, Y. Matsumura and K. Kataoka, *Cancer Research*, 2003, **63**, 8977-8983.

16. J. M. Chan, L. Zhang, K. P. Yuet, G. Liao, J. W. Rhee, R. Langer and O. C. Farokhzad, *Biomaterials*, 2009, **30**, 1627-1634.

17. L. Yang and P. Alexandridis, *Current Opinion in Colloid & Interface Science*, 2000, **5**, 132-143.

18. C. Allen, D. Maysinger and A. Eisenberg, *Colloids and Surfaces B: Biointerfaces*, 1999, **16**, 3-27.

19. C. Deng, Y. Jiang, R. Cheng, F. Meng and Z. Zhong, *Nano Today*, 2012, **7**, 467-480.

20. R. K. Jain and T. Stylianopoulos, *Nature Reviews Clinical Oncology*, 2010, **7**, 653-664.

21. T. Lammers, F. Kiessling, W. E. Hennink and G. Storm, *Journal of Controlled Release*, 2012, **161**, 175-187.

22. M. Talelli, M. Barz, C. J. F. Rijcken, F. Kiessling, W. E. Hennink and T. Lammers, *Nano Today*, 2015, **10**, 93-117.

23. F. Koizumi, M. Kitagawa, T. Negishi, T. Onda, S.-i. Matsumoto, T. Hamaguchi and Y. Matsumura, *Cancer Research*, 2006, **66**, 10048-10056.

24. G. S. Kwon, M. Yokoyama, T. Okano, Y. Sakurai and K. Kataoka, *Pharmaceutical Research*, 1993, **10**, 970-974.

25. K. K. Bansal, D. Kakde, L. Purdie, D. J. Irvine, S. M. Howdle, G. Mantovani and C. Alexander, *Polymer Chemistry*, 2015, **6**, 7196-7210.

26. S. Cajot, N. Lautram, C. Passirani and C. Jerome, *Journal of Controlled Release*, 2011, **152**, 30-36.

27. S. B. La, T. Okano and K. Kataoka, *Journal of Pharmaceutical Sciences*, 1996, **85**, 85-90.

28. J.-H. Kim, K. Emoto, M. Iijima, Y. Nagasaki, T. Aoyagi , T. Okano, Y. Sakurai and K. Kataoka, *Polymers for Advanced Technologies*, 1999, **10**, 647-654.

29. K. Van Butsele, P. Sibret, C. A. Fustin, J. F. Gohy, C. Passirani, J. P. Benoit, R. Jérôme and C. Jérôme, *Journal of Colloid and Interface Science*, 2009, **329**, 235-243.

30. K. K. Jette, D. Law, E. A. Schmitt and G. S. Kwon, *Pharmaceutical Research*, 2004, **21**, 1184-1191.

31. Y. Lu and K. Park, *International Journal of Pharmaceutics*, 2013, **453**, 198-214.

32. H. Otsuka, Y. Nagasaki and K. Kataoka, *Advanced Drug Delivery Reviews*, 2003, **55**, 403-419.

33. S. Cajot, N. Lautram, C. Passirani and C. Jérôme, *Journal of Controlled Release*, 2011, **152**, 30-36.

34. F. Meng, Z. Zhong and J. Feijen, *Biomacromolecules*, 2009, **10**, 197-209.

35. J.-H. Ryu, R. Roy, J. Ventura and S. Thayumanavan, *Langmuir*, 2010, **26**, 7086-7092.

36. J. Li, M. Huo, J. Wang, J. Zhou, J. M. Mohammad, Y. Zhang, Q. Zhu, A. Y. Waddad and Q. Zhang, *Biomaterials*, 2012, **33**, 2310-2320.

37. A. K. Jain, M. G. Gund, D. C. Desai, N. Borhade, S. P. Senthilkumar, M. Dhiman, N. K. Mangu, S. V. Mali, N. P. Dubash, S. Halder and A. Satyam, *Bioorganic Chemistry*, 2013, **49**, 40-48.

Chapter 5: ANTICANCER DRUG LOADED REDOX-RESPONSIVE REVERSIBLY CORE-CROSSLINKED MICELLES INDUCING APOPTOSIS IN BREAST CANCER CELLS

(This chapter has been published in Biomaterials Science, 2017,**5**, 532-550)

5.1. INTRODUCTION

Micelle-based drug carrier systems have emerged as promising tools for site-specific delivery and controlled release applications.[1, 2] Despite several advantages over conventional drugs (e.g. prolonged circulation time, improved drug bioavailability and, for cancer treatments enhanced accumulation in tumour sites, and fewer side effects of the encapsulated drug),[3-5] some limitations of micelle-based drug delivery have also been reported. These drawbacks include low stability *in vivo*, poor penetration, modest accumulation in tumour tissues, and inadequate control over drug release.[6-8] Furthermore, premature drug release in the bloodstream can decrease the efficacy and may increase the side effects of micelle-based drug delivery systems.[9]

To overcome such limitations, stimuli-responsive or smart polymeric nanocarriers have been developed. Such smart nanocarriers can release payload in response to internal or external stimulus such as light, magnetic field, temperature, enzymes, redox-potential, and reactive oxygen species.[10-12] Specifically, bio-responsive nanocarriers offer additional advantages over external stimuli-responsive (magnetic, temperature and light) nanocarriers. Bio-responsive nanocarriers have shown enhanced tumour uptake in tumour cells and triggered drug release at the target site without the need of an external device.[13]

The most well-known internal stimuli in cancerous regions include acidity (pH 6.5-7.2) associated with dysregulated metabolism in tumour tissues, higher levels of glutathione in the cytosol and cell nucleus, altered degradative enzymes in the lysosomes, and reactive oxygen species (ROS) in the mitochondria.[14-16] In addition, acidic pH in the endosomal and lysosomal compartments (pH 5.5-6.8, and 4.5-5.5, respectively), provide additional triggers for intracellular drug release. These intrinsic microenvironments can be exploited as internal stimuli to attain active drug release in the tumour tissues or cancer cells. Accordingly, nanocarriers which are responsive to these stimuli have shown greater *in vitro* and *in vivo* antitumour activities when compared to their non-responsive counterparts.[17-19] Additionally, owing to rapid release of payloads into the cancer cells, bio-responsive nano-carriers have also demonstrated their importance in reversing multidrug resistant cancers.[15]

In particular, redox-responsive polymeric nano-carriers have been of interest as bio-responsive drug delivery systems. Their rapid response to intracellular reducing conditions, and triggered release of payload in the cytosol and subsequent passage to the cell nucleus,[20] enables them to be good candidates for responsive drug delivery and controlled release application. It has been reported that the glutathione tripeptide (γ-glutamyl-cysteinyl-glycine) (GSH) is present in higher concentrations (2-10 mmol) in the cytosol than in the extracellular milieu (approximately 2-20 μmol).[21-23] Furthermore, the reducing potential inside certain cancerous

cells (e.g. human breast, prostate, colon and pancreatic cancer)[24] is considerably higher (approximately 100–1000 times) than that found in the extracellular environment and bloodstream.[25, 26] Redox states in cancer cells are controlled by complex and variable parameters,[27] however, the ranges of redox potential might be exploited for tumour specific drug delivery and controlled release applications.

Generally, redox responsive polymers have disulfide linkages that are stable in the normal extracellular environment but which undergo rapid cleavage in the presence of reducing agents, such as GSH, in the intracellular components.[10, 28]

Redox responsive disulfide bridges can be incorporated in the backbone of a polymer or in a side chain, or as crosslinker inside a nanocarrier using initiator, monomer or chain transfer mechanism.[22, 28] For instance, doxorubicin loaded core-shell micelles comprising intervening disulfide bonds between the hydrophilic PEG shell and the hydrophobic poly(ε-benzyloxycarbonyl-*L*-lysine) core have been developed. It was revealed that doxorubicin-loaded reduction responsive micelles inhibited cell proliferation to a greater extent in glutathione pre-treated human cervical cell line (HeLa cells) and human hepatoma cell line (HepG2 cells) as compared to the corresponding untreated cells.[29]

Moreover, redox responsive atorvastatin calcium loaded micelles have been constructed from amphiphilic copolymers of mPEG-SS-vitamin E succinate for metastatic breast cancer therapy. It was shown that the atorvastatin

content in tumours and lungs was significantly higher in the case of atorvastatin loaded micelles when compared to the free drug at 12-hours post administration. Furthermore, it was also revealed that atorvastatin loaded micelles could completely prevent liver and lung metastasis of breast cancer in a 4T1 orthotropic mammary tumour metastatic cancer model.[30]

Redox-responsive disulfide bridges can also be incorporated into nanocarriers by placing multiple disulfide bonds in a polymer backbone or by conjugating therapeutic agents to the side chain of the polymer via a disulfide linker. For instance, camptothecin-conjugated redox-responsive (PEG-PLL-SS-CPT) micelles demonstrated prolonged blood circulation and greater localisation in xenografts of AY27 rat urothelial carcinoma.[31] After Photofrin (a clinically approved photosensitizer) induced endosomal permeability, real-time confocal microscopy revealed the escape of camptothecin-conjugated redox-responsive (PEG-PLL-SS-CPT) micelles from endocytic vesicles into the cytosol of cancer cells. It was also observed that the drug release was higher in irradiated tissues when compared to the tissues without irradiation, hence enhanced the *in vivo* antitumour efficiency without any significant toxicity to normal tissues.

Another strategy to construct redox-responsive bridges is to crosslink the polymeric nanocarriers with a disulfide agent. Previously, it has been shown that polymeric micelles can dissociate, especially upon administration when they are diluted below their critical micelle concentration.[32] The stability of

polymeric micelles can be enhanced by chemical crosslinking.[33, 34] Various types of crosslinked micelles can be prepared, dependent on the localisation of the crosslinking,[35] *e.g.* shell crosslinked micelles,[36,37] and core crosslinked micelles.[9]

Shell crosslinked nanocarriers can offer better stability along with higher drug loading. For instance, doxorubicin (DOX) loaded shell-crosslinked disulfide bonded mPEG-$(Cys)_4$-PDLLA micelles stably retained the drug during circulation and delivered 7-fold higher drug concentrations to the tumour in contrast to the non-crosslinked PEG-*b*-PDLLA micelles.[38] Moreover, the same DOX-loaded crosslinked micelles completely suppressed the M109 tumour progression in mice within 2 weeks after post administration.

Additionally, doxorubicin loaded shell-crosslinked micelles based on hyaluronic acid-poly caprolactone (HA-PCL) block copolymer micelles have been prepared by crosslinking a hyaluronic acid shell with a bio-reducible disulfide crosslinker.[39] The doxorubicin loaded shell-crosslinked HA-PCL micelles significantly decreased drug release under physiological conditions, whereas, rapid drug release was observed in the presence of glutathione. *In vitro* and *in vivo* experiments showed that doxorubicin loaded shell-crosslinked HA-PCL micelles could successfully deliver the drug into the nuclei of SSC7 cells and also to the tumour when administrated into SSC7 tumours present at subcutaneous dorsa of athymic nude mice.

Shell crosslinked micelles can offer better stability along with higher drug loading, however, a challenge in preparation of shell-crosslinked micelles is the need for highly dilute conditions to circumvent undesired inter-micellar crosslinking, therefore making it difficult for large-scale preparation.[40] The inter-micellar crosslinking in shell cross-linked micelles may also cause the agglomeration of nanocarriers into larger particles which may lead to system instability and a weakened "enhanced permeability and retention" (EPR) effect.[41]

To overcome these limitations, reduction sensitive core-crosslinked micelles have been developed. Generally, these reduction-sensitive core-crosslinked micelles are designed from amphiphilic block copolymers that contain functional moieties (*e.g.* carboxylic acid, hydrazide, lipoyl, dithiopyridine, thiol and alkynyl) in the hydrophobic block as pendent or end-capped groups.[42] For instance, dithiodiethanoic acid was used as a crosslinker to prepare doxorubicin conjugated core-crosslinked micelles based on PEG-*b*-poly(methacrylic acid-*g*-hydrazone-DOX) block copolymer.[43] The resultant core-crosslinked micelles showed fast drug release in response to acidic and reductive conditions. Furthermore, reduction-sensitive reversibly core-crosslinked micelles based on PEG-*b*-poly(*N*-2-hydroxypropyl methacrylamide)−lipoic acid were developed for doxorubicin triggered release.[44] In this case, PEG-*b*-PHPMA block copolymers were synthesised by reversible addition−fragmentation chain transfer (RAFT) polymerisation. The lipoic acid was then conjugated by the

esterification of hydroxyl groups in the block copolymer and micelles were crosslinked with a catalytic amount of dithiothreitol. The core-crosslinked PEG-*b*-poly(*N*-2-hydroxypropyl methacrylamide)−lipoic acid micelles showed better drug loading and *in vitro* drug release experiments demonstrated significantly higher doxorubicin release in reducing conditions (10 mmol DTT) when compared to the drug release at physiological conditions. Empty core-crosslinked micelles were non-toxic up to 1 mg/mL concentration, whereas, doxorubicin loaded core-crosslinked PEG-b-PHPMA-LA micelles showed good antitumour activity in HepG2 and HeLa cells as revealed by MTT assays.

Moreover, core-crosslinked micelles based on poly(ethylene glycol)-*b*-poly(*L*-lysine) have also been constructed.[45] Specifically, some of the lysine groups of the copolymer were further modified with iminothiolane and a polyion complex was developed by intermingling the positively charged lysine residues with negatively charged siRNA. The core of the polyion complex was then crosslinked using iminothiolane via disulfide bonds. It was revealed that core-crosslinked polyion complex micelles demonstrated 100-fold higher siRNA transfection as compared with non-crosslinked polyion complex micelles. However, it is noteworthy that side reactions can occur when reacting 2-aminothiolane with primary amines, which may cause undesired impurities and may lead to degradation of the polymer.[9]

Redox-responsive core-crosslinked micelles have demonstrated good stability and better 'stealth' properties, however, the hydrophobic cores of most of the existing core-crosslinked micelles have been based on non-degradable polymers such as polyacrylamide or polyacrylate.[46, 47] The non-degradable constituent of the block copolymer may cause complications in clinical applications. Poly(*L*-lysine) which is a biodegradable polymer, has also been used to form the core of the reduction-responsive core-crosslinked micelle, however, this polymer is not biologically inert, for example, polycationic materials have been reported to alter cellular processes and cell division during transfection.[48, 49] Furthermore, activation of proteins and phospholipases by poly(*L*-lysine) has also been observed, which may affect membrane permeability.[50] Therefore, reduction-responsive core-crosslinked micelles comprising entirely of biologically inert or biocompatible polymers that are biodegradable would be better candidates for drug delivery and controlled release applications.

Polyesters are a class of biodegradable polymers and have been frequently used in various biomedical applications such as tissue engineering, drug delivery, and controlled release.[51] In the last few decades, various FDA approved[52] aliphatic polyesters e.g. poly(lactic-co-glycolic acid) (PLGA), poly(ε-caprolactone) (PCL), and poly(lactic acid) (PLA), have been intensively studied to exploit their potential in drug, gene and protein delivery and controlled release applications.[53] Such polyesters are mainly derived from ε-caprolactone, β-butyrolactone, lactide, glycolide, and

trimethyl carbonate.[54-56] It has been reported that several polyesters are biodegradable and biocompatible but most of these polyesters lack functional side chains, making it difficult to incorporate redox-responsive linkages to core-crosslink their micelles.

To address these issues, we have synthesised a functional biodegradable and biocompatible block copolymer based on mPEG-*b*-poly(εCL-*co*-αClεCL). The pendent chloro groups of the block copolymer were converted into azides using nucleophilic substitution reaction to produce mPEG-*b*-poly(εCL-*co*-αN_3CL) block copolymer as a precursor of reactive polymeric micelles. The synthesised polymers were characterised by ^{1}H NMR, FT-IR and size exclusion chromatography (SEC). Micelles were prepared using co-solvent or dialysis methods and methotrexate (MTX) (an anticancer drug) was loaded into the hydrophobic core of the reactive micelles. MTX is a folate antimetabolite and is a derivative of deoxyfolic acid. Folate dependent enzymes play an important role in the synthesis of the nucleoside thymidine, needed for DNA synthesis by both normal and cancer cells.[57] However, cancer cells require higher amounts of folate-dependent enzymes due to their increased rates of metabolism. Folic acid (as folate salt) is also important for the biosynthesis of purine and pyrimidine bases.[58] Dihydrofolate reductase (DHFR) is a vital enzyme in intracellular folate metabolism in which an inactive derivative (dihydrofolate) of folic acid is reduced into the active derivative (tetrahydrofolate) catalysed by DHFR.[59] MTX competitively inhibits DHFR, therefore obstructing the synthesis of

RNA and DNA. By inhibiting DHFR, cancer cells lose their ability to repair and replicate, leading to impairment of tumour growth and induction of cell death by secondary genotoxic effects or apoptosis.[60] MTX has been used against various malignancies including breast, lung, head and neck cancers, Hodgkin's disease, non-Hodgkin's lymphoma, osteosarcoma, and childhood acute lymphocytic leukemia.[61] MTX is commercially available, formulated as tablets, injections and capsules in various doses of 2.5, 7.5, 10 and 50 mg.

Despite several advantages of MTX in treating certain types of tumour, various dose-related side effects of MTX *e.g.* acute and chronic hepatotoxicity, bone marrow suppression, interstitial pneumonitis, nephrotoxicity, and leukopenia have been reported.[62] Furthermore, poor aqueous solubility (0.01 mg/mL, pKa; 4.7-5.5), low permeability and the short circulation half-life (2-10 hours) of the free acid form of MTX are major barriers in developing therapeutically successful formulations.[59, 63] Although, the methotrexate disodium salt exhibits better aqueous solubility and can be routinely administered through oral route, it should be noted that plasma MTX concentrations after oral administration have been reported to vary significantly due to interpatient differences in the rate of absorption.[64] Moreover, uptake of orally administered MTX through the gastrointestinal tract is mainly mediated via a saturable transporter, the reduced folate carrier (RFC).[65, 66] Therefore, bioavailability of orally administered MTX decreases at higher doses upon saturation of RFC and

increasing the dose may not help in overcoming the poor bioavailability.[65,67,68]

To overcome these limitations, MTX was encapsulated into the cores of micelles. Micelles were subsequently crosslinked by a redox-responsive bis-alkyne ethyl disulfide crosslinker. The size distributions and morphology of core-crosslinked micelles were assessed using dynamic light scattering (DLS) and transmission electron microscopy. The drug release studies were performed under simulated physiological and reductive conditions. Cellular uptake studies in human breast cancer cells (MCF7 cells) were performed using Oregon-green loaded core-crosslinked micelles.

The MCF7 cell line was used as an *in vitro* model for cellular uptake studies. It is a widely investigated epithelial cancer cell line derived from breast adenocarcinoma. When grown *in vitro*, this cell line retains ideal characteristics of mammary epithelium and is capable of developing domes and forming monolayer. Moreover, the MCF-7 cell line has been exploited to generate a reference collection of gene-expression profiles following treatment with nanomaterials.[69] The MCF-7 cell line has also been widely used to simulate the functional interactions of drug-loaded nano-carriers with the mammalian cells, previously.[70] Therefore, MCF-7 cell line can be a suitable *in vitro* model to mimic the breast cancers for cellular uptake studies of nanomaterials.

The Oregon-green dye was used a model fluorophore for cellular uptake studies because it shares numerous advantages over other fluorescein based probes. For instance, Oregon green is significantly less susceptible to photobleaching and is more stable as compare to the fluorescein, hence, permitting better acquisition of photons before photo-destruction of the fluorophore.[71] Additionally, Oregon green based probes have a lower pKa (pKa = 4.7) making their fluorescence essentially pH insensitive in the physiological pH range.[72] Therefore, Oregon green fluorophore can be a useful alternate to the fluorescein for imaging, cellular uptake and diagnosis.

The MTX-loaded core-crosslinked micelles were assessed for their cytotoxicity in human breast cancer cells by MTT assays. The apoptosis inducing potential of MTX-loaded core-crosslinked micelles was analysed using Hoechst/PI assays and was further probed by annexin-V/PI assays. The data obtained from these assays indicate that drug release from these cross-linked micelles can be controlled and that the redox-responsive micelles are more effective carriers for MTX than non-crosslinked analogues in the cell-lines tested.

5.2. RESULTS

5.2.1. Preparation and characterisation of MTX-loaded redox-responsive reversibly core-crosslinked micelles

To incorporate reduction sensitive bridges into the core of the micelles, a *bis*-alkyne-ethyl disulfide crosslinker was synthesised and the micelle-core was then crosslinked using CUAAC. The *bis*-alkyne-ethyl disulfide cross-linker was synthesised by reacting pentynoic acid with *bis*(2-hydroxyethyl) disulfide, using EDAC as a carboxylic acid activating agent and DMAP as a catalyst. (scheme 5-1).

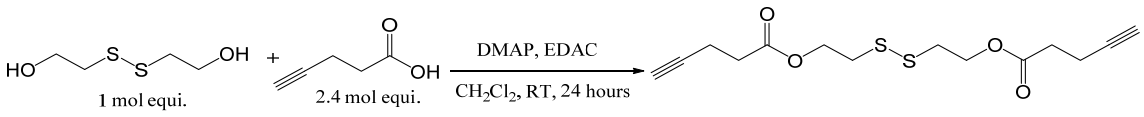

Scheme-5-1. Scheme for the synthesis of *bis*-alkyne ethyl disulfide redox-responsive crosslinker.

The reaction proceeded from the conversion of carboxylic acid by EDAC into an anhydride, which then formed an acylpyridinium intermediate with DMAP. This intermediate is highly reactive due to the electrophilic acylcarbonyl carbon of acylpyridinium, which is readily attacked by nucleophilic alcohols to produce the corresponding ester derivative.

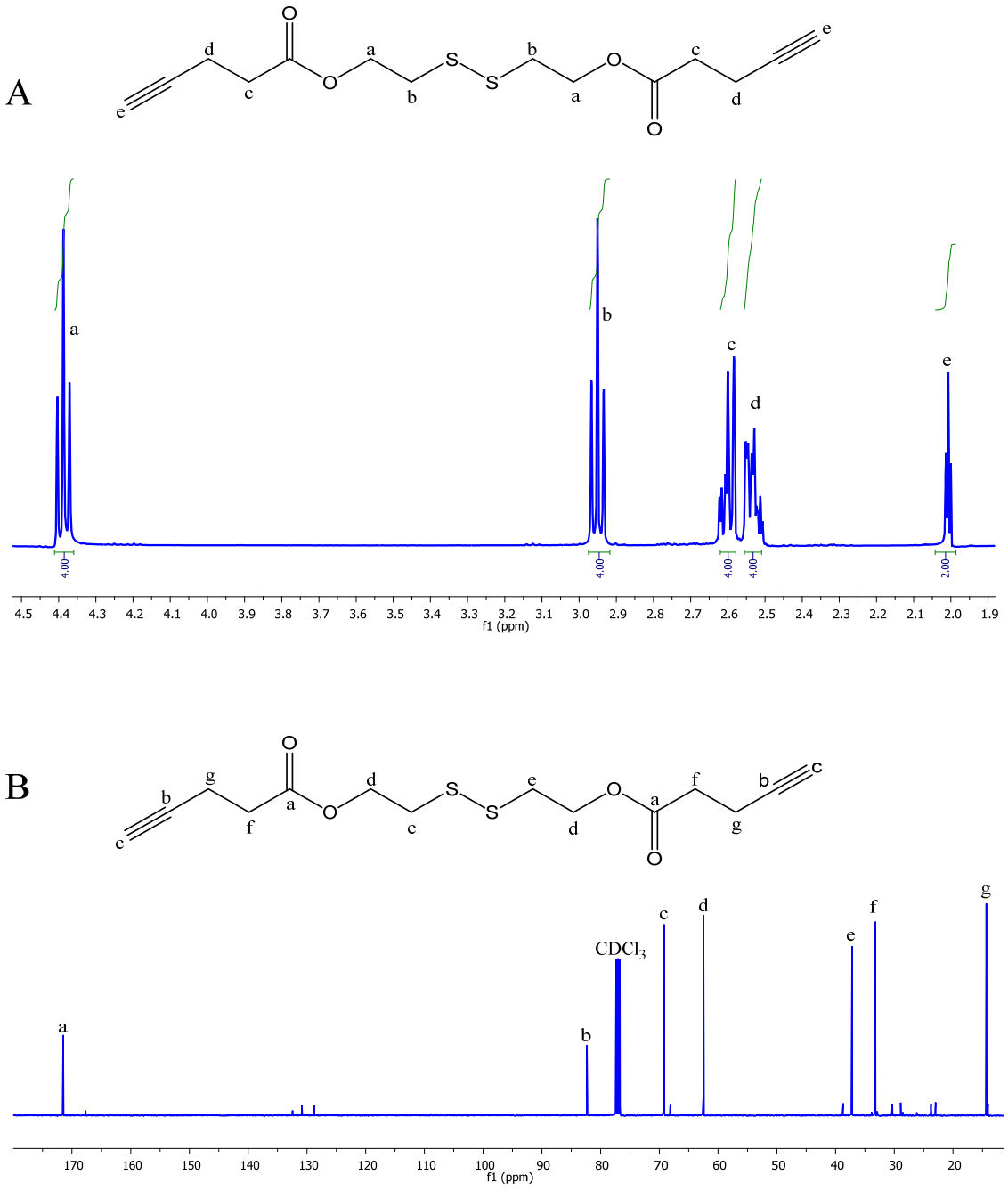

Figure 5-1. NMR characterisation of *bis*-alkyne ethyl disulfide redox-responsive crosslinker. (A) ^{1}H NMR spectrum and (B) ^{13}C NMR spectrum.

Hence, this redox-responsive *bis*-alkyne-ethyl disulfide cross-linker could be synthesised in one step. The resulting compound was purified by silica gel column chromatography (75% yield). The structure of *bis*-alkyne-ethyl disulfide cross-linker was confirmed by ^{1}H NMR and ^{13}C NMR (figure 5-1A and B, respectively). The ^{1}H NMR resonance at 4.39 ppm and ^{13}C NMR resonance at 62.48 ppm confirmed the formation of the crosslinker.

Reactive micelles based on mPEG-*b*-poly(εCL-*co*-αN$_3$εCL) were then prepared using a dialysis method in which DMSO was used as a co-solvent. Methotrexate was loaded into the hydrophobic block of the micelles which were then crosslinked by the bis-alkyne ethyl disulfide crosslinker using a copper catalysed azide-alkyne cycloaddition (scheme 5-1). The efficiency of the 'click' reaction was checked by FT-IR (figure 5-2). The infrared absorption peak at 2106 cm^{-1} (characteristic of the azide group) entirely disappeared in favour of a new peak at 1660 cm^{-1} (typical of the triazole ring), as also reported previously.[73]

The size distributions and morphologies of micelles were analysed using DLS and TEM, respectively. The average size of MTX-loaded (un-crosslinked) micelles was 53 ± 7 nm with a summated poly dispersity index (0.12 ± 0.05) as revealed by DLS (figure 5-3B). TEM analysis showed the predominantly spherical morphology of MTX-loaded micelles with average sizes of 46 nm (figure 5-3A). MTX-loaded core-crosslinked micelles were of slightly larger average size (67 ± 12 nm, and 63 nm) as determined by

DLS (figure 5-3D) and TEM (figure 5-3C), respectively, as compared with MTX-loaded un-crosslinked micelles.

The zeta potentials of the MTX-loaded un-crosslinked and MTX-loaded core-crosslinked micelles were observed to be near to neutral (-3.50 ± 1.25, and -2.30 ± 2.21 mv, respectively) as shown in figure 5-4.

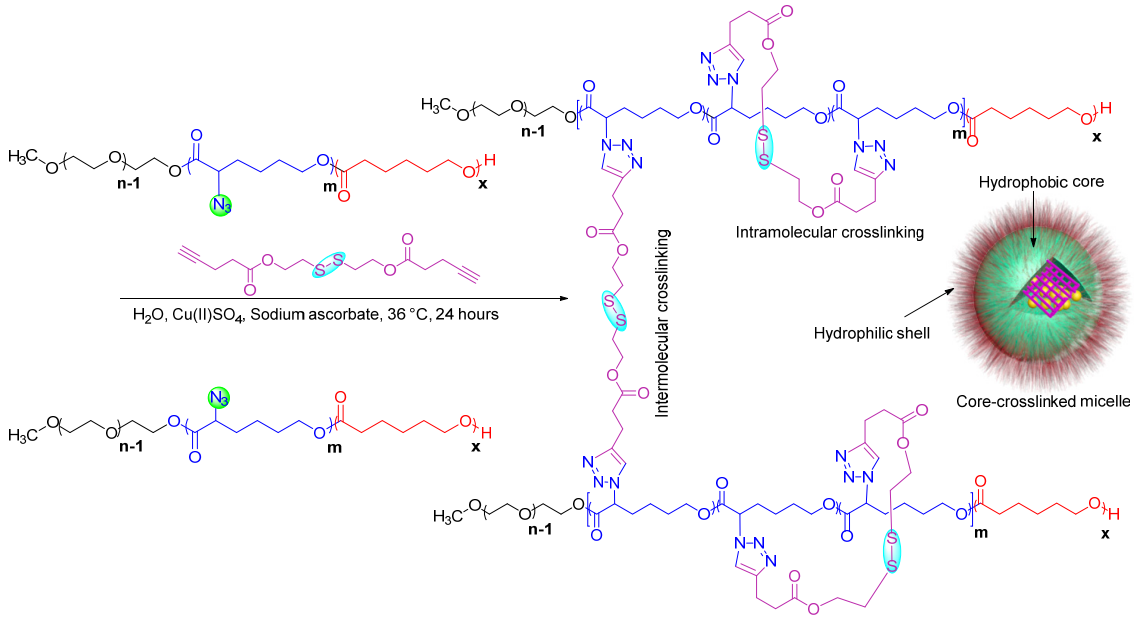

Scheme 5-1. Schematic representation of micelles crosslinking by copper catalysed azide-alkyne cycloaddition.

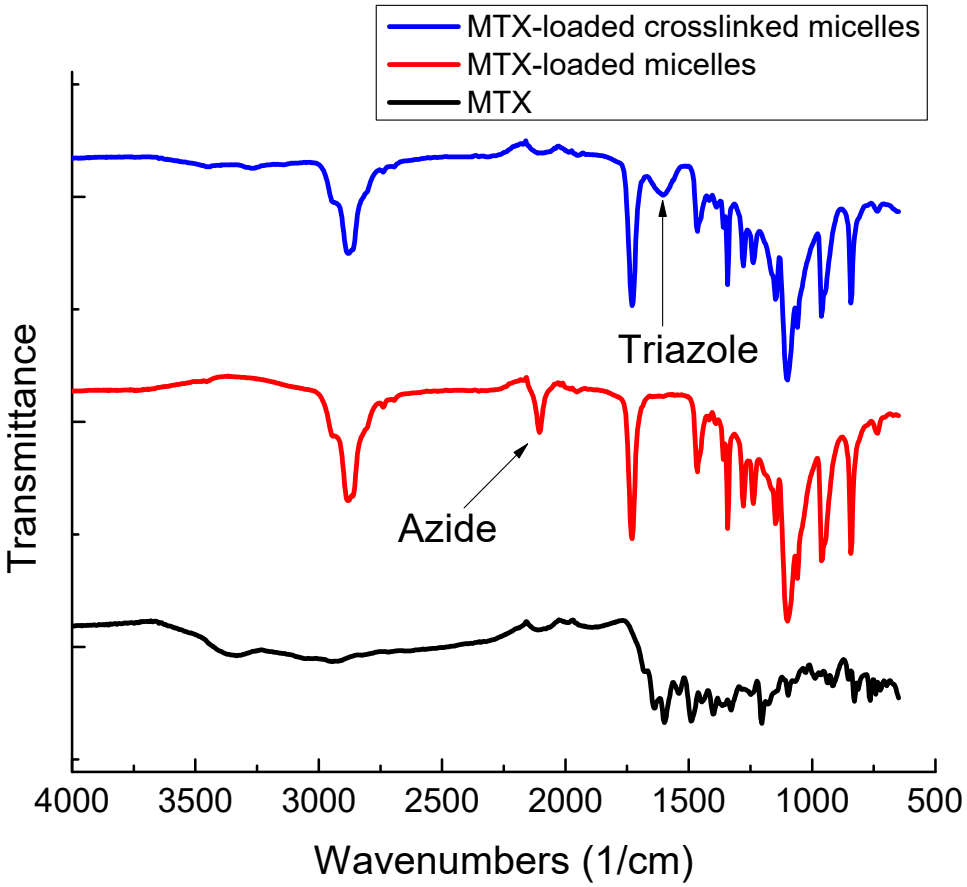

Figure 5-2. FT-IR characterisation of freeze dried MTX-loaded and MTX-loaded crosslinked micelles. In MTX-loaded crosslinked micelles, the IR absorption at 2106 cm^{-1} (characteristic of the azide) completely disappeared in corresponding to a new absorption at 1660 cm^{-1} (characteristic of the triazole ring).

Drug contents and encapsulation efficiency of MTX-loaded un-crosslinked and core-crosslinked micelles were determined by using UV-Vis spectrophotometry (λ_{max} = 304 nm) through a standard curve of MTX in DMSO. The core-crosslinked micelles showed higher drug contents (4.9 ± 0.6 wt. %) and better encapsulation efficiency (61.8 ± 7.4 %) as compared

with un-crosslinked micelles (3.1 ± 0.4 wt.%, and 39.3 ± 5.2 %, respectively), as shown in table 5-1.

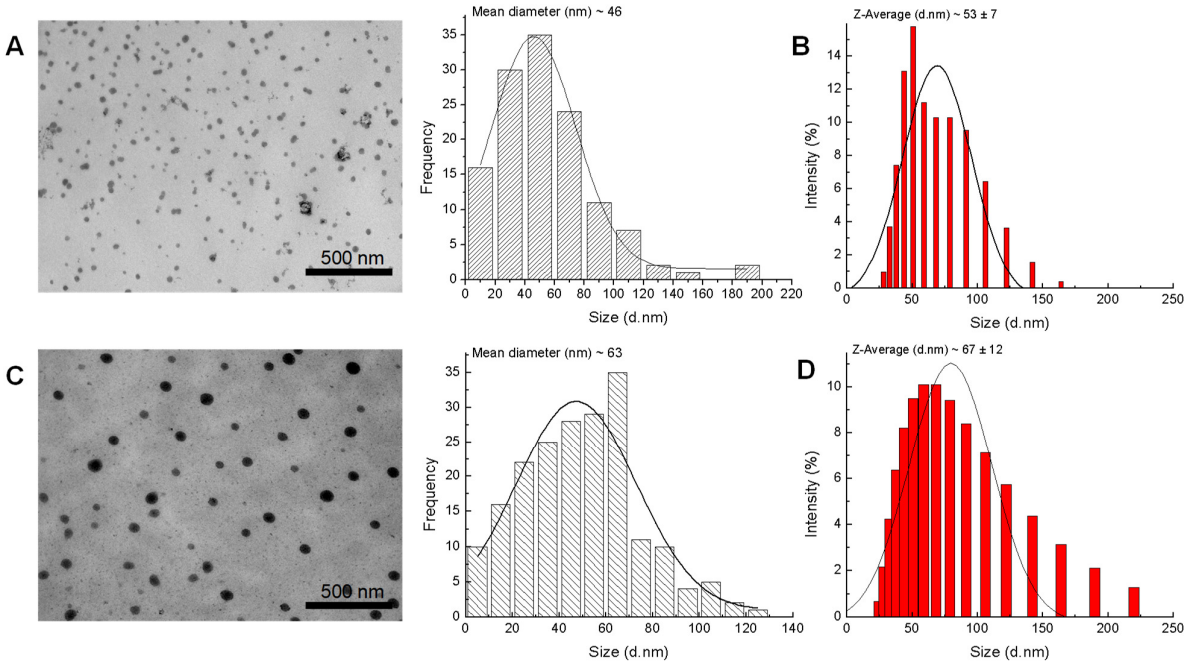

Figure 5-3. Size and morphological characterisation of drug-loaded micelles. (A) TEM micrograph and size distribution of MTX-loaded micelles, (B) Size distribution measured by DLS, (C) TEM micrograph and size distribution of MTX-loaded crosslinked micelles, and (D) Size distribution measured by DLS. Size distributions in TEM images were calculated using ImageJ software. Scale bars = 500 nm.

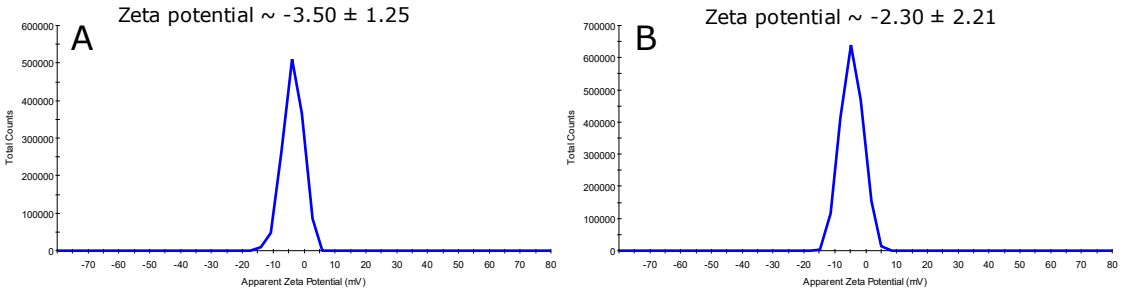

Figure 5-4. Zeta potential measurements of (A) MTX-loaded micelles, and (B) MTX-loaded crosslinked micelles.

Table 5-1. Characterisation data of empty, drug loaded, and drug loaded crosslinked micelles. (SD ~ standard deviation, NA~ not applicable, PDI ~ poly dispersity index, EE ~ encapsulation efficiency).

Micelles type	Size (d.nm) ± SD	PDI ± SD	Zeta potential (mv) ± SD	Drug content (Wt. %) ± SD	EE (%) ± SD
Empty micelles	36 ± 7	0.21 ± 0.02	-2.81 ± 0.91	NA	NA
MTX-loaded micelles	53 ± 9	0.12 ± 0.05	-3.50 ± 1.25	3.14 ± 0.42	39.31 ± 5.24
MTX-loaded crosslinked micelles	67 ± 12	0.24 ± 0.03	-2.30 ± 2.21	4.94 ± 0.60	61.83 ± 7.48

To study the cellular uptake of micelles, Oregon-green loaded and Oregon-green loaded core-crosslinked micelles were prepared in a similar method as described above. The synthesis of Oregon-green involved the methanesulfonic acid catalysed reaction of the 4-fluroresorcinol with the trimellitic anhydride (scheme 5-2).

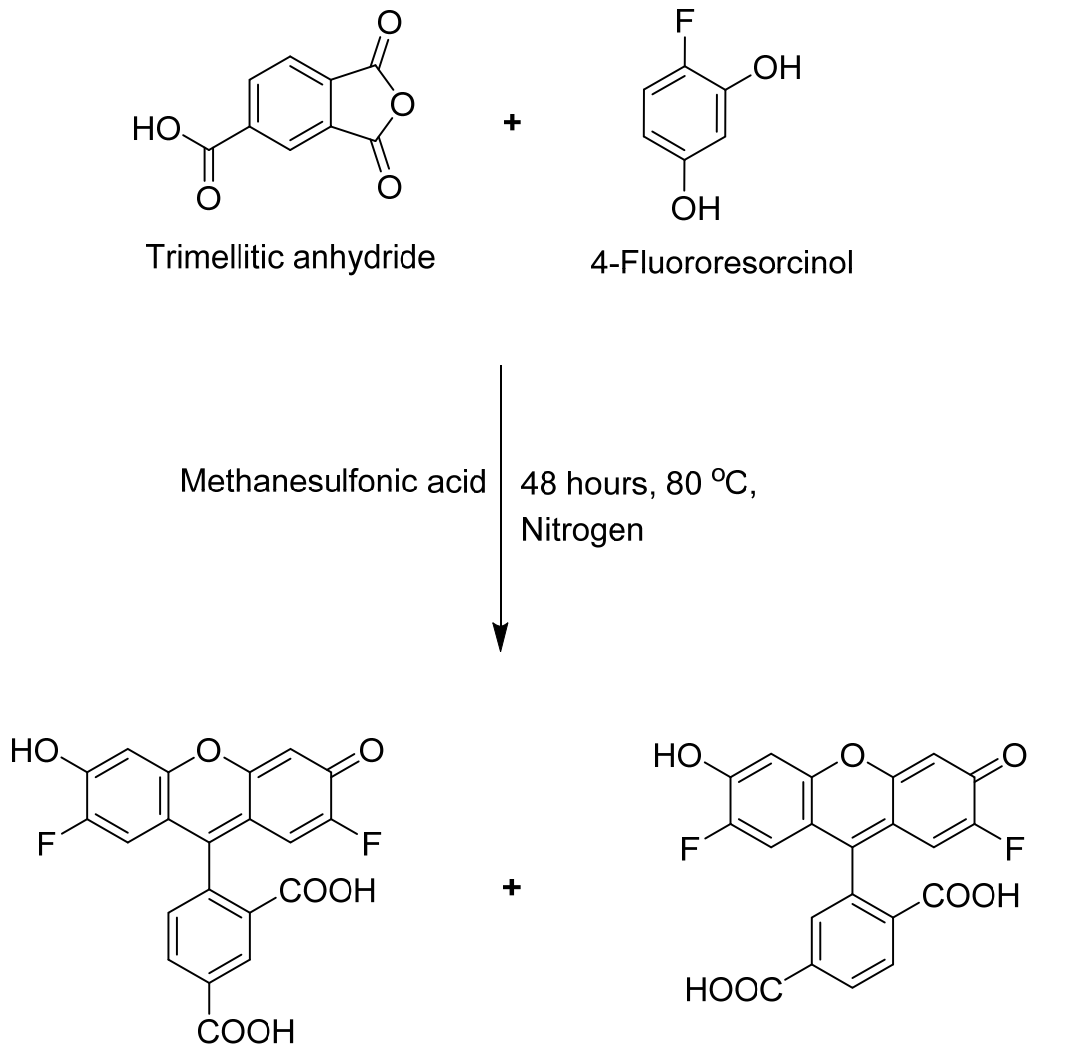

Scheme 5-2. Scheme for the synthesis of Oregon-green (mixed isomers).

The synthesised Oregon-green was analysed by ^{1}H NMR (figure 5-5) and electrospray ionisation mass spectrometry (see supplementary information, figure 8-2). The Oregon-green loaded micelles and Oregon-green loaded core-crosslinked micelles were of mean sizes of 43 and 52 nm, respectively, as revealed by DLS measurements (figure 5-6).

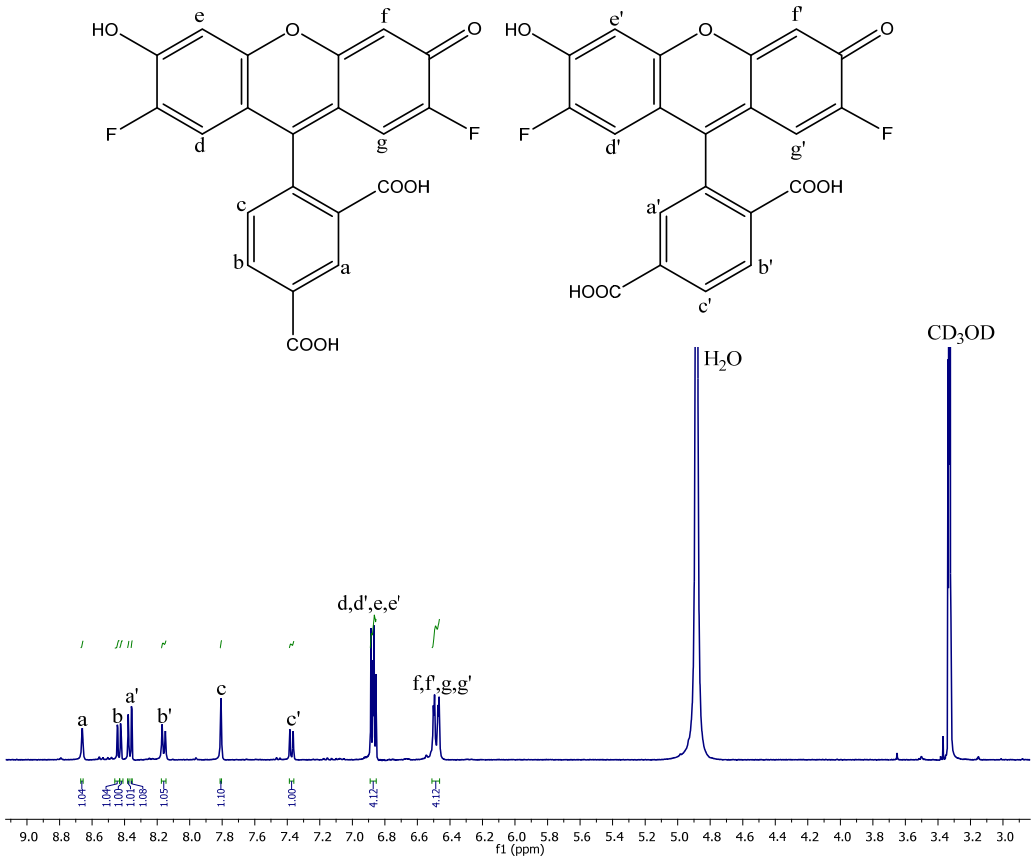

Figure 5-5. ^{1}H NMR spectrum of Oregon green (mixed isomers).

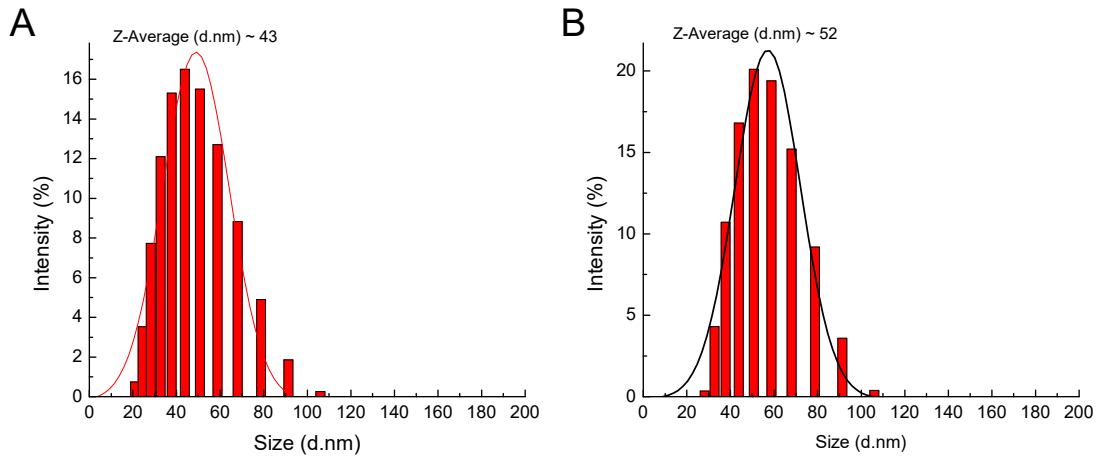

Figure 5-6. Size distribution of dye-loaded micelles measured by DLS. (A) Oregon-green loaded micelles, and (B) Oregon-green loaded core-crosslinked micelles.

5.2.2. *In vitro* drug release studies

In this study, drug release analysis of MTX-loaded and MTX-loaded core-crosslinked micelles was carried out under reducing and non-reducing conditions at 37 °C. Due to the complexities of the intracellular environment, in which many reducing species may be present at different times, GSH alone was not used in these model studies,[27] and instead DTT was used as a simple known reductant. The amount of drug release was determined using UV-Vis spectrophotometry monitoring at 304 nm. As shown in figure 5-7, in PBS (pH 7.4), MTX-loaded un-crosslinked micelles showed burst release of drug during first 12 hours (35 % drug release) followed by a steady and temporal drug release where 90 % drug was released up to 96 hours.

In contrast, core-crosslinked micelles exhibited a reduced burst release of MTX in non-reducing conditions, with ~ 20% MTX detected in the dialysate during the first 12 hours. Methotrexate was mostly retained by core-crosslinked micelles in PBS at 37 °C even up to 96 h, after which time 34 % MTX release was observed. In contrast MTX-loaded core-crosslinked micelles exhibited about 60 % drug release at 12 hours and 89 % drug release at 24 hours under the same reducing conditions (10 mmol DTT).

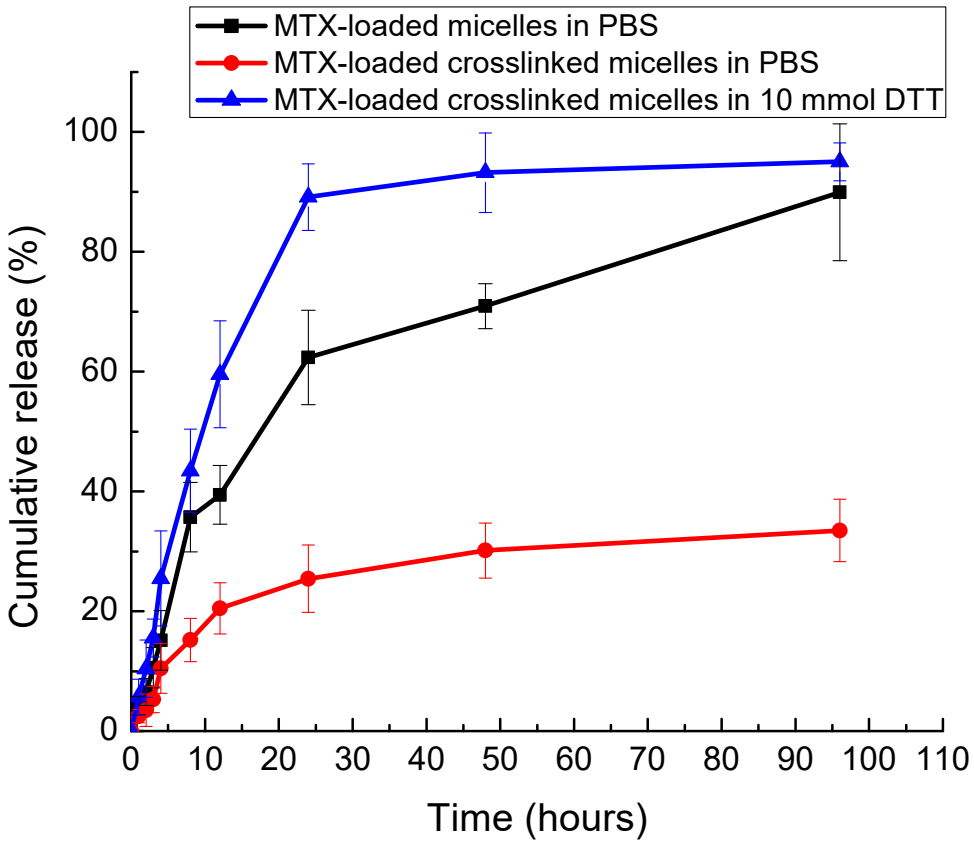

Figure 5-7. Analysis of methotrexate (MTX) release from MTX-loaded micelles and MTX-loaded core-crosslinked micelles at 37 °C.

5.2.3. *In vitro* cellular uptake

In vitro cellular uptake of un-crosslinked and reversibly core-crosslinked micelles was investigated using flow cytometry and confocal laser scanning microscopy. For this purpose, Oregon-green loaded and Oregon-green loaded core-crosslinked micelles were prepared and incubated for 3 hours with human breast cancer (MCF7) cells. Flow cytometry analysis showed that Oregon-green loaded and Oregon-green loaded core-crosslinked micelles were efficiently taken up by MCF7 cells (figure 5-8). Cells

incubated without micelles were used as a negative control to correct for auto fluorescence. The median fluorescence intensities arising from negative control, Oregon-green loaded (un-crosslinked) and Oregon-green loaded core-crosslinked micelles were 5.23, 62.08, and 63.35, (arbitrary units), respectively. To estimate the percentage of population which endocytosed the micelles, histograms of control and treated samples were overlaid. The overlapped area was subtracted from the total area under the curve. The bright sub-population of cells which ingested micelles shifted to the right, and the percentage of cells containing micelles were measured by integrating the shifted area, as reported previously.[74, 75]

Flow cytometry analysis revealed that the extent of uptake of un-crosslinked and core-crosslinked micelles were 93 and 94%, respectively, showing that crosslinking the micelle-core did not negatively affect cellular entry of micelles. Flow cytometry and fluorescence activated cell sorting (FACS) enabled the fast and quantitative high throughput quantitation of the cells which had taken up the micelles. However, it was not possible to distinguish the intracellular localization of micelles using FACS.

Therefore, confocal laser scanning microscopy was used to analyse the intracellular localization of micelles. MCF7 cells were incubated with Oregon-green loaded un-crosslinked and core-crosslinked micelles for 3 hours. Cell membranes were stained with CellMask™ deep red plasma membrane stain, whereas cell nuclei were stained with Hoechst dye.

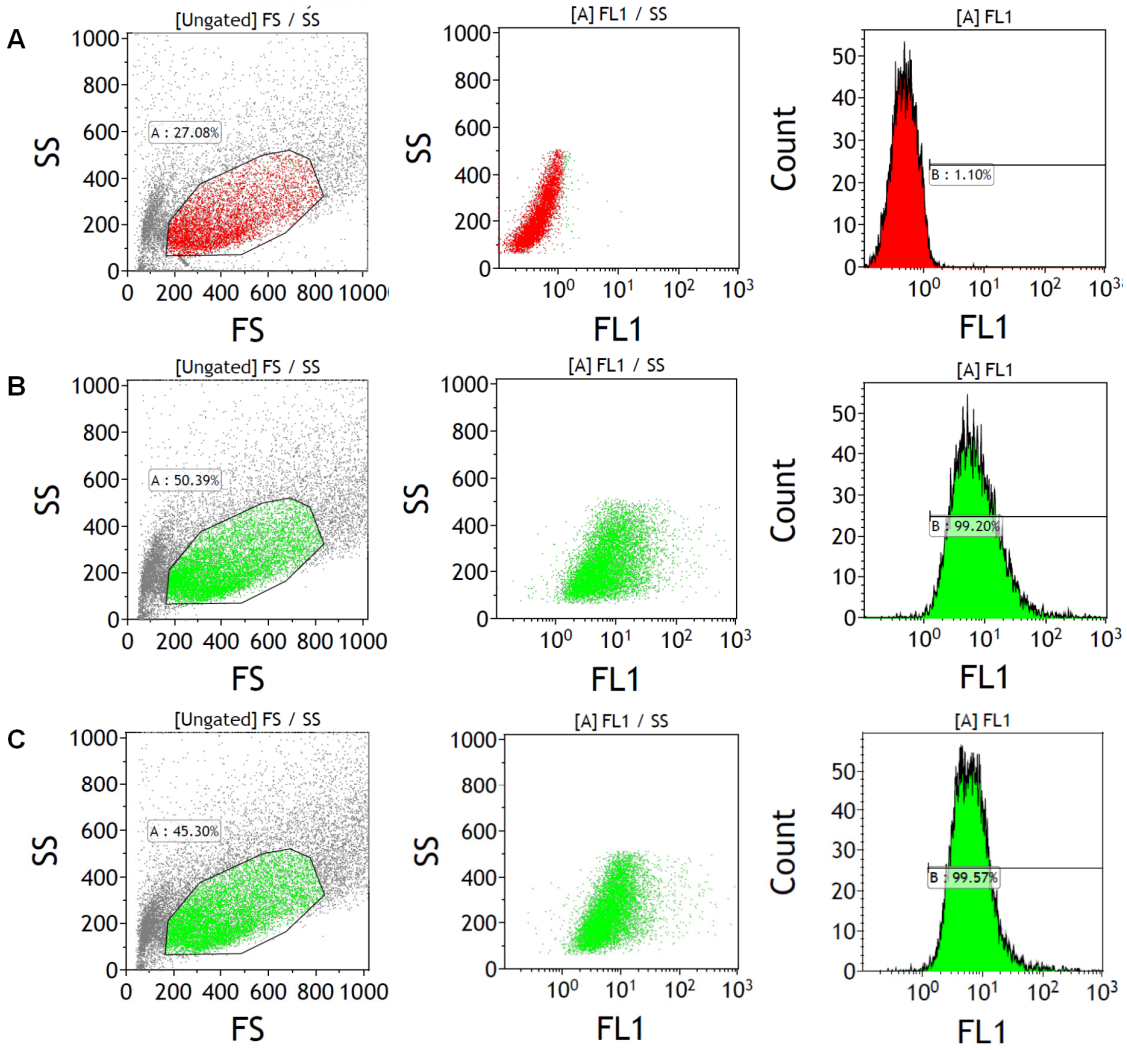

Figure 5-8. Fluorescence assisted cell sorting analysis of cellular uptake in MCF7 cells incubated with (A) Un-treated cells, (B) Oregon-green loaded micelles, and (C) Oregon-green loaded crosslinked micelles.

Figure 5-9 shows the CLSM images of cellular uptake of Oregon-green loaded un-crosslinked micelles. It is revealed that Oregon-green loaded micelles were internalised by MCF7 cells and were localised mostly in the cytoplasm at the 3-hr time-point.

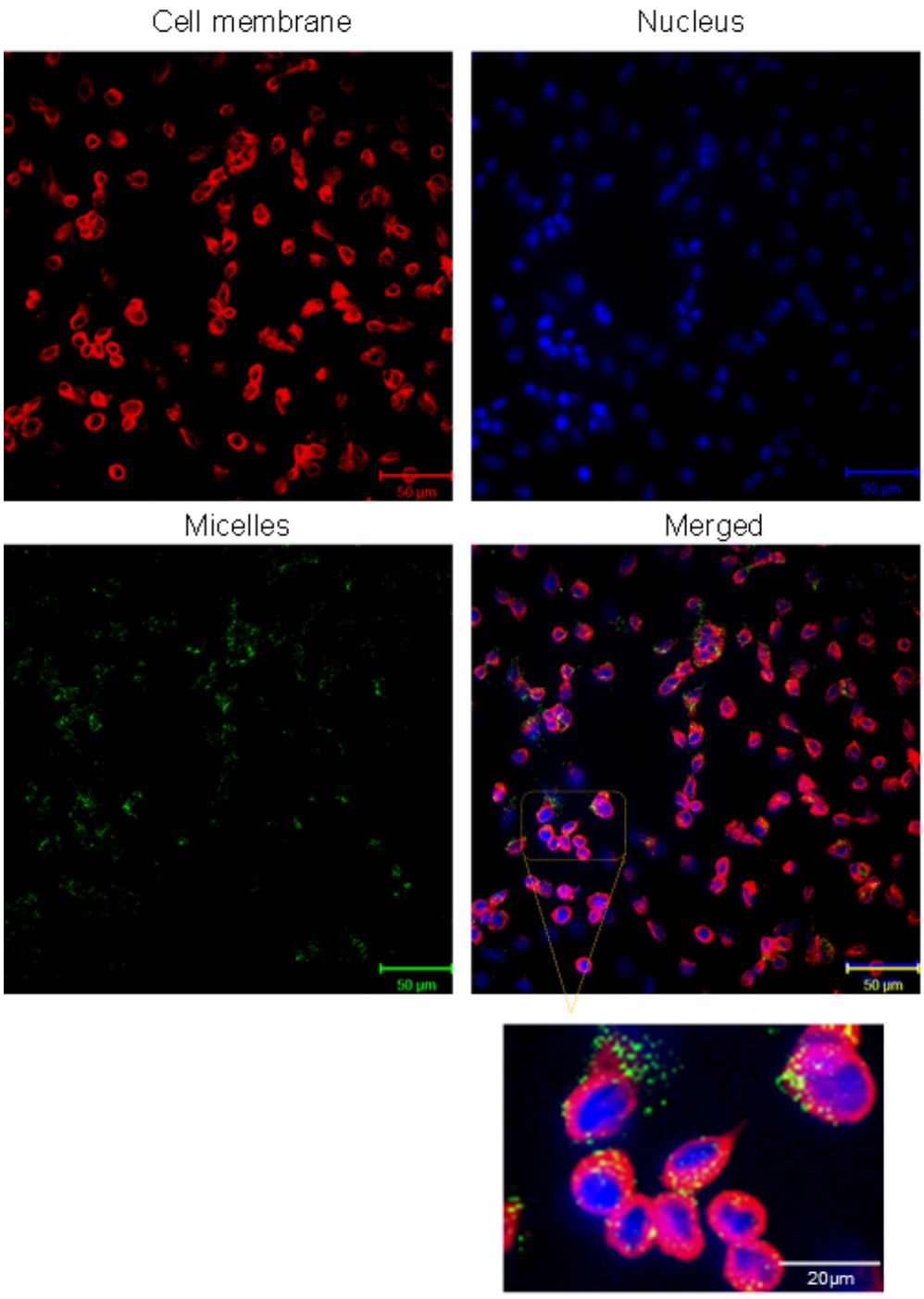

Figure 5-9. Confocal laser scanning microscopy images of cellular uptake in MCF7 cells cultured with Oregon-green loaded micelles. Nuclei of cells were stained with Hoechst (blue) and cell membranes were stained with CellMask™ deep red plasma membrane stain.

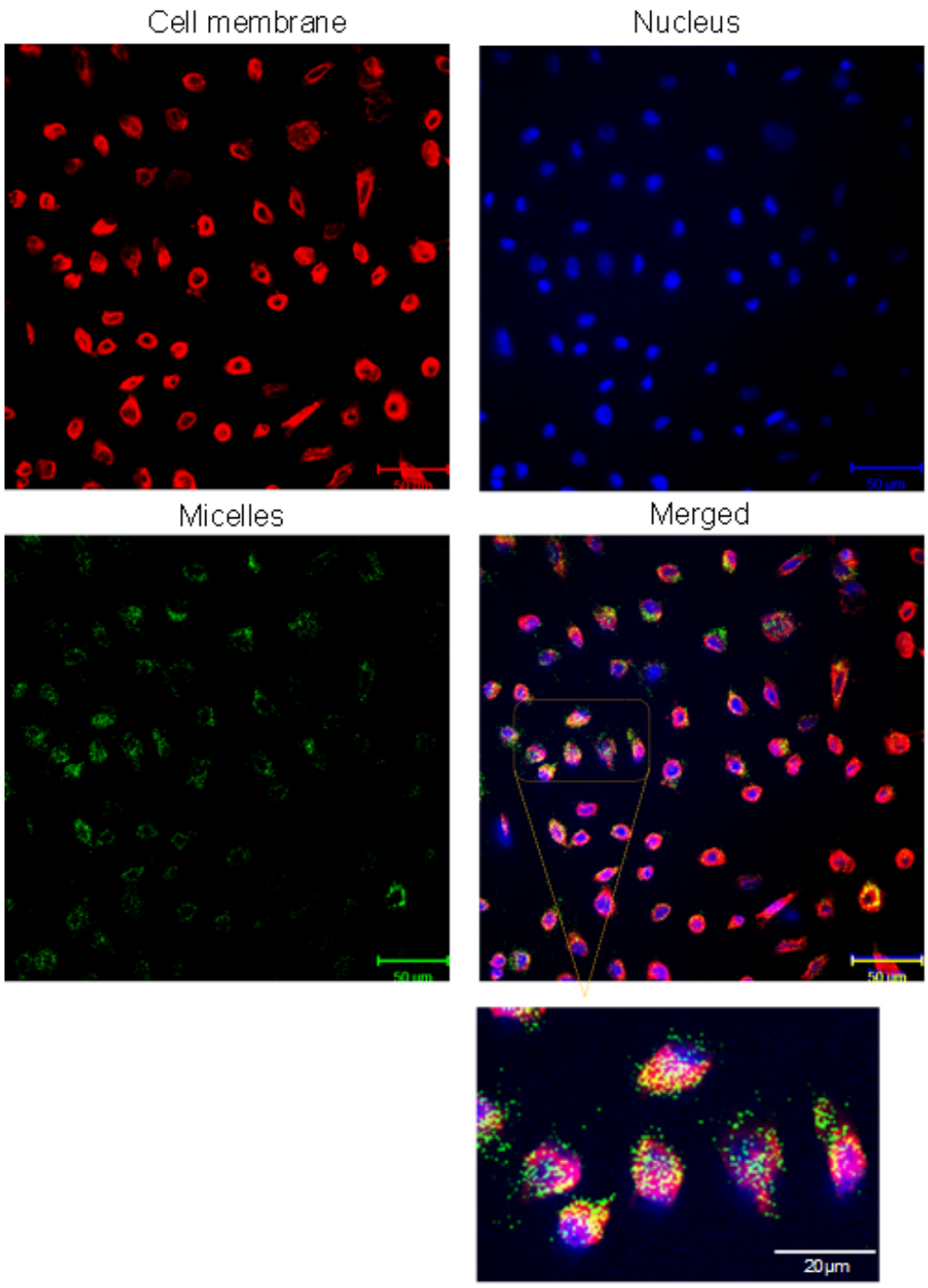

Figure 5-10. Confocal laser scanning microscopy images of cellular uptake in MCF7 cells cultured with Oregon-green loaded crosslinked micelles. Nuclei of cells were stained with Hoechst (blue) and cell membranes were stained with CellMask™ deep red plasma membrane stain.

Interestingly, Oregon-green loaded core-crosslinked micelles were localised both in the cytoplasm and in nuclei of MCF7 cells as shown by the Oregon-green fluorescence in merged CLMS images (figure 5-10). The observed green fluorescence located in the proximity of cell nuclei was probably due to the localisation of core-crosslinked micelles following endosomal escape as reported previously.[20]

5.2.4. MTT assay/cytotoxicity studies

For biomedical application of nanocarriers, cytotoxicity evaluation is necessary as nanomaterials may pose unidentified risks to biological systems. Specifically, cell compatibilities of micelles are important for drug delivery applications. In this study, *in vitro* effects of empty micelles based on mPEG-*b*-poly(εCL-*co*-αN_3εCL) and their crosslinked counter parts were investigated in MCF7 cells using MTT assays.

For this purpose, MCF7 cells were treated with various amounts of empty un-crosslinked and crosslinked micelles for 48 hours. The results of MTT assays are shown in figure 5-11. It was observed that both types of micelles were cytocompatible up to a concentration of 500 µg/mL (> 90% cell viability). Specifically, at maximum tested concentration of 1000 µg/mL, cells treated with un-crosslinked and core-crosslinked micelles showed metabolic activities of 90.8 ± 2.7, and 75 ± 2 %, respectively.

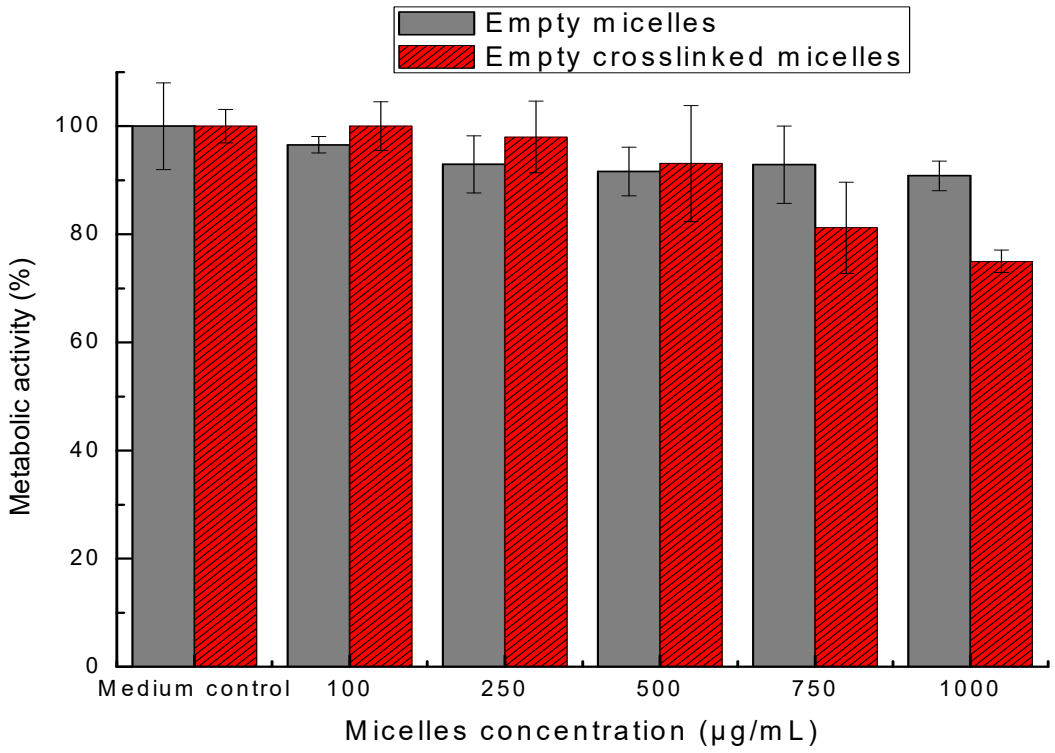

Figure 5-11. Cytotoxicity analysis of micelles cultured with MCF7 cells for 48 hours. (A) Empty mPEG-b-poly(εCL-co-αN$_3$εCL) micelles and, (B) Empty mPEG-b-poly(εCL-co-αN$_3$εCL) core-crosslinked micelles. Error bars showing standard deviation (n=3). MTT assay was used to analyse the metabolic activity of MCF7 cells.

In addition, cytotoxicities of MTX-loaded and MTX-loaded core-crosslinked micelles were also evaluated by MTT assays. The results are shown in figure 5-12. It was revealed that MTX-loaded and MTX-loaded core-crosslinked micelles decreased the metabolic activity of MCF7 cells in a dose dependent pattern. Specifically, MTX-loaded un-crosslinked micelles showed a metabolic activity of 50.8 ± 4 and 45.4 ± 2.5 % at concentrations of 500 and 1000 µg/mL, respectively.

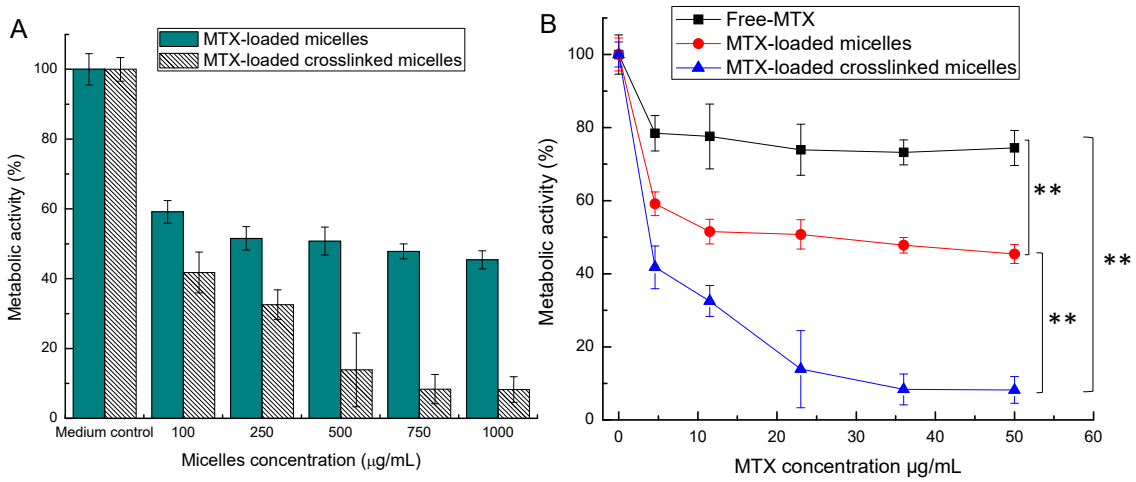

Figure 5-12. Cytotoxicity analysis of (A) MTX-loaded and MTX-loaded crosslinked micelles, and (B) Metabolic activity of MCF7 cells as a function of MTX concentration. Error bars show standard deviation (n=3). *= significant ($p < 0.05$) and **= very significant ($p < 0.01$).

Interestingly, MTX-loaded core-crosslinked micelles proved to be significantly more potent as compared to the free MTX (figure 5-12) and un-crosslinked counterparts. At concentrations of 500 and 1000 μg/mL, MTX-loaded core-crosslinked micelles decreased the metabolic activity of MCF7 cells to 14 ± 10.5, and 8.2 ± 3.6 %, respectively. As the drug contents of MTX-loaded un-crosslinked and core-crosslinked micelles were different, therefore, MTT assays were also repeated with calculated amounts of MTX-loaded un-crosslinked or core-crosslinked micelles, equivalent to various amounts of MTX (4.6, 11.5, 23, and 50 μg/mL). The metabolic activities of MCF7 cells as a function of MTX concentrations are shown in figure 5-1B. It was observed that metabolic activities of MCF7

cells treated with MTX-loaded core-crosslinked micelles, equivalent to 50 µg/mL of MTX, significantly decreased as compared to MTX-loaded un-crosslinked micelles and free MTX.

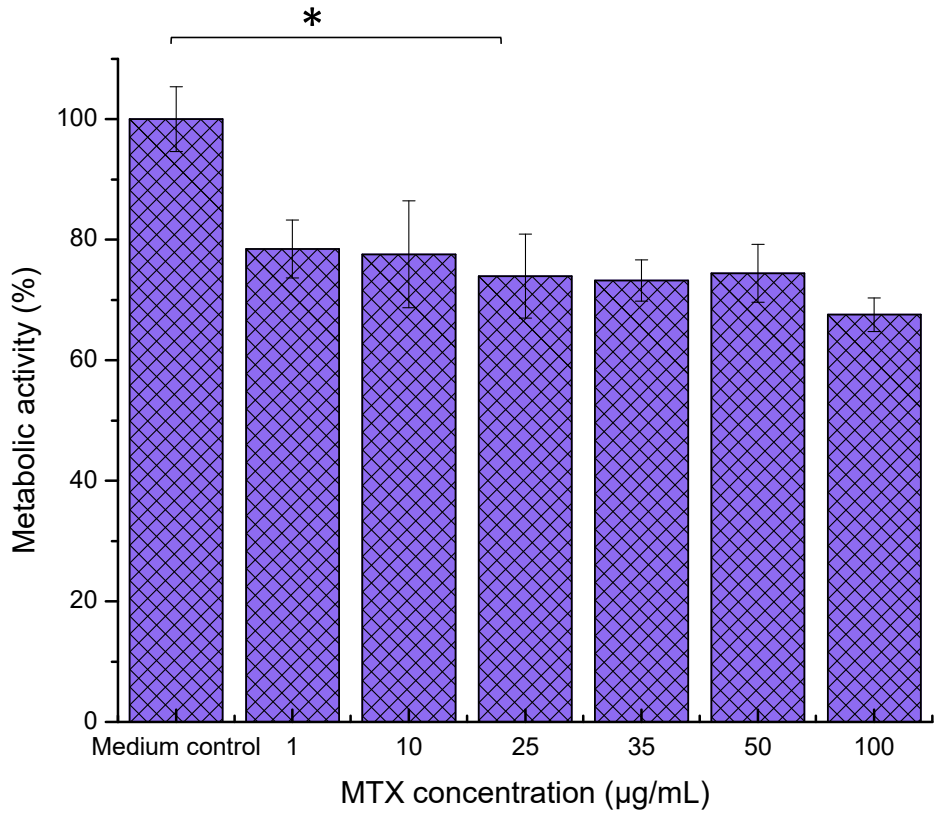

Figure 5-13. Cytotoxicity analysis of various concentrations of free MTX cultured with MCF7 cells for 48 hours. Error bars showing standard deviation (n=3). *= significant ($p < 0.05$).

These findings indicated that crosslinked micelles increased the cytotoxicity of the MTX to a greater extent as compared with the free MTX and MTX-loaded un-crosslinked micelles.

5.2.5. Apoptosis inducing potential of MTX-loaded core-crosslinked micelles

In order to investigate whether the cell death observed in MCF7 cells treated with the free MTX, MTX-loaded un-crosslinked and core-crosslinked micelles could be due to the apoptosis, Hoechst/PI double staining was performed. The morphological changes in cell nuclei were analysed by using the fluorescence microscopy. MCF7 cells incubated with different concentrations of the free MTX, MTX-loaded un-crosslinked and core-crosslinked micelles showed obvious morphological changes in cell nuclei after treatment for 48 hours, as compared with the control untreated cells. As shown in figure 5-14, untreated cells appeared to be regular and intact with less bright blue nuclei and without red fluorescence.

In contrast, cells treated with MTX-loaded un-crosslinked and core-crosslinked micelles, free MTX, and MTX-DMSO control (figure 5-15 to 5-18, respectively) showed characteristics features of apoptotic and dead cells. The percentages of live, apoptotic, and dead cells from the merged fluorescent microscopic images were calculated by using the Infinity Analyze software (Infinity Analyze 3^{R}, Lumenera Corporation). The percentage of apoptotic and dead cells correspondingly increased in a dose dependent pattern after treatment with MTX-loaded un-crosslinked and core-crosslinked micelles.

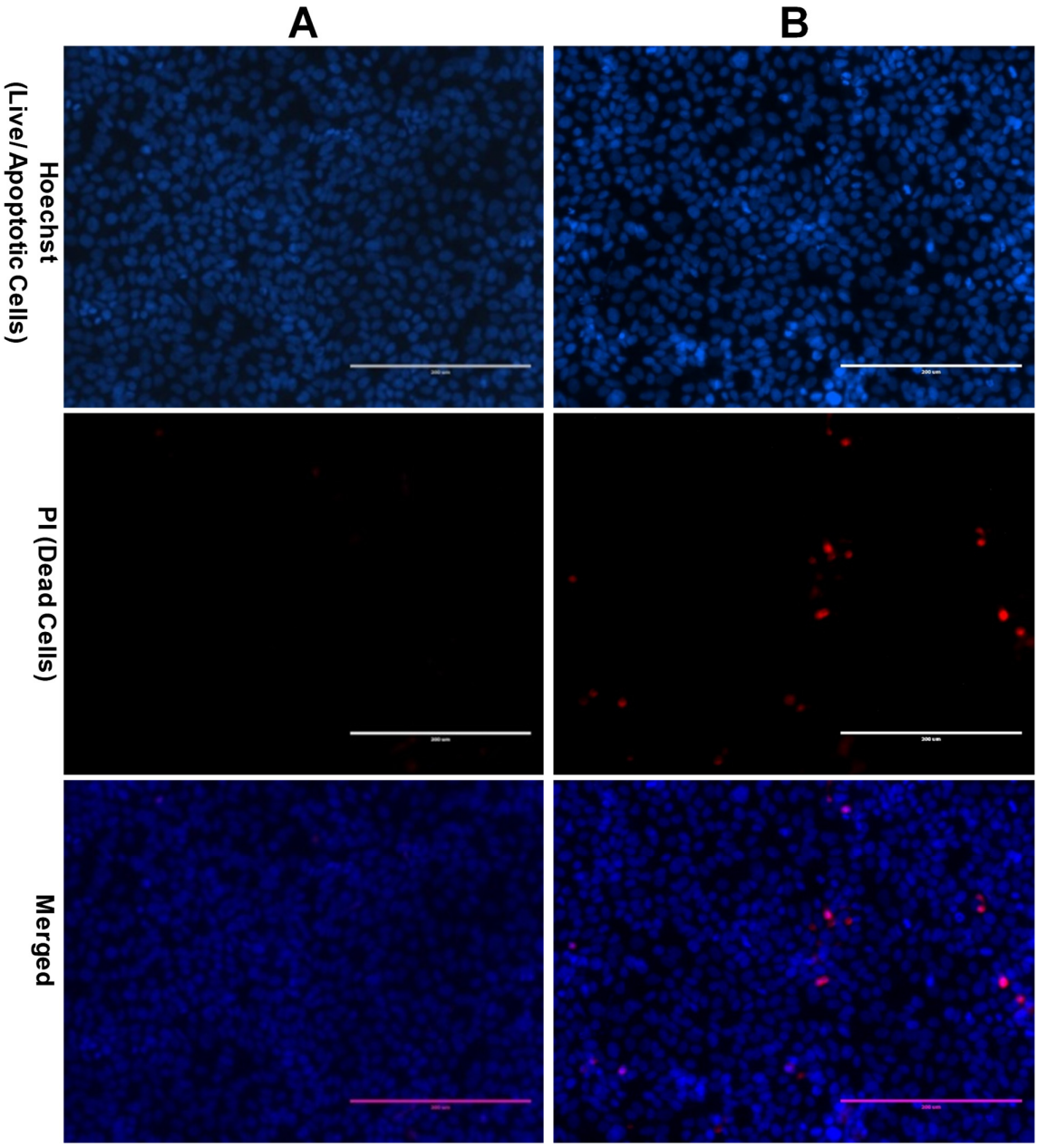

Figure 5-14. Fluorescence microscopy analysis of apoptotic and dead cells in MCF7 breast cancer cells cultured for 48 hours with (A) Medium control, (B) Medium-DMSO control. Hoechst 33342 dye was used to detect apoptotic cells, whereas propidium iodide (PI) was used to detect dead cells. Scale bars ~ 200 µm.

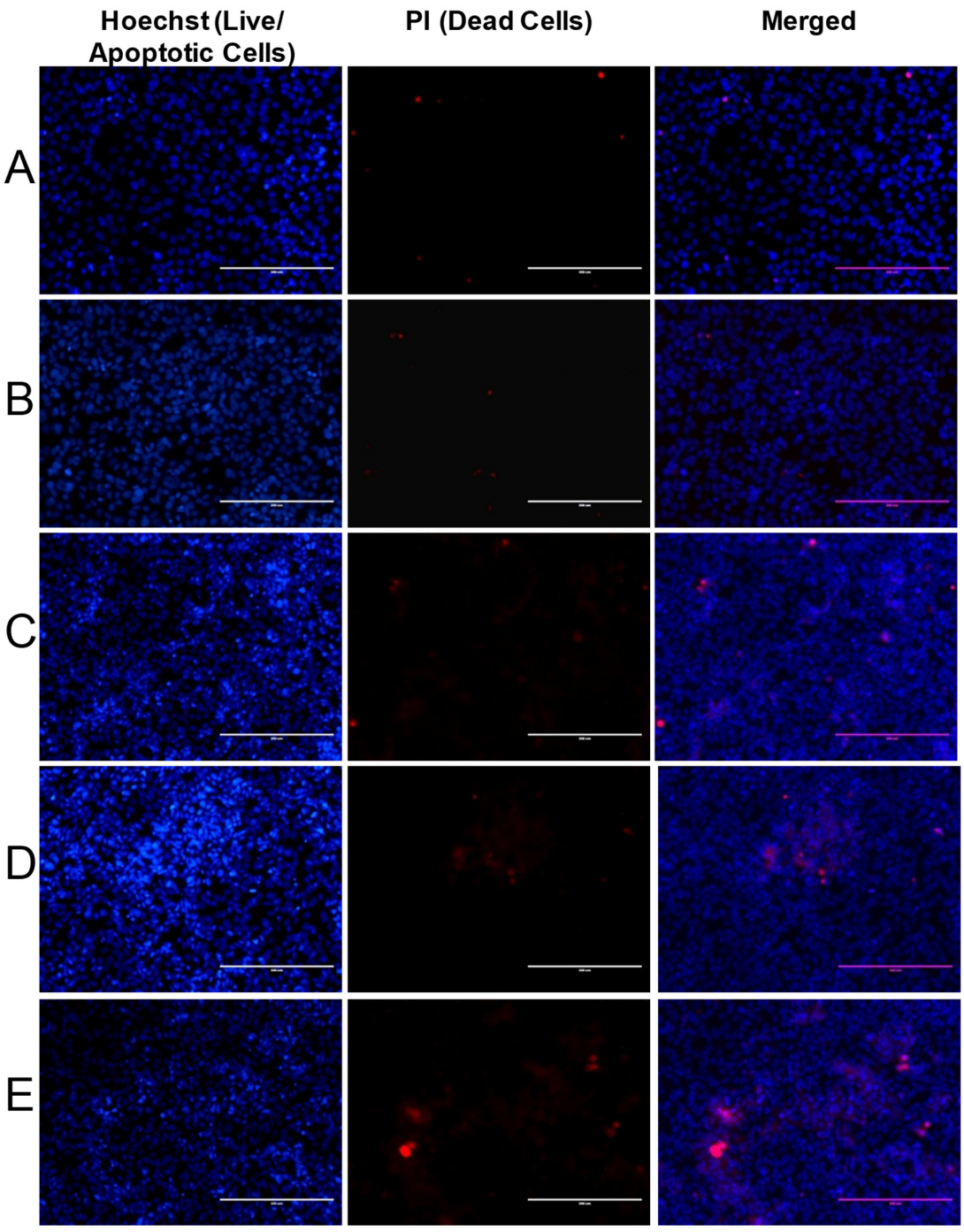

Figure 5-15. Fluorescence microscopy analysis of apoptotic and dead cells in MCF7 breast cancer cells cultured for 48 hours with MTX-loaded micelles. A, B, C, D, and E represent MTX-loaded micelles equivalent to various amounts of MTX (4.6, 11.5 23, 36, and 50 µg/mL, respectively). Scale bars ~ 200 µm.

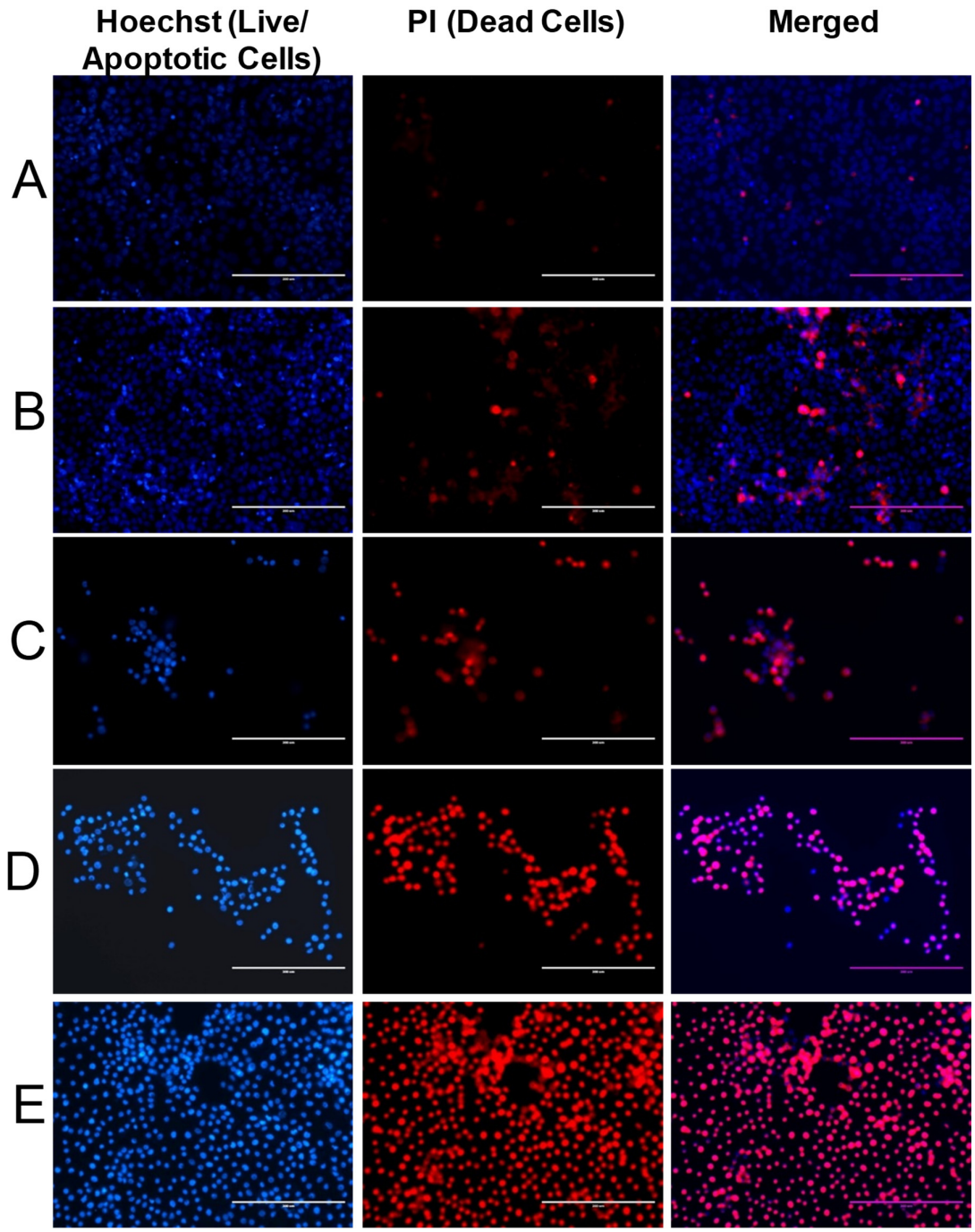

Figure 5-16. Fluorescence microscopy analysis of apoptotic and dead cells in MCF7 breast cancer cells cultured for 48 hours with MTX-loaded core-crosslinked micelles. A, B, C, D, and E represent MTX-loaded micelles equivalent to various amounts of MTX (4.6, 11.5 23, 36, and 50 μg/mL, respectively). Scale bars ~ 200 μm.

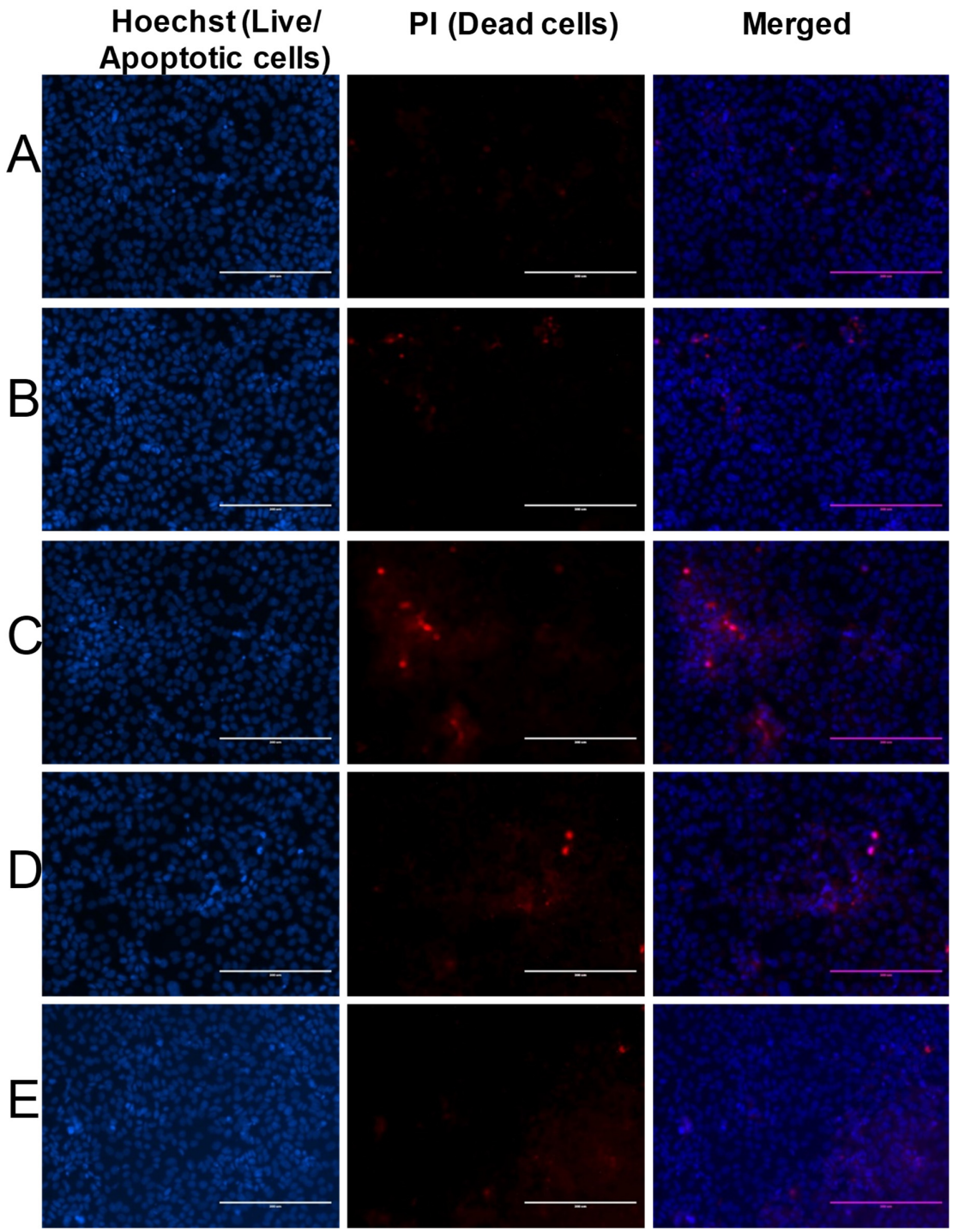

Figure 5-17. Fluorescence microscopy analysis of apoptotic and dead cells in MCF7 breast cancer cells cultured for 48 hours with various concentrations of free MTX. (A) 4.6 µg/mL, (B) 11.5 µg/mL, (C) 23 µg/mL (D) 36 µg/mL, and (E) 50 µg/mL. Scale bars ~ 200 µm.

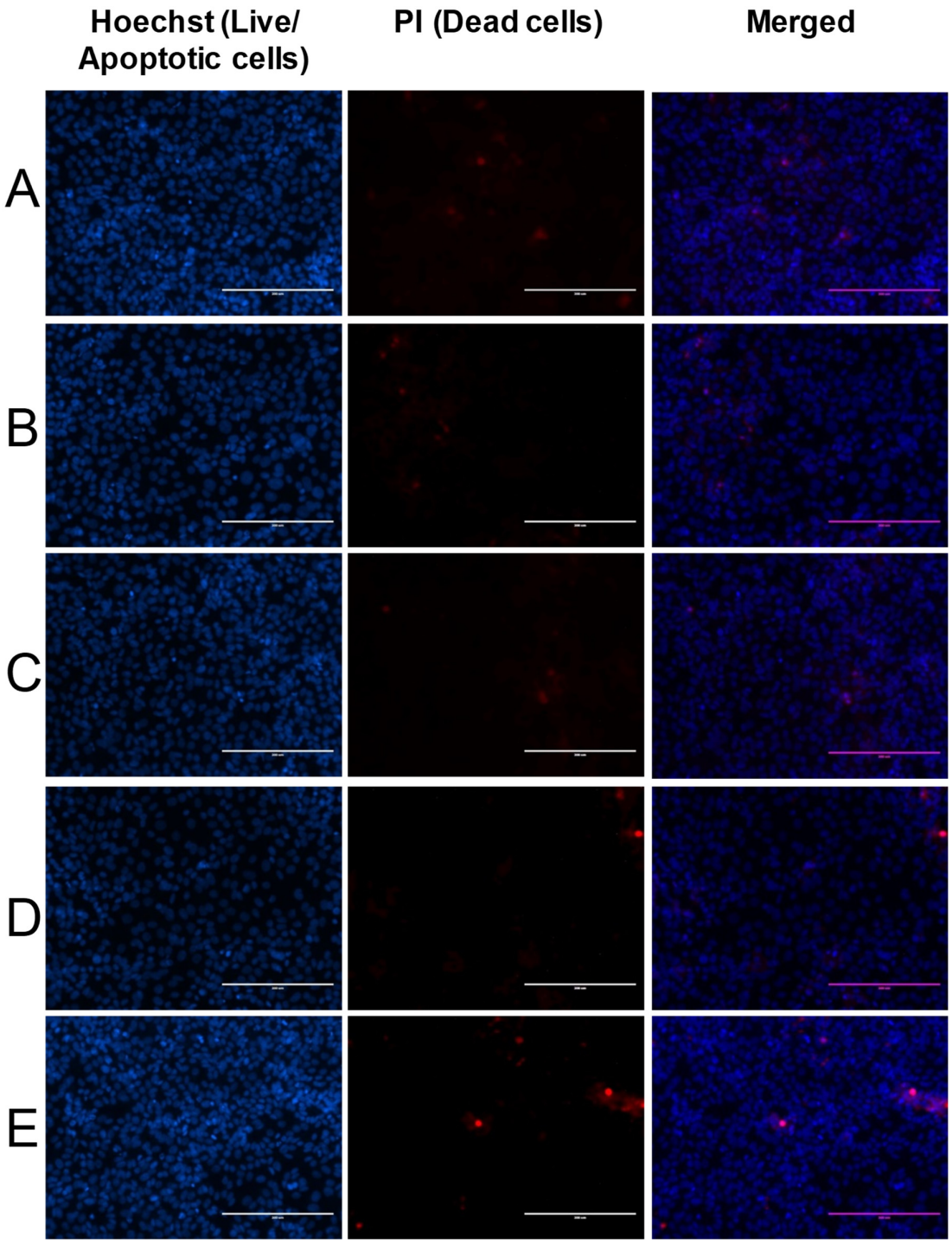

Figure 5-18. Fluorescence microscopy analysis of apoptotic and dead cells in MCF7 breast cancer cells cultured for 48 hours with various concentrations of free MTX-DMSO control. (A) 4.6 µg/mL, (B) 11.5 µg/mL, (C) 23 µg/mL (D) 36 µg/mL, and (E) 50 µg/mL. Scale bars ~ 200 µm.

Specifically, MTX-loaded un-crosslinked micelles at 50 µg/mL equivalent of MTX resulted in 20 ± 1.8 and 15 ± 2.3% apoptotic and dead cells, respectively, as shown in figure 4-20C. Interestingly, the percentage of apoptotic and dead cells increased after treatment with MTX-loaded crosslinked micelles (figure 5-19D) as compared with their un-crosslinked counterparts. Particularly, MTX-loaded core-crosslinked micelles at 23 µg/mL equivalent of MTX gave rise to approximately 46 ± 6 and 33 ± 5% apoptotic and dead cells, respectively. When the amount of MTX-loaded crosslinked micelles was increased to 50 µg/mL equivalent of MTX, the percentage of dead cells was also increased showing 78 ± 8% dead cells and 9 ± 4% apoptotic cells.

However, MCF7 cells treated with free MTX (figure 5-19E) showed lower percentages of apoptotic and dead cells as compared with MTX-loaded un-crosslinked and core-crosslinked micelles. At 50 µg/mL free MTX concentration, the percentages of apoptotic and dead cells were 10 ± 3 and 8 ± 2%, respectively. These findings were consistent with cytotoxicity results obtained by MTT assay.

To investigate the probability that low *in vitro* cytotoxicity of free MTX could be due to its poor aqueous solubility and less permeability, assays with MTX-DMSO control formulations were performed. For this purpose, MTX was first dissolved in DMSO and then diluted with cell culture medium to obtain the desired concentration. The various concentrations of MTX dissolved in DMSO-medium were incubated with MCF7 cells for 48 hours.

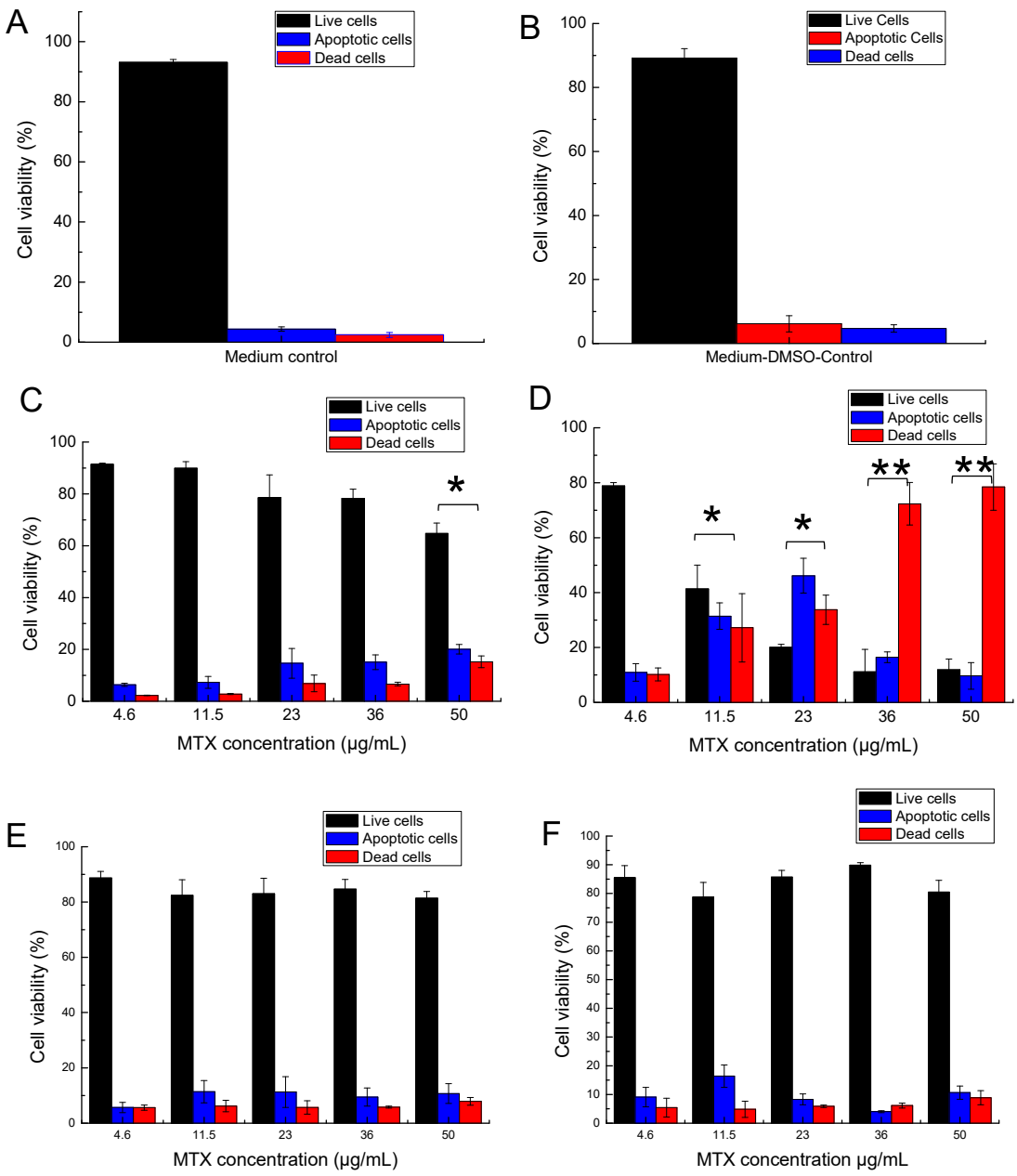

Figure 5-19. Quantification of live, apoptotic, and dead cells in MCF7 cells treated with (A) Medium control, (B) Medium-DMSO control, (C) MTX-loaded micelles, (D), MTX-loaded core-crosslinked micelles, (E) Free MTX, and (F) MTX-DMSO control. The percentage of live, apoptotic and dead cells was calculated by Infinity Analyse software. Error bars represent standard deviation. n=3. *= significant ($p < 0.05$) and **= very significant ($p < 0.01$).

The results are shown in figure 5-18 and 5-19F. Interestingly, there was no apparent difference found in the percentage of apoptotic and dead cells as compared with the free MTX (without DMSO) as a positive control.

To further confirm that cell death was induced via apoptosis by MTX-loaded un-crosslinked and core-crosslinked micelles, annexin V-FITC/PI assays were performed. The proportion of live, apoptotic, and dead cells stained with annexin V-FITC/PI assay were calculated using flow cytometry. The forward scattering (FS) and side scattering (SS) were integrated to provide information about cell size, and cell morphology, respectively. The percentages of live, apoptotic, and dead cells were calculated from FL1/FL3.

The results of annexin V-FITC/PI assays are shown in figures 5-20 to 5-23. The negative control cells (without treatment) appeared to be regular and with low fluorescence (i.e. auto fluorescence) as shown in figure 5-20A. The auto fluorescence generated by control cells was subtracted from the flow cytometry data of treated samples by applying appropriate gating.

The flow cytometry results revealed that MCF7 cells treated with MTX-loaded un-crosslinked micelles resulted in dose dependent increases in the proportions of apoptotic and dead cells (figure 5-21, and 5-23B) as compared to untreated cells (figure 5-20A, and 5-23A). MTX-loaded un-crosslinked micelles at 50 μg/mL equivalent of MTX gave rise to 23 ± 4 and 8 ± 5% apoptotic and dead cells, respectively.

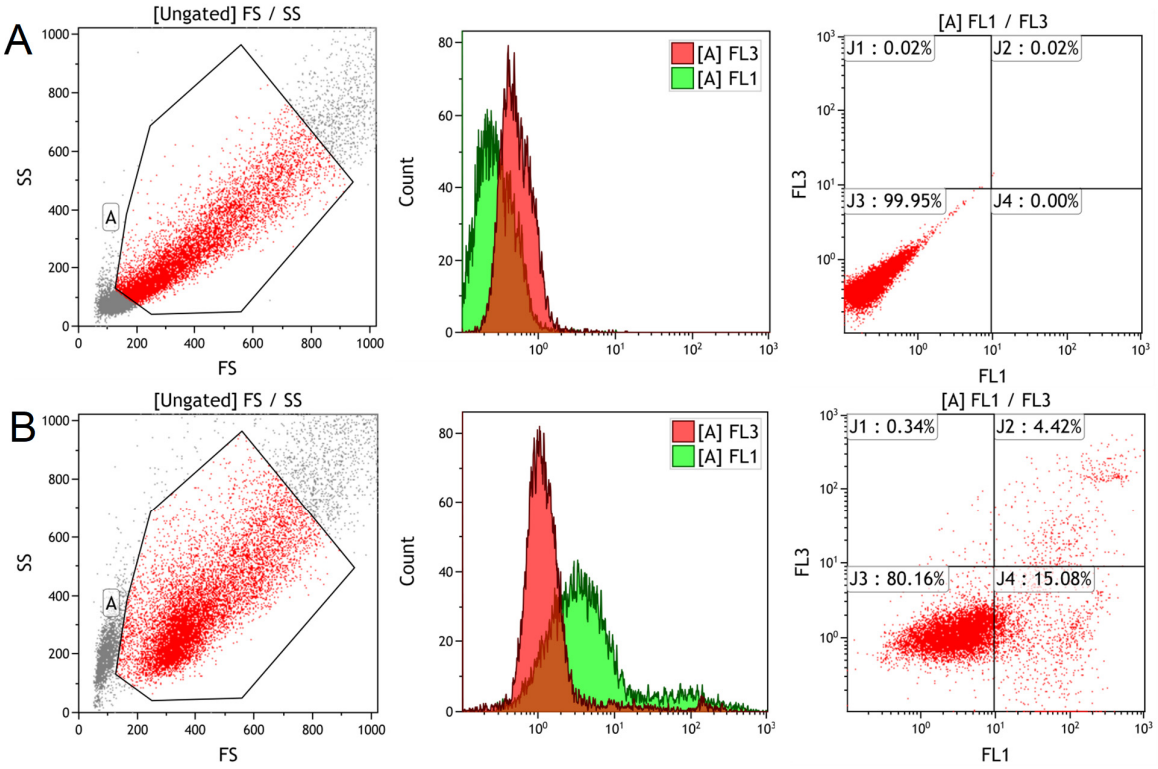

Figure 5-20. Flow cytometry analysis to measure the apoptotic and dead cells in MCF7 breast cancer cells cultured with (A) Medium control and (B) MTX control (50 µg/mL). The percentages of live, apoptotic, and dead cells were calculated from FL1/FL3. Annexin-V-FITC was used to detect apoptotic cells, and propidium iodide (PI) was used to detect dead cells. J1~ necrotic cells, J2 ~ dead cells, J3 ~ live cells, and J4 ~ apoptotic cell.

On the other hand, MTX-loaded core-crosslinked micelles enhanced the proportion of apoptotic and dead cells even at moderate concentrations of 23 µg/mL equivalent of MTX, showing approximately 50 ± 9 and 39 ± 11% apoptotic and dead cells, respectively (figure 5-22, and 5-23C).

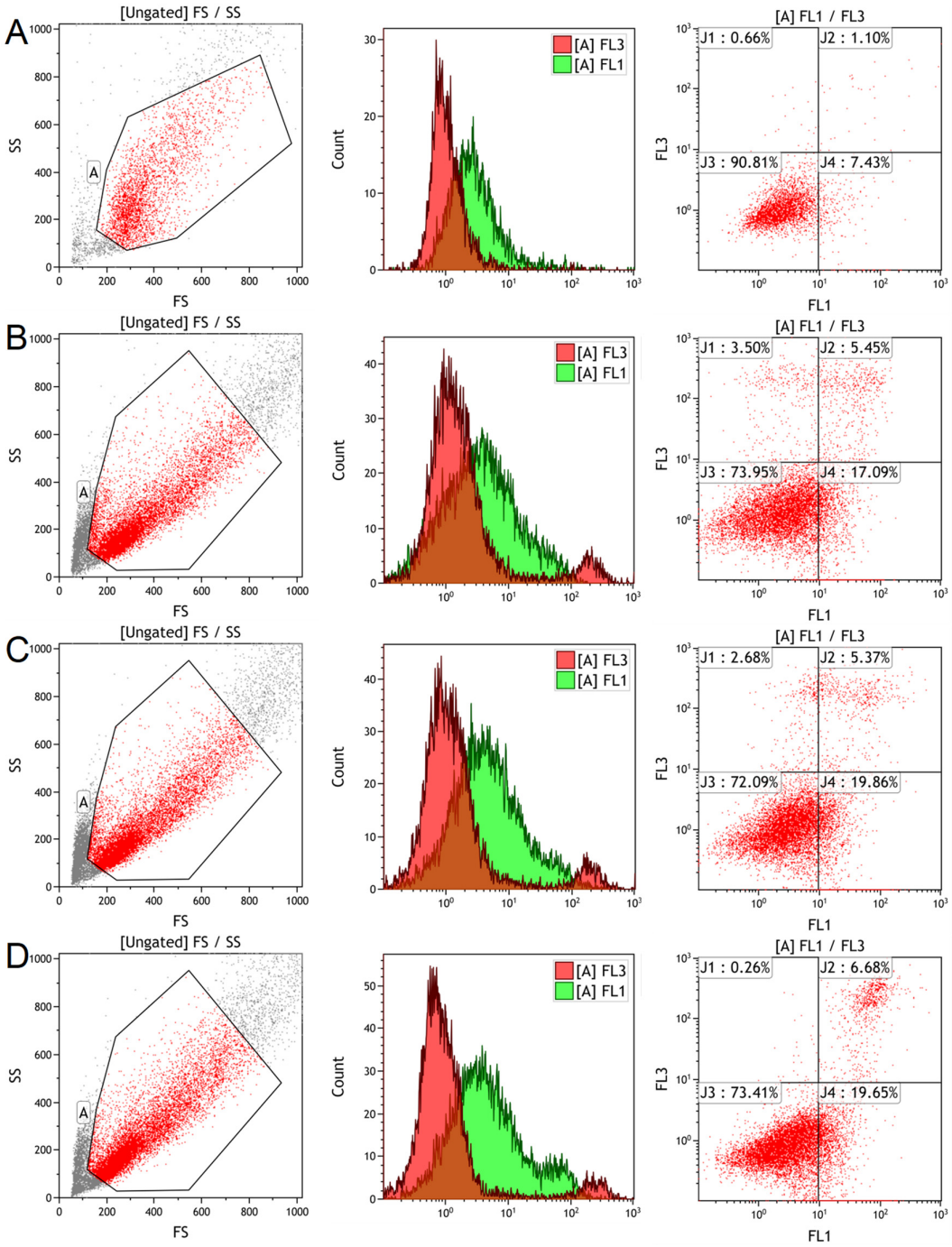

Figure 5-21. Flow cytometry analysis to measure the apoptotic and dead cells in MCF7 breast cancer cells cultured with MTX-loaded micelles. A, B, C, and D represent MTX-loaded micelles equivalent to various amounts of the MTX (4.6, 11.5, 23, and 50 µg/mL, respectively). J1~ necrotic cells, J2 ~ dead cells, J3 ~ live cells, and J4 ~ apoptotic cell.

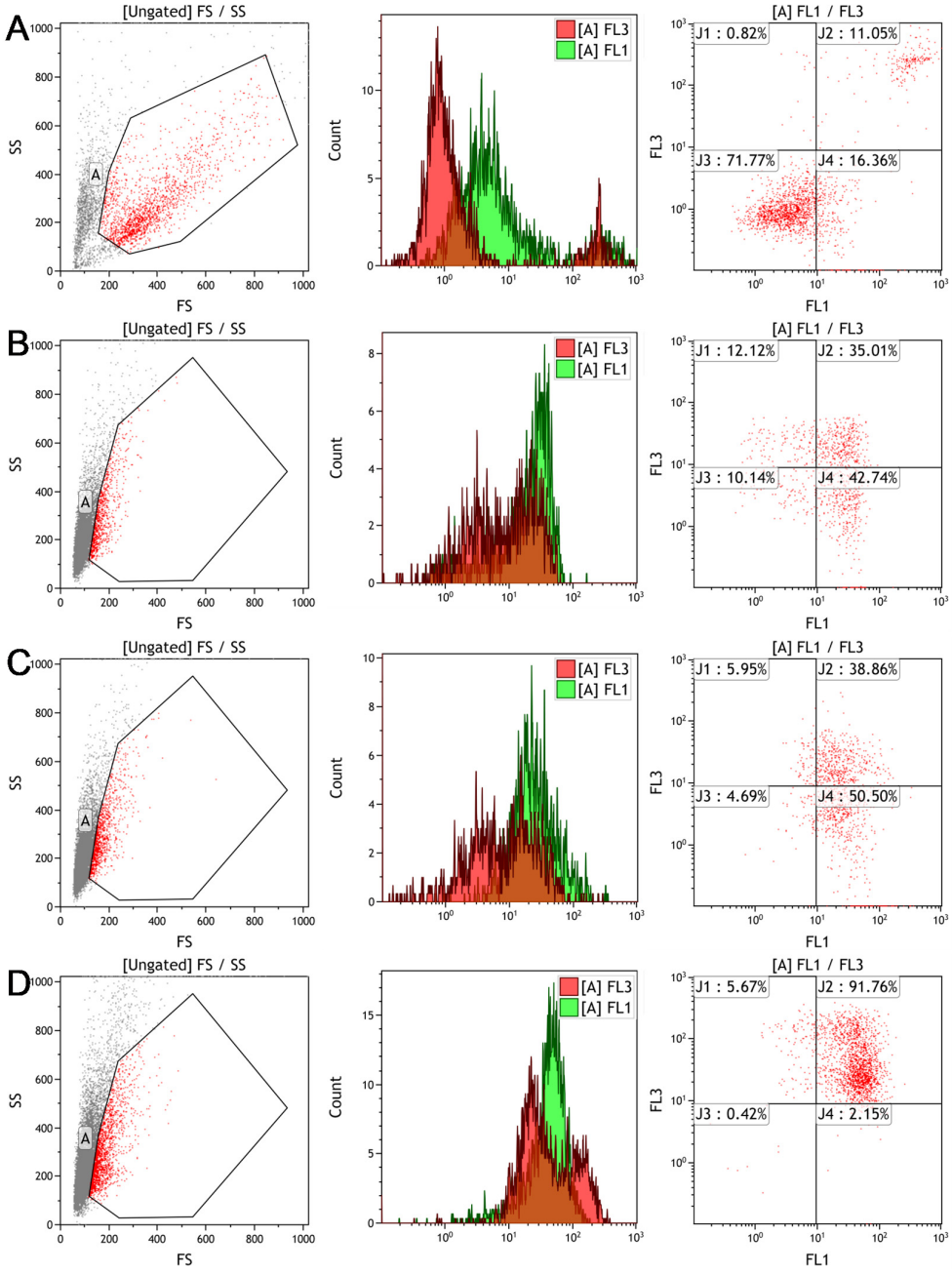

Figure 5-22. Flow cytometry analysis to measure the apoptotic and dead cells in MCF7 breast cancer cells cultured with MTX-loaded core-crosslinked micelles. A, B, C, and D represent the MTX-loaded core-crosslinked micelles equivalent to various amounts of MTX (4.6, 11.5, 23, and 50 μg/mL, respectively). J1~ necrotic cells, J2 ~ dead cells, J3 ~ live cells, and J4 ~ apoptotic cell.

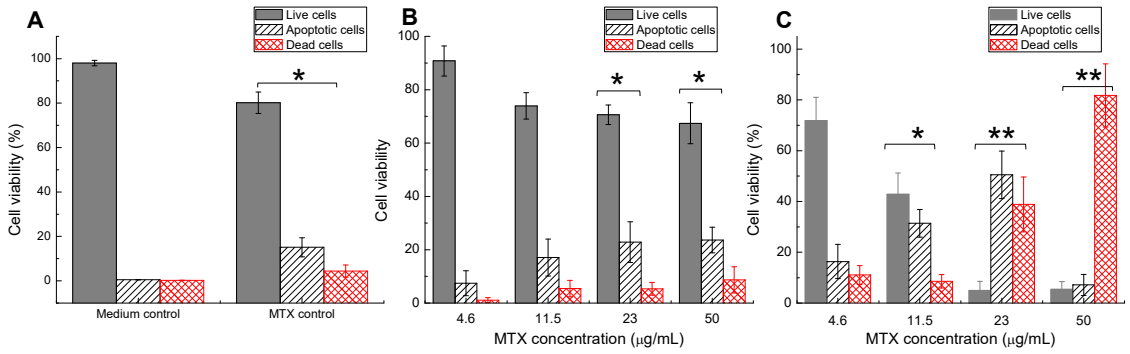

Figure 5-23. Flow cytometric quantification of live, apoptotic, and dead cells from MCF7 cells treated with (A) Medium and free MTX control (50 μg/mL), (B) MTX-loaded un-crosslinked micelles, and (C) MTX-loaded core-crosslinked micelles.

The higher concentrations of crosslinked micelles (50 μg/mL equivalent of MTX) were very effective against MCF7 cells (82 ± 12 % dead cells). In contrast, assays in which cells were treated with free MTX control (50 μg/mL) resulted in fewer apoptotic (approximately 15 ± 4 %) and dead cells (4 ± 3 %), as shown in figure 5.20B and 5-23A. The findings obtained from annexin V-FITC/PI assay were in agreement with Hoechst/PI double staining and MTT assays.

5.3. DISCUSSION

The MTX-loaded redox-responsive reversible core-crosslinked micelles were derived from a biodegradable amphiphilic block copolymer (mPEG-*b*-poly(εCL-*co*-αN$_3$εCL)) and formulated using a dialysis method. In order to concentrate the *bis*-alkyne ethyl disulfide crosslinker in the hydrophobic

part of the micelles, the crosslinker was directly added in the DMSO along with the copolymer and MTX. Upon drop-wise addition of this mixture into the water, it was intended that the *bis*-alkyne ethyl disulfide crosslinker would be retained in the hydrophobic region of the micelles, but still be accessible to $Cu(II)SO_4$ and ascorbic acid sodium salt as the click reaction proceeded between the pendent azide groups of the copolymer backbone and the alkyne groups of the crosslinker as the DMSO and aqueous phases mixed.

The MTX-loaded core-crosslinked micelles were larger than their un-crosslinked counterparts. The larger sizes of the core-crosslinked micelles were likely due to conformational rearrangements driven by triazole ring formation, which in turn caused decreased free movement of chains of the copolymer, leading to larger cores of micelles, as has been reported previously.[35] The hydrodynamic diameters of micelles in all formulations as measured by DLS were larger than those of air dried micelles measured by TEM, as expected based on the hydration of the polyethylene glycol shell of the copolymeric micelles in solution.[76] The zeta potential measurements showed close to neutral surface charges of micelles, again attributable to the neutral hydrophilic PEG shell that extended out into the aqueous phase and inhibited the aggregation of micelles through steric stabilisation.

The drug loading analysis of core-crosslinked micelles revealed that the crosslinking step increased the drug content compared to un-crosslinked micelles. The better encapsulation efficiency of crosslinked micelles could

be attributed to a more tightly packed core with interconnected networks of crosslinked bridges providing more effective diffusion barriers to egress of MTX from the formulation. Various other factors have been reported to influence drug loading of polymeric micelles, including polymer-drug compatibility,[77] size of the micelle core,[78] presence and extent of micellar crosslinking, presence of specific functional groups in the copolymer,[79] and molecular weight and chemical structure of the encapsulated agent. Moreover, the preparation method of micelles, aqueous solubility of the drug, hydrogen bonding, π-π stacking, electrostatic and dipole-dipole interactions between the drug and hydrophobic core of micelles were likely to affect the drug incorporation in these MTX-loaded micelles. Furthermore, the crystallinity and glass transition temperature of the hydrophobic block of copolymer have been shown to influence the drug loading and encapsulation efficiency of micelles.[80]

From *in vitro* release experiments, it was apparent that un-crosslinked micelles showed greater burst release of MTX compared to core-crosslinked micelles. The latter retained most of the drug payload in the absence of exogenous reducing agent, however, rapid release of MTX was observed in reducing environments for disulfide-crosslinked polymer micelles.

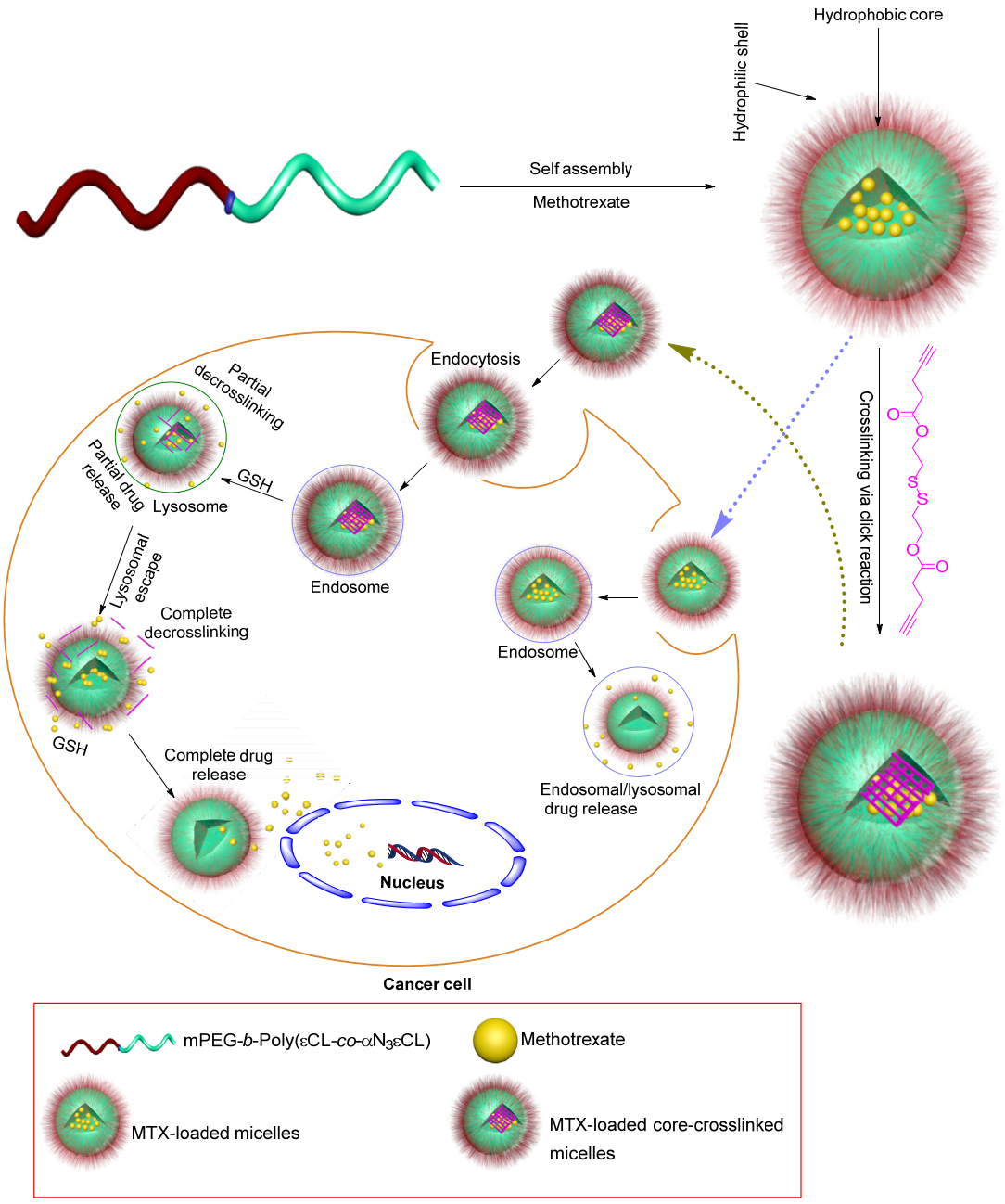

Figure 5-24. Schematic illustration for the preparation of MTX-loaded redox-responsive reversibly core-crosslinked micelles and intracellular uptake and drug release.

Various factors are known to affect the drug release from polymeric micelles such as polymer degradation, wettability, molecular weights of hydrophilic and hydrophobic blocks, glass transition temperature, binding affinity between the drug and copolymer.[81] The incorporated drug may accumulate at various places inside the micelle *e.g.* at the interface between the core and shell of the micelle, within the micelle-core and to a lesser extent within the corona or shell of the micelle. Therefore, the localisation of the drug within the micelle can play an important role in the release kinetics of the encapsulated drug. The incorporated drug can be released from polymeric nanocarriers by several routes i.e. diffusion through the polymer matrix, by the degradation (by surface or bulk erosion) of the polymer, and by solubilisation or diffusion through nano-channels that may exist in the polymer matrix or those created by erosion.[82]

In this study, MTX release rate was not expected to be influenced by polymer degradation owing to the known slow hydrolysis rate of PCL, as reported previously.[83] Therefore, the initial 'burst release' from un-crosslinked micelles was likely to have been due to the rapid contact of the aqueous medium with a fraction of the MTX localised on the corona or at the interface between the corona and micelle-core.[84] The steady or temporal drug release phase was probably due to the drug diffusion from the micelle-core into the release medium, as previously described.[82] In contrast, MTX-loaded core-crosslinked micelles released lower amounts of drug under non-reducing conditions showing that core-crosslinked micelles

more efficiently contained the drug payload compared to un-crosslinked systems.

The fast MTX release from core-crosslinked micelles under a reducing environment was primarily due to the cleavage of disulfide bridges (figure 5-24) resulting in cleavage of crosslinker and 'opening' of the micellar core. Overall, redox-responsive reversibly core-crosslinked micelles efficiently restricted MTX release in non-reducing buffer conditions, however, introduction of the DTT into micellar suspensions caused cleavage of internal micelle crosslinks, which subsequently facilitated the drug release.

The analysis of the cellular uptake of micelles was performed using Oregon-green as a fluorescent probe. Oregon-green based labels share several advantages over other fluorescein dyes, e.g. good photo-stability and lower pK_a. For this purpose, Oregon-green was synthesised as already reported in literature.[85] Oregon-green loaded un-crosslinked and Oregon-green loaded core-crosslinked micelles were efficiently taken up by MCF7 cells and there was no apparent difference found in the magnitude of the cellular uptake of both type of micelles, as observed by flow cytometry and confocal microscopy studies. However, confocal microscopy revealed that un-crosslinked micelles were mostly localised in cytoplasmic regions of MCF7 cells, whereas, core-crosslinked micelles were accumulated both in cytoplasmic and in perinuclear regions of MCF7 cells.

It has been reported that nanocarriers can penetrate into certain solid tumours due to the leaky vascular system existing in these types of cancer tissues. This phenomenon is known as the "Enhanced Permeability and Retention (EPR) effect",[86] and has been shown to allow materials above a hydrodynamic volume threshold to partition selectively from the circulation into tumour tissues. If, after penetrating the target site, the retained nano-carriers can release a drug payload in the vicinity of cancer cells, an effective localisation of drug can be obtained, which is better in terms of the therapeutic window for the drug. In addition, many tumours lack effective lymphatic drainage, hence increasing the retention of nanoscale drug delivery systems in the target site.[87] This retention of nanocarriers contributes to the further accumulation of the drug at the tumour locality.

Typically, to exploit the enhanced permeability and retention effect, drug delivery systems must be within a narrow size range (10-100 nm). After systemic injection, the mononuclear phagocytic system and the renal clearance compete with the tumour for nanoparticles.[88] In general, macromolecules, polymers and nanoparticles smaller than 10 nm are removed through renal and hepatobiliary clearance or by extravasation,[89] whereas, larger materials (100-200 nm) are cleared by the reticuloendothelial system.[90]

Polymeric micelles are considered to be good candidates to take advantage of the EPR effect due to the possibility that micelle-size can easily be tuned by controlling the molecular weights of hydrophilic and hydrophobic blocks

and other parameters. However, it is also noteworthy that certain tumours do not exhibit enhanced permeability and retention (EPR) effect and the permeability of vessels is not consistent throughout a single solid tumour.[88]

In any clinical application, drug-loaded nanocarriers must pass through various transport barriers to reach their targets. Specifically, translocation of injected drug delivery systems across the plasma membrane barrier is a prerequisite.[87] Plasma membranes are complicated components of the body and play an important role in control of cellular communication and cell division regulated by endocytosis. Cells use endocytosis for internalisation of important nutrients, extracellular fluids, proteins, and lipids, and in downregulation of growth factor receptors and in controlling the cell signalling.[91]

It can be assumed that cellular uptake of Oregon-green loaded and Oregon-green loaded core-crosslinked micelles was through passive caveolin-mediated endocytosis,[92] as no targeting ligands were grafted to micelles. For instance, Oregon-green loaded poly(vinyl alcohol)-graft-poly(lactide-co-glycolide) nanoparticles have been investigated for their cellular uptake, previously.[93] It was demonstrated that the uptake of Oregon-green loaded nanoparticles followed caveolin-mediated endocytosis pathway.[93]

Thus, after being internalised, the nanocarriers were likely to have been entrapped into endocytic vesicles, and trafficked into endo/lysosomal compartments. The endosomes and lysosomes are acidic vesicles

containing multiple enzymes that can degrade certain foreign particles.[94, 95] Therefore, in this study, the localisation of Oregon-green loaded un-crosslinked micelles mostly in non-nuclear regions of MCF7 cells could be attributed to the dis-assembly of micelles, and ultimately release of Oregon-green in the endosomes or lysosomes. This might have restricted un-crosslinked micelles to cytoplasmic regions of MCF7 cells. In contrast, due to better colloidal stability and more robust cores, crosslinked micelles may have been able to survive lysosomal degradation. This might in turn have enabled more rapid transport out of lysosomal compartments, passage into the cytosol and transport or facilitated delivery of Oregon-green to nuclei of MCF7 cells.[20]

The metabolic activity investigations using MTT assays showed that both un-crosslinked and core-crosslinked micelles were essentially non-toxic to MCF7 cells. The MTT (methyl-thiazolyl-tetrazolium) assay is a colorimetric test and has been widely used to examine the cell viability, cytotoxicity, and proliferation analysis in cell biology.[96] MTT is a water-soluble salt that gives a yellow colour in aqueous solution, which on reduction by NAD(P)H-dependent oxidoreductase enzymes present in metabolically active cells, produces a water insoluble formazan. The lipid soluble formazan has a purple colour and may be extracted with organic solvents and can be quantified by spectrophotometry. It is assumed that the quantity of MTT formazan is directly proportional to the number of live or metabolically active cells.[97] .

The MTT assay results suggested that empty un-crosslinked and core-crosslinked micelles had low cytotoxicities. In contrast, MTX-loaded formulations significantly enhanced the cytotoxicity of MTX. Specifically, MTX-loaded core-crosslinked micelles were found to be more toxic to breast cancer cells as shown by the declined cell viability of 8.2 % at 50 μg/mL equivalent to MTX, as compared with same concentrations of free-MTX (74 % cell viability) and MTX-loaded un-crosslinked micelles (45 % cell viability).

In order to check whether the cell death in tumour cells treated with MTX-loaded formulations was due to the onset of the apoptosis, confirmatory tests were implemented. Typically, the initiation of the apoptosis in cells results in condensation or fragmentation of the chromatin due to the condensed nuclei of apoptotic cells, which can be detected by fluorescence microscopy using a cell permeable nucleic acid labelling blue fluorescent dye, Hoechst 33342. Concurrently, dead cells can be detected by staining with the propidium iodide (a dye which exhibits strong fluorescence on DNA-binding). The propidium iodide cannot cross cell-membranes of live cells, however, dead or necrotic cells can be stained with the PI due to their compromised cell membrane integrity.[98]

The MCF7 cells treated with MTX-loaded un-crosslinked and core-crosslinked micelles, free MTX, and MTX-DMSO control showed characteristics features of the apoptosis such as chromatin condensation

and fragmentation, cell shrinkage, and formation of apoptotic bodies (figure 5-25).

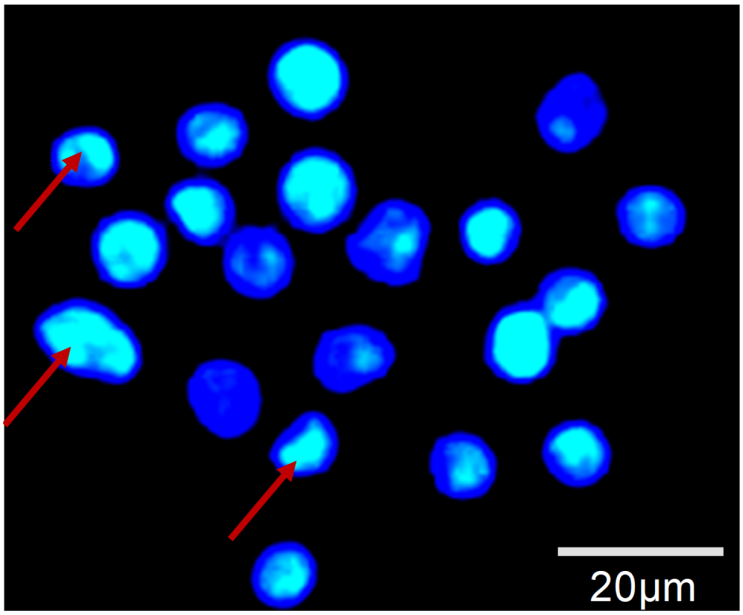

Figure 5-25. Representative fluorescence microscopy image of MCF7 cells in apoptosis stage. Arrows showing bright blue condensed or fragmented chromatin, a characteristic feature of cells entering apoptosis.

Specifically, apoptotic nuclei clearly exhibited bright blue fluorescence with condensed or fragmented chromatin.[99] Dead or late apoptotic cells showed the pink fluorescence. The findings of Hoechst/PI assays were consistent with MTT assays, showing that MTX-loaded core-crosslinked micelles induced greater apoptosis and subsequently increased the cell death in breast cancer cells, as compared with the free-MTX and MTX-loaded un-crosslinked micelles.

It should be noted that the free-MTX was less potent in inducing apoptosis as compared with MTX-loaded nanocarriers. The low apoptosis inducing potency of the free-MTX may have been a consequence of its low solubility in aqueous media. To investigate this phenomenon, a control experiment was designed in which MTX was first dissolved in DMSO and then mixed with the cell culture medium. However, no apparent difference was found in apoptotic activity as compared with the free-MTX directly dissolved in cell culture media. These findings suggested that along with the low aqueous solubility, some other factors (e.g. low permeability and influx, higher efflux of MTX, and drug resistance etc.) might be responsible for low cytotoxicity of free MTX. Comparison with the formulated sodium salt of methotrexate was not carried out, as for a breast cancer indication, the conventional oral methotrexate sodium tablet formulation would not be suitable.

To further confirm that cell death was induced via apoptosis (as observed in the Hoechst/PI assay) by MTX-loaded micelles, annexin V-FITC/PI assays were performed. Annexin V is a calcium-dependent, phospholipid-binding protein that can selectively bind to the cells that express negatively charged phospholipids (phosphatidyl serine) on the outer surface of plasma membrane, a distinctive feature of cells entering apoptosis. In contrast, healthy cells express phosphatidyl serine on the inner side of the plasma membrane. Upon entering apoptosis, the negatively charged phosphatidyl serine is translocated by a protein known as scramblase to the outer cell

surface.[100] Therefore, annexin V labelled with a fluorescent dye such as FITC can be used to detect apoptotic cells.[101] After binding to the phosphatidyl serine, annexin V assembles into a trimeric cluster comprising of three annexin V units bound to each other by non-covalent protein-protein interactions. The building of annexin V cluster on the plasma membrane greatly amplifies the fluorescence intensity of the FITC, which can be detected by using flow cytometry.[102]

The findings of the annexin V-FITC/PI assay also revealed that MTX-loaded core-crosslinked micelles induced the apoptosis and finally cell death in tumour cells to a greater extent as compared with MTX-loaded un-crosslinked micelles and free-MTX. Therefore, the findings of annexin V-FITC/PI assays were in agreement with Hoechst/PI and MTT assays.

In order to achieve better therapeutic effects, anticancer drugs must enter cancer cells and need high concentrations. In terms of passive transmembrane diffusion, repulsive interactions between the negatively charged plasma membrane and the MTX in its sodium salt form may cause difficulties in permeation of the MTX into the cell membrane, consequently decreasing the therapeutic effectiveness.[103] Furthermore, after being transported into the cytosol, higher cellular levels of the MTX must be maintained, since the affinity of dihydrofolate reductase enzyme is greater to folate than MTX.[104] However, maintaining high intracellular levels of the MTX is difficult due to the limited influx and spontaneous efflux of the MTX.[103]

It is also important to note that internalisation of the free MTX can occur via reduced-folate-carrier (RFC) mediated transport.[105] The reduced-folate-carrier is an integral plasma membrane protein that mediates cellular transport of folates and antifolates (such as MTX).[106,107] However, saturation of the reduced-folate-carrier at high MTX concentrations may occur which can inhibit the further uptake of the drug, therefore decreasing the therapeutic effectiveness.[108] In contrast, MTX-loaded un-crosslinked and crosslinked micelles are assumed to follow a different path of internalisation such as passive endocytosis. In addition, the approximately neutral charge of MTX-loaded un-crosslinked and crosslinked micelles may not have induced repulsive interactions at the negatively charged plasma membranes. Therefore, uptake of MTX-loaded un-crosslinked and core-crosslinked micelles by endocytic routes might have been more efficient than diffusion of free MTX alone, hence enhancing the influx of MTX within polymer micelles as compared to the reduced-folate-carrier route of free MTX.

It has also been reported that some anticancer drug loaded nanocarriers exhibit lower cytotoxicity and apoptosis inducing potential as compared to free drugs themselves.[109] This phenomenon is observed in some cases due to the endosomal or lysosomal entrapment of drug-loaded nanocarriers. However, in this study, the free MTX showed low *in vitro* cytotoxicity and apoptosis inducing potential as compared with MTX-loaded micelles. The low *in vitro* cytotoxicity of the free MTX might have been due to its poor

aqueous solubility and lower permeability.[59,63,110] Furthermore, the low cytotoxicity of the free MTX may have been a consequence of its reduced intracellular retention, caused by the P-glycoprotein-mediated drug efflux. On the other hand, the higher cytotoxicity of MTX-loaded nanocarriers suggested that there were other factors relating to drug efficacy in MCF7 cells. The cytotoxic activity of MTX-loaded micelles further increased after the crosslinking step due most likely to the enhanced drug loading and retention in the core cross-linked micelles and accelerated drug release within the cancer cells.

The findings of higher *in vitro* anti-cancer activity of MTX-loaded core-crosslinked micelles against MCF7 cells were consistent with the cellular uptake experiments. From cellular internalisation data, it could be deduced that MTX-loaded core-crosslinked micelles were more stable to dissociation both outside and inside the target cells. Thus, greater *in vitro* anti-cancer efficacy of MTX-loaded core-crosslinked micelles may have been due to the greater accumulation of MTX-loaded core-crosslinked micelles or release of MTX in cytoplasmic regions of MCF7 cells which were distant from efflux pump protein. These data together suggest that further development of, redox-responsive reversibly core-crosslinked micelles could be promising for tumour therapy and bio-responsive drug delivery applications.

5.4. CONCLUSIONS

In this study, functional micelles based on mPEG-*b*-poly(εCL-*co*-αN$_3$εCL) block copolymer were developed by using a co-solvent method. An anticancer drug (methotrexate) was loaded into the hydrophobic core of the micelles, which were further crosslinked by a redox responsive crosslinker to generate redox-responsive reversibly core-crosslinked micelles. The encapsulation efficiency of micelles greatly improved after crosslinking as compared to un-crosslinked micelles. The redox-responsive reversibly core-crosslinked released lower amounts of the drug under simulated simplified (serum free) physiological conditions, however, rapid drug release was observed in reducing environments. The cellular uptake studies revealed that core-crosslinked micelles were internalised by MCF7 cells quantitatively and mostly localised near the vicinity of cell nuclei. In contrast, un-crosslinked micelles were mostly localised in the cytoplasm of MCF7 cells. The cytotoxicity studies showed that empty un-crosslinked and core-crosslinked micelles were nontoxic to MCF7 cells. The MTX-loaded core-crosslinked micelles greatly inhibited the metabolic activity of MCF7 in a dose dependent manner, as compared to the MTX-loaded un-crosslinked micelles and free MTX. The apoptosis assays revealed that MTX-loaded core-crosslinked micelles induced apoptosis and cell death in MCF7 cells to a greater extent as compared to the MTX-loaded un-crosslinked micelles and free MTX. Therefore, redox-responsive reversibly core-crosslinked

micelles might in future be promising candidates for bio-responsive drug delivery applications and tumour therapy.

5.5. EXPERIMENTAL

5.5.1. Synthesis of mPEG-*b*-poly(εCL-*co*-αN$_3$εCL)

The functional amphiphilic block copolymer based on mPEG-*b*-poly(εCL-*co*-αN$_3$εCL) was synthesised according to the procedure described in chapter 3. The block copolymer coded as MG14 (M_n ~ 10.1 kDa, D_p of PCL ~ 35, D_p of poly(αN$_3$εCL) ~ 7, CMC ~ 6 µg/mL (see appendix, figure 8-1)) was used for all drug loading, micelles crosslinking, and cell culture experiments.

5.5.2. Synthesis of *bis*-alkyne ethyl disulfide crosslinker [disulfanediyl-*bis*(ethane-2,1-diyl) *bis*(pent-4-ynoate)]

Anhydrous CH_2Cl_2 (40 mL) was cooled to 0 °C in a clean dry round bottom flask using an ice bath. The solvent was purged with the nitrogen gas and 1.31 g (8.49 mmol) 2-hydroxyethyl disulfide, 3.90 g (20.34 mmol) *N*-(3-dimethylaminopropyl)-*N*'-ethylcarbodiimide hydrochloride (EDC), and 4-pentynoic acid (2 g, 20.38 mmol) were introduced into the system. 0.25 g (2.05 mmol) 4-(dimethylamino) pyridine was dissolved in a small amount of dry CH_2Cl_2 and was subsequently introduced into the reaction mixture drop wise under magnetic stirring. The reaction contents were stirred for

48 hours at RT. Afterwards, the organic phase was washed with 3 x 100 mL of 1M hydrochloric acid solution, 3 x 100 mL of 1M sodium hydroxide solution, and 200 mL of 1M NaCl solution. The water residues in the organic phase were removed with anhydrous $MgSO_4$. After filtration, the solvent was removed under reduced pressure to obtain a transparent viscous liquid. The final product was purified by silica gel column chromatography (hexane: ethyl acetate 4:3, R_f 0.36, 75 % yield), and characterised by electrospray ionisation mass spectrometry, ^{1}H NMR, and ^{13}C NMR.

^{1}H NMR (400 MHz, $CDCl_3$) δ (ppm): 4.40 (-C$\underline{H}_2$-O-C=O, t, *J* = 6.6 Hz, 4H), 2.95 (-S-S-C$\underline{H}_2$-CH_2-O-C=O, t, *J* = 6.6 Hz, 4H), 2.60 (O=C-C$\underline{H}_2$-CH_2-C≡CH, dd, *J* = 7.9 Hz, *J* = 5.4 Hz, 4H), 2.56–2.51 (O=C-CH_2-C$\underline{H}_2$-C≡CH, m, 2H), 2.01 (C≡C$\underline{H}$, t, *J* = 2.5 Hz, 2H). ^{13}C NMR (101 MHz, $CDCl_3$) δ (ppm): 171.49 (C=O), 82.31 ($\underline{C}$≡CH), 69.18 (C≡$\underline{C}$H), 62.48 ($\underline{C}H_2$-O-C=O), 38.38 (-S-S-$\underline{C}H_2$-CH_2-O-C=O), 33.22 (O=C-$\underline{C}H_2$-CH_2-C≡CH, 14.65 (O=C-CH_2-$\underline{C}H_2$-C≡CH). Data were compared with the previously reported results by Gao *et al.*[111]

5.5.3. Synthesis of Oregon-green mixed isomers [4-(2,7-difluoro-6-hydroxy-3-oxo-3*H*-xanthen-9-yl)isophthalic acid, and 2-(2,7-difluoro-6-hydroxy-3-oxo-3H-xanthen-9-yl)terephthalic acid]

Oregon-green (mixed isomers) was synthesised adapting a method described in the literature with some modifications.[85] Briefly, 4-Fluororesorcinol (500 mg, 3.90 mmol) was dissolved in 3 mL methanesulfonic acid. The system was deoxygenated using nitrogen gas for 30 minutes before adding trimellitic anhydride (394 mg, 1.95 mmol). Afterwards, the reaction was stirred for 48 h at 80 °C and was then allowed to cool down and poured into 7 volumes of cold water. The resultant precipitate was filtered and dried using rotary evaporator. Finally, the solid was dissolved in a small amount of methanol and precipitated again in cold water. The solid was subsequently dried using a rotary evaporator, and the final product was characterised by ^{1}H NMR and electrospray ionisation mass spectrometry (see appendix figure 8-2). ^{1}H NMR (400 MHz, CD_3OD) δ (ppm): 8.38 (s, 1H), 8.20 (d, 1H), 7.40 (d, 1H), 6.85 (s,s, 2H), 6.50 (s,s 2H). Data were compared with the previously reported results.[85]

5.5.4. Preparation of empty and drug/dye loaded micelles

Empty micelles of the mPEG-*b*-poly(εCL-*co*-αN$_3$εCL) copolymer were prepared using a dialysis method with DMSO as co-solvent. Briefly, 50 mg

of copolymer was dissolved in 5 mL DMSO and was introduced into Milli-Q water (20 mL) under vigorous stirring, using a syringe pump with a flow rate of 0.20 mL/min. The solution was stirred for 2 hours at room temperature and polymer micelles were purified by dialysis overnight against 1 L of Milli-Q water using a cellulose dialysis membrane (Spectrapor, cut-off 3500) to remove the DMSO. Drug/dye loaded micelles were prepared in a similar procedure in which 4 mg methotrexate (MTX) or Oregon-green dye and 50 mg copolymer were dissolved in 5 mL DMSO. The micellar solution was filtered through a membrane syringe filter (pore size: 0.22 μm) (Millex-LG, Millipore Co., USA) before further characterisation.

5.5.5. Preparation of empty and drug/dye loaded cross-linked micelles

For the preparation of cross-linked micelles, 50 mg (approximately 0.005 mmol) of mPEG-*b*-poly(εCL-*co*-αN$_3$εCL) copolymer and 12 mg (0.038 mmol) of *bis*-alkyne-ethyl disulfide cross-linker were dissolved in DMSO. Afterwards, under vigorous stirring, this mixture was dropwise introduced into 20 mL Milli-Q water, using a syringe pump with a flow rate of 0.20 mL/min. The micellar solution was stirred for 2 hours at room temperature. Afterwards, copper(II) sulfate (0.20 mol equivalent to azide groups) and sodium ascorbate (0.20 mol equivalent to azide groups) were introduced

into the system. The crosslinking reaction was carried out at 36 °C for 24 hours. Afterwards, EDTA (2 mol equiv. vs. Cu) was introduced into the system and the cross-linked micelles were dialyzed against 1 L of deionised H_2O. Drug/dye loaded cross linked micelles were prepared in a similar method in which 4 mg methotrexate (MTX) or Oregon-green dye and 50 mg copolymer were dissolved in 5 mL DMSO in presence of cross-linker.

5.5.6. Determination of drug contents and encapsulation efficiency

Drug contents and encapsulation efficiency were determined by dissolving a known amount (5 mg) of freeze dried MTX-loaded micelles or MTX-loaded core-cross-linked micelles in DMSO. The quantification of methotrexate was performed using UV-Vis spectrophotometry (monitoring at λmax = 304 nm). The amount of loaded drug was calculated using a standard curve of MTX in DMSO. Drug content (wt. %) and encapsulation efficiency (wt. %) were calculated according to the following equations:

$$\text{Drug content (wt. \%)} = \frac{\text{(weight of MTX in micelles)}}{\text{(weight of copolymer used)}} \times 100$$

$$\text{Encapsulation Efficiency \%} = \frac{\text{(weight of MTX in micelles)}}{\text{(weight of MTX in feed)}} \times 100$$

5.5.7. Drug release analysis

The *in vitro* drug release studies from MTX-loaded un-cross-linked and MTX-loaded cross-linked micelles were carried out in non-reducing (PBS, pH 7.4) and reducing (10 mmol DTT in PBS, pH 7.4) media, containing Tween 80 (1% v/v) in order to improve the solubility of MTX. Samples (5 mg) of freeze dried MTX-loaded or MTX-loaded cross-linked micelles were re-dispersed in 2mL PBS (pH 7.4) and the solution was placed in a dialysis device (Slide-A-Lyzer™ mini dialysis device, 3.5K MWCO, Thermo Scientific). The micellar solution was dialysed against 45 mL of release media at 37 °C and samples (1 mL) were taken at appropriate time points and replaced with 1 mL fresh medium. The collected samples were freeze dried and dissolved in DMSO. The amount of MTX was calculated using UV-Vis spectrophotometry (λ_{max} =304 nm) via a standard calibration curve of MTX in DMSO containing Tween 80 (1% v/v).

5.5.8. Cellular uptake analysis using confocal microscopy

Human breast cancer cells (MCF7) were cultured in Dulbecco's Modified Eagle Medium (DMEM) containing 10% fetal bovine serum (FBS) and 1% L-glutamine at 37 °C with 5% CO_2. For cellular uptake studies, MCF7 cells (3 x 10^4 cells/well) were seeded on a collagen coated cover glass in a 6-

well plate for 24 hours. Cell culture medium was removed and cells were then treated with fresh medium containing Oregon-green loaded un-cross-linked or Oregon-green loaded cross-linked micelles (100 µg/mL each) and incubated for 3 hours. Cell culture medium was removed again and cells were washed with PBS (3 times). To label cell membranes, cells were incubated with CellMask™ deep red plasma membrane stain (working solution concentration 1µL/mL) for 10 minutes at 37 °C. After washing with PBS (3 times), cells were incubated with Hoechst dye (working solution concentration 1 µL/mL) for 30 minutes at 37 °C to label cell nuclei. After removing the labelling solution, cells were washed with PBS and were fixed with 4% paraformaldehyde for 15 min at room temperature. After fixation, cells were washed with PBS and cover glasses were mounted on glass microscope slides using fluorescence mounting medium. The uptake of Oregon-green loaded micelles or Oregon-green loaded cross-linked micelles was examined using a Zeiss 510 Meta Confocal microscope.

5.5.9. Cellular uptake analysis using flow cytometry

For cellular uptake studies by flow cytometry, MCF7 cells were seeded on a 12-well plate at a density of 7.5×10^4 cells/well in 1 mL of Dulbecco's Modified Eagle Medium (DMEM) containing 10% fetal bovine serum (FBS) and 1% L-glutamine for 24 hours (37 °C, 5% CO_2). Cell culture medium was removed and was replaced with fresh medium containing Oregon-

green loaded un-cross-linked or Oregon-green loaded cross-linked micelles (100 µg/mL each) and incubated for 3 hours. Cell culture medium was removed again and cells were washed with PBS (3 times). Cells were then incubated with 100 µL of 1×trypsin/EDTA solution for 3 minutes (37 °C and 5% CO_2). PBS (0.9 mL) was then added into each well and cells were collected in labelled FACS tubes and were then centrifuged at 1200 RPM for 5 minutes. Supernatant was removed and cells were re-suspended in 500 µL PBS and analysed using a Beckman Coulter FC 500 flow cytometer. The untreated cells (without micelles) were used as a negative control and data were analysed using Kaluza 1.3 software.

5.5.10. *In vitro* metabolic activity analysis

The effects of empty un-crosslinked and cross-linked micelles, MTX-loaded un-cross-linked and MTX-loaded core-cross-linked micelles on the metabolic activities of MCF-7 cells were analysed by MTT assay. MCF7 cells were seeded on a 96-well plate at a density of 5×10^3 cells per well in 200 µL of Dulbecco's Modified Eagle Medium (DMEM) containing 10% fetal bovine serum (FBS) and 1% L-glutamine at 37 °C with 5% CO_2 for 24 hours. Cell culture medium was removed and replaced with fresh medium containing various concentrations of empty un-cross-linked or empty cross-linked micelles and MTX-loaded un-crosslinked, and MTX-loaded crosslinked micelles ranging from 100, 250, 500, 750, and 1000 µg/mL.

Cells were incubated for 48 hours and then 50 µL MTT solution (4 mg/mL) was added into each well. Cells were incubated for another 4 hours and medium containing MTT solution was removed and replenished by 150 µL DMSO to dissolve any resulting formazan purple crystals. The optical densities at 570 nm were measured using a BioTek microplate reader. The MTT assay was also repeated with a calculated amount of MTX-loaded un-crosslinked or crosslinked micelles equivalent to 4.6, 11.5 23, 36, and 50 µg/mL of MTX, and also with the same amount of free-MTX as a positive control. The percentage of cell metabolic activity was calculated using untreated cells (without micelles) as a negative control (100% metabolic activity).

5.5.11. Apoptosis detection by fluorescence microscope-Hoechst/PI assay

MCF7 cells were seeded on a 24-well plate at a density of 2×10^4 cells per well in DMEM containing 10% FBS and 1% *L*-glutamine at 37 °C with 5% CO_2 for 24 hours. Cell culture medium was removed and replaced with fresh medium containing a calculated amount of MTX-loaded un-crosslinked or crosslinked micelles, equivalent to various amounts of the MTX (4.6, 11.5 23, 36, and 50 µg/mL). Cells were incubated for 48 hours and cell culture medium was then removed and cells were washed with ice cold PBS. Afterwards, cells were incubated with 1 mL Hoechst 33342 solution (10

μL/mL in ice cold PBS) at 37 °C for 15 minutes. After removing the labelling solution and washing the cells with ice cold PBS, cells were incubated with 1 mL propidium iodide (PI) solution (5 μL/mL in ice cold PBS) at room temperature for 15 minutes in dark. The PI labelling solution was removed and cells were washed (3 times) with ice cold PBS and were observed immediately under an inverted-fluorescence microscope (EVOS™ FL Cell Imaging System). The untreated cells (without micelles) were used as a negative control and cells treated with various amounts of free MTX (4.6, 11.5 23, 36, and 50 μg/mL) dissolved in cell culture medium were used as positive controls. Cells were also treated with various amount of MTX dissolved in DMSO-medium as another positive control. A stock solution of MTX was prepared by first dissolving MTX in 200 μL DMSO, and volume was made up to 10 mL with DMEM. This stock solution was further diluted with DMEM to obtain the required concentration of MTX. The percentages of live, apoptotic, and dead cells were calculated using Infinity Analyze software (Infinity Analyze 3R, Lumenera Corporation).

5.5.12. Annexin-V/PI apoptosis assay

MCF7 cells were seeded on a 24-well plate at a density of 7.5×10^4 cells/well in DMEM containing 10% FBS and 1% L-glutamine for 24 hours (37 °C, 5% CO_2). Cell culture medium was removed and replaced with fresh medium containing a calculated amount of MTX-loaded un-crosslinked or MTX-

loaded crosslinked micelles, equivalent to various amounts of MTX (4.6, 11.5, 23, and 50 μg/mL) and cells were then incubated for 48 hours. After the incubation period, floating cells were collected into labelled FACS tubes on ice (4 °C) and attached cells were trypsinised and pooled together with corresponding floating cells. Samples were centrifuged at 1200 rpm for 5 min at 4 °C and supernatants were then discarded and cells were re-suspended in 5 μL annexin V-FITC (Sigma Aldrich) along with 100 μL 1 × annexin V binding buffer (Sigma Aldrich). Samples were incubated for 15 min at room temperature in the dark and were then treated with 10 μL PI (50 μg/mL in 1 × annexin V binding buffer) along with an extra 400 μL annexin V binding buffer and were incubated in the dark at (4 °C) for 10 min. Samples were analysed using a Beckman Coulter FC-500 flow cytometer and data were analysed using Kaluza 1.3 software.

5.5.13. Statistical analysis

All experiments were performed at least three times and data are expressed as mean ± standard deviation. The significance of the results was evaluated by Student's t-test. The difference between two groups was considered statistically significant for $p < 0.05$, and very significant for $p < 0.01$.

5.6. REFERENCES

1. R. Cheng, F. Meng, C. Deng and Z. Zhong, *Nano Today*, 2015, **10**, 656-670.
2. D. Peer, J. M. Karp, S. Hong, O. C. Farokhzad, R. Margalit and R. Langer, *Natre Nanotechnology*, 2007, **2**, 751-760.
3. J. Hrkach, D. Von Hoff, M. M. Ali, E. Andrianova, J. Auer, T. Campbell, D. De Witt, M. Figa, M. Figueiredo, A. Horhota, S. Low, K. McDonnell, E. Peeke, B. Retnarajan, A. Sabnis, E. Schnipper, J. J. Song, Y. H. Song, J. Summa, D. Tompsett, G. Troiano, T. Van Geen Hoven, J. Wright, P. LoRusso, P. W. Kantoff, N. H. Bander, C. Sweeney, O. C. Farokhzad, R. Langer and S. Zale, *Science Translational Medicine*, 2012, **4**, 128ra139-128ra139.
4. S. Eliasof, D. Lazarus, C. G. Peters, R. I. Case, R. O. Cole, J. Hwang, T. Schluep, J. Chao, J. Lin, Y. Yen, H. Han, D. T. Wiley, J. E. Zuckerman and M. E. Davis, *Proceedings of the National Academy of Sciences*, 2013, **110**, 15127-15132.
5. H. Cabral and K. Kataoka, *Journal of Controlled Release*, 2014, **190**, 465-476.
6. C. Deng, Y. Jiang, R. Cheng, F. Meng and Z. Zhong, *Nano Today*, 2012, **7**, 467-480.
7. R. K. Jain and T. Stylianopoulos, *Nature Reviews Clinical Oncology*, 2010, **7**, 653-664.

8. T. Lammers, F. Kiessling, W. E. Hennink and G. Storm, *Journal of Controlled Release*, 2012, **161**, 175-187.

9. M. Talelli, M. Barz, C. J. F. Rijcken, F. Kiessling, W. E. Hennink and T. Lammers, *Nano Today*, 2015, **10**, 93-117.

10. E. Fleige, M. A. Quadir and R. Haag, *Advanced Drug Delivery Reviews*, 2012, **64**, 866-884.

11. Z. Ge and S. Liu, *Chemical Society Reviews*, 2013, **42**, 7289-7325.

12. C. S. Kim, B. Duncan, B. Creran and V. M. Rotello, *Nano Today*, 2013, **8**, 439-447.

13. J.-O. You, D. Almeda, G. J. Ye and D. T. Auguste, *Journal of Biological Engineering*, 2010, **4**, 1-13.

14. S. Mura, J. Nicolas and P. Couvreur, *Nature Materials*, 2013, **12**, 991-1003.

15. Q. Yin, J. Shen, Z. Zhang, H. Yu and Y. Li, *Advanced Drug Delivery Reviews*, 2013, **65**, 1699-1715.

16. A. Jhaveri, P. Deshpande and V. Torchilin, *Journal of Controlled Release*, 2014, **190**, 352-370.

17. G. H. Gao, M. J. Park, Y. Li, G. H. Im, J. H. Kim, H. N. Kim, J. W. Lee, P. Jeon, O. Y. Bang, J. H. Lee and D. S. Lee, *Biomaterials*, 2012, **33**, 9157-9164.

18. T. Suma, K. Miyata, Y. Anraku, S. Watanabe, R. J. Christie, H. Takemoto, M. Shioyama, N. Gouda, T. Ishii, N. Nishiyama and K. Kataoka, *ACS Nano*, 2012, **6**, 6693-6705.

19. J. H. Ryu, R. T. Chacko, S. Jiwpanich, S. Bickerton, R. P. Babu and S. Thayumanavan, *Journal of the American Chemical Society*, 2010, **132**, 17227-17235.

20. Y. Lili, M. Ruihua, L. Li, L. Fei, Y. Lin and S. Li, *International Journal of Pharmaceutics*, 2016, **498**, 195-204.

21. F. Q. Schafer and G. R. Buettner, *Free Radical Biology & Medicine*, 2001, **30**, 1191-1212.

22. J. Li, M. Huo, J. Wang, J. Zhou, J. M. Mohammad, Y. Zhang, Q. Zhu, A. Y. Waddad and Q. Zhang, *Biomaterials*, 2012, **33**, 2310-2320.

23. J. M. Estrela, A. Ortega and E. Obrador, *Critical Reviews in Clinical Laboratory Sciences*, 2006, **43**, 143-181.

24. A. Acharya, I. Das, D. Chandhok and T. Saha, *Oxidative Medicine and Cellular Longevity*, 2010, **3**, 23-34.

25. G. K. Balendiran, R. Dabur and D. Fraser, *Cell Biochemistry and Function*, 2004, **22**, 343-352.

26. N. Ballatori, S. M. Krance, S. Notenboom, S. Shi, K. Tieu and C. L. Hammond, *Biological chemistry*, 2009, **390**, 191-214.

27. L. Flohé, *Biochimica et Biophysica Acta: General Subjects*, 2013, **1830**, 3139-3142.

28. D. Roy, J. N. Cambre and B. S. Sumerlin, *Progress in Polymer Science*, 2010, **35**, 278-301.

29. J. Ding, J. Chen, D. Li, C. Xiao, J. Zhang, C. He, X. Zhuang and X. Chen, *Journal of Materials Chemistry B*, 2013, **1**, 69-81.

30. P. Xu, H. Yu, Z. Zhang, Q. Meng, H. Sun, X. Chen, Q. Yin and Y. Li, *Biomaterials*, 2014, **35**, 7574-7587.

31. H.-C. Yen, H. Cabral, P. Mi, K. Toh, Y. Matsumoto, X. Liu, H. Koori, A. Kim, K. Miyazaki, Y. Miura, N. Nishiyama and K. Kataoka, *ACS Nano*, 2014, **8**, 11591-11602.

32. Y. Lu and K. Park, *International Journal of Pharmaceutics*, 2013, **453**, 198-214.

33. F. Q. Hu, G. F. Ren, H. Yuan, Y. Z. Du and S. Zeng, *Colloids and Surfaces B: Biointerfaces*, 2006, **50**, 97-103.

34. L. Zhang, K. Katapodi, T. P. Davis, C. Barner-Kowollik and M. H. Stenzel, *Journal of Polymer Science Part A: Polymer Chemistry*, 2006, **44**, 2177-2194.

35. S. Cajot, N. Lautram, C. Passirani and C. Jérôme, *Journal of Controlled Release*, 2011, **152**, 30-36.

36. K. Zhang, H. Fang, Z. Wang, J.-S. A. Taylor and K. L. Wooley, *Biomaterials*, 2009, **30**, 968-977.

37. K. Zhang, H. Fang, Z. Wang, J. S. A. Taylor and K. L. Wooley, *Biomaterials*, 2009, **30**, 968-977.

38. S.-Y. Lee, S. Kim, J. Y. Tyler, K. Park and J.-X. Cheng, *Biomaterials*, 2013, **34**, 552-561.

39. H. S. Han, T. Thambi, K. Y. Choi, S. Son, H. Ko, M. C. Lee, D.-G. Jo, Y. S. Chae, Y. M. Kang, J. Y. Lee and J. H. Park, *Biomacromolecules*, 2015, **16**, 447-456.

40. H. Wang, L. Tang, C. Tu, Z. Song, Q. Yin, L. Yin, Z. Zhang and J. Cheng, *Biomacromolecules*, 2013, **14**, 3706-3712.

41. Z. Yang, S. Zheng, W. J. Harrison, J. Harder, X. Wen, J. G. Gelovani, A. Qiao and C. Li, *Biomacromolecules*, 2007, **8**, 3422-3428.

42. H. Sun, F. Meng, R. Cheng, C. Deng and Z. Zhong, *Antioxidants & Redox Signaling*, 2014, **21**, 755-767.

43. C. Wei, J. Guo and C. Wang, *Macromolecular Rapid Communications*, 2011, **32**, 451-455.

44. R. Wei, L. Cheng, M. Zheng, R. Cheng, F. Meng, C. Deng and Z. Zhong, *Biomacromolecules*, 2012, **13**, 2429-2438.

45. S. Matsumoto, R. J. Christie, N. Nishiyama, K. Miyata, A. Ishii, M. Oba, H. Koyama, Y. Yamasaki and K. Kataoka, *Biomacromolecules*, 2009, **10**, 119-127.

46. X. Jiang, S. Liu and R. Narain, *Langmuir*, 2009, **25**, 13344-13350.

47. Z. Zhang, L. Yin, C. Tu, Z. Song, Y. Zhang, Y. Xu, R. Tong, Q. Zhou, J. Ren and J. Cheng, *ACS Macro Letters*, 2013, **2**, 40-44.

48. W. C. Shen and H. J. Ryser, *Proceedings of the National Academy of Sciences of the United States of America*, 1978, **75**, 1872-1876.

49. E. Kundahl, R. Richman and R. A. Flickinger, *Journal of Cellular Physiology*, 1981, **108**, 291-298.

50. A. E. Gad, M. Bental, G. Elyashiv, H. Weinberg and S. Nir, *Biochemistry*, 1985, **24**, 6277-6282.

51. H. Seyednejad, A. H. Ghassemi, C. F. van Nostrum, T. Vermonden and W. E. Hennink, *Journal of Controlled Release*, 2011, **152**, 168-176.

52. S. K. Sahoo and V. Labhasetwar, *Drug Discovery Today*, 2003, **8**, 1112-1120.

53. N. Saito, N. Murakami, J. Takahashi, H. Horiuchi, H. Ota, H. Kato, T. Okada, K. Nozaki and K. Takaoka, *Advanced Drug Delivery Reviews*, 2005, **57**, 1037-1048.

54. L. Buttafoco, N. P. Boks, P. Engbers-Buijtenhuijs, D. W. Grijpma, A. A. Poot, P. J. Dijkstra, I. Vermes and J. Feijen, *Journal of Biomedical Materials Research Part B: Applied Biomaterials*, 2006, **79B**, 425-434.

55. S.-H. Hyon, K. Jamshidi and Y. Ikada, *Biomaterials*, 1997, **18**, 1503-1508.

56. R. J. Pounder and A. P. Dove, *Polymer Chemistry*, 2010, **1**, 260-271.

57. Y. Chen, W. Zhang, J. Gu, Q. Ren, Z. Fan, W. Zhong, X. Fang and X. Sha, *International Journal of Pharmaceutics*, 2013, **452**, 421-433.

58. G. Caldwell, M. G. Meirim, D. D. N'da and E. W. Neuse, *Journal of Applied Polymer Science*, 2006, **100**, 3415-3424.

59. Y. Huang, J. Liu, Y. Cui, H. Li, Y. Sun, Y. Fan and X. Zhang, *BioMed Research International*, 2014, **2014,** 1-11.

60. Y. Chen, X. Sha, W. Zhang, W. Zhong, Z. Fan, Q. Ren, L. Chen and X. Fang, *International Journal of Nanomedicine*, 2013, **8**, 1463-1476.

61. Y. Zhang, T. Jin and R. X. Zhuo, *Colloids and Surfaces B: Biointerfaces*, 2005, **44**, 104-109.

62. B. Kumar, J. G. Meher, A. Gupta, V. K. Pawar, Y. Singh and M. K. Chourasia, *Journal of Biomaterials and Tissue Engineering*, 2014, **4**, 700-709.

63. G. Yousefi, S. M. Foroutan, A. Zarghi and A. Shafaati, *Chemical and Pharmaceutical Bulletin*, 2010, **58**, 147-153.

64. R. Zhao, N. Diop-Bove, M. Visentin and I. D. Goldman, *Annual Review of Nutrition*, 2011, **31**, 10.1146/annurev-nutr-072610-145133.

65. F. M. Balis, J. Mirro, Jr., G. H. Reaman, W. E. Evans, C. McCully, K. M. Doherty, R. F. Murphy, S. Jeffries and D. G. Poplack, *Journal of Clinical Oncology*, 1988, **6**, 1882-1886.

66. H. Tian and B. N. Cronstein, *Bulletin of the NYU Hospital for Joint Diseases*, 2007, **65**, 168-173.

67. A. Rozin, D. Schapira, A. Balbir-Gurman, Y. Braun-Moscovici, D. Markovits, D. Militianu and M. A. Nahir, *Annals of the Rheumatic Diseases*, 2002, **61**, 756-757.

68. J. Wegrzyn, P. Adeleine and P. Miossec, *Annals of the Rheumatic Diseases*, 2004, **63**, 1232-1234.

69. S. Cajot, P. Lecomte, C. Jerome and R. Riva, *Polymer Chemistry*, 2013, **4**, 1025-1037.

70. K. L. Robertson and J. L. Liu, *Wiley Interdisciplinary Reviews: Nanomedicine and Nanobiotechnology*, 2012, **4**, 511-524.

71. O. Gladkovskaya, V. A. Gerard, M. Nosov, Y. K. Gun'ko, G. M. O'Connor and Y. Rochev, *RSC Advances*, 2015, **5**, 42250-42258.

72. X. Zhao, Z. Poon, A. C. Engler, D. K. Bonner and P. T. Hammond, *Biomacromolecules*, 2012, **13**, 1315-1322.

73. X. Ke, V. W. L. Ng, R. J. Ono, J. M. W. Chan, S. Krishnamurthy, Y. Wang, J. L. Hedrick and Y. Y. Yang, *Journal of Controlled Release*, 2014, **193**, 9-26.

74. C. Allen, D. Maysinger and A. Eisenberg, *Colloids and Surfaces B: Biointerfaces*, 1999, **16**, 3-27.

75. J. Gou, S. Feng, H. Xu, G. Fang, Y. Chao, Y. Zhang, H. Xu and X. Tang, *Biomacromolecules*, 2015, **16**, 2920-2929.

76. C. Ma, P. Pan, G. Shan, Y. Bao, M. Fujita and M. Maeda, *Langmuir*, 2015, **31**, 1527-1536.

77. T. Niwa, H. Takeuchi, T. Hino, N. Kunou and Y. Kawashima, *Journal of Controlled Release*, 1993, **25**, 89-98.

78. S. Y. Kim, I. L. G. Shin, Y. M. Lee, C. S. Cho and Y. K. Sung, *Journal of Controlled Release*, 1998, **51**, 13-22.

79. P. Jarrett, C. V. Benedict, J. P. Bell, J. A. Cameron and S. J. Huang, in *Polymers as Biomaterials*, eds. S. W. Shalaby, A. S. Hoffman, B. D. Ratner and T. A. Horbett, Springer US, Boston, MA, 1984, DOI: 10.1007/978-1-4613-2433-1_13, pp. 181-192.

80. Y. Teng, M. E. Morrison, P. Munk, S. E. Webber and K. Procházka, *Macromolecules*, 1998, **31**, 3578-3587.

81. W.-C. Sun, K. R. Gee, D. H. Klaubert and R. P. Haugland, *The Journal of Organic Chemistry*, 1997, **62**, 6469-6475.

82. Y. Matsumura and H. Maeda, *Cancer Research*, 1986, **46**, 6387-6392.

83. V. P. Chauhan and R. K. Jain, *Nature Materials*, 2013, **12**, 958-962.

84. S. Wilhelm, A. J. Tavares, Q. Dai, S. Ohta, J. Audet, H. F. Dvorak and W. C. W. Chan, *Nature Reviews Materials*, 2016, **1**, 16014.

85. S. V. Vinogradov, T. K. Bronich and A. V. Kabanov, *Advanced Drug Delivery Reviews*, 2002, **54**, 135-147.

86. L. Ilium, S. S. Davis, C. G. Wilson, N. W. Thomas, M. Frier and J. G. Hardy, *International Journal of Pharmaceutics*, 1982, **12**, 135-146.

87. T.-G. Iversen, T. Skotland and K. Sandvig, *Nano Today*, 2011, **6**, 176-185.

88. K. Miyata, N. Nishiyama and K. Kataoka, *Chemical Society Reviews*, 2012, **41**, 2562-2574.

89. M. Elsabahy and K. L. Wooley, *Chemical Society Reviews*, 2012, **41**, 2545-2561.

90. J. C. Stockert, A. Blazquez-Castro, M. Canete, R. W. Horobin and A. Villanueva, *Acta Histochemica*, 2012, **114**, 785-796.

91. J. van Meerloo, G. J. Kaspers and J. Cloos, *Methods in Molecular Biology (Clifton, N.J.)*, 2011, **731**, 237-245.

92. S. N. Syed Abdul Rahman, N. Abdul Wahab and S. N. Abd Malek, *Evidence-Based Complementary and Alternative Medicine*, 2013, **2013**, 14.

93. S. Rello, J. C. Stockert, V. Moreno, A. Gámez, M. Pacheco, A. Juarranz, M. Cañete and A. Villanueva, *Apoptosis*, 2005, **10**, 201-208.

94. M. van Engeland, L. J. Nieland, F. C. Ramaekers, B. Schutte and C. P. Reutelingsperger, *Cytometry*, 1998, **31**, 1-9.

95. G. Koopman, C. P. Reutelingsperger, G. A. Kuijten, R. M. Keehnen, S. T. Pals and M. H. van Oers, *Blood*, 1994, **84**, 1415-1420.

96. G. Zhang, V. Gurtu, S. R. Kain and G. Yan, *BioTechniques*, 1997, **23**, 525-531.

97. J.-M. Oh, M. Park, S.-T. Kim, J.-Y. Jung, Y.-G. Kang and J.-H. Choy, *Journal of Physics and Chemistry of Solids*, 2006, **67**, 1024-1027.

98. L. H. Matherly and Z. Hou, *Vitamins and Hormones*, 2008, **79**, 145-184.

99. R. Zhao, N. Diop-Bove and I. D. Goldman, *Molecular Pharmacology*, 2014, **85**, 310-321.

100. L. H. Matherly, in *Progress in Nucleic Acid Research and Molecular Biology*, Academic Press, 2001, vol. 67, pp. 131-162.

101. E. E. Sierra, K. E. Brigle, M. J. Spinella and I. D. Goldman, *Biochemical Pharmacology*, 1995, **50**, 1287-1294.

102. A. Hamid, M. Kiran, S. Rana and J. Kaur, *IUBMB Life*, 2009, **61**, 236-243.

103. Y. Huang, J. Liu, Y. Cui, H. Li, Y. Sun, Y. Fan and X. Zhang, *BioMed Research International*, 2014, **2014**, 11.

104. D. R. Nogueira, L. Tavano, M. Mitjans, L. Perez, M. R. Infante and M. P. Vinardell, *Biomaterials*, 2013, **34**, 2758-2772.

105. H. Gao and K. Matyjaszewski, *Macromolecules*, 2006, **39**, 4960-4965.

Chapter 6: MTX-CONJUGATED MICELLES FOR RECEPTOR MEDIATED ENHANCED CELLULAR UPTAKE AND ANTITUMOR ACTIVITY

6.1. INTRODUCTION

Cancer is one of the most overwhelming ailments, with over 14 million new cases ever year,worlwide.[1] However, with the use of advanced technologies and due to the better understanding of the cancer biology, improved diagnostics and therapy, mortality rate has decreased over the last decade. Surgery, radiation and chemotherapy are the existing cancer treatments, however, these techniques pose certain risks and serious side effects. In case of conventional anticancer chemotherapeutics, they can accumulate non-selectively in the body affecting both normal and cancer cells.[2] Therefore, it is desirable to construct therapeutics that exclusively target the tumour site or cancer cells.

To overcome these limitations, targeted drug delivery systems using nano-carriers has been developed.[3] These nano-carriers generally rely on passive targeting, with the aim of exploiting the enhanced permeability and retention (EPR) effect present in certain tumour tissues.[4] Although passive drug targeting routes using nano-carriers offer certain advantages over conventional drugs, they also suffer from several drawbacks.[5] In addition, nano-carrier based passive targeting is not inherently selective to tumour tissues as administered nano-carriers have been reported to accumulate in organs including the liver, lungs and spleen, resulting in non-specific toxicities.[6] Therefore more selective targeting is required to achieve a

better therapeutic effect and to avoid undesirable side effects while treating these malignancies.

To overcome these drawbacks, active drug targeting has been proposed in which nano-carriers are functionalised to enhance their affinity for target cells.[7-9] The active targeting may be attained by grafting specific agents (e.g. antibodies, ligands, nucleic acids and peptides) to the surface of nanocarriers.[10] These targeting agents can selectively bind to specific receptors overexpressed on the surface of cancer cells.[11] Examples of these overexpressed recognition sites include the folate receptor,[12] transferrin receptor,[13] and epidermal growth factor receptor, etc.[14,15] For example, antibodies attached to the surface of drug loaded nano-carriers have shown enhanced accumulation of drugs in certain tumour cells resulting in better anti-tumour activity.[16-19] However, high production cost, low reproducibility and compatibility of antibodies with several drugs and undesirable interactions with immune system components can limit their applications.[20-22]

An alternative route frequently investigated for drug targeting is the folate receptor (FR), which is a glycosylphosphatidylinositol-anchored glycoprotein.[23] The FR has been reported to overexpress on the surface of a variety of tumour cells including breast, ovarian, kidney and endometrial cancers.[24-28] In contrast, FRs are rarely overexpressed in normal cells, with the exceptions of the placenta and to a lesser extent on thyroid and kidney

cells.[29] The existence of high levels of folate receptor in several human cancers renders these as a good targets for selective drug delivery to these disorders. The corresponding ligand for folate receptors is folic acid (usually in its ionised folate salt form) and has extensively been studied for its targeting ability to deliver therapeutic molecules to the tumour cells. The low immunogenicity, good stability, low molecular weight, and high binding affinity of folic acid at folate receptors are certain advantages of folic acid over other types of target ligands.[23, 30] Moreover, the good compatibility of folic acid with several solvents provides an opportunity for further modification and ease in organic synthesis.[31]

To exploit folate receptors for enhanced cellular uptake and better antitumor activity, various drug-loaded nano-carriers functionalised with folic acid have been developed.[31-33] For instance, folic acid conjugated liposomes have shown better uptake in KB oral carcinoma cells and the same liposomes loaded with paclitaxel induced 3.8-fold higher cytotoxicity as compared to the paclitaxel loaded control liposome without folic acid.[34] In another approach, folic acid was conjugated to PEG–phosphatidylethanolamine and was subsequently used to modify the surface of doxorubicin loaded PLGA nanoparticles.[33] The *in vivo* experiments in mice bearing human nasopharyngeal carcinoma KB cells demonstrated that FA–PEG–PE-modified doxorubicin loaded PLGA nanoparticles exhibited greater antitumor activity than non-modified counterparts.

In this work, we synthesised a multifunctional amphiphilic block copolymer based on α-amino-PEG-*b*-poly(εCL-*co*-αN_3εCL) for folate receptor mediated active targeting of tumour cells. Methotrexate (MTX) was conjugated on the hydrophilic block by reacting amine group of PEG with the γ carboxylic acid of the MTX. The synthesised polymers were characterised by ^{1}H NMR, FT-IR, and size exclusion chromatography (SEC). Micelles of multifunctional block copolymers were prepared using a dialysis method. Furthermore, an alkyne bearing fluorescent probe (FITC-alkyne) was grafted on the hydrophobic backbone via CuAAC. The size distributions and morphology of multifunctional micelles were assessed using dynamic light scattering (DLS) and transmission electron microscopy. Cellular uptake studies of MTX-conjugated-FITC-functionalised micelles were assessed in human breast cancer cells (MCF7 cells). The cytotoxicities of multifunctional micelles were assessed using MTT assays and apoptosis inducing potentials of MTX conjugated multifunctional micelles were analysed using annexin-V/PI assays. As MTX is structurally analogous to the folic acid, the working hypothesis was that by conjugating the MTX on the hydrophilic PEG of amphiphilic block copolymer, it would not only provide active and passive targeting opportunities but would also deliver an anticancer drug to cancer cells.

6.2. RESULTS

6.2.1. Synthesis and characterisation of multifunctional block copolymers

To conjugate MTX on the hydrophilic block of copolymers, we synthesised a multifunctional block copolymer based on α-amine-PEG-*b*-poly(εCL-*co*-αN_3εCL) via ring opening polymerisation using stannous octoate as a catalyst. For this purpose, hetero-functional PEG (α-azide-ω-hydroxyl PEG) was used as an initiator. The α-azide-ω-hydroxyl PEG was synthesised from commercially available PEG_{4000} in two steps as shown in scheme 6-1. First, a highly reactive intermediate i.e. α-tosyl-ω-hydroxyl PEG (PEG-OTs) was obtained by reacting equimolar amounts of PEG with *p*-toluenesulfonyl chloride. The chemical shift at 2.46 ppm in the ^{1}H NMR spectrum of PEG-OTs in deuterated chloroform (figure 6-1A) corresponded to methyl protons of tosyl goroup, whereas, the chemical shift at 4.17 ppm represnts the methylene protons of PEG next to the tosyl group.

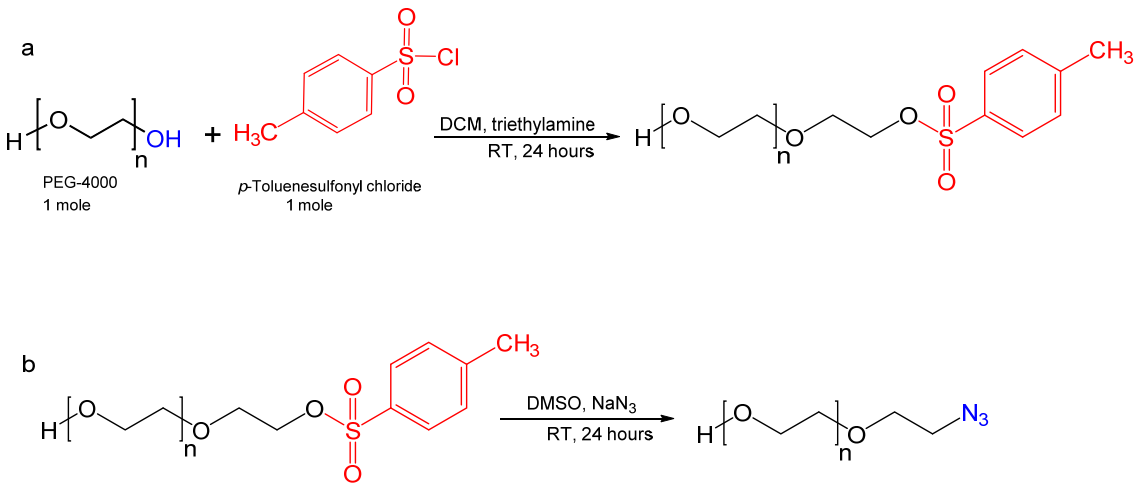

Scheme 6-1. Schematic representation for the synthesis of hetero-functional PEG. (a) α-tosyl-ω-hydroxyl PEG and (b) α-azide-ω-hydroxyl PEG.

The chemical shifts at 7.37 and 7.82 ppm corresponded to aromatic protons of tosyl group. These signals confirmed the synthesis of PEG-OTs. The monotosylation nature of the PEG-OTs was confirmed by performing ^{1}H NMR spectroscopy in the deuterated DMSO. The chemical shift corresponding to hydroxyl protons was observed at 4.57 ppm (a triplet. 1H, figure 6-1B), which was well separated from the PEG backbone peaks and did not broaden or shifted with the variation of the concentration showing quantitative conversion of PEG to PEG-OTs. In a second step, the tosyl group of the PEG-OTs was replaced with an azide group via nucleophilic substitution reaction using sodium azide to obtain α-azide-ω-hydroxyl PEG (PEG-N_3). The synthesis of PEG-N_3 was confirmed by ^{1}H NMR and FTIR sepectroscopy.

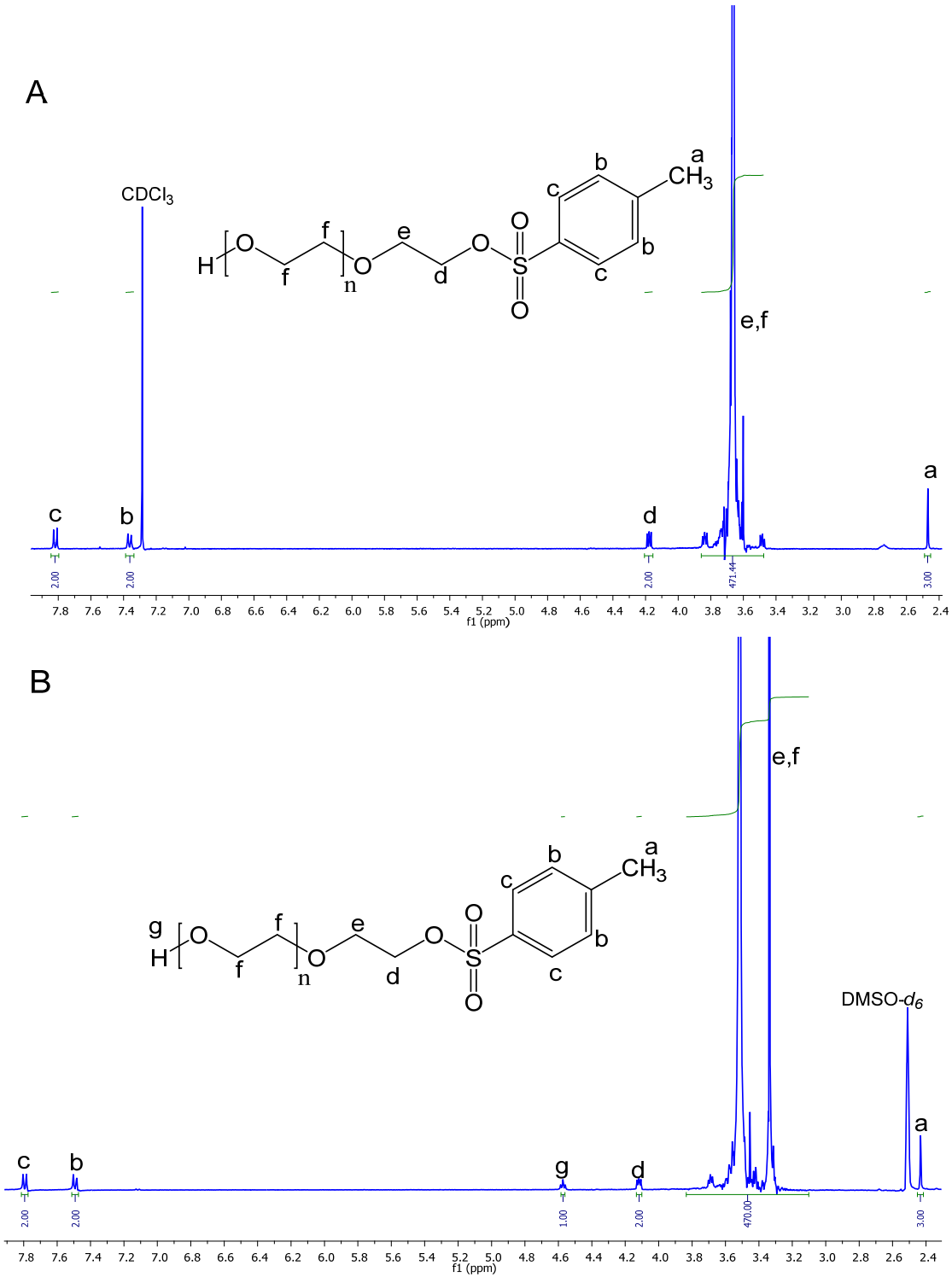

Figure 6-1. ^{1}H NMR spectrum of α-tosyl-ω-hydroxyl PEG (PEG-OTs) in (A) C*D*Cl$_3$ and (B) in DMSO-d_6).

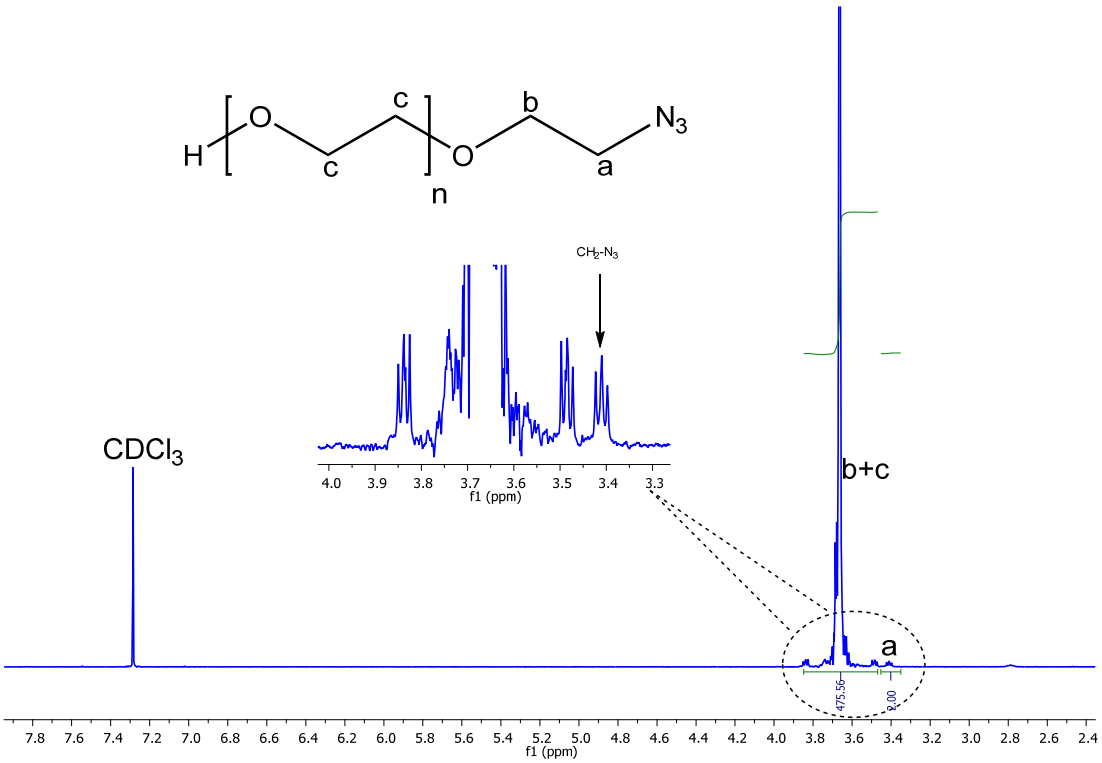

Figure 6-2. ^{1}H NMR spectrum of α-azide-ω-hydroxyl PEG (PEG-N_3).

The complete disappearance of protons corresponding to the tosyl group in ^{1}H NMR spectrum of PEG-N_3 (figure 6-2) and appearance of a new peak at 3.41 ppm (corresponding to methylene protons next to the azide group) confirmed the synthesis of PEG-N_3.

The synthesis of PEG-N_3 was further confirmed by FTIR spectroscopy. The appearance of a new infrared absorption peak at 2106 cm^{-1} in the FTIR spectrum of PEG-N_3 (figure 6-3) confirmed the incorporation of azide groups. The size exclusion chromatography showed unimodal peaks without shoulder indicating similar molar mass distributions of PEG, PEG-OTs, and PEG-N_3 without any apparent degradation as shown in figure 6-

4. The data were in good agreement with the previously reported results in the literature.[35,36]

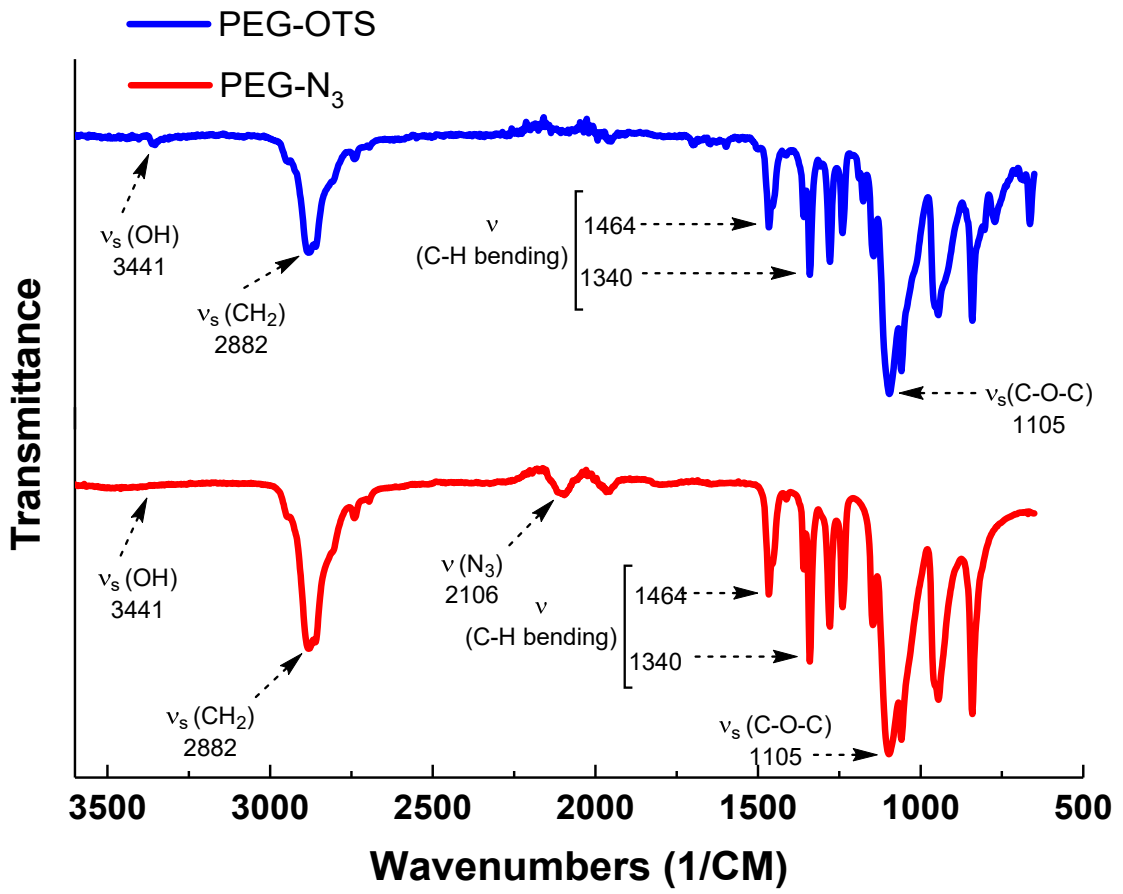

Figure 6-3. FT-IR characterisation of α-tosyl-ω-hydroxyl PEG (PEG-OTs) and α-azide-ω-hydroxyl PEG (PEG-N_3).

The α-azido-ω-hydroxyl PEG (PEG-N_3) was used as an initiator for ring opening polymerisation of εCL and αClεCL using tin octoate as a catalyst to obtain copolymer of α-azido-PEG-*b*-poly(εCL-*co*-αClεCL) (scheme 6-2).

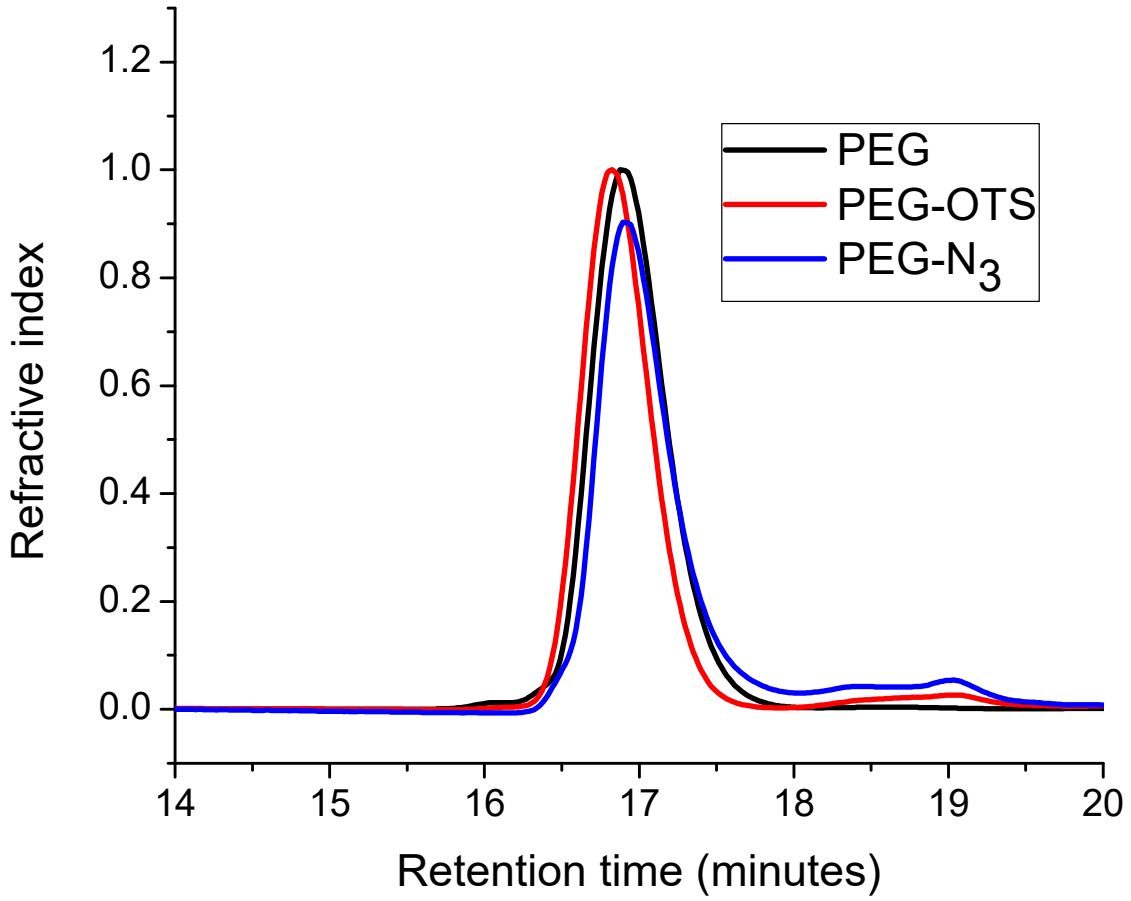

Figure 6-4. SEC traces of PEG, α-tosyl-ω-hydroxyl PEG (PEG-OTs) and α-azide-ω-hydroxyl PEG (PEG-N_3) in THF.

The synthesised block copolymers were purified by precipitation in diethyl ether to remove un-converted monomer and catalyst residues. ^{1}H NMR spectrum of α-azide-PEG-*b*-poly(εCL-*co*-αClεCL) is shown in figure 6-5. The disappearance of the monomer signals in ^{1}H NMR spectrum revealed the complete conversion of both monomers after 24 hours.

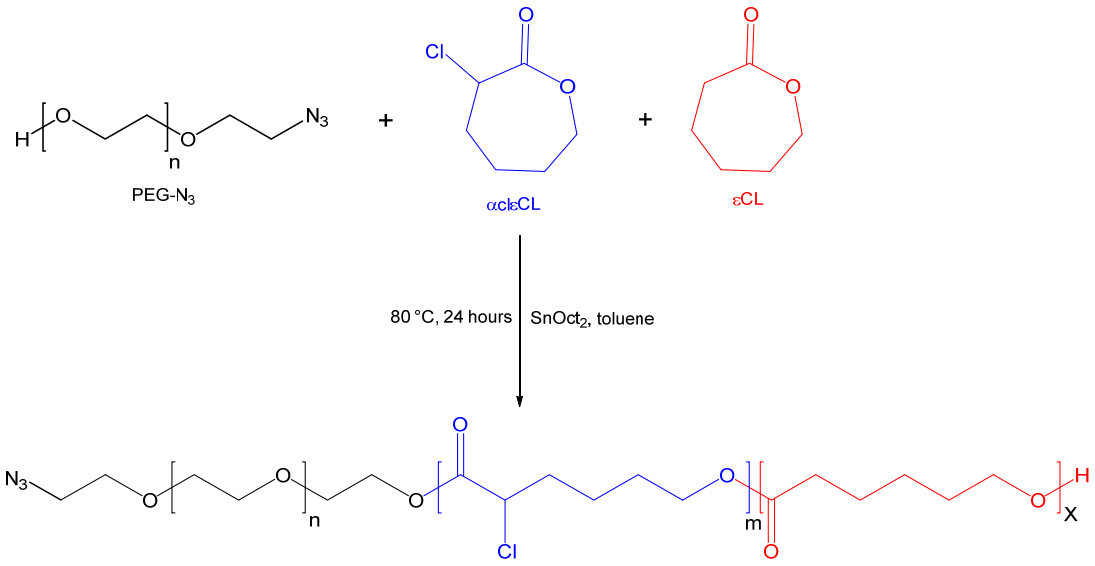

Scheme 6-2. Ring-opening polymerisation to synthesise α-azido-PEG-*b*-poly(εCL-*co*-αClεCL).

The molar mass of α-azide-PEG-*b*-poly(εCL-*co*-αClεCL) block copolymer was calculated by the comparison of the relative intensity of the proton of PCL at 2.33 ppm ($C\underline{H_2}$-C(O), peak "k", in figure 6-5) and relative intensity of the proton of poly(αClεCL) at 4.21 ppm (CO–CH(Cl)–CH_2–CH_2–CH_2–$C\underline{H_2}$–O–, peak "j") with the methylene protons next to azide group (3.41 ppm, peak "a") of PEG-N_3. The calculated molar mass (9810 g/mol) was in good agreement with theoretically calculated molar mass.

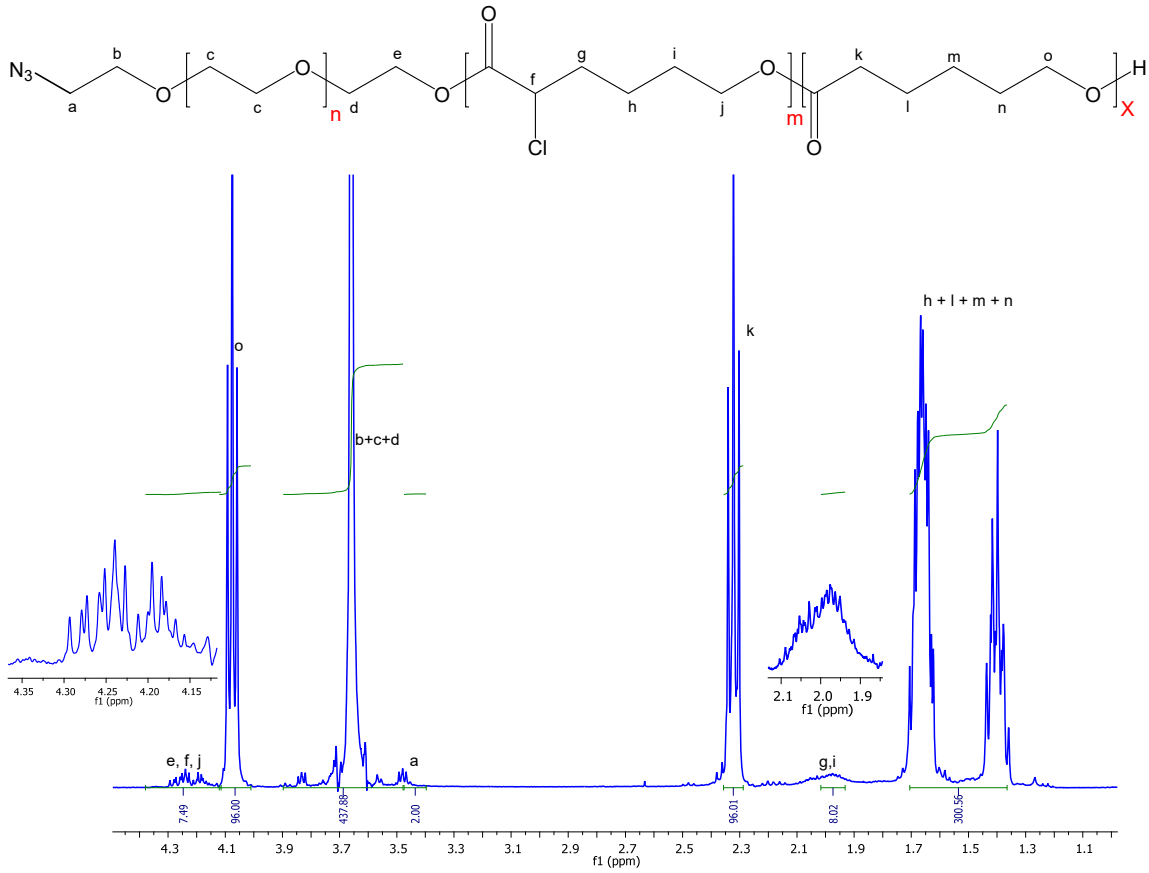

Figure 6-5. ^{1}H NMR spectrum of α-azido-PEG-*b*-poly(εCL-*co*-αClεCL) in C*D*Cl_3.

The SEC chromatography of α-azide-PEG-*b*-poly(εCL-*co*-αClεCL) block copolymers showed a unimodal peak (figure 6-6) and lower elution time as compared to the PEG-N_3, proving growing molar mass without apparent transesterification.

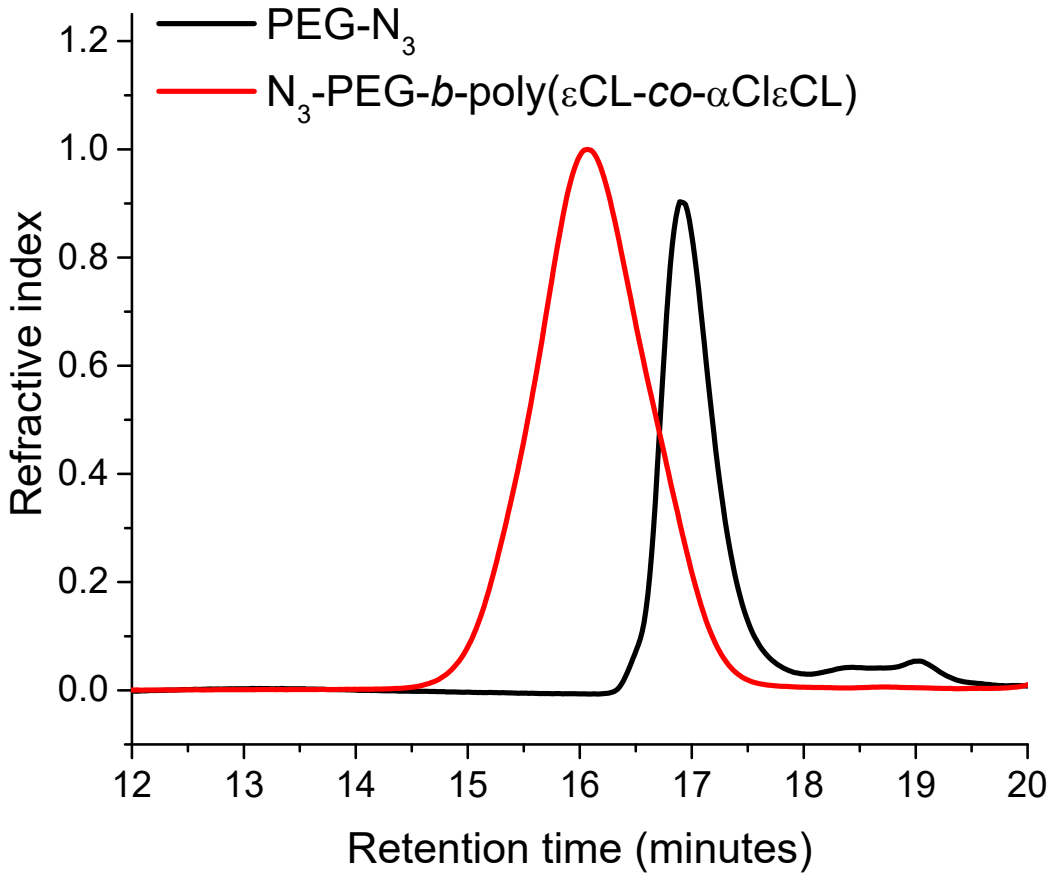

Figure 6-6. SEC traces of α-azido-PEG-*b*-poly(εCL-*co*-αClεCL) in THF.

After synthesis of α-azido-PEG-*b*-poly(εCL-*co*-αClεCL), the azide group of multifunctional block copolymer was reduced to the corresponding amine by reacting with triphenylphosphine as illustrated in scheme 6-3. The reaction was carried out in mild conditions at room temperature using mixed solvents of chloroform and methanol (1:1).

The absence of methylene protons next to the azide group in ^{1}H NMR spectrum (figure 6-7) and appearance of a new chemical shift at 2.85 ppm

(corresponding to methylene protons next to the amine group) confirmed the synthesis of α-amine-PEG-*b*-poly(εCL-*co*-αClεCL).

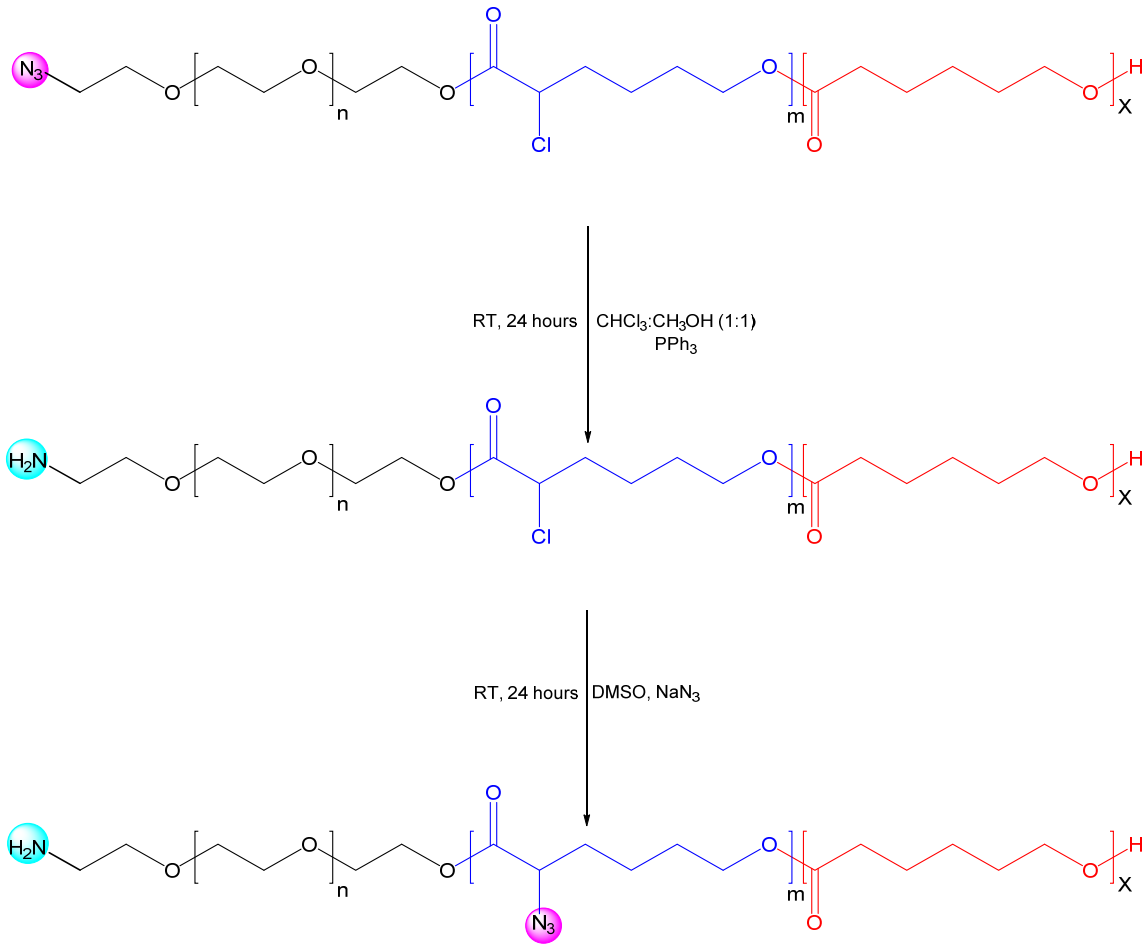

Scheme 6-3. Scheme for the synthesis of α-amino-PEG-*b*-poly(εCL-*co*-αClεCL) and α-amino-PEG-*b*-poly(εCL-*co*-αN_3εCL).

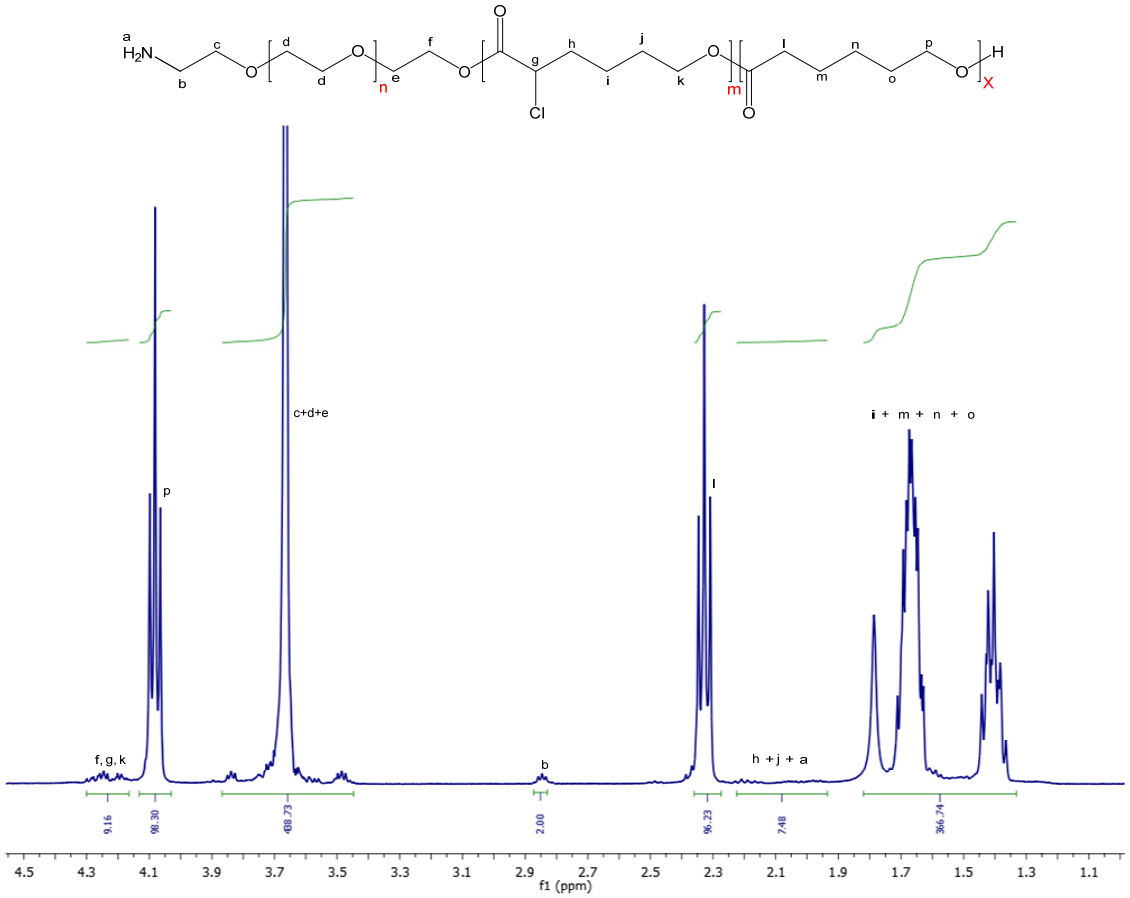

Figure 6-7. ^{1}H NMR spectrum of α-amino-PEG-*b*-poly(εCL-*co*-αClεCL) in C*D*Cl_3.

In the next step, chloro atoms of the hydrophobic backbone of multifunctional block copolymer were reacted with sodium azide. ^{1}H NMR spectroscopy of α-amino-PEG-*b*-poly(εCL-*co*-αN_3εCL) revealed the complete conversion of chloro atoms into azides. Specifically, the chemical shifts at 4.27 ppm for the C<u>H</u>-Cl protons in ^{1}H NMR spectrum completely disappeared in the favour of a new peak at 3.89 ppm, typical of C<u>H</u>-N_3 as shown in figure 6-8.

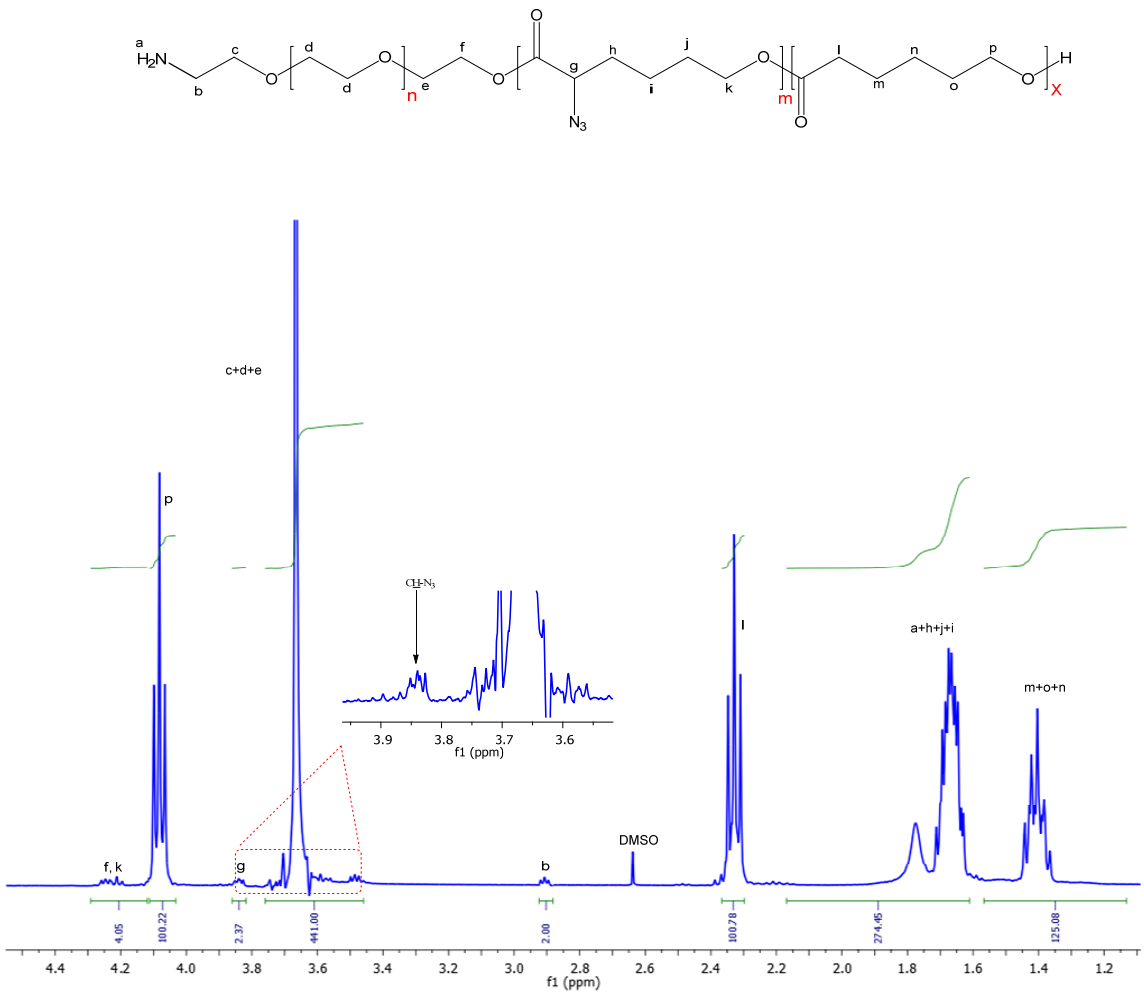

Figure 6-8. ^{1}H NMR spectrum of α-amino-PEG-*b*-poly(εCL-*co*-αN_3εCL) in C*D*Cl_3.

The substitution reaction was further confirmed by FTIR spectroscopy. The appearance of new infrared absorption peak at 2106 cm^{-1} in FTIR spectrum (figure 6-9) confirmed the substitution to an azide group.

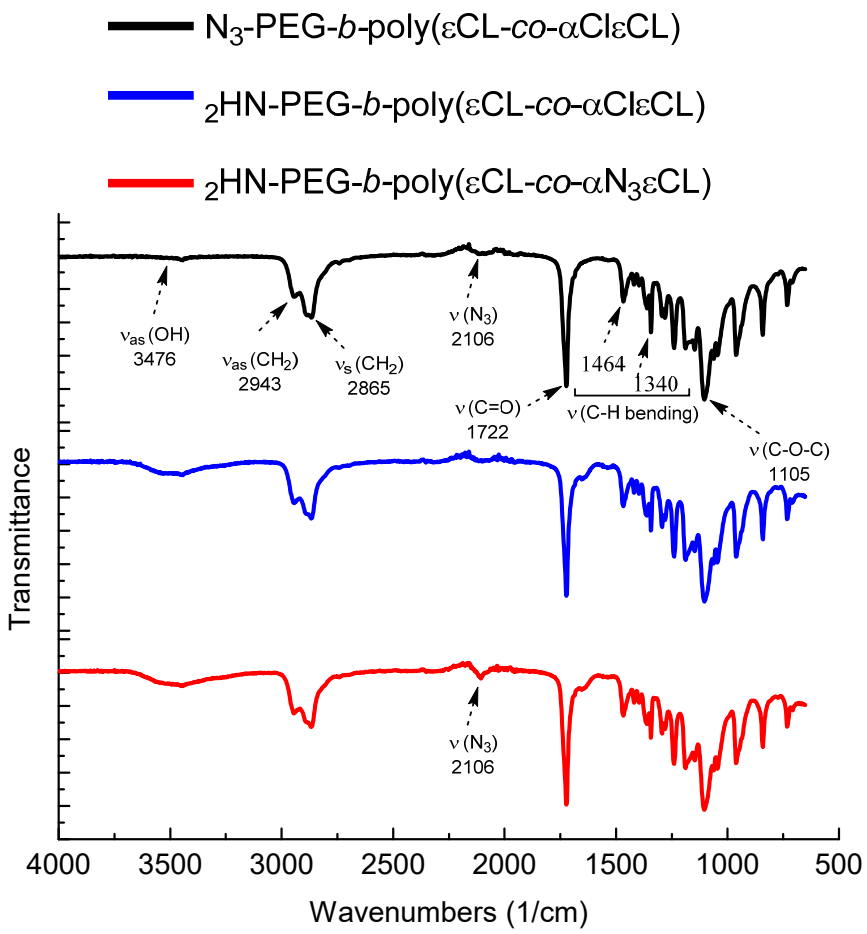

Figure 6-9. FT-IR spectra of (A) α-azide-PEG-*b*-poly(εCL-*co*-αClεCL), (B) α-amine-PEG-*b*-poly(εCL-*co*-αClεCL), and (C) α-amine-PEG-*b*-poly(εCL-*co*-αN_3εCL). IR absorption peaks at 2106 cm^{-1} represents the azide functionality.

6.2.2. Conjugation of MTX to hydrophilic block of multifunctional copolymer

MTX was conjugated to the PEG block of multifunctional copolymer by reacting the γ-carboxylic acid of MTX with the amine group of α-amine-PEG-*b*-poly(εCL-*co*-αN_3εCL) forming an amide bond as illustrated in scheme

6-4.

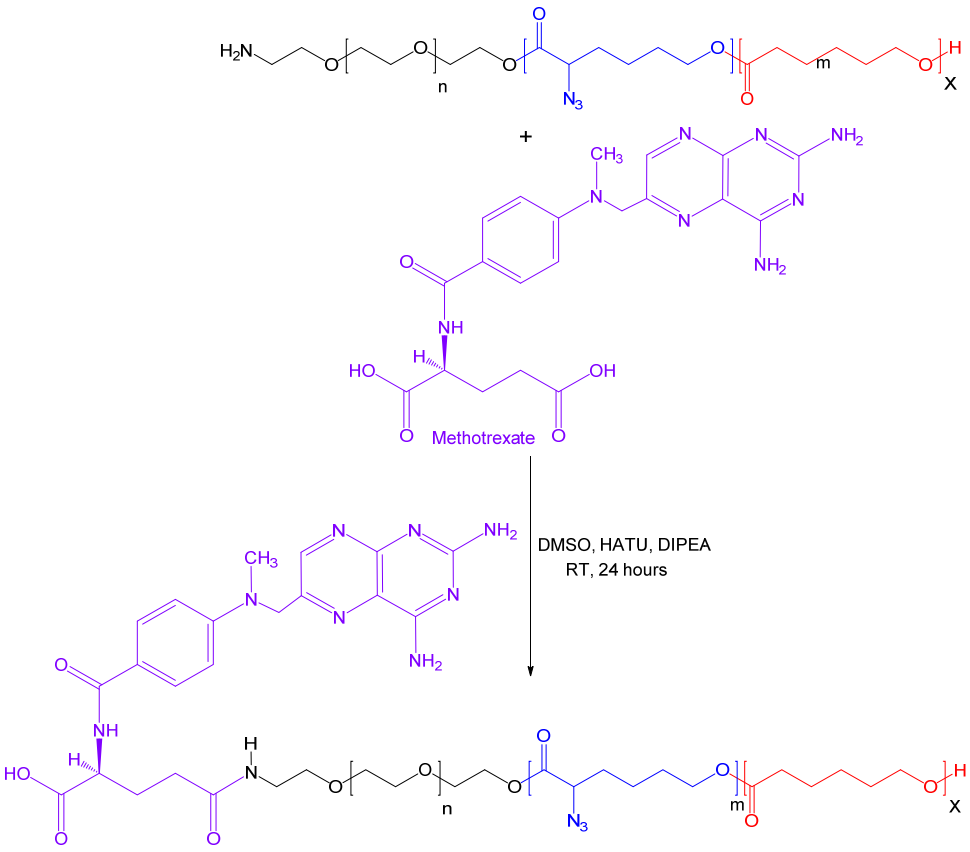

Scheme 6-4. Scheme for the conjugation of MTX to the hydrophilic block of multifunctional block copolymer.

The reaction was carried out under mild conditions at room temperature using DMSO as an organic solvent, HATU as carboxylic acid activating agent and *N,N*-diisopropylethylamine (DIPEA) as a catalyst. The unreacted MTX and other impurities were removed by aqueous dialysis and MTX conjugated block copolymer (MTX-PEG-*b*-poly(εCL-*co*-αN$_3$εCL) was recovered by freeze drying. The synthesis of MTX-PEG-*b*-poly(εCL-*co*-

αN$_3$εCL) block copolymer was confirmed by ^{1}H NMR (figure 6-10).

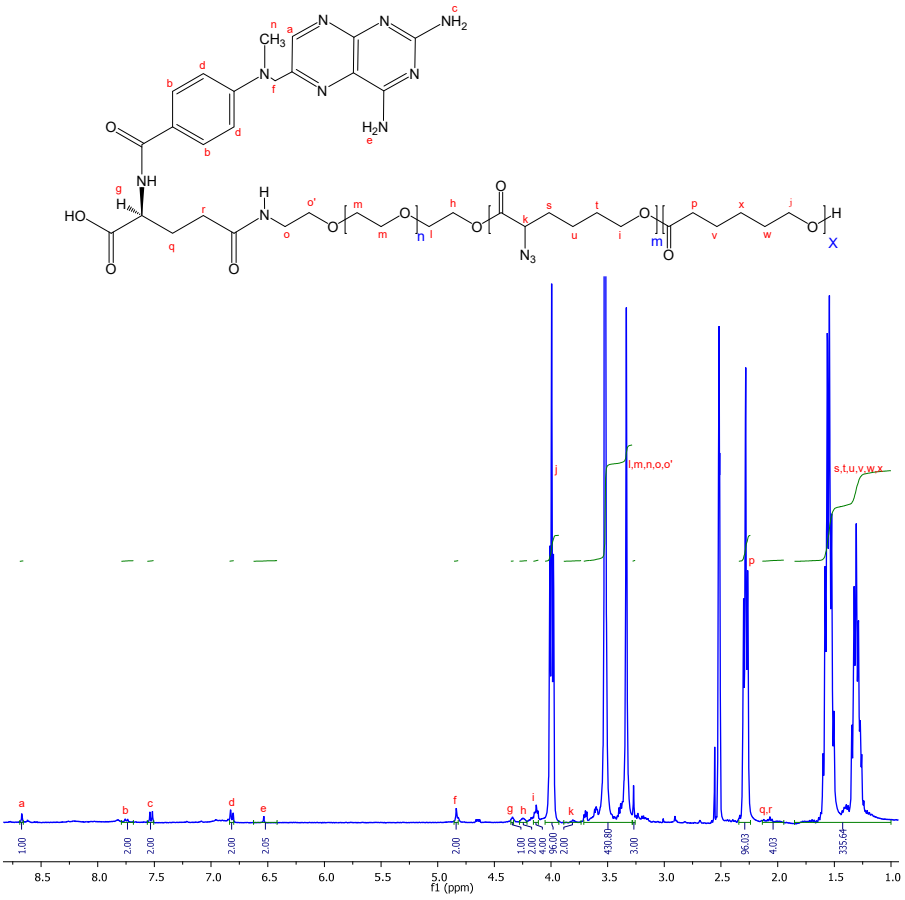

Figure 6-10. ^{1}H NMR spectrum of MTX-PEG-*b*-poly(εCL-*co*-αN$_3$εCL) in DMSO-d_6.

The ^{1}H NMR spectrum of MTX-PEG-*b*-poly(εCL-*co*-αN$_3$εCL) block copolymer clearly showed chemical shifts corresponding to MTX in addition to chemical shifts of block copolymer. The MTX contents and molecular weight of MTX-PEG-*b*-poly(εCL-*co*-αN$_3$εCL) were determined by the integration of aromatic proton signals at 8.6-6.7 ppm (corresponding to MTX) region of the

spectrum in relation to the methylene protons of PEG next to the amide bond.

6.2.3. Preparation of micelles and post-functionalisation with FITC-alkyne

Micellisation of α-amino-PEG-*b*-poly(εCL-*co*-αN_3εCL) and MTX-PEG-*b*-poly(εCL-*co*-αN_3εCL) block copolymers was performed by a dialysis method using DMSO as an organic solvent as described in chapter 4 (section 4-2.1). The size distributions of micelles were measured by DLS and morphologies were analysed using TEM. The micelles prepared from α-amino-PEG-*b*-poly(εCL-*co*-αN_3εCL) resulted into an average size of 73 ± 6 nm as revealed by DLS analysis (figure 6-11A, left image), whereas, MTX-PEG-*b*-poly(εCL-*co*-αN_3εCL) block copolymer showed an average size of 77 ± 9 nm by DLS (figure 6-11B, left image). The TEM investigations showed almost spherical morphologies of both type of micelles as shown in figure 6-11AB (right images).

The post functionalisation of micelles with FITC-alkyne was carried out via CuAAC as illustrated in scheme 6-5. The reaction was continued until the FTIR absorption peak at 2106 cm^{-1} (characteristic of the azide group) completely disappeared and a new absorption peak at 1660 cm^{-1} (corresponding to triazole unsaturation) observed (figure 6-12).

The DLS analysis of FITC functionalised micelles showed an average size of 88 ± 7 as shown in figure 6-13A with spherical morphologies as revealed by TEM investigations (figure 6-13B). Whereas, MTX-conjugated-FITC functionalised micelles showed an average sized of 96 ± 13 nm (measured by DLS, figure 6-13C) and spherical morphologies as shown in TEM image (figure 6-13D).

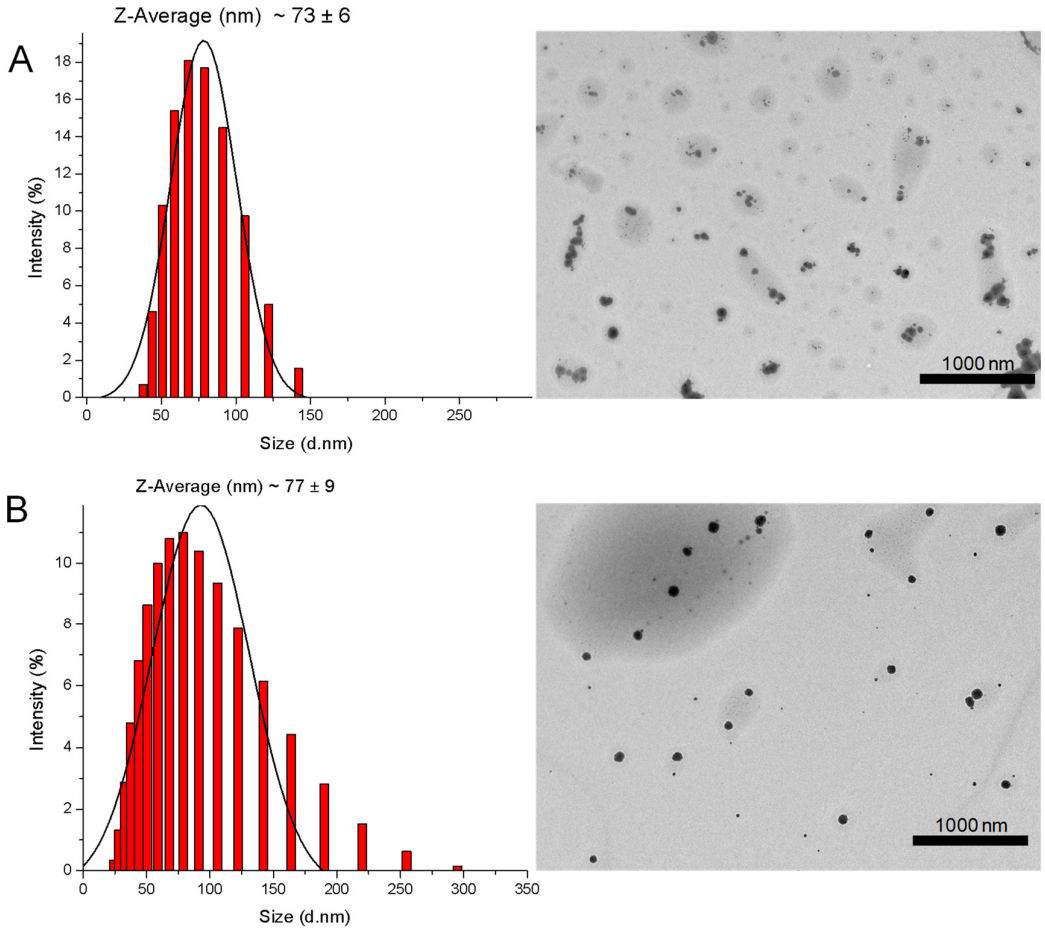

Figure 6-11. Size distributions by DLS (left images) and TEM micrographs (right images) of micelles prepared from (A) α-amino-PEG-*b*-poly(εCL-*co*-αN_3εCL), and (B) MTX-PEG-*b*-poly(εCL-*co*-αN_3εCL).

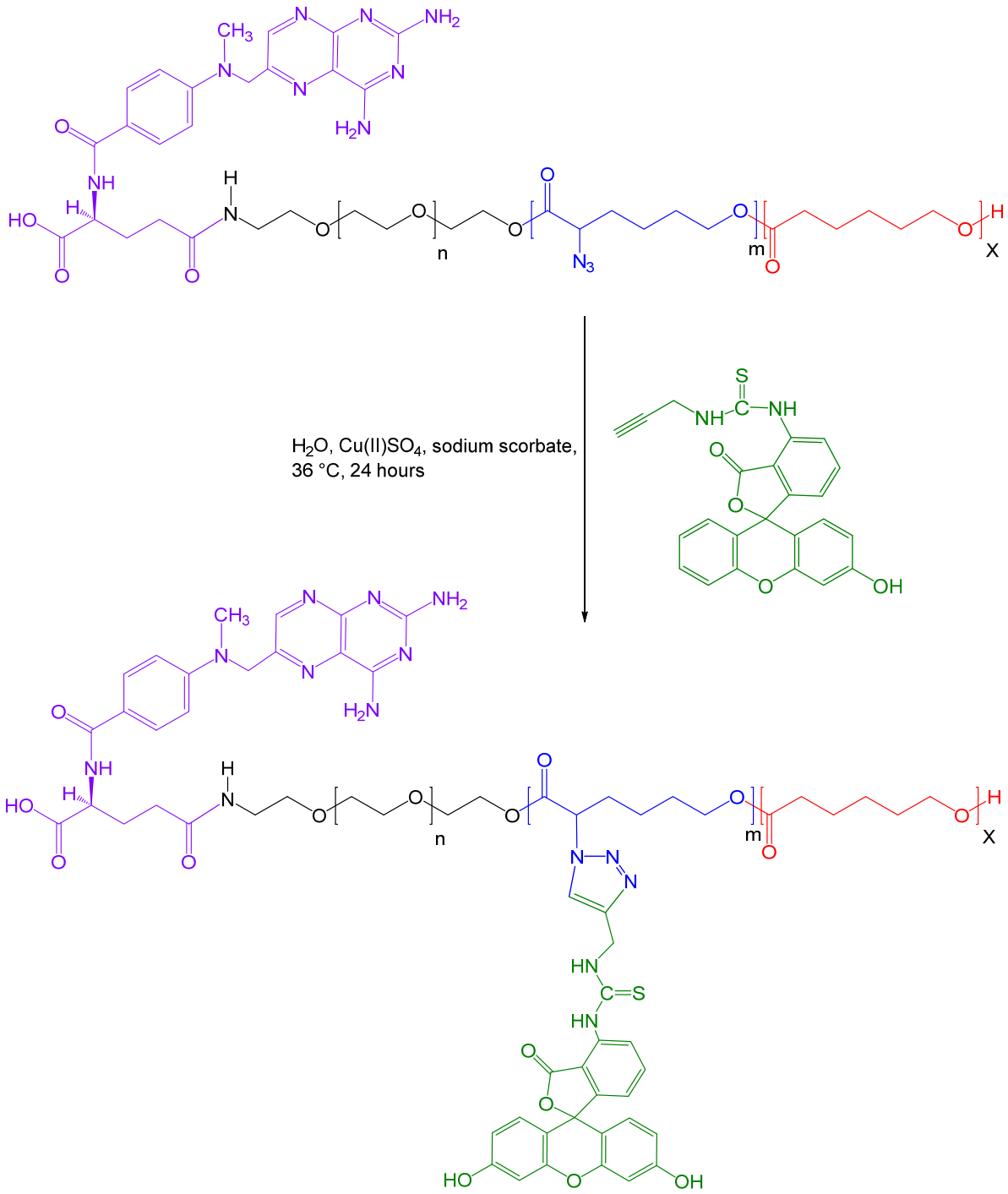

Scheme 6-5. Post-functionalisation of micelles with FITC-alkyne via copper catalysed alkyne-azide cycloaddition (CuAAC).

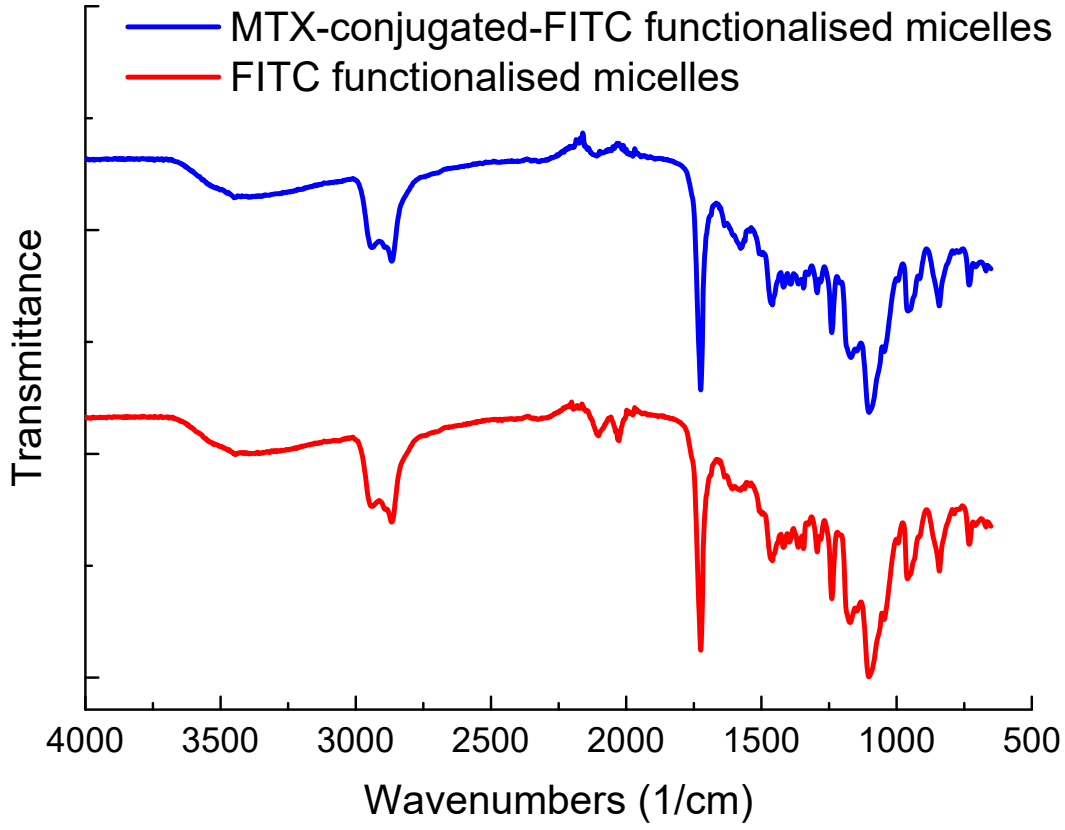

Figure 6-12. FT-IR spectra of FITC functionalised and MTX-conjugated-FITC functionalised micelles.

6.2.4. *In vitro* cellular uptake

In vitro cellular uptake of FITC-functionalised micelles and MTX-conjugated-FITC-functionalised micelles was tested in MCF7 cells using confocal laser scanning microscopy and flow cytometry. For this purpose, both types of micelles were incubated for 3 hours with human breast cancer cells (MCF7).

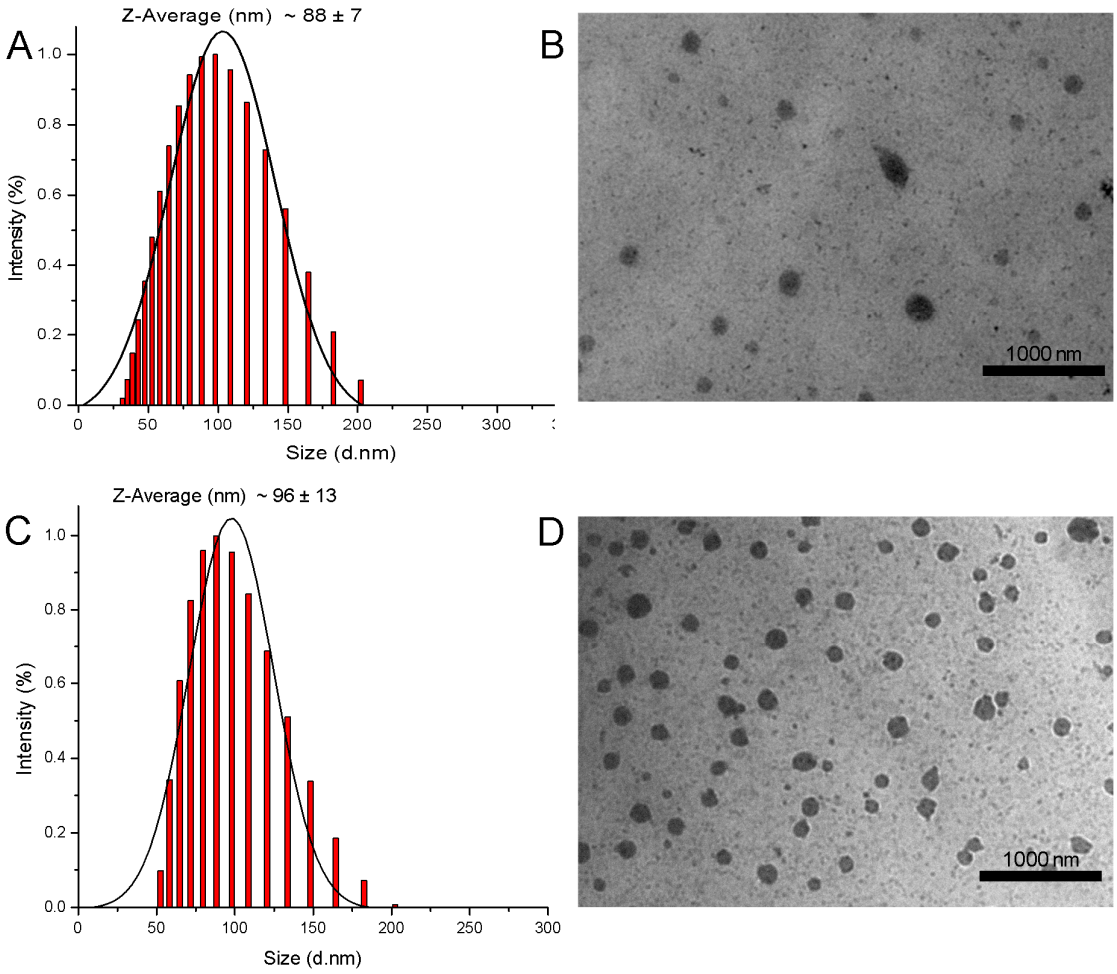

Figure 6-13. Characterisation of FITC-functionalised and MTX-conjugated-FITC functionalised micelles. (A) Size distributions of FITC-functionalised micelles determined by DLS and (B) TEM micrograph (C) Size distributions of MTX-conjugated-FITC-functionalised micelles determined by DLS, and (D) TEM micrograph.

Figure 6-14 shows the CLSM images of cellular uptake studies. It is revealed that both types of micelles were taken up by MCF7 cells as represented by the green fluorescence in merged CLMS images. However, the visible intensity of green fluorescence in MCF7 cells treated with MTX-conjugated

micelles (figure 6-14B) appeared higher than un-conjugated micelles (figure 6-14A). Nevertheless, it was difficult to quantify the cellular uptake by confocal microscopy in this study.

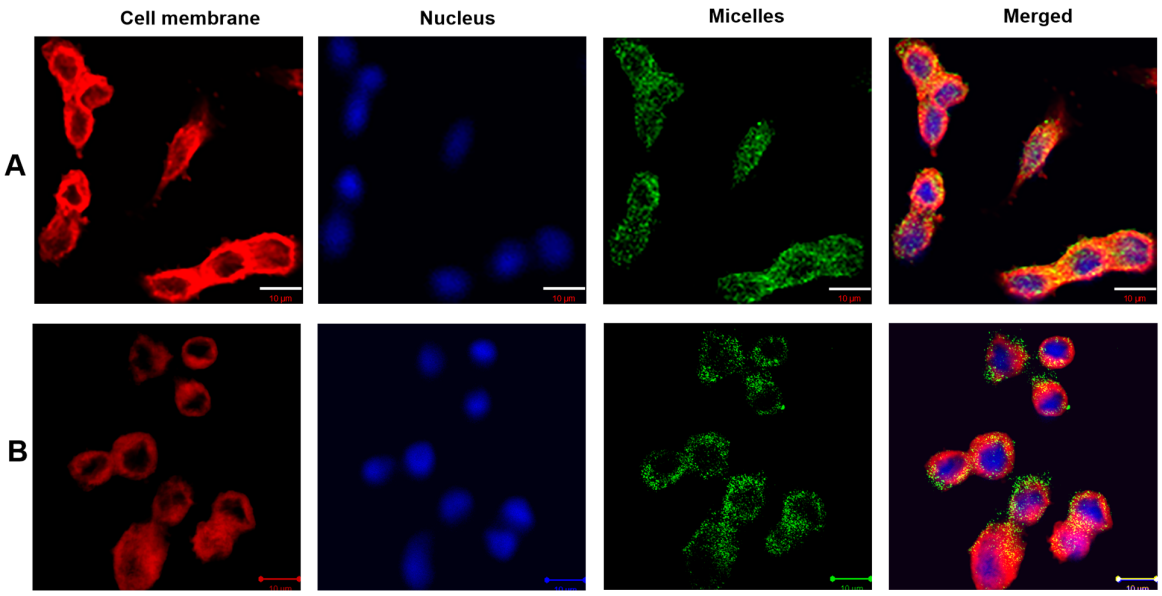

Figure 6-14. Confocal laser scanning microscopy images of cellular uptake in MCF7 cells cultured with (A) FITC-functionalised micelles and (B) MTX-conjugated-FITC functionalised micelles. Nuclei of cells were stained with Hoechst dye (blue fluorescence) and cell membranes were stained with CellMask™ deep red plasma membrane stain (red fluorescence). Scale bars ~ 10 µm.

To quantify the cellular uptake, fluorescence assisted cell sorting (FACS) was used and results are shown in figure 6-15.

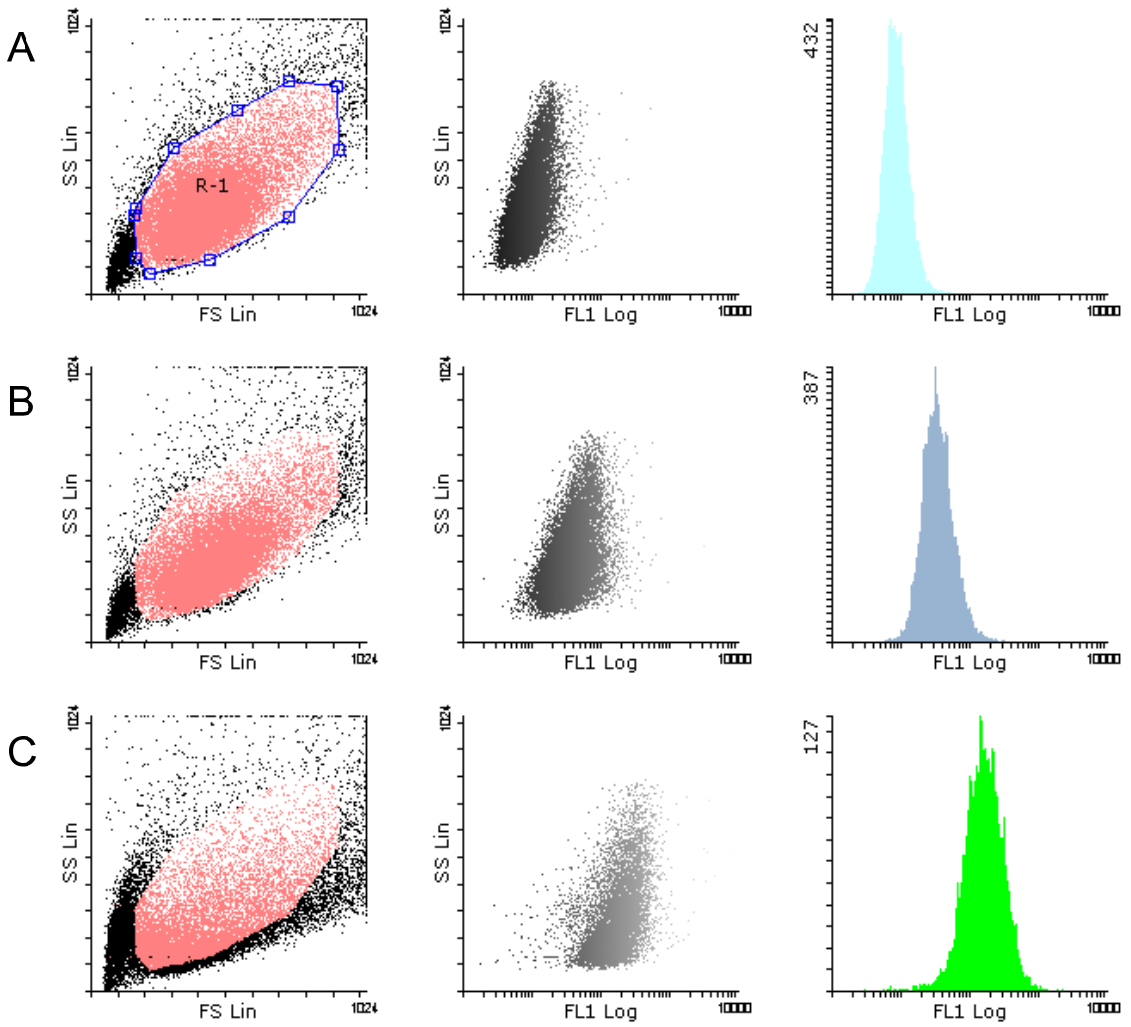

Figure 6-15. Fluorescence assisted cell sorting of cellular uptake in MCF7 cells incubated with (A) Control, (B) FITC-functionalised micelles, and (C) MTX conjugated FITC functionalised micelles.

The cells incubated without micelles were used as a negative control to correct the auto fluorescence. The FACS analysis showed that MTX-conjugated micelles were more efficiently taken up by MCF7 cells as compared to micelles without MTX-conjugation. Specifically, median

fluorescent intensities arising from negative control, non-conjugated and MTX-conjugated micelles were 5, and 72, and 171 (a.u) respectively, indicating 2.3-fold higher uptake of MTX-conjugated micelles as compared with micelles without MTX-conjugation.

6.2.5. MTT assay/cytotoxicity studies

The *in vitro* cytotoxic effects of empty micelles were investigated in MCF7 cells using MTT assays. For this purpose, MCF7 cells were incubated with various amounts of empty micelles (ranging from 100 to 1000 µg/mL) for 48 hours. The results of MTT assays are shown in figure 6-16A. It was revealed that empty micelles did not inhibit the metabolic activity of MC7 cells to a greater extent showing more than 90% cell viability (metabolic activity) up to 500 µg/mL concentrations. At maximum tested concentration of 1000 µg/mL, most of the cells were alive as revealed by more than 80% metabolic activities.

In addition, *in vitro* antitumour activities of free MTX and MTX conjugated micelles were also assessed using MTT assays. The results are shown in figure 6-16B. The MTX conjugated micelles showed greater *in vitro* antitumour activity in MCF7 cells in a dose dependent pattern as compared with free MTX. Specifically, at the maximum tested concentration of 40 µg/mL equivalent to MTX, the MTX-conjugated micelles inhibited the metabolic activity of MCF7 cells to 45 % of their normal levels. In contrast,

the same amount of free MTX was less potent, inhibiting the metabolic activity of MCF7 cells to 64% of baseline, as compared with the negative control.

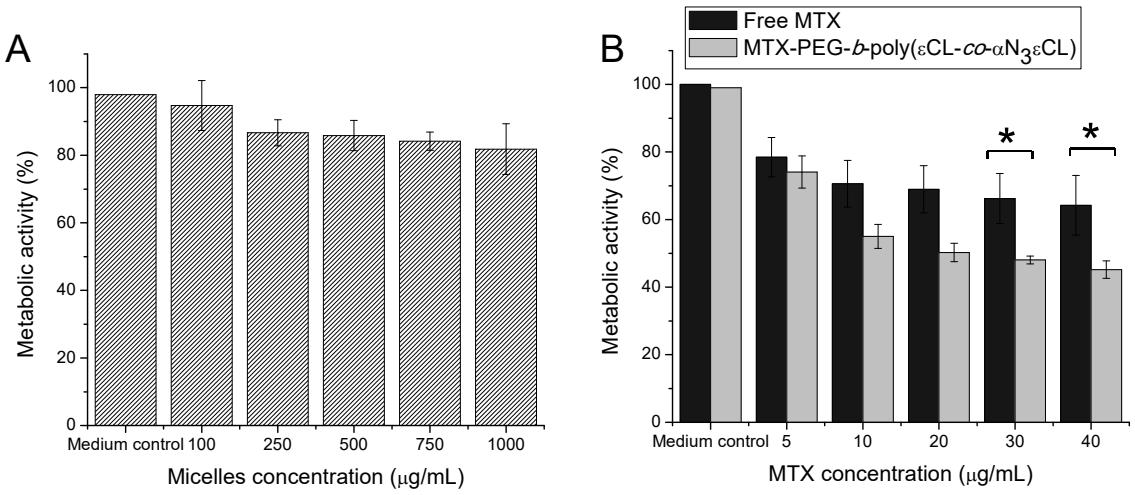

Figure 6-16. Cytotoxicity analysis of micelles cultured with MCF7 cells for 48 hours. (A) α-amino-PEG-*b*-poly(εCL-*co*-αN_3εCL) and (B) MTX-PEG-*b*-poly(εCL-*co*-αN_3εCL). Error bars represent standard deviation (n=3). MTT assays were used to analyse the metabolic activity of MCF7 cells.

6.2.6. Annexin V-FITC/PI assay

The results obtained from MTT assays were further confirmed by annexin V-FITC/PI assays using flow cytometry. The data obtained from annexin V-FITC/PI assays are shown in figures 6-17. The negative control cells (without treatment) appeared to be regular and with low fluorescence (i.e. auto fluorescence) as shown in figure 6-16A. The auto fluorescence

generated by control cells was subtracted from the flow cytometry data of treated samples by applying appropriate gates. The flow cytometry data showed that MCF7 cells treated with MTX-conjugated micelles resulted in dose dependent increases in the percentages of apoptotic and dead cells (figure 6-17C-D) as compared to the untreated cells (figure 6-17A).

Specifically, MTX conjugated micelles at 10 µg/mL equivalent to free-MTX, resulted in 12 % apoptotic and 5 % dead cells. The same formulation at 40 µg/mL equivalent to free-MTX, gave rise to 32 and 21 % apoptotic and dead cells, respectively. On the other hand, MCF7 cells treated with free MTX control (40 µg/mL) resulted into 14 % apoptotic and less than 2 % apoptotic cells (figure 6-17B). The findings obtained from annexin V-FITC/PI assays were in agreement with MTT assays.

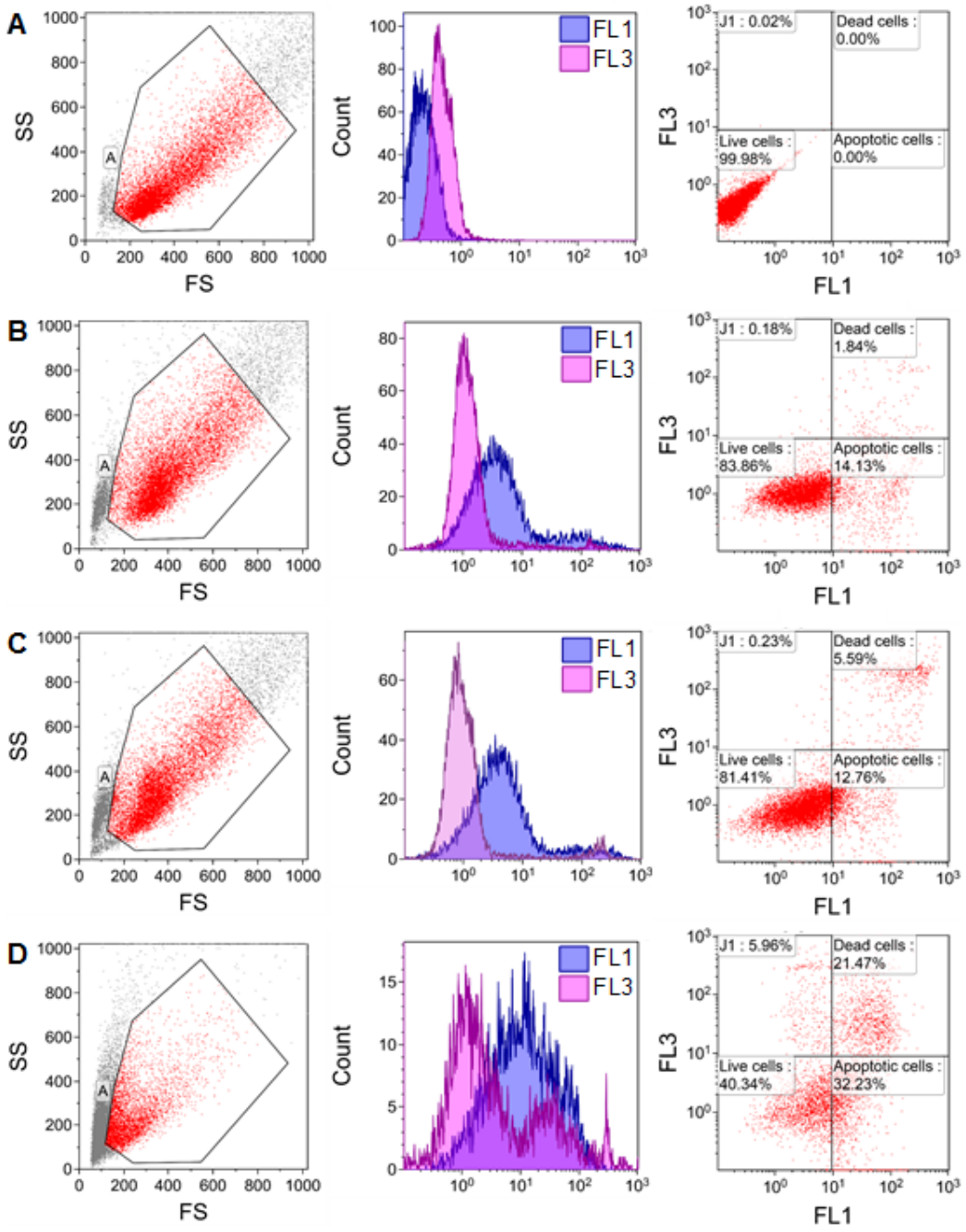

Figure 6-17. Flow cytometry investigation to calculate the percentage of apoptotic and dead cells in MCF7 breast cancer cells treated with (A) Medium control, (B) MTX control (40 µg/mL), (C) MTX conjugated micelles at 10 µg/mL equivalent to free-MTX, and (D) 40 µg/mL equivalent to free-MTX. J1~ necrotic cells.

6.3. DISCUSSION

In this study, multifunctional amphiphilic block copolymers were synthesised for folate receptor mediated active targeting of tumour cells. For this purpose, a heterofunctional macro-initiator i.e. α-azide-ω-hydroxyl PEG was synthesised in a two-step method. In the first step, a highly reactive intermediate (α-tosyl-ω-hydroxyl PEG) was obtained by the mono-tosylation of polyethylene glycol by reacting equimolar amounts of PEG and *p*-toluenesulfonyl chloride using triethylamine as a catalyst.

The mono-tosylation nature and degree of functionalisation was determined by ^{1}H NMR using deuterated chloroform. However, protons signals of alcohol functionality were not detected. Therefore, to confirm the mono-tosylation of PEG, ^{1}H NMR spectroscopy was performed in deuterated DMSO.

The chemical shift corresponding to the hydroxyl proton was observed at 4.57 ppm, which was well separated from PEG backbone peaks and did not broaden or shifted with the variation of the concentration showing quantitative conversion of PEG to PEG-OTs. Furthermore, size exclusion chromatography showed only unimodal peaks without any shoulder, indicating similar molar mass distributions of PEG and PEG-OTs.

The tosylate is a good leaving group in contrast to the hydroxyl group and may serve as a good substrate for nucleophilic substitution reactions.[36] Therefore, the tosylate group in polyethylene glycol is a useful functionality

and can be replaced by various functional groups such as azide, thiols, and -thioacetate to obtain functional polyethylene glycol derivatives.[35] The tosyl group of PEG-OTs was subsequently replaced with azide via nucleophilic substitution reactions to obtain the α-azido-ω-hydroxyl PEG (PEG-N_3). The complete disappearance of protons corresponding to the tosyl group in the ^{1}H NMR spectrum of PEG-N_3 (figure 6-2) and the appearance of a new peak at 3.41 ppm (corresponding to methylene protons next to azide group) confirmed the quantitative substitution of tosyl group. Furthermore, the appearance of a new infrared absorption peak at 2106 cm^{-1} in FTIR spectrum of PEG-N_3 (figure 6-3) validated the incorporation of azide group as reported previously.[35, 36]

The heterofunctional PEG (i.e. α-azido-ω-hydroxyl polyethylene glycol) was used as an initiator for tin octoate catalysed ring opening polymerisation of εCL and functional caprolactone (αClεCL) to obtain multifunctional amphiphilic block copolymer based on α-azide-PEG-*b*-poly(εCL-*co*-αClεCL). The azide functionality of PEG block of multifunctional copolymer was subsequently reduced to the primary amine using triphenylphosphine via a Staudinger-type reaction.[37] This reaction was performed at room temperature and proceeded through the formation of a linear phosphazide intermediate by the attack of phosphorus on the nitrogen. The phosphazide intermediate is highly unstable and readily undergoes intramolecular rearrangement to yield a second intermediate (iminophosphorane) with concomitant loss of N_2. In the presence of water, the iminophosphorane

undergoes spontaneous hydrolysis to yield a primary amine and triphenylphosphine oxide.[38] The reduction of the azide into the amine was complete as validated by the disappearance of methylene protons next to azide and the appearance of a new peak at 2.85 ppm (corresponding to methylene protons next to the amine) in ^{1}H NMR (figure 6-7), as further validated by the absence of stretching vibration bands of the azide in the FTIR spectrum (figure 6-9).

In subsequent step, chloro atoms of the hydrophobic backbone of α-amino-PEG-*b*-poly(εCL-*co*-αClεCL) were substituted into azide to obtain a block copolymer of α-amino-PEG-*b*-poly(εCL-*co*-αN_3εCL) with multiple functional groups. The multifunctional block copolymer with amine functionality on the hydrophilic block and azide functionalities on the hydrophobic backbone was designed to be a 'platform' copolymer. For instance, the azide group on the hydrophobic backbone could be used to attach an alkyne functionalised fluorescent probe or an anticancer therapeutic agent via CuAAC, whereas the amine functionality on the hydrophilic block might be used to conjugate a targeting ligand for receptor mediated drug delivery.

In this study, we used methotrexate (MTX) as a targeting ligand for folate receptor mediated active targeting in human breast cancer (MCF7) cells. The chemical structure of the MTX is similar to the folic acid, except some minor variations as shown in figure 6-18. Therefore, MTX may not only be used as an antitumor agent but also as a targeting ligand.

To test this hypothesis, MTX was conjugated to the PEG block of multifunctional copolymer by reacting the γ-carboxylic acid of MTX with the primary amine of α-amine-PEG-*b*-poly(εCL-*co*-αN$_3$εCL) using HATU as a coupling agent and *N,N*-diisopropylethylamine (DIPEA) as a catalyst.[39] The ^{1}H NMR spectrum of MTX-PEG-*b*-poly(εCL-*co*-αN$_3$εCL) block copolymer clearly showed chemical shifts corresponding to the MTX in addition to chemical shifts of block copolymer (figure 6-10) confirming the successful synthesis of the desired MTX conjugated block copolymer.[40]

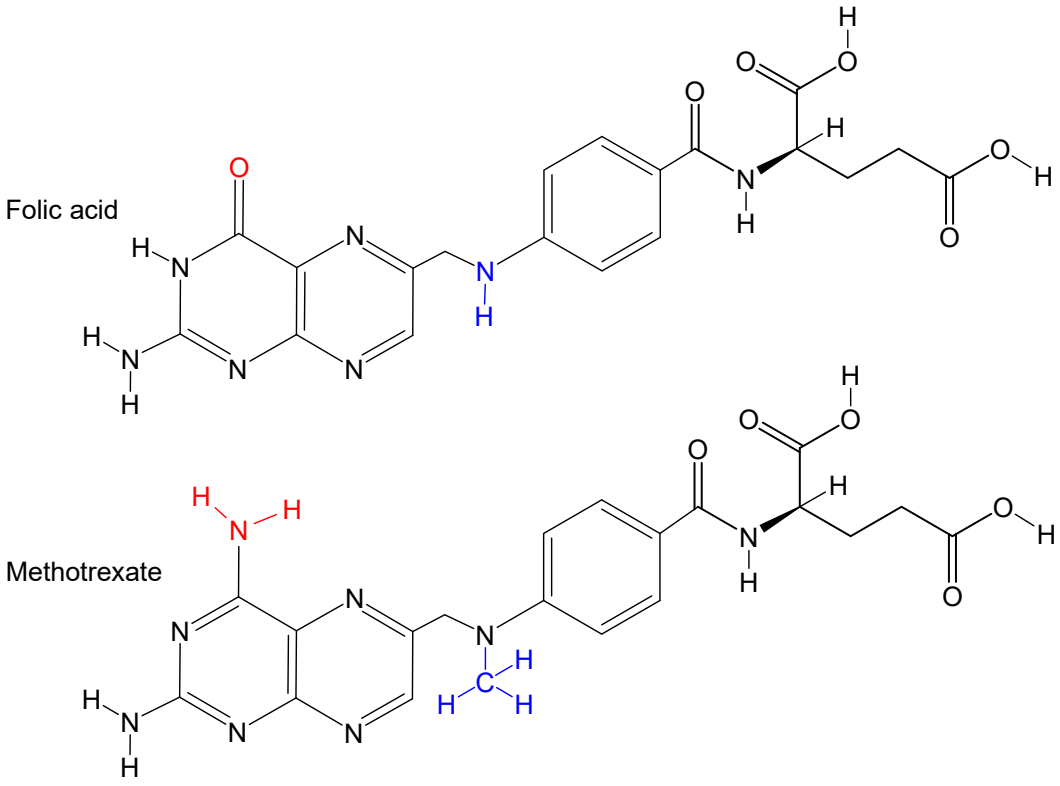

Figure 6-18. Structure comparison of folic acid (top) and the anti-cancer drug methotrexate (bottom).

The micelles of blank and MTX-conjugated block copolymers were prepared using a dialysis method and showed uniform size distributions and approximately spherical morphologies. Interestingly, a slight increase in the average micellar size was observed in MTX conjugated block copolymers as compared with MTX-free block copolymers (blank micelles) suggesting that surface modification of micelles with MTX did not greatly affect the hydrophilicity of micelles. To investigate the cellular uptake of MTX conjugated and non-conjugated micelles, a fluorescent probe (FITC-alkyne) was covalently grafted onto the hydrophobic block of micelles via CuAAC. The FITC-grafted micelles were of larger average sizes as compared with the same micelles without FITC. The larger size of FITC grafted micelles might be due to the accumulation of FITC in the core of micelles along with conformation rearrangement driven by the triazole ring formation during click reaction as reported earlier.[41]

In vitro cellular uptake of FITC-functionalised and MTX-conjugated-FITC-functionalised micelles was examined in MCF7 cells using confocal laser scanning microscopy and flow cytometry. It is observed that both types of micelles were taken up by MCF7 cells as represented by the green fluorescence in merged CLMS images (figure 6-14). However, it was difficult to quantify the cellular uptake by confocal microscopy alone. Therefore, cellular uptake of both types of micelles was quantified using flow cytometry and showed 2.3-fold higher uptake of MTX-conjugated micelles as compared with the micelles without MTX-conjugation (figure 6-

15). These results suggest that surface modification of micelles with MTX enhanced the cellular uptake by folate receptor mediated active targeting.[42]

The blank micelles did not show apparent cytotoxic effects in MCF7 cells at low concentrations as revealed by MTT assays. On the other hand, MTX-conjugated micelles greatly reduced the metabolic activities of MCF7 cells in a dose dependent pattern as compared with the free MTX. The results obtained from MTT assays were further confirmed using annexin V-FITC/PI assays and revealed that MTX-conjugated micelles induced apoptosis and finally cell death to tumour cells in a greater extent as compared with the free-MTX. The low apoptosis inducing potential of free-MTX can be attributed to its low aqueous solubility, less permeability across cell membranes, and higher efflux of MTX, and drug resistance.[43]

In contrast, carrier-bound MTX might have internalised via folate receptor mediated endocytosis and accumulated in the cytoplasm of MCF7 cells resulting into greater cytotoxic effect as compared with the free-MTX. The receptor mediated uptake of folic acid or MTX-conjugated micelles initiates with conjugate binding to the folate receptor overexpressed on the cell membrane of cancer cell as illustrated in figure 6-19. The cell membrane subsequently invaginates to create an endocytic vesicle (endosome) resulting in internalisation of the MTX-conjugated micelles into cancer cells.[44]

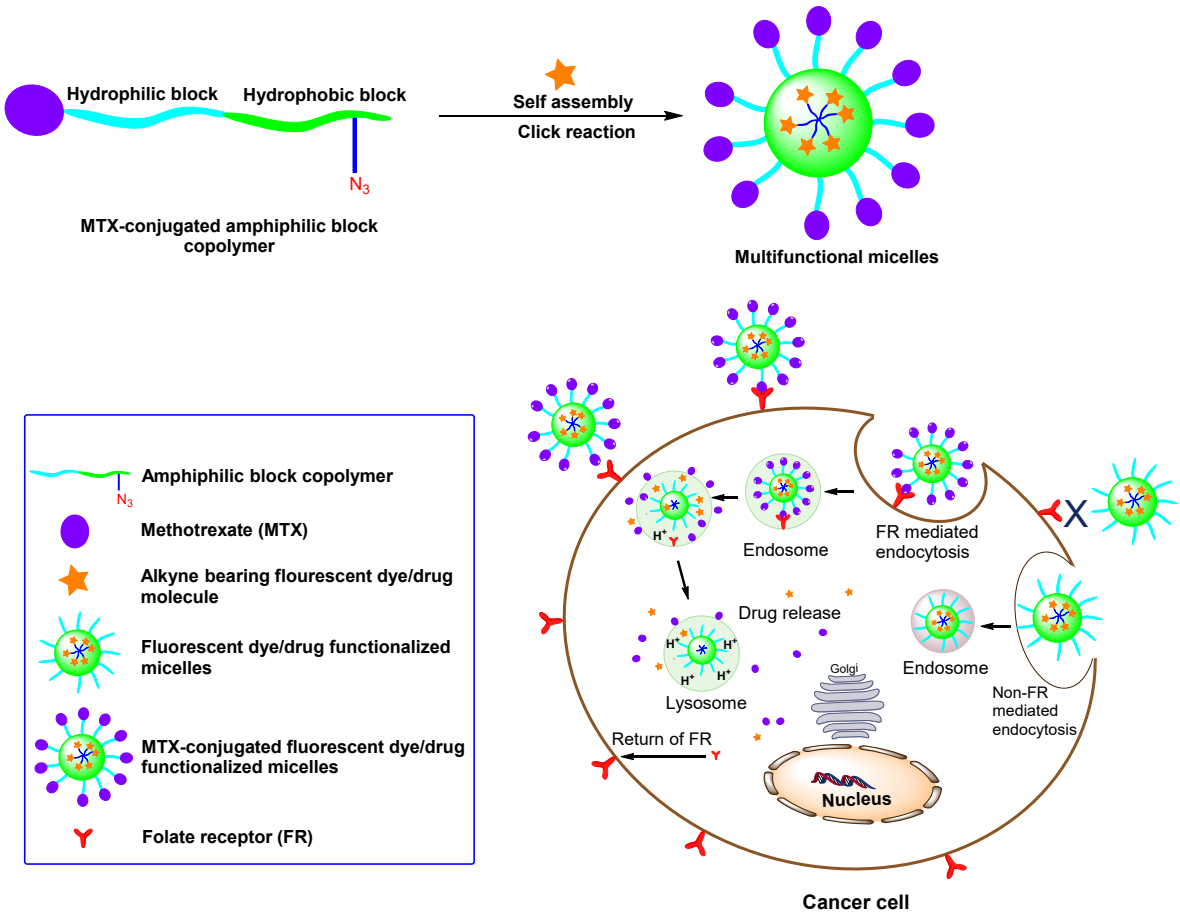

Figure 6-19. Schematic illustration of receptor mediated endocytosis of MTX-conjugated amphiphilic block copolymeric micelles in breast cancer cells. MTX-conjugated micelles bind to the folate receptor overexpressed on the cell membrane of cancer cells, which subsequently invaginates to form an endosome.

Since binding of the folate or MTX-conjugate with the folate receptors relies on the pH, therefore, acidic environment (pH ~ 4.3-6.9) in the endosome may cause cleavage of the folate or MTX conjugate from the folate receptor.[45,46] The cleaved folate or MTX conjugate escapes the endosome by an unknown mechanism resulting into drug accumulation in the

cytoplasm.[32] It is thought that cleaved folate receptors are mainly recycled back to the cell membrane permitting uptake of additional folate or MTX-conjugated micelles.

To achieve a required therapeutic effectiveness, the MTX molecules must be internalised into the cancer cells with high concentration. However, repulsive interactions between the negatively charged plasma membrane and ionic MTX may cause difficulties in permeation of MTX into the cell membrane, consequently decreasing therapeutic effectiveness.[47] Furthermore, internalisation of free MTX is considered via reduced-folate-carrier (RFC) mediated transport.[48-50] However the RFC path is not considered very effective as saturation of reduced-folate-carrier at high MTX concentration has been reported, consequently decreasing the therapeutic effectiveness.[51] In contrast, MTX-conjugated micelles might have followed several different path of internalisation in addition to folate receptor mediated endocytosis. Therefore, uptake of MTX-conjugated micelles by folate receptor mediated endocytosis route might have allowed breast cancer cells to engulf greater amounts of MTX resulting into better anticancer activity.

The findings of higher *in vitro* anti-tumour activity of MTX-conjugated micelles against MCF7 cells were consistent with the cellular uptake experiments. From cellular uptake data, it can be seen that MTX-conjugated micelles were internalised by MCF7 cells in a greater extent (2.3 fold higher)

than micelles without MTX conjugation. These MTX-conjugated amphiphilic block copolymeric micelles could be promising candidates for targeted drug delivery and tumour therapy.

6.4. CONCLUSIONS

In this work, a multifunctional amphiphilic block copolymer based on α-amine-PEG-*b*-poly(εCL-*co*-αN$_3$εCL) was synthesised and subsequently was used to conjugate methotrexate on the hydrophilic block for receptor mediated targeting of breast cancer cells. Furthermore, an alkyne bearing fluorescent probe (FITC-alkyne) was grafted on the hydrophobic backbone via CuAAC to analyse cellular uptake of micelles. Cellular uptake studies revealed 2.3-fold higher uptake of MTX-conjugated micelles as compared with un-conjugated micelles. The blank micelles showed low cytotoxicities in breast cancer cells, however, MTX-conjugated micelles exhibited greater antitumour activities in contrast to free-MTX. Therefore, MTX-conjugated micelles based on MTX-PEG-*b*-poly(εCL-*co*-αN$_3$εCL) could be promising nanocarriers for targeted drug delivery and tumour therapy.

6.5. EXPERIMENTAL

6.5.1. Synthesis of α-tosyl-ω-hydroxyl PEG

The α-tosyl-ω-hydroxyl polyethylene glycol (PEG-OTs) was synthesised using the procedure previously described in the literature with some modifications.[36] Briefly, PEG_{4000} (10 g, 2.50 mmol) was dried by azeotropic distillation in toluene and was subsequently dissolved in 50 mL of anhydrous DCM in a round bottom flask. Afterwards, *p*-toluenesulfonyl chloride (0.50 g, 2.62 mmol) and triethylamine (14 mL) were introduced into the system. The reaction mixture was stirred at room temperature for 24 hours. Afterwards, the product mixture was neutralised with 1M HCl solution and filtered. An excess of sodium bicarbonate was then added and the organic phase was collected using a separating funnel and aqueous residues were removed by magnesium sulfate before filtration. The organic phase was concentrated using a rotary evaporator and polymer was recovered by precipitating in diethyl ether and dried under reduced pressure until constant weight was achieved (72% yield). ^{1}H NMR (400 MHz, $CDCl_3$) δ (ppm): 7.83-7.81 (meta protons of benzene ring, d, *J* = 8.3 Hz, 2H), 7.37-7.35 (ortho protons of benzene ring, d, *J* = 8.0 Hz, 2H), 4.18 ($C\underline{H}_2$-O-S-, m, 2H), 3.86–3.47 (O–$C\underline{H}_2$–$C\underline{H}_2$–O–, m, 471H), 2.47 ($C\underline{H}_3$ s, 3H). ^{1}H NMR (400 MHz, DMSO) δ (ppm): 7.79 ((meta protons of *p*-toluene sulfonyl, d, *J* = 8.2 Hz, 2H), 7.49 (ortho protons of *p*-toluene sulfonyl, d, *J* = 8.1 Hz, 2H), 4.57 ($\underline{C}H_2$-OH, t, *J* = 5.4 Hz, 1H), 4.13 – 4.11 ($C\underline{H}_2$-O-S-,

m, 2H), 3.72–3.26 (O–C$\underline{H}_2$–C$\underline{H}_2$–O–, m, 470H), 2.43 (C$\underline{H}_3$, s, 3H). ^{13}C NMR (101 MHz, $CDCl_3$) δ (ppm): 144.80 (para carbon of *p*-toluene sulfonyl), 133.06 ($\underline{C}$-CH_3 of *p*-toluene sulfonyl), 129.85 (ortho carbon of *p*-toluene sulfonyl), 128.00 (meta carbon of *p*-toluene sulfonyl), 72.62 ($\underline{C}H_2$-CH_2-OH), 70.61 [(-O-$\underline{C}H_2$-$\underline{C}H_2)_n$], 69.28 (-O-$\underline{C}H_2$-CH_2-O-S), 68.70 (-O-CH_2-$\underline{C}H_2$-O-S), 61.72 (CH_2-$\underline{C}H_2$-OH), 21.68 ($\underline{C}H_3$). IR: ν max/cm^{-1}: 1105 (C-O-C stretching), 1340 (C-H bending), 1464 (C-H bending), 2882 (CH_2 stretching). 3441 (OH stretching).

6.5.2. Synthesis of α-azide-ω-hydroxyl PEG

The α-azide-ω-hydroxyl polyethylene glycol (PEG-N_3) was synthesised by reacting PEG-OTs with sodium azide. Briefly, 5 g of PEG-OTs (approximately 1.20 mmol) and sodium azide (0.78 g, 12 mmol) were dissolved in 10 mL of DMSO and reaction mixture was stirred at room temperature for 24 h. The polymer was recovered by precipitation in anhydrous diethyl ether and the resulting precipitates were dissolved in toluene, and mixture was subsequently centrifuged (4000 rpm, 10 min, RT) to remove insoluble salts. Finally, the azide bearing polymer was recovered by recrystallization in anhydrous diethyl ether, filtered and was dried under reduced pressure to a constant weight. (84 % yield). ^{1}H NMR (400 MHz, $CDCl_3$) δ (ppm): 3.86–3.47 (O–C$\underline{H}_2$–C$\underline{H}_2$–O–, m, 475H), 3.41 (C$\underline{H}_2$–N_3, t, 2H). IR: ν max/cm^{-1}: 1105 (C-O-C stretching), 1340 (C-H bending), 1464

(C-H bending), 2106 (N_3 stretching), 2882 (CH_2 stretching). 3441 (OH stretching).

6.5.3. Synthesis of α-azide-PEG-*b*-poly(εCL-co-αClεCL)

Briefly, 3.5 g of α-azido-ω-hydroxyl PEG (0.87 mmol approximately) and αClεCL (0.26 g, 1.75 mmol) were dissolved in anhydrous toluene and dried by azeotropic distillations in a glass reactor. Afterwards, 5 mL of εCL (5.15 g, 45.12 mmol) and 20 mL of anhydrous toluene were introduced via a rubber septum using a glass syringe and the mixture was stirred for 15 minutes under nitrogen. Afterwards, $SnOct_2$ (0.19 g in anhydrous toluene) was finally added (under nitrogen) and the reaction was stirred at 80 °C for 24 hours. Finally, the reaction mixture was cooled to room temperature and concentrated to a small volume using a rotary evaporator. The copolymer was recovered by precipitation in anhydrous diethyl ether, filtered and dried under reduced pressure.

M_n = 9810 g/mol (^{1}H NMR). ^{1}H NMR (400 MHz, $CDCl_3$) δ (ppm): 4.30 (C$\underline{H}_2$–O–CO, t, 2H), 4.27 (CO–C$\underline{H}$(Cl)–CH_2–CH_2–CH_2–CH_2–O–, t, 2H), 4.21 (CO–CH(Cl)–CH_2–CH_2–CH_2–C$\underline{H}_2$–O–, t, 4H), 4.08 (CO–CH_2–CH_2–CH_2–CH_2–C$\underline{H}_2$–O–H, t, 96H), 3.86–3.47 (O–C$\underline{H}_2$–C$\underline{H}_2$–O–, m, 438H), 3.41 (C$\underline{H}_2$–N_3, t, 2H), 2.33 (CO–C$\underline{H}_2$–CH_2–CH_2–CH_2–CH_2–O–H, t, 96H), 2.0 (CO-CH(Cl)–C$\underline{H}_2$–CH_2–C$\underline{H}_2$–CH_2–O–, m, 8H), 1.76-1.32 (CO–CH_2–C$\underline{H}_2$– C$\underline{H}_2$–C$\underline{H}_2$–CH_2–O–

and, CO–CH(Cl)–CH_2–C$\underline{H}_2$–CH_2–CH_2–O–, m, 300H). IR: ν max/cm^{-1} 735, 841, 958, 1103, 1148, 1239, 1278, 1341, 1466, 1731, 1954, 2106, 2885. IR: ν max/cm^{-1}: 1105 (C-O-C stretching), 1340 (C-H bending), 1465 (C-H bending), 1722 (C=O stretching), 2106 (N_3 stretching), 2865 (symmetric CH_2 stretching), 2943 (asymmetric CH_2 stretching) 3476 (OH stretching).

6.5.4. Synthesis of α-amino-PEG-*b*-poly(εCL-co-αClεCL)

The α-azide-PEG-*b*-poly(εCL-*co*-αClεCL) (4 g, 0.40 mmol approximately) was dissolved in 25 mL of DCM in a round bottom flask. To this rapidly stirring mixture, triphenylphosphine (0.31 g, 1.2 mmol, in 25 mL of methanol) was added and the reaction mixture was stirred at 40 °C for 24 h. The organic solvents were removed under reduced pressure. The crude product was dissolved in 10 mL of DCM and copolymer was recovered by recrystallization in anhydrous diethyl ether, filtered and dried under reduced pressure.

M_n = 9784 g/mol (^{1}H NMR).

^{1}H NMR (400 MHz, $CDCl_3$) δ (ppm): 4.30 (C$\underline{H}_2$–O–CO, t, 2H), 4.27 (CO–C$\underline{H}$(Cl)–CH_2–CH_2–CH_2–CH_2–O–, t, 2H), 4.21 (CO–CH(Cl)–CH_2–CH_2–CH_2–C$\underline{H}_2$–O–, t, 4H), 4.08 (CO–CH_2–CH_2–CH_2–CH_2–C$\underline{H}_2$–O–H, t, 96H), 3.86–3.47 (O–C$\underline{H}_2$–C$\underline{H}_2$–O–, m, 438H), 2.85 (C$\underline{H}_2$–NH_2, t, 2H), 2.33 (CO–C$\underline{H}_2$–CH_2–CH_2–CH_2–CH_2–O–H, t, 96H), 2.0-1.8 (CO-CH(Cl)–C$\underline{H}_2$–CH_2–C$\underline{H}_2$–CH_2–O–,and N$\underline{H}_2$, m, 10H), 1.76-1.32 (CO–CH_2–C$\underline{H}_2$– C$\underline{H}_2$–C$\underline{H}_2$–CH_2–O– and,

CO–CH(Cl)–CH_2–C$\underline{H}_2$–CH_2–CH_2–O–, m, 300H). 1105 (C-O-C stretching), 1340 (C-H bending), 1465 (C-H bending), 1722 (C=O stretching), 2865 (symmetric CH_2 stretching), 2943 (asymmetric CH_2 stretching) 3476 (OH stretching).

6.5.5. Synthesis of α-amino-PEG-*b*-poly(εCL-*co*-αN_3εCL)

Briefly, 2 g (0.20 mmol approximately) of α-amino-PEG-*b*-poly(εCL-*co*-αClεCL) was dissolved in 5 mL of DMSO. Afterwards, sodium azide (0.04 g, 0.60 mmol) was added into the system and the reaction mixture was stirred at room temperature for 24 hours. DMSO was removed by extraction with anhydrous diethyl ether and the resulting product was dissolved in toluene, and was subsequently centrifuged (4000 rpm, 10 min, RT) to remove insoluble salts. Finally, the azide bearing copolymer was recovered by recrystallization in anhydrous diethyl ether, filtered and was dried under vacuum.

M_n = 9798 g/mol (^{1}H NMR). ^{1}H NMR (400 MHz, $CDCl_3$) δ (ppm) 4.30 (C$\underline{H}_2$–O–CO, t, 2H), 4.23 (CO–CH(N_3)–CH_2–CH_2–CH_2–C$\underline{H}_2$–O–, t, 4H), 4.08 (CO–CH_2–CH_2–CH_2–CH_2–C$\underline{H}_2$–O–H, t, 96H), 3.89 (CO–C$\underline{H}$(N_3)–CH_2–CH_2–CH_2–CH_2–O–, t, 2H) 3.86–3.47 (O–C$\underline{H}_2$–C$\underline{H}_2$–O–, m, 438H), 2.85 (C$\underline{H}_2$–NH_2, t, 2H), 2.33 (CO–C$\underline{H}_2$–CH_2–CH_2–CH_2–CH_2–O–H, t, 96H), 2.00-1.32 (N$\underline{H}_2$, CO-CH(N_3)–C$\underline{H}_2$–C$\underline{H}_2$–C$\underline{H}_2$–CH_2–O–, and CO–CH_2–C$\underline{H}_2$– C$\underline{H}_2$–C$\underline{H}_2$–CH_2–O, 368H). IR: ν max/cm^{-1}: 1105 (C-O-C stretching), 1340 (C-H bending),

1465 (C-H bending), 1722 (C=O stretching), 2106 (N_3 stretching), 2865 (symmetric CH_2 stretching), 2943 (asymmetric CH_2 stretching) 3476 (OH stretching).

6.5.6. Synthesis of MTX-PEG-*b*-poly(εCL-co-αN$_3$εCL)

Briefly, 500 mg (0.05 mmol approximately) of α-amine-PEG-*b*-poly(εCL-co-αN$_3$εCL) was dissolved in 3 mL of DMSO in a glass reaction tube and the system was purged with nitrogen gas under stirring for 15 minutes. Afterwards, methotrexate (27 mg, 0.06 mmol), HATU (23 mg, 0.06 mmol) and 100 µL (0.06 mmol) of *N,N*-Diisopropylethylamine was added and the reaction mixture was stirred at room temperature for 24 h. The MTX-conjugated block copolymer was purified by dialysis for 48 h against 1 L of HPLC grade water using a cellulose dialysis membrane (Spectrapor, cut-off 3500). Finally, the MTX-conjugated block copolymer was recovered by freeze drying. M_n = 10251 g/mol (^{1}H NMR).

^{1}H NMR (400 MHz, DMSO-d_6) δ (ppm): 8.67 (-C-N=C<u>H</u> of aromatic ring of MTX, s, 1H), 7.79-7.68 (O=C-C=C<u>H</u> of aromatic ring of MTX, d, 2H, *J* = 8.6 Hz), 7.53 (N<u>H</u>$_2$ of aromatic ring of MTX, s, 2H), 6.82 ($_3$HC-N-C=C<u>H</u> of aromatic ring of MTX, d, *J* = 9.1 Hz, 2H), 6.53 (N=C-N<u>H</u>$_2$ of aromatic ring of MTX, s, 2H), 4.83 ($_3$HC-N-C<u>H</u>$_2$ of aromatic ring of MTX, s, 2H), 4.34 (HOOC-C-C<u>H</u> of aromatic ring of MTX, m, 1H), 4.30 (CH_2-C<u>H</u>$_2$-O-C=O, m, 2H), 4.23 (CO–CH(N_3)–CH_2–CH_2–CH_2–C<u>H</u>$_2$–O–, m, 4H), 4.08 (CO–CH_2–

CH_2–CH_2–CH_2–C$\underline{H}_2$–O–H, t, *J* = 6.4 Hz, 96H), 3.89 (CO–C$\underline{H}$(N_3)–CH_2–CH_2–CH_2–CH_2–O–, m, 2H), 3.70–3.28 (O–(C$\underline{H}_2$–C$\underline{H}_2$)$_n$–O–, m, 430H), 3.27 (N-C$\underline{H}_3$ of aromatic ring of MTX, s, 3H), 2.33 (CO–C$\underline{H}_2$–CH_2–CH_2–CH_2–CH_2–O–H, t, *J* = 7.2 Hz, 96H), 2.14-2.00 (HOOC-CH-C$\underline{H}_2$-C$\underline{H}_2$-CONH, m, 4H), 1.85-1.00 (CO-CH(N_3)–C$\underline{H}_2$–C$\underline{H}_2$–C$\underline{H}_2$–CH_2–O–, and CO–CH_2–C$\underline{H}_2$– C$\underline{H}_2$–C$\underline{H}_2$–CH_2–O–H, m, 355H).

6.5.7. Synthesis of FITC-alkyne

Fluorescein isothiocyanate (FITC) (50 mg, 0.12 mmol) was dissolved in 5 mL of THF in a glass reaction tube and the mixture was purged with argon for 15 minutes under continuous stirring before adding propargylamine (9.8 µL, 0.15 mmol). Afterwards, 1 µL of triethylamine was added into the reaction mixture (under argon) and the reaction contents were stirred for 72 hours at room temperature in the dark. The organic solvents were removed under reduced pressure using a Schlenk line. The crude product was dissolved in 2 mL of THF and FITC-alkyne was recovered by precipitation in cold heptane. ^{1}H NMR (400 MHz, CD_3OD) δ (ppm): 8.15 (aromatic, s, 1H,), 7.72 (aromatic, d, *J* = 2.1 Hz, 1H), 7.69 (aromatic, d, *J* = 1.5 Hz, 1H aromatic), 7.13 (aromatic, d, *J* = 2.9 Hz, 1H), 7.07 (aromatic, d, *J* = 2.2 Hz, 1H), 6.75-6.51 (aromatic, m, 4H), 4.04 (CH≡C-CH_2-N$\underline{H}$, d, *J* = 2.5 Hz, 1H). 3.75 (CH≡C-C$\underline{H}_2$-NH, m, 2H), 1.90 (C≡C$\underline{H}$, s, 1H).

6.5.8. Preparation of micelles

Briefly, 50 mg of α-amino-PEG-*b*-poly(εCL-*co*-αN_3εCL) or MTX-PEG-*b*-poly(εCL-*co*-αN_3εCL) were dissolved in 5 mL of DMSO and introduced into Milli-Q water (20 mL) under vigorous stirring, using a syringe pump with a flow rate of 0.20 mL/min. The solution was stirred for 2 hours at room temperature and micelles were purified by dialysis overnight against 1 L of Milli-Q water using a cellulose dialysis membrane (Spectrapor, cut-off 3500) to remove the DMSO.

6.5.9. Post-functionalisation of micelles with FITC-alkyne

50 mg of α-amine-PEG-*b*-poly(εCL-*co*-αN_3εCL) or MTX-PEG-*b*-poly(εCL-*co*-αN_3εCL) and FITC-alkyne (1.50 mol equivalent vs. azide groups) were dissolved in 5 mL of DMSO. This mixture was dropwise added into 20 mL Milli-Q water under vigorous stirring, using a syringe pump with a flow rate of 0.20 mL/min. The micellar solution was stirred for 2 hours at room temperature. Afterwards, copper(II) sulfate (0.20 mol equivalent vs. azide groups) and sodium ascorbate (0.20 mol equivalent vs. azide groups) were introduced into the system. The reaction was carried out at 36 °C for 24 hours. Afterwards, EDTA (2 mol equivalent vs. Cu) was introduced into the system and micelles were dialysed against 1 L of deionised water for 48 h using a cellulose dialysis membrane (Spectrapor, cut-off 3500) to remove DMSO and un-reacted FITC-alkyne.

6.5.10. *In vitro* cell culture experiments

The *in vitro* cellular uptake, cytotoxicities and apoptosis inducing potential of multifunctional micelles were tested in MCF7 cells according to the procedures described in the experimental section of chapter 5.

6.6. REFERENCES

1. *Global Cancer Facts & Figures 3rd Edition*, Atlanta, Georgia., 2012.
2. F. Danhier, O. Feron and V. Préat, *Journal of Controlled Release*, 2010, **148**, 135-146.
3. G. Tiwari, R. Tiwari, B. Sriwastawa, L. Bhati, S. Pandey, P. Pandey and S. K. Bannerjee, *International Journal of Pharmaceutical Investigation*, 2012, **2**, 2-11.
4. Y. Matsumura and H. Maeda, *Cancer Research*, 1986, **46**, 6387-6392.
5. U. Kedar, P. Phutane, S. Shidhaye and V. Kadam, *Nanomedicine: Nanotechnology, Biology and Medicine*, 2010, **6**, 714-729.
6. R. K. Jain, *Scientific American*, 1994, **271**, 58-65.
7. Y. H. Bae and K. Park, *Journal of Controlled Release*, 2011, **153**, 198-205.
8. C. H. J. Choi, C. A. Alabi, P. Webster and M. E. Davis, *Proceedings of the National Academy of Sciences*, 2010, **107**, 1235-1240.

9. K. Y. Choi, H. Chung, K. H. Min, H. Y. Yoon, K. Kim, J. H. Park, I. C. Kwon and S. Y. Jeong, *Biomaterials*, 2010, **31**, 106-114.
10. A. Béduneau, P. Saulnier and J.-P. Benoit, *Biomaterials*, 2007, **28**, 4947-4967.
11. L. E. van Vlerken, T. K. Vyas and M. M. Amiji, *Pharmaceutical Research*, 2007, **24**, 1405-1414.
12. E. Gullotti and Y. Yeo, *Molecular Pharmaceutics*, 2009, **6**, 1041-1051.
13. X. Pan and R. J. Lee, *Expert Opinion on Drug Delivery*, 2004, **1**, 7-17.
14. T. Kakudo, S. Chaki, S. Futaki, I. Nakase, K. Akaji, T. Kawakami, K. Maruyama, H. Kamiya and H. Harashima, *Biochemistry*, 2004, **43**, 5618-5628.
15. A. Kikuchi, S. Sugaya, H. Ueda, K. Tanaka, Y. Aramaki, T. Hara, H. Arima, S. Tsuchiya and T. Fuwa, *Biochemical and Biophysical Research Communications*, 1996, **227**, 666-671.
16. S. Acharya, F. Dilnawaz and S. K. Sahoo, *Biomaterials*, 2009, **30**, 5737-5750.
17. F. Fay and C. J. Scott, *Immunotherapy*, 2011, **3**, 381-394.
18. N. Karra, T. Nassar, A. N. Ripin, O. Schwob, J. Borlak and S. Benita, *Small (Weinheim an der Bergstrasse, Germany)*, 2013, **9**, 4221-4236.
19. F. Fay and C. J. Scott, *Immunotherapy*, 2011, **3**, 381-394.

20. M. Arruebo, M. Valladares and Á. González-Fernández, *Journal of Nanomaterials*, 2009, **2009**, 24.

21. B. A. Teicher and R. V. J. Chari, *Clinical Cancer Research*, 2011, **17**, 6389-6397.

22. P. Chames, M. Van Regenmortel, E. Weiss and D. Baty, *British Journal of Pharmacology*, 2009, **157**, 220-233.

23. O. Bucur, B. Pennarun, A. L. Stancu, M. Nadler, M. S. Muraru, T. Bertomeu and R. Khosravi-Far, *Apoptosis*, 2013, **18**, 1154-1162.

24. J. Sudimack and R. J. Lee, *Advanced Drug Delivery Reviews*, 2000, **41**, 147-162.

25. D. J. O'Shannessy, E. B. Somers, J. Maltzman, R. Smale and Y.-S. Fu, *SpringerPlus*, 2012, **1**, 22.

26. J. Sudimack and R. J. Lee, *Advanced Drug Delivery Reviews*, 2000, **41**, 147-162.

27. Z. Zhang, J. Wang, D. E. Tacha, P. Li, R. E. Bremer, H. Chen, B. Wei, X. Xiao, J. Da, K. Skinner, D. G. Hicks, H. Bu and P. Tang, *Archives of Pathology & Laboratory Medicine*, 2014, **138**, 890-895.

28. L. C. Hartmann, G. L. Keeney, W. L. Lingle, T. J. H. Christianson, B. Varghese, D. Hillman, A. L. Oberg and P. S. Low, *International Journal of Cancer*, 2007, **121**, 938-942.

29. A. C. Antony, *Blood*, 1992, **79**, 2807-2820.

30. S. D. Weitman, R. H. Lark, L. R. Coney, D. W. Fort, V. Frasca, V. R. Zurawski, Jr. and B. A. Kamen, *Cancer Research*, 1992, **52**, 3396-3401.

31. J. A. Reddy, V. M. Allagadda and C. P. Leamon, *Current Pharmaceutical Biotechnology*, 2005, **6**, 131-150.

32. L. Nair K, S. Jagadeeshan, A. Nair S and G. S. V. Kumar, *PLOS ONE*, 2013, **8**, e70697.

33. S. Wang and P. S. Low, *Journal of Controlled Release*, 1998, **53**, 39-48.

34. G. Wu, Z. Wang, X. Bian, X. Du and C. Wei, *Pharmaceutical Biology*, 2014, **52**, 978-982.

35. J. Wu, Q. Liu and R. J. Lee, *International Journal of Pharmaceutics*, 2006, **316**, 148-153.

36. R. Mahou and C. Wandrey, *Polymers*, 2012, **4**, 561.

37. Y. Zhang, Q. Zhao, H. Shao, S. Zhang and X. Han, *Advances in Materials Science and Engineering*, 2014, **2014**, 6.

38. H. Staudinger and J. Meyer, *Helvetica Chimica Acta*, 1919, **2**, 635-646.

39. F. L. Lin, H. M. Hoyt, H. van Halbeek, R. G. Bergman and C. R. Bertozzi, *Journal of the American Chemical Society*, 2005, **127**, 2686-2695.

40. E. Valeur and M. Bradley, *Chemical Society Reviews*, 2009, **38**, 606-631.

41. J. Lin, Y. Li, Y. Li, F. Cui, F. Yu, H. Wu, L. Xie, F. Luo, Z. Hou and C. Lin, *Journal of Materials Chemistry B*, 2015, **3**, 7707-7717.

42. S. Cajot, N. Lautram, C. Passirani and C. Jérôme, *Journal of Controlled Release*, 2011, **152**, 30-36.

43. W. Dang, O. M. Colvin, H. Brem and W. M. Saltzman, *Cancer Research*, 1994, **54**, 1729-1735.

44. Y. Zhang, T. Jin and R. X. Zhuo, *Colloids and Surfaces B: Biointerfaces*, 2005, **44**, 104-109.

45. A. R. Hilgenbrink and P. S. Low, *Journal of Pharmaceutical Sciences*, 2005, **94**, 2135-2146.

46. A. Kumar, V. Chelvam, M. Sakkarapalayam, G. Li, P. Sanchez-Cruz, N. S. Pinero, P. S. Low and A. E. Alegria, *Open Journal of Medicinal Chemistry*, 2016, **6**, 1-17.

47. T. Wileman, C. Harding and P. Stahl, *Biochemical Journal*, 1985, **232**, 1-14.

48. J.-M. Oh, M. Park, S.-T. Kim, J.-Y. Jung, Y.-G. Kang and J.-H. Choy, *Journal of Physics and Chemistry of Solids*, 2006, **67**, 1024-1027.

49. R. Zhao, N. Diop-Bove and I. D. Goldman, *Molecular Pharmacology*, 2014, **85**, 310-321.

50. L. H. Matherly, in *Progress in Nucleic Acid Research and Molecular Biology*, Academic Press, 2001, Volume 67, 131-162.

51. E. E. Sierra, K. E. Brigle, M. J. Spinella and I. D. Goldman, *Biochemical Pharmacology*, 1995, **50**, 1287-1294.

52. A. Hamid, M. Kiran, S. Rana and J. Kaur, *IUBMB Life*, 2009, **61**, 236-243.

Chapter 7: GENERAL CONCLUSIONS AND FUTURE WORK

7.1. GENERAL CONCLUSIONS

In this project, a functional caprolactone (α-chloro-ε-caprolactone) was synthesised as a precursor of functional amphiphilic block copolymers. The ring opening polymerisation of functional lactone monomer was carried out to generate amphiphilic block copolymers based on mPEG-*b*-poly(αClεCL) and mPEG-*b*-poly(εCL-*co*-αClεCL) comprising various molar masses (chapter 3). The characterisation data revealed good quantitative conversion of monomers generating amphiphilic block copolymers of predictable molecular weights and narrow polydispersity without apparent transesterification. In a second step, pendent chloro groups of amphiphilic block copolymers were substituted by azide via nucleophilic substitution.

The reactive micelles based on mPEG-*b*-poly($\alpha N_3\varepsilon CL$) and mPEG-*b*-poly(εCL-*co*-$\alpha N_3\varepsilon CL$) amphiphilic block copolymers comprising various molecular weights and different ratios of functional groups were then prepared using dialysis method (chapter 4). The block copolymer of mPEG-*b*-poly(εCL-*co*-$\alpha N_3\varepsilon CL$) (M_n ~ 10.1 kDa, D_p of PCL ~ 35, D_p of poly($\alpha N_3\varepsilon CL$) ~ 7) resulted into uniform sized micelles with narrow poly dispersity index, and therefore, was used for further applications. The azide-bearing hydrophobic backbone of the selected amphiphilic block copolymer was used to conjugate an alkyne functionalised model molecule (HCA-linker) to develop the redox-responsive polymer-dye conjugate as a model responsive drug delivery system. The resultant micelles of HCA-linker

grafted block copolymer efficiently retained the HCA in non-reducing medium, however, temporal release of HCA was observed in reducing medium.

In another strategy (chapter 5), an anticancer drug (methotrexate) was loaded into the hydrophobic core of the micelles, which were further crosslinked by a redox responsive crosslinker to generate redox-responsive reversibly core-crosslinked micelles. The encapsulation efficiency of micelles greatly improved after crosslinking as compared to the un-crosslinked micelles. The redox-responsive reversibly core-crosslinked released lower amounts of the drug under simplified (serum free) physiological conditions, however, rapid drug release was observed in reducing environments. The cellular uptake studies revealed that core-crosslinked micelles were internalised by MCF7 cells quantitatively and mostly localised near the vicinity of cell nuclei. In contrast, un-crosslinked micelles were mostly localised in the cytoplasm of MCF7 cells. The cytotoxicity studies showed that empty un-crosslinked and core-crosslinked micelles were nontoxic to MCF7 cells. The MTX-loaded core-crosslinked micelles greatly inhibited the metabolic activity of MCF7 in a dose dependent manner, as compared to the MTX-loaded un-crosslinked micelles and free MTX. The apoptosis assays revealed that MTX-loaded core-crosslinked micelles induced apoptosis and cell death in MCF7 cells to a greater extent as compared to the MTX-loaded un-crosslinked micelles and free MTX.

In another strategy (chapter 6), a multifunctional amphiphilic block copolymer based on α-amine-PEG-*b*-poly(εCL-*co*-αN_3εCL) was synthesised and subsequently was used to conjugate methotrexate on the hydrophilic block for receptor mediated targeting of breast cancer cells. Furthermore, an alkyne bearing fluorescent probe (FITC-alkyne) was grafted on the hydrophobic backbone via CuAAC to analyse cellular uptake of micelles. Cellular uptake studies revealed 2.3-fold higher uptake of MTX-conjugated micelles as compared with un-conjugated micelles. The blank micelles showed low cytotoxicities in breast cancer cells, however, MTX-conjugated micelles exhibited greater antitumor activities in contrast to free-MTX. Therefore, these functional micelles might in future be promising candidates for bio-responsive drug delivery applications, active tumour targeting and therapy.

7.2. FUTURE WORK

The redox-responsive and multi-functional micelles proved promising and potential candidates as drug delivery vehicles. Despite the success of *in vitro* investigations, *in vivo* studies are required to assess the efficiency of functional micelles for clinical applications. Furthermore, dual stimuli responsive micelles can be developed by incorporating acid-labile and reduction responsive linkages in the hydrophobic core of the micelles to exploit multiple intrinsic stimuli present in the tumour microenvironment.

Furthermore, it would be worth conjugating or encapsulating more than one drug inside the cores of the functional micelles to achieve combinatory tumour therapy.

Chapter 8: APPENDIX

8.1. Theory of DLS and zeta potential

8.1.1. DLS

In the DLS experiments, suspensions of nanoparticles were illuminated by a laser beam and fluctuations in the intensity of scattered light caused by the Brownian motion of particles, were detected at a known scattering angle using a fast photon detector. The intensity of scattered light fluctuates at a rate which is dependent on the size of the nanoparticles. The smaller particles cause the light to fluctuate faster than larger particles. The velocity of the Brownian motion can be estimated by analysing these fluctuations in the intensities of scattered light. The estimated velocity of Brownian motion can be converted into particle size using the Stokes-Einstein relationship.[1]

8.1.2. Zeta Potential

Zeta potential is one of the important parameters affecting the stability of colloids or nanoparticles in a liquid. In particular, the existence of a net charge on a particle dispersed in a liquid affects the distribution of ions surrounding it, resulting in an increase in the magnitude of counter-ions. The area over which this effect extends is known as electrical double layer, comprising an inner and an outer layer. The inner region is known as Stern layer, where ions are firmly bound. The outer layer is called as diffuse layer

which holds loosely bound ions.[2] When particles move through solution, the associated ions also move, however, there is a "boundary" at some distance from the particle, beyond which ions do not move with the particle. This region of the outer or diffuse layer is called as slipping plane or surface of hydrodynamic shear and the potential at this boundary is known as zeta potential. Simply, it is the potential difference between the dispersion medium and the stationary layer of the fluid attached to the dispersed particle. Zeta potential of nanocarriers can be estimated by applying an electric field across the colloids or nanoparticles dispersion and then by measuring the electrophoretic mobility by laser doppler velocimetry. The measured electrophoretic mobility can be converted into zeta potential using Henry equation:

$$\mu_E = \frac{2\varepsilon\, \zeta\, f(ka)}{3\eta}$$

ζ = zeta potential, μ_E = electrophoretic mobility, ε = dielectric constant, η = viscosity, and f (ka) = Henry's function.

Dispersions of nanocarriers having zeta potential values more than +25 mV or less than -25 mV are usually considered to be 'colloidally stable'. On the other hand, dispersions with a low zeta potential value are unstable and will eventually agglomerate due to Van-Der Waal inter-particle attractions.

8.2. Supplementary figures

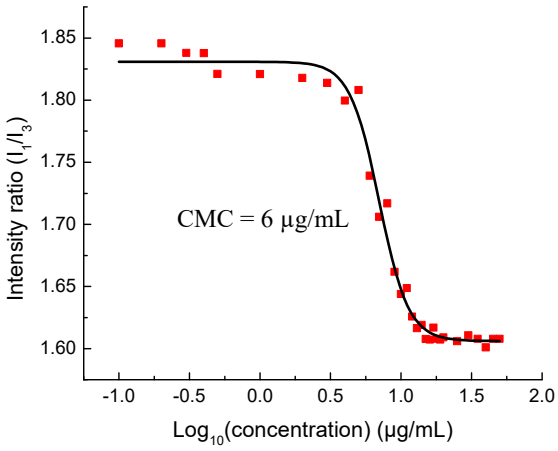

Figure 8-1. CMC plot for mPEG-*b*-poly(εCL-*co*-αN$_3$εCL) (M_n ~ 10.1 kDa, D_p of PCL ~ 35, D_p of poly(αN$_3$εCL) ~ 7).

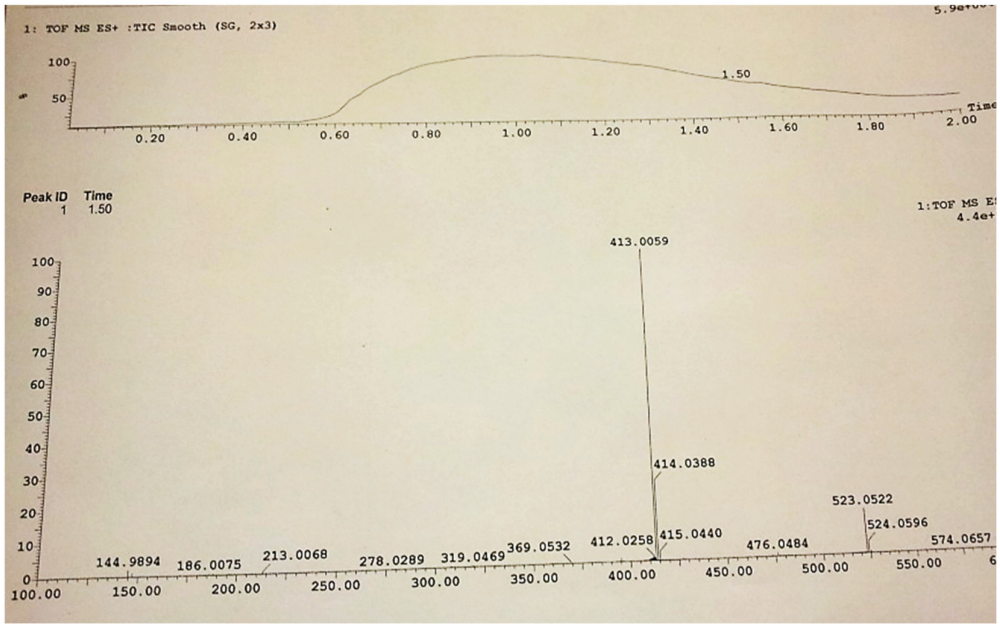

Figure 8-2. Electrospray ionisation mass spectrum of Oregon-green.

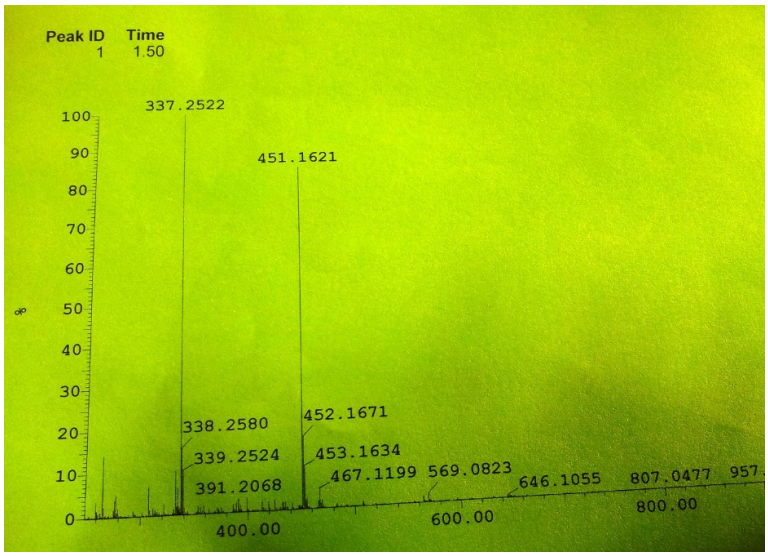

Figure 8-3. Electrospray ionisation mass spectrum of *bis*-alkyne disulfide crosslinker.

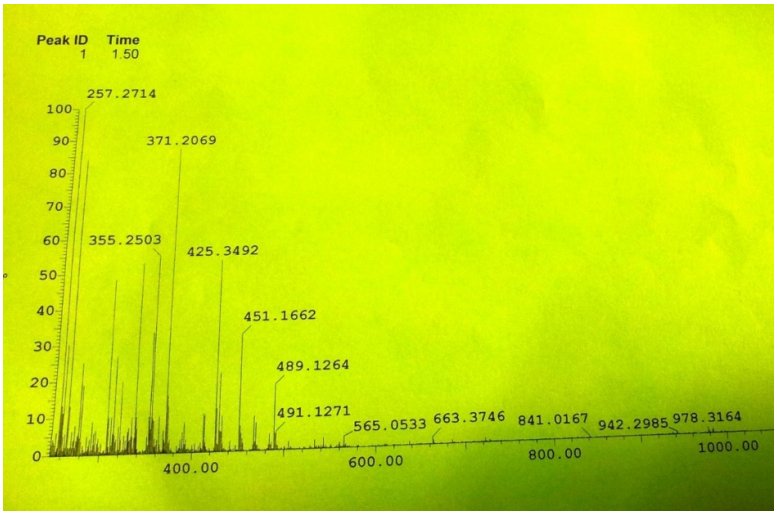

Figure 8-4. Electrospray ionisation mass spectrum of bi-functional redox-responsive spacer.

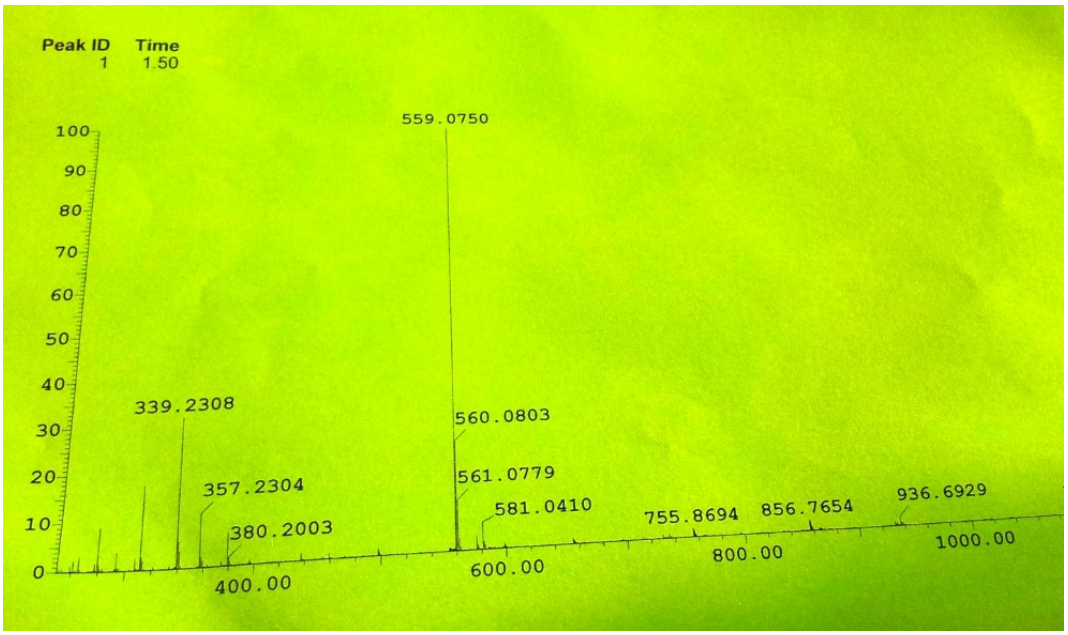

Figure 8-5. Electrospray ionisation mass spectrum of 7-hydroxycoumarinyl-spacer complex (HCA-Linker).

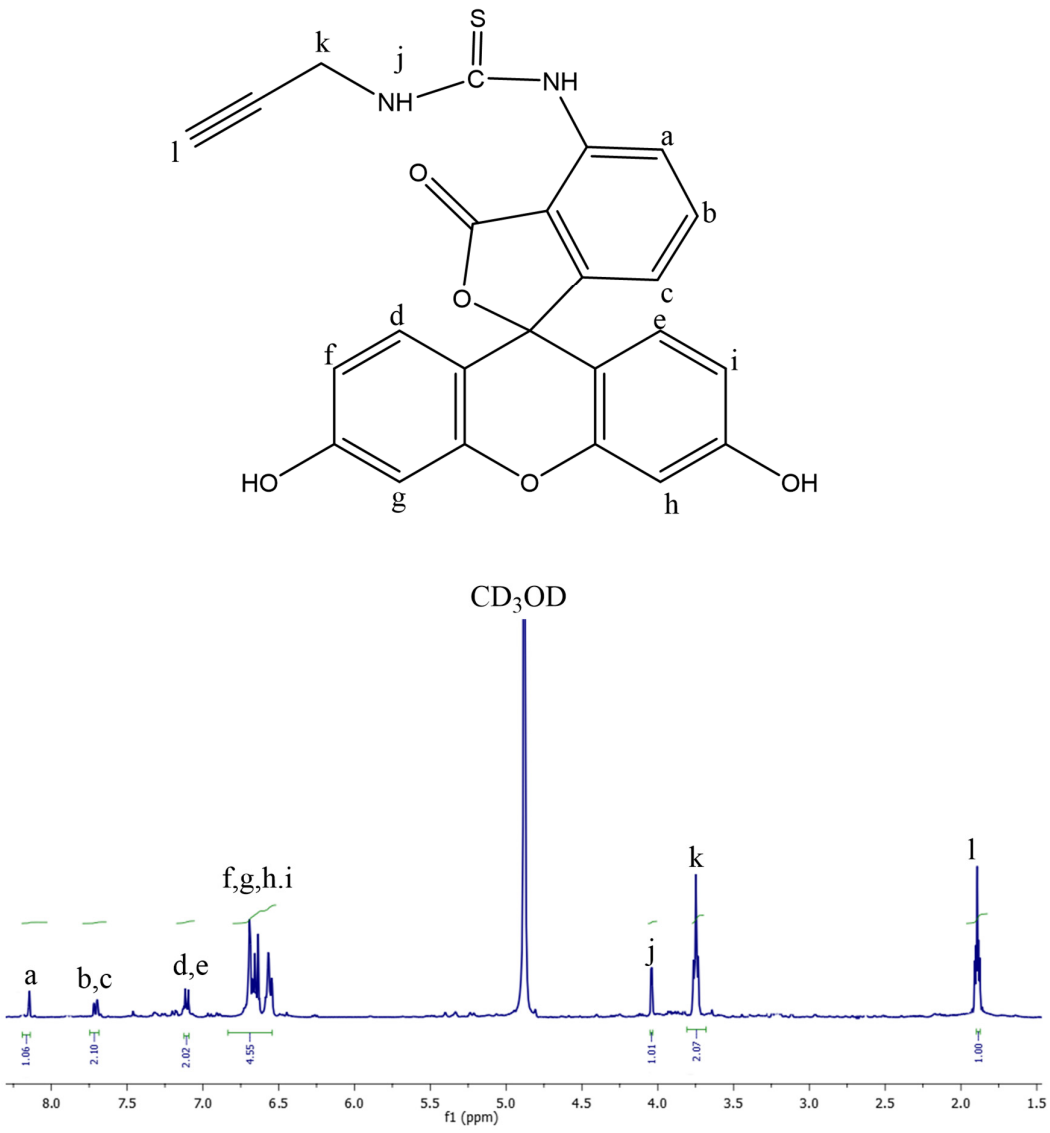

Figure 8-6. ^{1}H NMR spectrum of FITC-alkyne in CD_3OD.

8.3. REFERENCES

1. R. Pecora, *Journal of Nanoparticle Research*, 2000, **2**, 123-131.

2. J. D. Clogston and A. K. Patri, *Methods in Molecular Biology (Clifton, N.J.)*, 2011, **697**, 63-70.